Jarrah Ali Al-Tubaikh
Maximilian F. Reiser

Congenital Diseases and Syndromes

An Illustrated Radiological Guide

Springer

Congenital Diseases and Syndromes

"*This page left intentionally blank.*"

Jarrah Ali Al-Tubaikh
Maximilian F. Reiser

Congenital Diseases and Syndromes

An Illustrated Radiological Guide

Springer

Dr. Jarrah Ali Al-Tubaikh
Universitätsklinikum München
Klinikum Großhadern
Institut für Klinische Radiologie
Marchioninistr. 15
81377 München
Germany
Tabeebjarah@hotmail.com

Prof. Dr. Maximilian F. Reiser, FRCR, FACR
Universitätsklinikum München
Klinikum Großhadern
Institut für Klinische Radiologie
Marchioninistr. 15
81377 München
Germany
mreiser@med.uni-muenchen.de

Radiologist, Medical Illustrator
Department of Diagnostic Radiology
Sabah Hospital, Kuwait

All illustrations marked with  were drawn by the author.

ISBN: 978-3-642-00159-8 e-ISBN: 978-3-642-00160-4

DOI: 10.1007/978-3-642-00160-4

Springer Dordrecht Heidelberg London New York

Library of Congress Control Number: 2009921988

© Springer-Verlag Berlin Heidelberg 2009

This work is subject to copyright. All rights are reserved, whether the whole or part of the material is concerned, specifically the rights of translation, reprinting, reuse of illustrations, recitation, broadcasting, reproduction on microfilm or in any other way, and storage in data banks. Duplication of this publication or parts thereof is permitted only under the provisions of the German Copyright Law of September 9, 1965, in its current version, and permission for use must always be obtained from Springer. Violations are liable to prosecution under the German Copyright Law.

The use of general descriptive names, registered names, trademarks, etc. in this publication does not imply, even in the absence of a specific statement, that such names are exempt from the relevant protective laws and regulations and therefore free for general use.

Product liability: The publishers cannot guarantee the accuracy of any information about dosage and application contained in this book. In every individual case the user must check such information by consulting the relevant literature.

Cover design: eStudioCalamar, Figueres/Berlin

Printed on acid-free paper

Springer is part of Springer Science+Business Media (www.springer.com)

This book is dedicated to my mother, my father, my family, and my beloved country Kuwait.

"*This page left intentionally blank.*"

Preface

Radiology to me is an art more than a science; an art of imaging the human body, and an art of extracting information from an image. Radiology today is a vital specialty that almost no other medical specialty can work without. Congenital anomalies and syndromes are complex subjects in all medical specialties. They require knowledge of the normal anatomy and of the embryological basis of organogenesis. The importance of recognizing a congenital malformation or an anomaly, which can be the tip of an iceberg of a more complex syndrome, is to prevent future manifestations of a syndrome if possible or to reduce its severity. Due to this concept, I had an interest in studying how to use the radiological modalities in diagnosing congenital malformations as early as possible. Although radiology offers very powerful tools for diagnosis, the basics of medicine are still the main tools to be used for diagnosis. History, observation, clinical examination, and laboratory investigations are essential elements for diagnosis, which need to be used before radiology investigations are initiated.

The idea of this book is based on a simple principle: it is to link radiology to these basic medical tools. The book is written for junior radiologists, radiology students, and doctors interested in congenital malformations and syndromes in any specialty. Each disease is represented with a definition, description, etiology, diagnostic criteria, main symptoms, and its typical diagnostic radiological features on the modern radiological modalities available today. Important clinical manifestations, rare radiological signs, gross pathological morphology, or special classifications are illustrated by using digital medical illustrations and digital photo manipulation.

Radiology is a visual science, and no matter how well-written the description of a sign, if you do not see the sign, it is usually difficult to identify it in a real situation. As a radiologist, artist, professional graphic designer, and medical illustrator, I used to collect and draw the difficult and rare signs by using digital media. Over time, a huge archive of disease signs accumulated in my computer, from where this book came into life.

When I started studying congenital diseases and their radiological features, I faced many difficulties in finding definitions of the anomalies and their descriptions. There is no clear-cut line that tells the junior radiologist which case is a specialized case and which case is a general congenital anomaly that he/she should be aware of. You can easily get caught up in details and be sidetracked when reading a big reference textbook. For example, if you want to study a case of dwarfism, you will find yourself reading about case one, which has a similarity to case two, that will refer you to case three, and so on. In this book, I tried to collect and illustrate many of the cases in which radiology plays an important diagnostic role. Moreover, I included congenital malformations that are commonly mentioned in the radiological board examinations,

or can be faced occasionally in a busy radiological department. Some of the cases included are rare and considered to be specialty-related cases, but in my opinion they are interesting to know about.

The main goal of this book is to serve as a visual guide for radiology students and doctors interested in congenital diseases. The book is not intended as a substitute for standard radiological textbooks or common reference texts. Readers who are interested in more details are kindly requested to refer to the selected references supplied or to any specialized medical textbook.

Finally, I hope this book and its illustrations serve the reader by simplifying the congenital diseases and malformations for him/her. After all, increasing the quality and precision of diagnosis is the aim of any doctor.

Munich, Germany

Jarrah Ali Al-Tubaikh
Maximilian F. Reiser

Acknowledgments

I would like to thank the people who contributed to this project by supplying me with many of the cases illustrated in this book from their private archives:

Alaa Abou-Beih, Bader Al-Mahdi, Khaled Al-Sayyed, Magdi Al-Taweel, Tarek Al-Zayat, Ibrahim Helmi, and Rajae Makar.

Also, I would like to thank the people who supported me and this project, and helped me in many ways to accomplish it:

Samar Al-Farra, Moneera Al-Husaini, Ahmed Al-Mutairi, Mohammed Sami Khalifa (MD), Ibrahim Al-Abdulhadi (MD), Salman Al-Haqqan, Jalal Al-Baghli, Salman Jamal, Bashar Al-Shawaf, Ali Al-Shubbar, Adel Reda (MD), Mohammed Awad, Sameer Abu-Rabea, and Wieland Sommer (MD).

"*This page left intentionally blank.*"

Contents

"*This page left intentionally blank.*"

Contributors

Rajae Makar Department of Diagnostic Radiology, Sabah Hospital, Kuwait

Ibrahim Helmi Department of Diagnostic Radiology, Chest Hospital, Kuwait

Bader Al-Mahdi Cardiology Care Unit, Adan Hospital, Kuwait

Alaa Abou-Beih Department of Ear, Nose and Throat, Zain Hospital, Kuwait, Lecturer, Otolaryngology Department, Faculty of Medicine, Mansoura University, Mansoura, Egypt

Tarek Al-Zayat Department of Diagnostic Radiology, Al-Azhar University Hospitals, Cairo, Egypt

Magdi Al-Taweel Department of Diagnostic Radiology, Al-Azhar University Hospitals, Cairo, Egypt

Khaled Al-Sayyed Department of Diagnostic Radiology, Sabah Hospital, Kuwait

"*This page left intentionally blank.*"

Abbreviations

CT	computed tomography
MRI	Magnetic resonance image
T1W	T1-weighted
T2W	T2-weighted
US	ultrasound

Chapter 1

The CNS

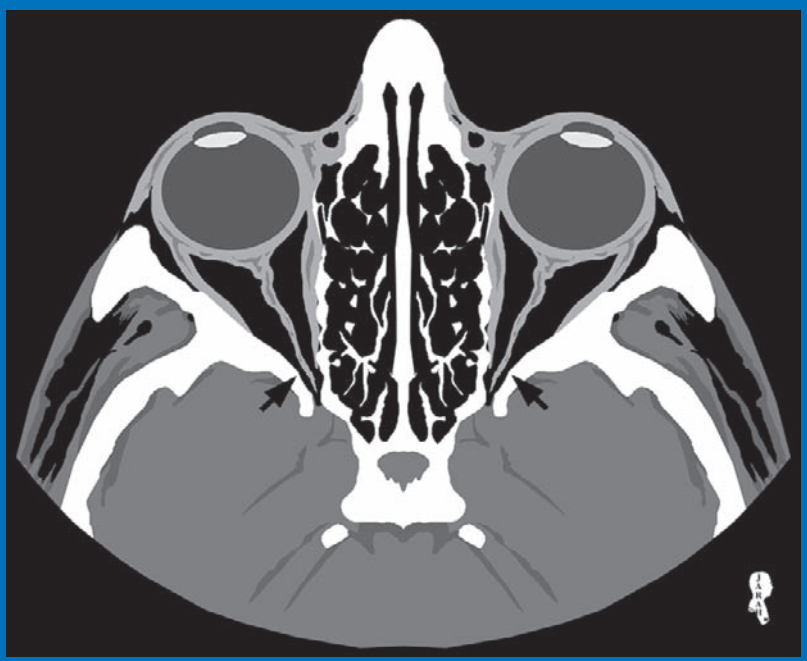

CONTENTS

J. A. Al-Tubaikh, M. F. Reiser: *Congenital Diseases and Syndromes* – An Illustrated Radiological Guide
DOI: 10.1007/978-3-642-00160-4_1, © Springer-Verlag Berlin Heidelberg 2009

1.1

Anencephaly (Acrania)

Anencephaly is a congenital brain malformation characterized by a partial or complete failure of the brain and skull to develop, resulting in small or missing brain hemispheres (Fig. 1.1.1). It is usually associated with spinal dysraphism.

Anencephaly is thought to be caused by antiepileptic drug use during pregnancy, mechanical insults, radiation exposure, and chromosomal anomalies.

Anencephaly can be detected during pregnancy by measuring the level of alpha-fetoprotein (AFP) in the amniotic fluid via amniocentesis, which will be abnormally high. Serum maternal AFP level will also be high with a low estriol level (highly suggestive of anencephaly). Additionally, anencephaly can be reliably diagnosed with Maternal ultrasonography between the 10th and 14th week of pregnancy.

A dietary supplement with folic acid during pregnancy reduces the incidence of anencephaly and spinal dysraphism.

Maternal–fetal MRI can play a role in diagnosing anencephaly, confirming the US findings, or differentiating it from other malformations (e.g., encephaloceles).

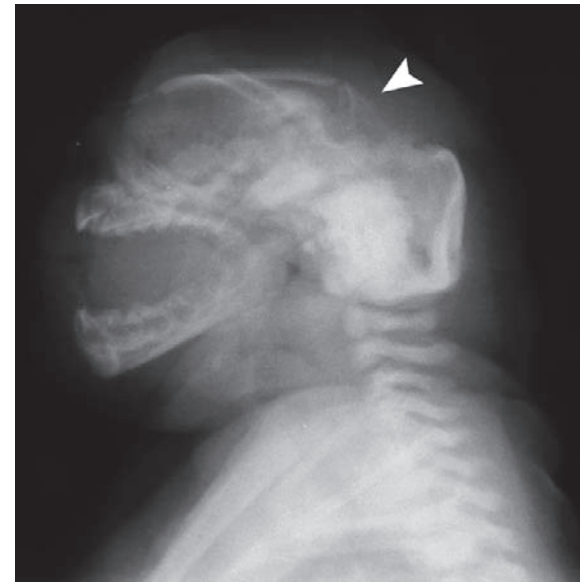

Fig. 1.1.1. A lateral plain radiograph of a dead infant with anencephaly shows absence of the brain and the skull (*arrowhead*)

For Further Reading

1. Ashwal S et al. Anencephaly: Clinical determination of brain death and neurological studies. Pediatr Neurol 1990; 6:233–239
2. Calzolaro F et al. Anencephaly: MRI findings and pathogenetic theories. Pediatr Radiol 2004;34:1012–1016

1.2

Encephalocele

Encephalocele is a congenital anomaly characterized by herniation of the intracranial structures through a defect in the cranium. There are different types of encephaloceles according to the contents of the herniated tissue:

- **Meningocele:** herniation of the meninges with cerebrospinal fluid.
- **Encephalomeningocele:** herniation of the meninges with brain parenchyma (but not the ventricles).
- **Encephalocystomeningocele:** herniation of the meninges, brain parenchyma, and ventricle.

There are different types of encephaloceles according to the area of defect:

Occipital Encephalocele (71%)

The defect of the cranium is located in the occipital bone. Typically the patient has microcephaly.
Occipital encephalocele is divided into three grades:

- **High occipital cephalocele:** herniation in the occipital bone above the foramen magnum (Fig. 1.2.1).

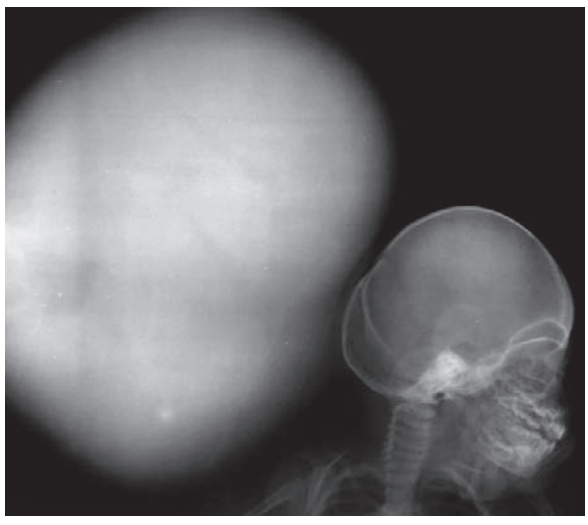

Fig. 1.2.1. Lateral plain radiograph of a patient with high occipital encephalocele shows very large herniated sac attached to the posterior margin of the cranium

Fig. 1.2.2. Lateral plain radiograph of a patient with cervico-occipital encephalocele (Chiari III malformation)

- **Low occipital cephalocele:** herniation in the occipital bone that reaches the foramen magnum.
- **Cervico-occipital cephalocele:** cervico-occipital defect that includes the posterior arches of C1–C2. It is also called "Chiari malformation type III" and it contains almost the whole cerebellum (Fig. 1.2.2).

Parietal Encephalocele (10%)

Parietal encephalocele is a defect of the cranium in the midline, near the midpoint of the sagittal suture, or posterior to the anterior fontanelle. Corpus callosum agenesis and Dandy-Walker malformation may be associated with parietal encephalocele.

Nasofrontal Encephalocele (9%)

The defect of the cranium occurs between two deformed orbits, producing hypertelorism and glabellar mass. The hernia typically includes the meninges, olfactory tract, and anterior–inferior frontal lobe.

Sphenoethmoidal Cephaloceles (Rare)

Sphenoethmoidal cephalocele is a brain herniation through the floor of the sella turcica just anterior to dorsum sella

and medial to the cavernous sinus. It results in hypertelorism, broad nasal septum, and endocrine dysfunction.

Meckel-Gruber syndrome: is a rare fatal disease characterized by encephalocele, polydactyly, and polycystic renal disease. The disease has an autosomal recessive mode of inheritance, and is usually detected by fetal US during the first trimester.

For Further Reading

1. Deasy NP et al. Intrasphenoid cephalocele: MRI in two cases. Neuroradiology 1999;41:497–500
2. Zhao X et al. A five-generation family with occipital encephalocele. Clin Neurol Neurosurg 2007;109:81–84
3. Häberle J et al. Cervical encehalocele in a newborn – Chiari III malformation. Case report and review of the literature. Child's Nerv Syst 2001;17:373–375
4. Hoving EW. Nasal encephaloceles. Child's Nerv Syst 2000; 16:702–706
5. Thijssen HOM et al. Acquired basal encephalocele. Neuroradiology 1976;11:209–213
6. Tanriverdi HA et al. Meckel Gruber syndrome: A first trimerster diagnosis of a recurrent case. Eur J Ultrasound 2002; 15:69–72

1.3

Holoprosencephaly

Holoprosencephaly is a congenital disease characterized by failure in the formation of the midline brain segments including the anterior part of the corpus callosum, falx cerebri, and septum pellucidum. Holoprosencephaly means "total prosencephalon," which is one of the three primitive vesicles of the early human brain. In holoprosencephaly, both lateral ventricles and the third ventricle become one big ventricle. The incidence is 1 in every 16,000 births.

Holoprosencephaly can be associated with hypotelorism, trisomy 13, Kallmann syndrome (congenital absence of the olfactory nerve with hypogonadotrophic hypogonadism), and trisomy 18. Moreover, it is commonly associated with facial anomalies such as:

- **Cyclopia:** both orbits and eyes are fused into one eye.
- **Ethmocephaly:** both orbits are very near each other but not fused.
- **Cebocephaly:** small flat nose with single nostril.
- **Cleft lip**.

There are three types of holoprosencephaly:

Alobar Holoprosencephaly

In alobar holoprosencephaly, the brain is made up of a big balloon of cerebrospinal fluid with no lateral or third ventricles. The cortex has three shapes referred to as pancake (Fig. 1.3.1), cup (Fig. 1.3.2), and ball type (Fig. 1.3.3) alobar holoprocencephaly.

Fig. 1.3.1. Axial CT illustration shows "pancake type" alobar holoprocencephaly. Only the frontal lobe is present with both basal ganglia and thalami fused in the middle within the frontal lobe parenchyma

Fig. 1.3.2. Axial CT illustration shows "cup type" alobar holoprocencephaly. The brain is much more developed with both thalami fused together as one mass in the middle. Part of the occipital lobe is present

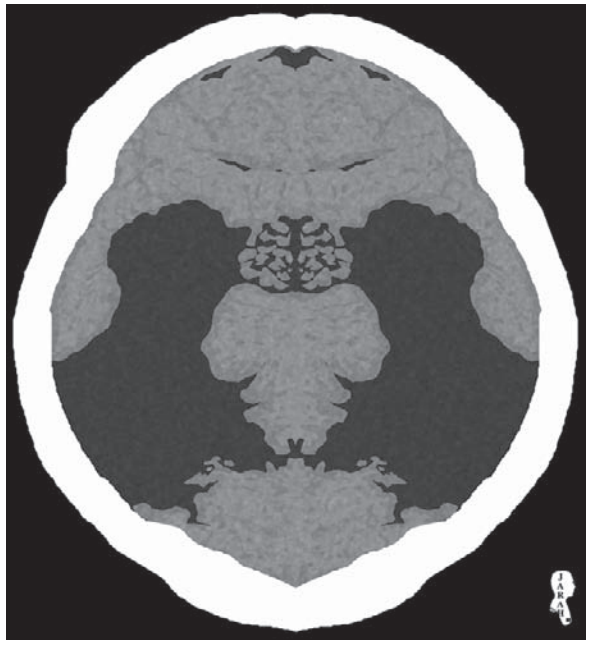

Fig. 1.3.3. Axial CT illustration shows "ball type" alobar holoprocencephaly. There is complete covering of the monoventricle by brain tissue with no falx. The midline fused thalami give the ventricle an "inverted U shape"

Signs on CT and MRI

- Absence of the falx cerebri, septum pellucidum, and the anterior portion of the corpus callosum (Fig. 1.3.4).
- Single-lobed brain tissue (frontal lobe only) with single monoventricle (Fig. 1.3.4).
- The middle cerebral vessels, the straight sinus, and the superior sagittal sinus are absent.
- The anterior cerebral arteries are fused into a single azygos artery, usually seen at angiography (Fig. 1.3.5).

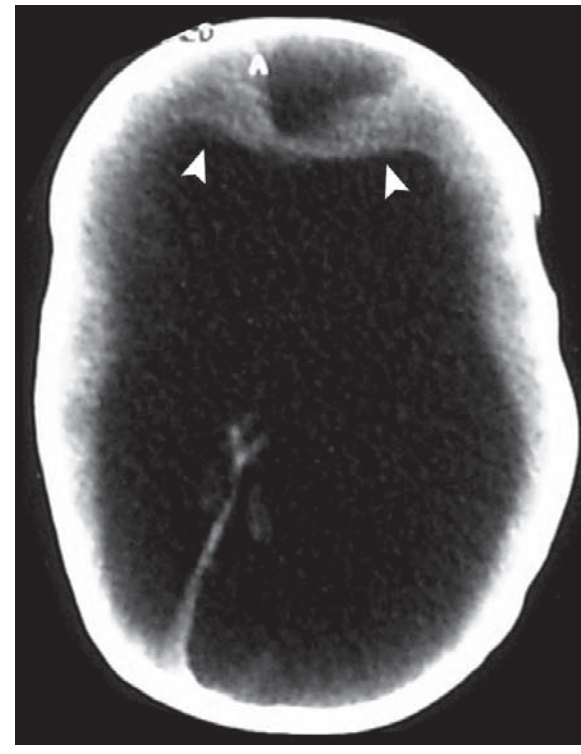

Fig. 1.3.4. Axial CT in a patient with alobar holoprocencephaly. Most of the brain parenchyma is absent with only part of the frontal lobe seen bilaterally (*arrowheads*)

Fig. 1.3.5. Axial MR angiography illustration of the circle of Willis shows single anterior cerebral artery, known as "azygos anterior cerebral artery" (*arrowhead*). It results from abnormal fusion of the two anterior cerebral arteries into a single vessel

Semilobar Holoprosencephaly

In semilobar holoprosencephaly, there is a partial attempt of brain differentiation and lobe formation.

Signs on CT and MRI

- H-shaped monoventricle with partially developed occipital and temporal horns (Fig. 1.3.6).
- Occipital horns of the lateral ventricles are developed and connected with each other across the midline with no anterior horns (the two frontal lobes are continuous without interruption by the anterior horns) (Fig. 1.3.6).
- The falx cerebri is rudimentary with fused basal ganglia.
- The temporal horns of the lateral ventricles are rudimentary.

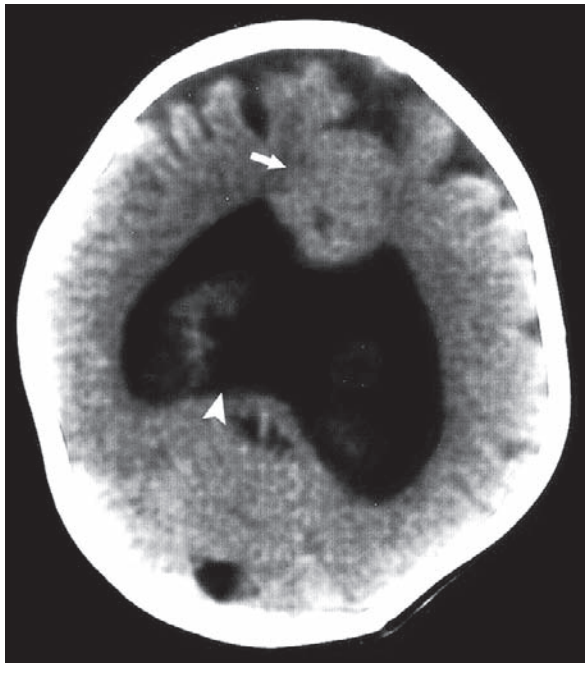

Fig. 1.3.6. Axial CT image of a patient with semilobar holoprocencephaly. The frontal lobes are continuous without interruption by the anterior horns of the lateral ventricles (*arrow*). Also, note the H-shaped lateral ventricles (*arrowhead*)

Lobar Holoprosencephaly

In lobar holoprosencephaly, there is almost complete brain formation with well-lobulated ventricles.

Signs on CT and MRI

- The frontal horns of the lateral ventricles are abnormally narrow with an absent septum pellucidum causing them to have a box-like shape (Fig. 1.3.7).
- The occipital horns are well formed and separated.
- The interhemispheric fissure and the falx cerebri are almost totally formed.

Fig. 1.3.7. Axial CT illustration shows lobar holoprocencephaly with absent septum pellucidum and "box-shape" frontal horns of the lateral ventricles (*arrow*)

For Further Reading

1. Fitz CR. Holoprosencephaly and related entities. Neuroradiology 1983;25:225–238
2. Sener RN. Anterior callosal agenesis in mild, lobar holoprosencephaly. Pediatr Radiol 1995;25:385–386
3. Osaka K et al. Dysgenesis of the deep venous system as a diagnostic criterion for holoprosencephaly. Neuroradiology 1977;13:231–238
4. Maki Y et al. Angiographic features of alobar holoprosencephaly. Neuroradiology 1974;6:270–276

1.4

Hydranencephaly

Hydranencephaly is a rare congenital disease characterized by absence of the majority of the brain parenchyma and replacement of the cerebral hemispheres by a large cerebrospinal fluid (CSF) pool in a normal-sized cranium. It occurs in less than 2 per 10,000 births worldwide.

Hydranencephaly is thought to be caused by occlusion of the bilateral internal carotid arteries in fetal life, mainly during or after the second trimester due to a variety of causes (e.g., congenital infections).

Signs on CT and MRI

- The CT or the MRI scan shows absent cerebral hemispheres; only the occipital lobes, part of the temporal lobes, or the thalami are present (Figs. 1.4.1 and 1.4.2).
- In contrast to holoprosencephaly, the falx cerebri is present (Fig. 1.4.2).
- Absence of the middle and the anterior coronary arteries on cerebral angiography.
- The posterior fossa content is morphologically normal and present (Fig. 1.4.1).

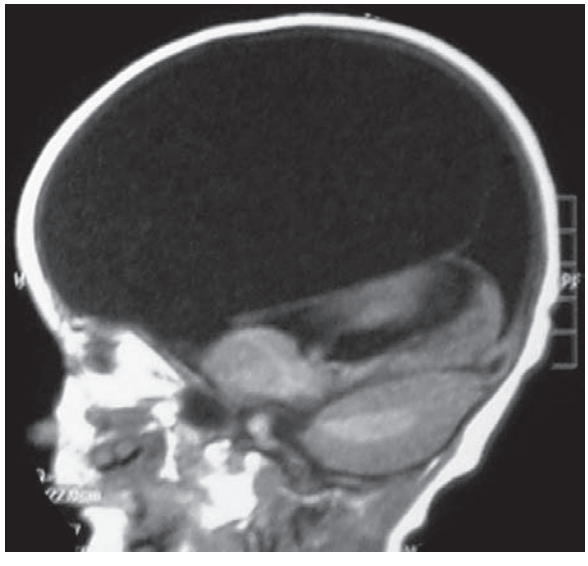

Fig. 1.4.1. Sagittal CT image shows a patient with hydranencephaly. Note absence of the cerebral hemispheres with filling of most of the cranium by CSF. Note also formation of parts of the occipital lobe, temporal lobe, and cerebellum

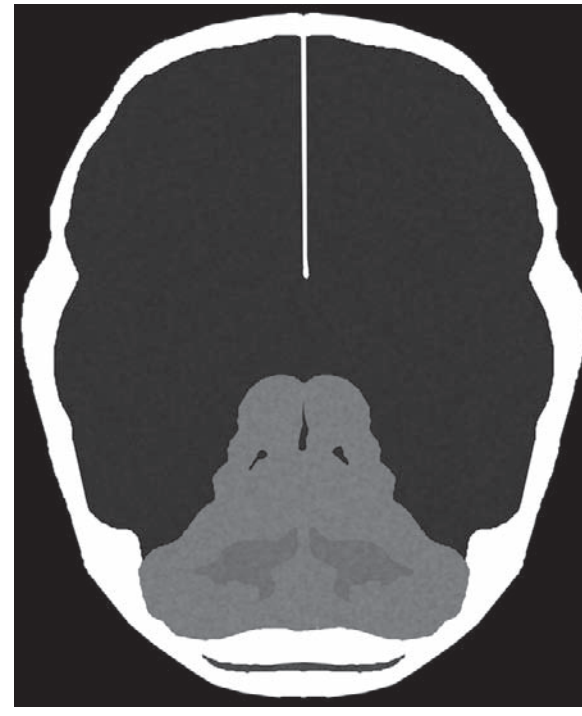

Fig. 1.4.2. Axial CT illustration of hydranencephaly shows presence of the falx cerebri with parts of the occipital lobes

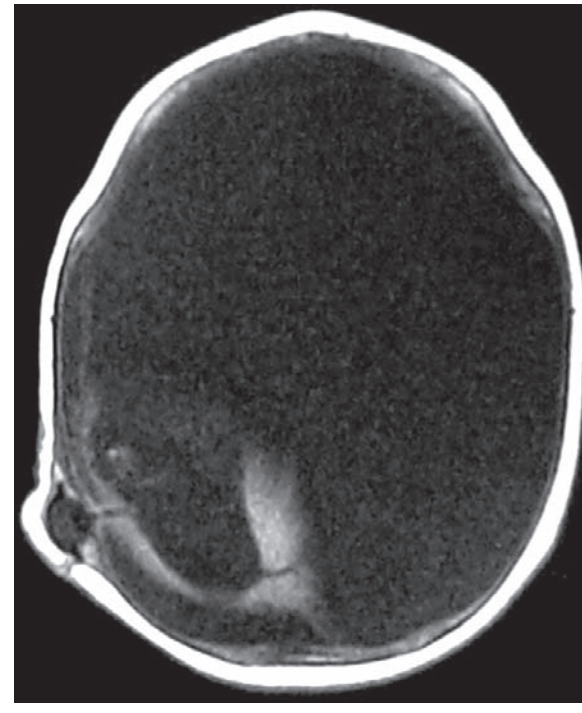

Fig. 1.4.3. Axial CT image of the same patient in a higher section shows filling of most of the cranium by CSF with very minimal brain parenchyma

For Further Reading

1. Nau H-E et al. Hydranencephaly-clinical and neuropathological aspects. Acta Neurochirurgica 1979;47:219–233
2. Hochmuth A et al. MR-angiographic findings in a case of hydranencephaly: Correlation of vascular and MR-tomographic features. Klin Neuroradiol 2003;13:84–87
3. Raybaud C. Destructive lesions of the brain. Neuroradiology 1983;25:265–291

1.5

Schizencephaly

Schizencephaly is a congenital disease characterized by presence of a cleft within the brain lined by gray matter allowing communication between the subarachnoid spaces laterally and the ventricular system medially.

Schizencephaly is thought to be caused by vascular insult during early neuroembryogenesis, cytomegalovirus infection, trauma, and exposure to drugs such as warfarin during pregnancy.

Schizencephaly is usually unilateral, but can be bilateral and symmetrical in some cases. It is usually associated with an absent septum pellucidum.
There are two types of schizencephaly:

Open-Lip Schizencephaly (Type 1)

Open-lip schizencephaly is characterized by a parenchymal cleft that reaches and communicates with the ventricles. It can be associated with septo-optic dysplasia.

Signs on MRI

An open cleft within the brain parenchyma lined by gray matter substance that extends from the subarachnoid space to the lateral ventricles (Fig. 1.5.1).

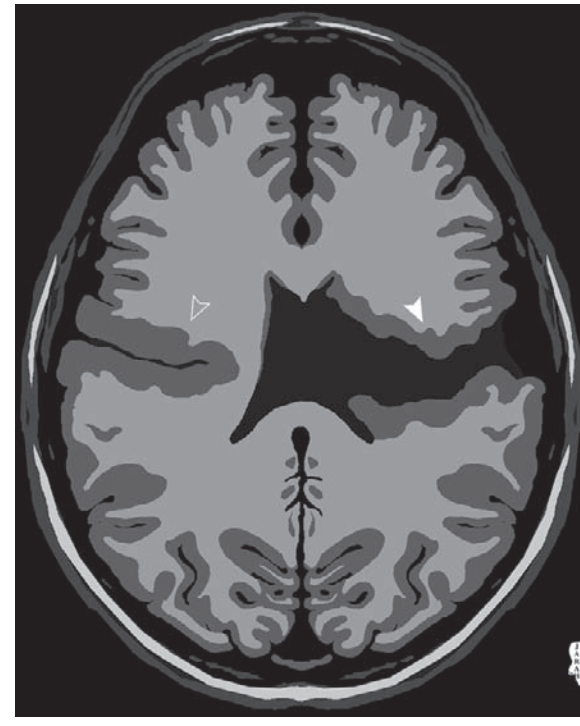

Fig. 1.5.1. Axial T1-weighted MR illustration shows different types of schizencephaly. Open-lip schizencephaly is seen as a cleft within the brain parenchyma, lined by gray matter, and communicates with the ventricular system (*white arrowhead*). Closed-lip schizencephaly is seen as a cleft within the brain parenchyma, lined by gray matter, and do not communicate with the ventricular system (*open arrowhead*). Note absence of septum pellucidum

Closed-Lip Schizencephaly (Type 2)

Closed-lip schizencephaly is characterized by a parenchymal cleft that does not reach the ventricles (Fig. 1.5.2).

Q: The differential diagnosis for open-lip schizencephaly is poroencephalic cyst; how can you differentiate between the two conditions?

Schizencephaly is lined by gray matter, while poroencephalic cyst is lined by white matter.

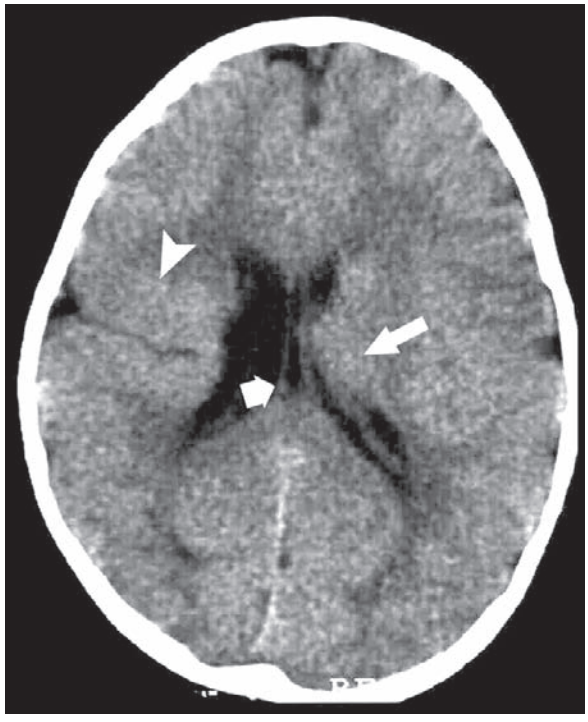

Fig. 1.5.2. Axial CT image shows closed-lip schizencephaly (*arrowhead*). Note also the subependymal gray matter heterotopia (*long arrow*), and cavum vergae (*short arrow*)

For Further Reading

1. Barkovich AJ et al. Malformations of cortical development. Neuroimag Clin N Am 2004;14:401–423
2. Deblaere K et al. Structural magnetic resonance imaging in epilepsy. Eur Radiol 2008;18:119–129
3. Denis D et al. Schizencephaly: Clinical and imaging features in 30 infantile cases. Brain Dev 2000;22:475–483
4. Hayashi N et al. Morphological features and associated anomalies of schizencephaly in the clinical population: Detailed analysis of MR images. Neuroradiology 2002;44: 418–427
5. Fernandez-Bouzas A et al. Schizencephaly with occlusion or absence of middle cerebral artery. Neuroradiology 2006; 48:171–175

1.6

Septo-optic Dysplasia (de Morsier Syndrome)

Septo-optic dysplasia (SOD) is a heterogeneous brain anomaly characterized by complete or partial absence of the septum pellucidum, hypoplasia of the optic nerves, dysgenesis of the olfactory bulbs, and pituitary insufficiency with endocrine abnormalities

Up to 50% of patients have dwarfism due to growth hormone deficiency as a consequence of pituitary-hypothalamic axis abnormalities. Other features include blindness, nystagmus, and hypotonia.

SOD can be associated with schizencephaly in 50% of cases.

Signs on CT and MRI

- Absence of the septum pellucidum in 50–75% of cases, resulting in a squared-off appearance of the frontal horns of the lateral ventricles (Fig. 1.6.1).
- Dilatation of the suprasellar cistern.
- Bilateral, small, hypoplastic optic nerves and chiasm with thinning of the nerves gradually toward the optic foramina (Fig. 1.6.2).
- Occasional dysgenesis of the corpus callosum.

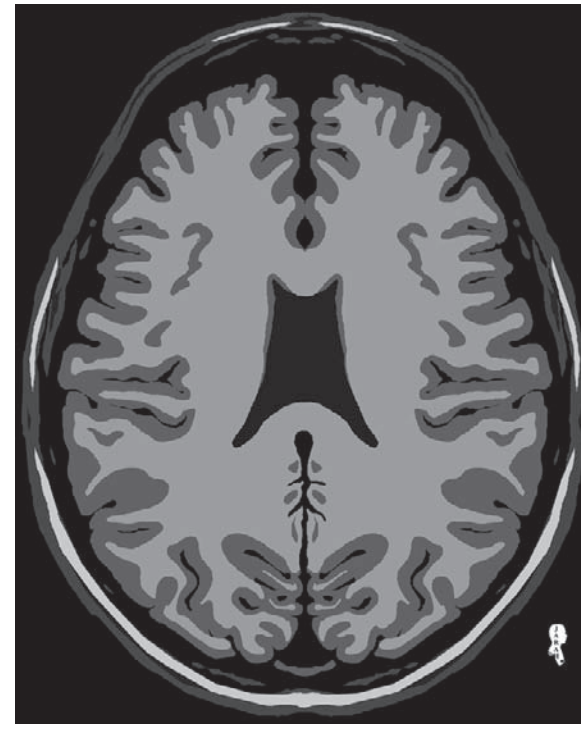

Fig. 1.6.1. Axial T1-weighted illustration shows the absent septum pellucidum with squared-off appearance of the lateral ventricles

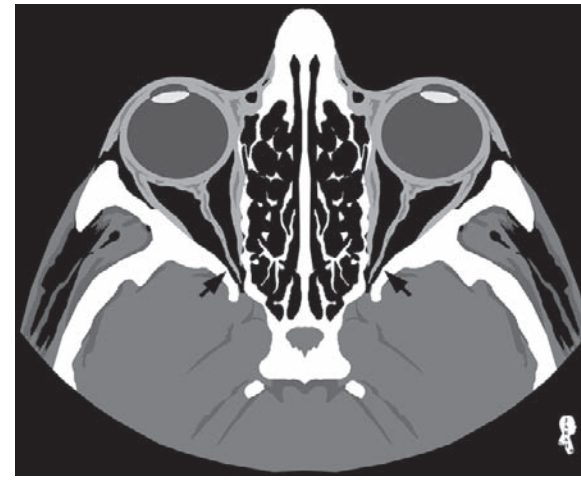

Fig. 1.6.2. Axial CT illustration of the orbit shows hypoplastic optic nerves with thinning of the nerves gradually toward the optic foramina (*arrows*)

For Further Reading

1. Riedl S et al. Refining clinical phenotypes in septo-optic dysplasia based on MRI findings. Eur J Pediatr 2008;167:1269–1276. doi 10.1007/s00431-007-0666-x
2. Nuri Sener R. Septo-optic dysplasia associated with total absence of the corpus callosum: MR and CT features. Eur Radiol 1993;3:551–553
3. Hayashi M et al. Septo-optic dysplasia with cerebellar hypoplasia in Cornelia de Lange syndrome. Acta Neuropathol 1996;92:625–630
4. Fitz CR. Holoprosencephaly and related entities. Neuroradiology 1983;25:225–238

1.7

Corpus Callosum Dysgenesis

The corpus callosum (CC) is composed of interhemispheric commissural nerve fibers, connecting the right cerebral hemisphere to the left hemisphere. Corpus callosum dysgenesis (CCD) is a term used to describe a common group of cerebral malformations that can occur as an isolated anomaly or as a part of several congenital cerebral malformations.

The CC is formed during the 10th–12th week of gestation, from anterior to posterior, and it reaches the adult form in the 20th week of gestation.
The following types of CCD are found:

Corpus Callosum Agenesis/Hypoplasia

Normally, CC formation starts from front to back; the rostrum is the last portion to form. In agenesis of the CC, there is complete absence of CC fibers between the cerebral hemispheres, while in hypoplasia of the CC, there is absence of the posterior segments only (rostum and splenium).

Signs on CT and MRI

- Absence of the CC genu or splenium on axial images.
- *Colpocephaly*: is enlargement of the occipital and the temporal horns of the lateral ventricles. It is a characteristic feature of the ventricles seen on axial images in cases of CC agenesis (Fig. 1.7.1).
- On coronal images, the shape of the lateral ventricles exhibits a characteristic "steer-horns appearance" due to the loss of the CC (Fig. 1.7.2).
- On sagittal images, there is complete absence of the body of the CC (Fig. 1.7.3).

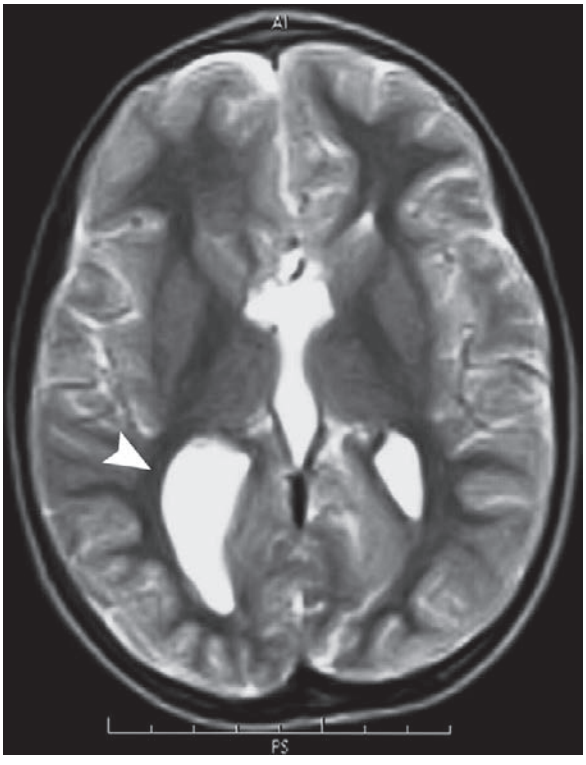

Fig. 1.7.1. Axial T2-weighted MR image shows enlargement of the occipital horn (colpocephaly) of the right lateral ventricle in a patient with CC agenesis (*arrowhead*)

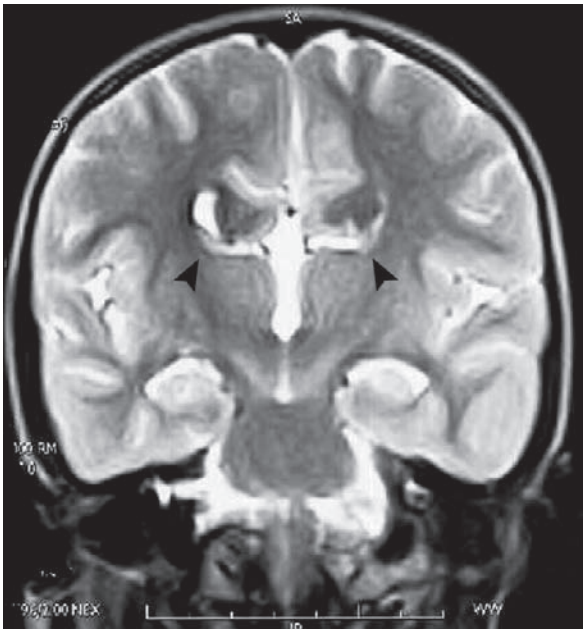

Fig. 1.7.2. Coronal T2-weighted MR image of the same patient shows "steer-horn appearance" of the lateral ventricles (*arrowheads*)

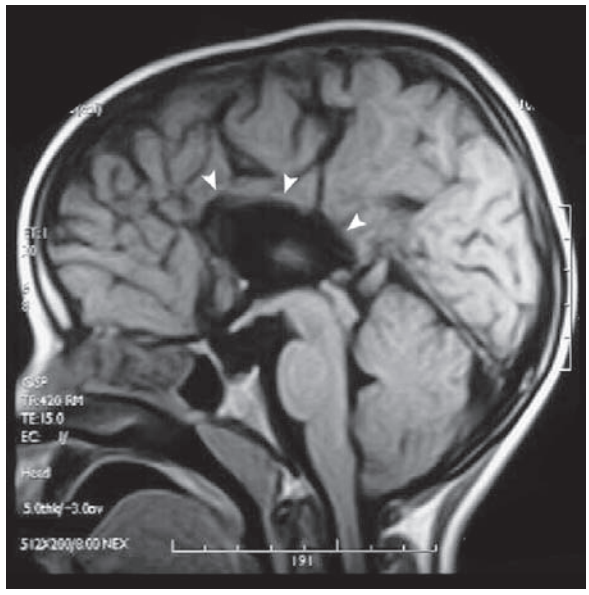

Fig. 1.7.3. Sagittal T1-weighted MR image of another patient with CC agenesis shows complete absence of the corpus callosum (*arrowheads*)

Acrocallosal (Schinzel) Syndrome

Acrocallosal syndrome is a rare, autosomal recessive disorder characterized by agenesis/hypoplasia of the CC, characteristic facial features, digital malformations (e.g., polydactyly), and severe mental and growth retardation.

Corpus Callosum Lipoma

In some cases of CC agenesis, the CC space is occupied by lipoma (fatty tissue seen along the interhemispheric fissure). CC lipoma most commonly occurs at the interhemispheric fissure (50%), the quadrigeminal cistern (25%), and the cerebellopontine angle (10%).

Pai Syndrome

Pai syndrome is a very rare syndromic frontonasal dysplasia characterized by upper lip median cleft, bifid nose, and CC lipoma.

Signs on CT and MRI

A bulky, fat-density mass located at the site of the CC with complete CC agenesis (Fig. 1.7.4).

Fig. 1.7.4. Axial CT section in a young patient shows CC lipoma. Note the hypodense, fat-dense mass located at the interhemispheric fissure (*white arrowhead*), with absence of the genu and splenium of the CC (*open arrowheads*)

For Further Reading

1. Sytritha L. Spectrum of corpus callosum agenesis. Pediatr Neurol 2005;32:94–101
2. Francesca M et al. Agenesis of the corpus callosum: Clinical and genetic study in 63 young patients. Pediatr Neurol 2006;34:186–193
3. Vaccarella F et al. Phenotypic variability of Pai syndrome: Report of a two patients and review of the literature. Int J Oral Maxillofac Surg 2008;37:1059–1064. doi:10.1016/j.ijom.2008.06.007
4. Shilpa BJ et al. Acrocallosal syndrome. J Indian Soc Pedod Prev Dent 2006;24:45–49

1.8

Gyral Abnormalities

Gyral abnormalities are a group of congenital brain malformations characterized by an abnormal shape and number of the brain cortical gyri. Gyral abnormalities include lissencephaly, pachygyria, polymicrogyria, and hemimegalencephaly. All gyral abnormalities are associated with epilepsy.

Lissencephaly (Agyria)

Lissencephaly is a rare congenital cortical malformation characterized by a smooth brain appearance due to no gyral formation.

The exact cause is unknown, although some cases are linked to in utero cytomegalovirus infection.

There are three types of lissencephaly:

Type 1 lissencephaly: characterized by microcephaly with dismorphic facial features. Lissencephaly type I is also called *Miller-Dieker syndrome*.

Type 2 lissencephaly: lacks the dismorphic facial features and exhibits macrocephaly, hydrocephalus, and retinal dysplasia. It is usually associated with posterior fossa anomalies such as Dandy-Walker malformation.

Type 3 lissencephaly: isolated areas of cerebral and cerebellar lissencephaly.

Signs on Brain CT and MRI

- Smooth brain with or without pachygyria. The brain shows a classic "hour-glass configuration" (Fig. 1.8.1).
- Bilateral vertical sylvian fissures (Fig. 1.8.1).
- Corpus callosum hypoplasia or subcortical heterotopias may be seen.

Pachygyria

Pachygyria is a congenital cortical malformation characterized by focal or diffuse few, broad, and flat gyri. The gyri exhibit abnormally thick four-layered cortices, and commonly exist with lissencephaly.

Signs on Brain CT and MRI

Broad and flat brain gyri with or without lissencephaly (Fig. 1.8.2).

Fig. 1.8.1. Axial brain CT shows lissencephaly. Note the lack of cortical gyri, few areas of pachygyria (*open arrowhead*), the hour-glass appearance of the brain, and the vertical sylvian fissures (*white arrowheads*)

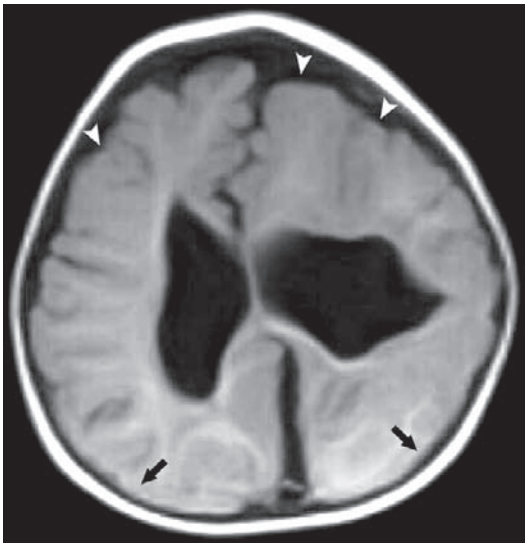

Fig. 1.8.2. Axial T1-weighted MR image of the brain shows pachygyria. There are multiple bilateral broad and flat gyri (*white arrowheads*). Note the coexistence of lissencephaly affecting the posterior occipital lobes (*black arrows*)

Zellweger (Cerebrohepatorenal) Syndrome

Zellweger syndrome is a rare autosomal recessive disorder associated with peroxisome deficiency and characterized by neural migration disorders (e.g., pachygyria), diffuse white matter demyelination, hypotonia, liver dysfunction with jaundice, renal cortical cysts, and craniofacial dysmorphism.

Polymicrogyria

Polymicrogyria is a congenital cortical malformation characterized by multiple small, irregular gyri in the inner and outer cortical surface with an irregular cortical–subcortical junction. It can be focal and unilateral, bilateral symmetric, or bilateral asymmetric.

Polymicrogyria commonly affects the frontal and parietal lobes; however, it can present in any part of the brain. Up to 80% of polymicrogyria cases involve at least one of the sylvian fissures.

Polymicrogyria can be associated with schizencephaly, subcotical heterotopias, and localized megalencephaly.

Congenital Bilateral Perisylvian Syndrome

Congenital bilateral perisylvian syndrome is a sporadic disease characterized by bilateral perisylvian polymicrogyria, pseudobulbar palsy, epilepsy, and cognitive impairment.

Signs on Brain MRI

Irregular cortical–subcortical junction with multiple festoon-like small gyri (Figs. 1.8.3 and 1.8.4).

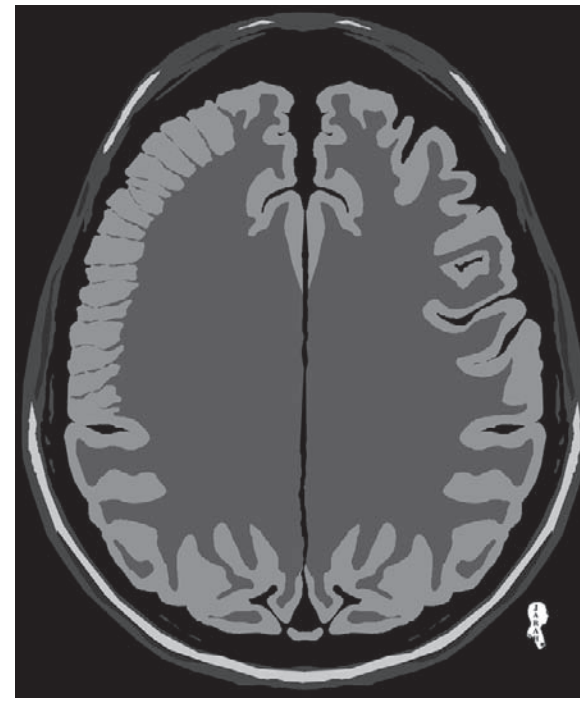

Fig. 1.8.3. Axial FLAIR MR illustration shows small, festoon-like, and crowded cortical gyri on the right hemisphere (polymicrogyri)

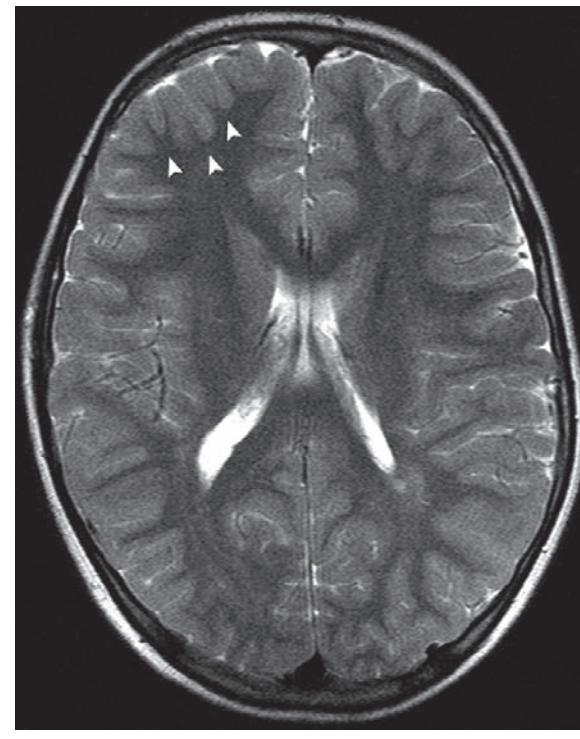

Fig. 1.8.4. Axial T2-weighted MR image shows localized polymicrogyria affecting the right frontal lobe in a patient with epilepsy disorder (*arrowheads*)

Hemimegalencephaly (Unilateral Megalencephaly)

Hemimegalencephaly is a congenital cortical malformation characterized by enlargement and thickening of one cerebral hemisphere due to focal or diffuse hamartomatous overgrowth of the affected hemisphere. Hamartoma is a lesion composed of normal cells in an abnormal arrangement.

Up to 90% of hemimegalencephaly cases occur in the right cerebral hemisphere. It can be seen with diseases like neurofibromatosis type I and tuberous sclerosis.

Signs on Brain CT and MRI

- Enlarged unilateral hemisphere, usually the right hemisphere (Fig. 1.8.5).
- Enlargement of the anterior horn of the lateral ventricle of the affected hemisphere (Fig. 1.8.5).

Fig. 1.8.5. Axial T2-weighted MR illustration shows hemimegalencephaly. Note the unilateral overgrowth of the right cerebral hemisphere (*white arrowhead*), with enlargement of the frontal and the occipital horns of the right lateral ventricle (*black arrowheads*)

For Further Reading

1. Malcolm Stewart RM et al. Lissencephaly and pachygyria. An architectonic and topographical analysis. Acta neuropath (Berl) 1975;31:1–12
2. Watanabe M et al. Focal pachygyria with unusual vascular anomaly. Neuroradiology 1990;32:237–240
3. Raybaud C. Destructive lesions of the brain. Neuroradiology 1983;25:265–291
4. Barkovich AJ et al. Malformations of cortical development. Neuroimag Clin N Am 2004;14:401–423
5. Deblaere K et al. Structural magnetic resonance imaging in epilepsy. Eur Radiol 2008;18:119–129
6. Hayashi N et al. Polymicrogyria without porencephaly/schizencephaly. MRI analysis of the spectrum and the prevalence of macroscopic findings in the clinical population. Neuroradiology 2002;44:647–655
7. Spalice A et al. Bilateral perysilvian polymicrogyria in Chiari I malformation. Child Nerv Syst 2006;22:1635–1637.
8. James A et al. Malformations of cortical development. Neuroimag Clin N Am 2004;14:401–423
9. King A et al. A case of Miller-Dieker syndrome in a family with neurofibromatosis type I. Acta Neuropathol 2000;99:425–427

1.9

Gray Matter Heterotopias

Gray matter heterotopia is a group of diseases characterized by the presence of ectopic gray matter in an abnormal location within the white matter.

In the normal embryonic brain, the gray matter neurons are formed at the subependymal layer of the ventricles and then start to migrate to their normal position at the cortex. Heterotopia occurs when the gray matter neurons fail to migrate fully into their cortical spaces, remaining embedded within the white matter.

All types of heterotopias are associated with seizures.

The differential diagnoses of heterotopia include metastasis and tuberus sclerosis. The main difference between ectopic gray matter and tuberus sclerosis or subependymal metastasis is the contrast enhancement. Heterotopias do not enhance after contrast material injection because they are composed of normal neurons, while tuberus sclerosis lesions and metastasis will enhance after injection of contrast material.

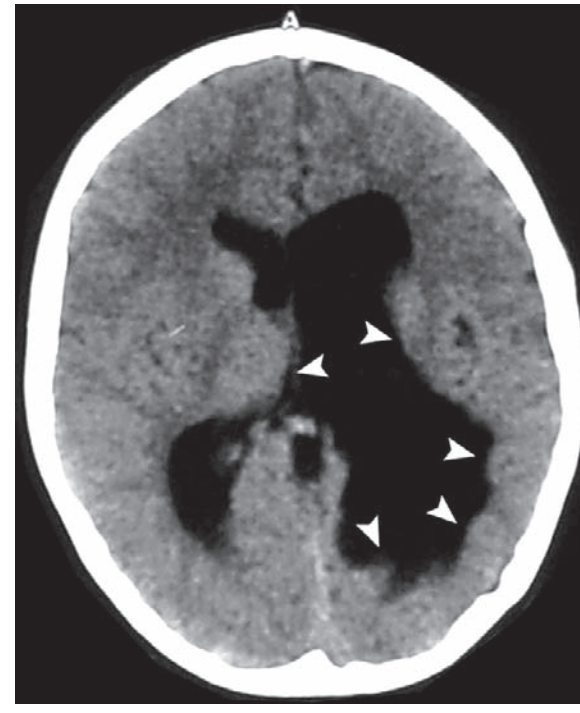

Fig. 1.9.1. Axial noncontrast-enhanced CT image of the brain shows multiple nodular masses along the subependymal layer of both lateral ventricles, typical of gray matter heterotopia (*arrowheads*)

Signs on CT and MRI

- Focal nodular or broad masses are seen in the subependymal, periventricular, or subcortical regions with no perifocal edema or contrast enhancement (Figs. 1.9.1 and 1.9.2).
- The mass exhibits the same density and signal intensity of gray matter on CT and MRI in all pulse sequences.

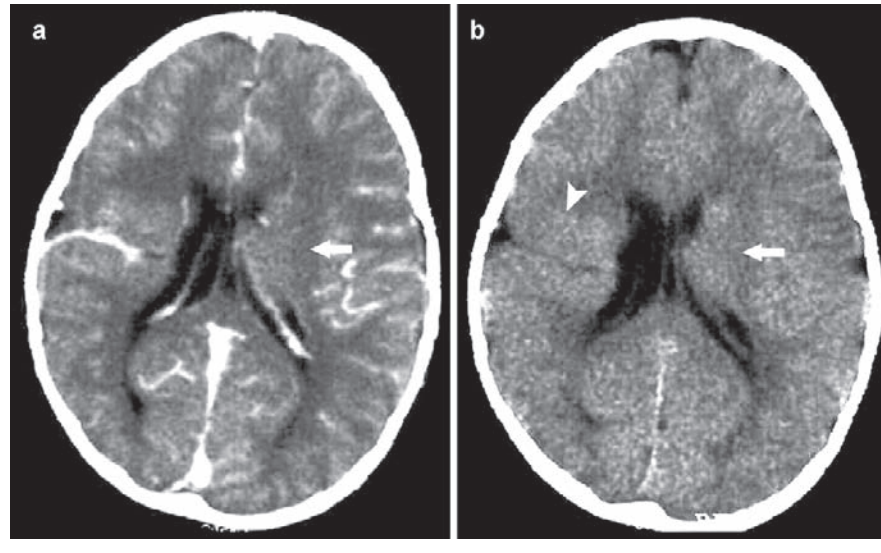

Fig. 1.9.2. Pre- (**b**) and postcontrast (**a**) axial CT images of the brain show subependymal heterotopia (*arrow*) with closed-lip schizencephaly (*arrowhead*). Note the lack of enhancement of the heterotopia in **a**

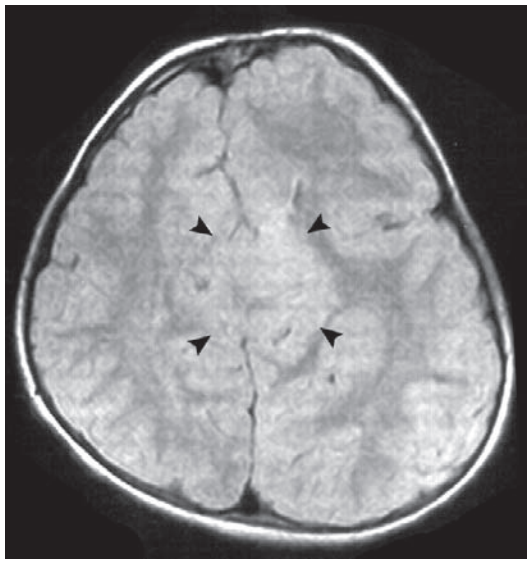

Fig. 1.9.3. Axial T1-weighted MR image shows a mass of multiple subependymal heterotopia (*arrowheads*)

There are three forms of heterotopia:

- **Subependymal heterotopia:** is the presence of a smooth, oval, gray matter mass embedded in and indenting the ventricular wall (Figs. 1.9.1 and 1.9.3).
- **Focal heterotopia:** is the presence of gray matter embedded within white matter.
- **Diffuse band heterotopia (double cortex syndrome):** is a very rare condition in which all the neurons during migration stop halfway within the white matter, causing the brain to have a double cortex appearance. Signs on CT and MRI include bilateral symmetrical bands of gray matter between the cortex and the ventricular walls, separated from both by layers of white matter (Fig. 1.9.4). Band heterotopia syndrome is considered a diffuse migration disorder, and patients with this syndrome are usually severely retarded.

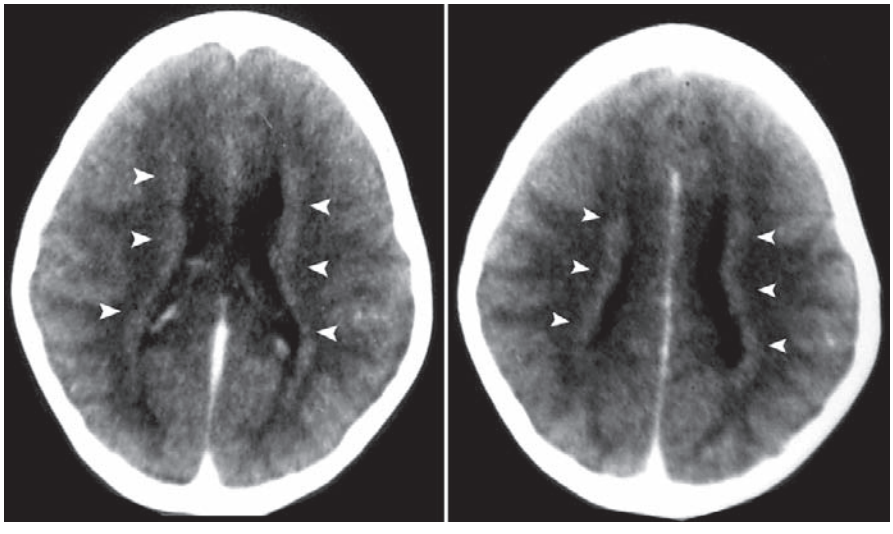

Fig. 1.9.4. Axial noncontrast-enhanced CT images of the brain show bilateral, symmetrical gray matter density band along the lateral ventricle margins (*arrowheads*) with no contrast enhancement after contrast material injection (not shown). Diagnosis is band heterotopia syndrome

For Further Reading

1. Barkovich AJ et al. Malformations of cortical development. Neuroimag Clin N Am 2004;14:401–423
2. Deblaere K et al. Structural magnetic resonance imaging in epilepsy. Eur Radiol 2008;18:119–129
3. Wetyburger CL et al. Gray matter heterotopia and acute necrotizing encephalopathy in trichothiodystrophy. Pediatr Neurol 1998;19:392–394
4. Soto Ares G et al. Unusual MRI findings in grey matter heterotopia. Neuroradiology 1998;40:81–87
5. Hashimoto R et al. The "double cortex" syndrome on MRI. Brain Dev 1993;15:57–60

1.10

Arnold-Chiari Malformations

Arnold-Chiari malformation (ACM) is a congenital group of diseases characterized by herniation of the cerebellum through the foramen magnum into the spinal canal. The herniated tissue blocks the circulation of cerebrospinal fluid (CSF), resulting in hydrocephalus or fluid cavities within the spinal cord (syringomyelia). There are four types of Chiari malformations:

Arnold-Chiari Malformation Type I

The main anomaly in type I is an abnormal defect in the base of the skull bones. The brain and its contents are normal, while the cranium is deficient at its base allowing herniation of the cerebellar tonsils into the superior part of the spinal canal.

Patients with ACM type I present in adulthood with headache, vertigo, and progressive cerebellar signs. The headache is characteristically associated with neck pain, and exacerbated by coughing, straining, or laughing.

Signs on MRI

- The cisterna magna is absent, and the cerebellar tonsils protrude more than 6 mm below the foramen magnum into the level of the first cervical (C1) vertebra or the upper border of the second cervical (C2) vertebra (Fig. 1.10.1).
- The fourth ventricle is elongated in 25% of cases.
- Associated malformations may include syringomyelia (Fig. 1.10.2), hydrocephalus (25%), and Klippel-Feil anomaly.

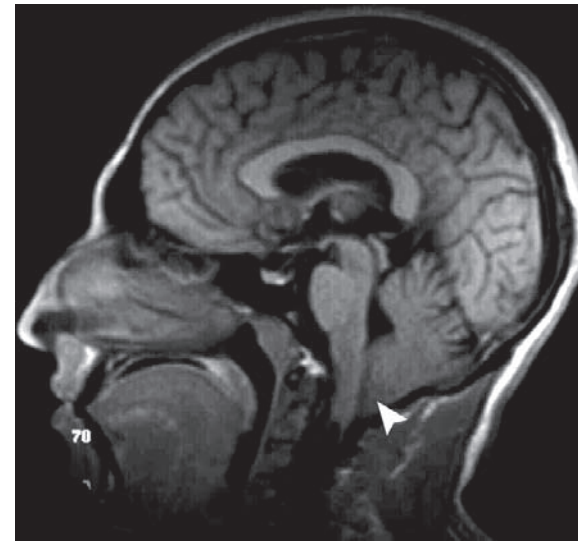

Fig. 1.10.1. Sagittal T1-weighted MR image of a patient with ACM type I shows protrusion of the cerebellar tonsils below the level of the foramen magnum into the superior portion of the spinal canal (*arrowhead*)

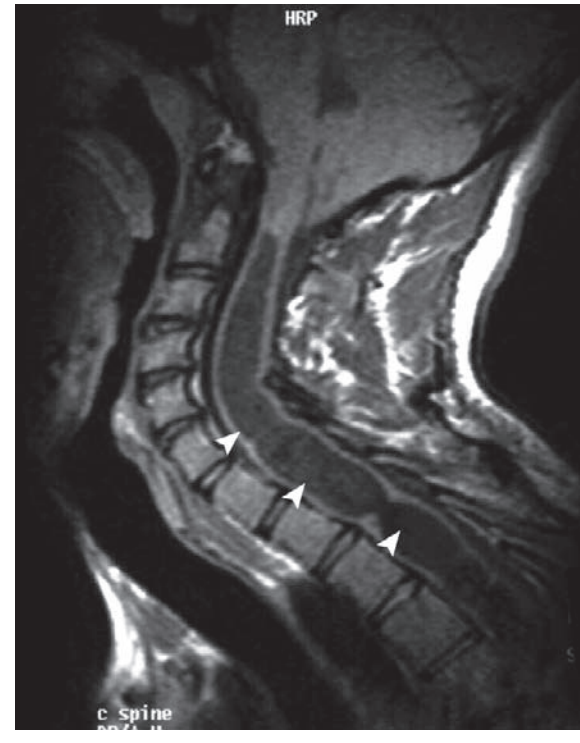

Fig. 1.10.2. Sagittal T1-weighted MR image of the same patient with ACM type I shows cystic dilatation of the spinal canal (syringomyelia) (*arrowheads*)

Arnold-Chiari Malformation Type II

The main anomaly in type II occurs in the brain itself, while the skull base bones are normal. In type II malformation, there is herniation of the medulla and the posterior cerebellar vermis into the spinal canal, which blocks the CSF circulation resulting in hydrocephalus. ACM type II is almost always associated with myelomenengiocele.

ACM type II is a complex anomaly that has three levels of changes seen on brain MRI:

- At the level of the posterior fossa
  - Small posterior fossa.
  - Concave clivus.
  - Thinning and elongation of the fourth ventricle.
- At the level of the upper cervical canal
  - The cerebellum and medulla oblongata are seen located behind the spinal cord (Fig. 1.10.3). The medulla oblongata is in vertical alignment with the spinal cord in 30% of cases, and kinked behind the spinal cord making a spur in 70% of cases.
  - Spinal dysraphism (menengiocele and syringiomylia).
- At the level of the supratentorial brain
  - Supratentorial hydrocephalus.
  - Large third ventricle with the shape of an "inverted 3 figure," where the two indentations that form the number are the caudate and thalamic nuclei indenting the dilated anterior horns of the lateral ventricles.
  - Peaked tectum (Fig. 1.10.4).
  - The confluence of dural venous sinuses (torcular herophili) is in an abnormally low position, with the straight sinus sometimes descending steeply from the vein of Galen (Fig. 1.10.5).

Q: How can you differentiate between Arnold-Chiari II anomaly affecting the third ventricle from cerebral aqueduct obstructive hydrocephalus?

Brain changes and anomalies are much more common in ACM type II malformation. Cerebral aqueduct obstruction makes the third ventricle look like a big sphere, while the ACM type II malformation gives the third ventricle an "inverted 3" figure.

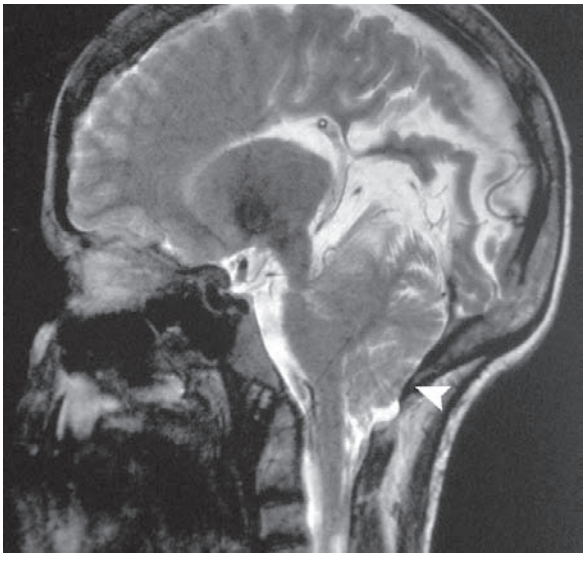

Fig. 1.10.3. Sagittal T2-weighted MR image of a patient with ACM type II shows protrusion of the cerebellum into the spinal canal (*arrowhead*)

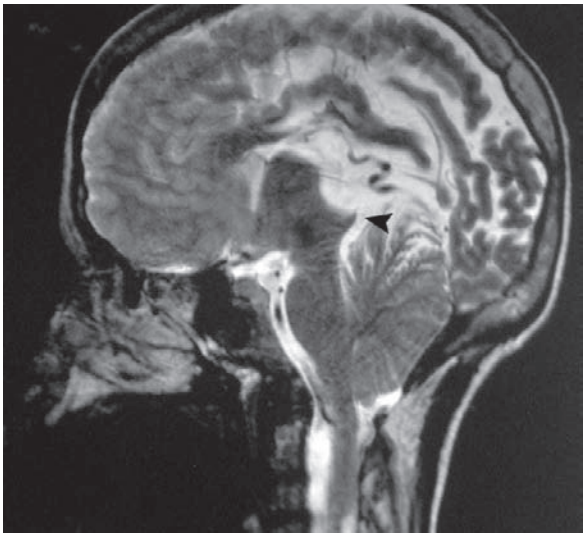

Fig. 1.10.4. Sagittal T2-weighted MR image of the patient in another section shows peaked tectum (*arrowhead*)

Fig. 1.10.5. MR venography illustration shows abnormally low-lying torcular herophili (*arrowhead*) with steeply descending straight sinus (*arrows*)

Arnold-Chiari Malformation Type III

ACM type III malformation is a very rare anomaly characterized by cervico-occipital encephalocele containing the cerebellum, occipital lobe, midbrain, and the fourth ventricle (Fig. 1.2.2).

The herniated structures are usually abnormally formed.

Patients with ACM type III frequently suffer from respiratory insufficiency and cranial nerve dysfunction.

Arnold-Chiari Malformation Type IV

ACM type IV malformation is also a very rare anomaly characterized by severe cerebellar hypoplasia, small brain stem, and large, CSF-filled posterior fossa. It can be misdiagnosed as Dandy-Walker malformation.

For Further Reading

1. Niesen CE. Malformations of the posterior fossa: Current perspectives. Semin Pediatr Neurol 2002;9(4):320–334
2. Ziadeh MJ et al. Arnold-Chiari malformation with syrinx presenting as carpal tunnel syndrome: A case report. Arch Phys Med Rehabil 2004;85:158–161
3. Archer CR et al. The Arnold-Chiari malformation presenting in adult life: a report of thirteen cases and a review of the literature. J Chron Dis 1977;30:369–382
4. Cure JK et al. Congenital and acquired abnormalities of the dural venous sinuses. Semin Ultrasound CT MRI 1994;15(6): 520–539

1.11

Dandy-Walker Malformation

Dandy-Walker malformation (DWM) is a rare congenital brain anomaly affecting the posterior fossa, characterized classically by the triad of cystic dilatation of the fourth ventricle, cerebellar vermis hypoplasia, and hydrocephalus. DWM is commonly associated with an enlarged posterior fossa, high confluence of the dural venous sinuses (torcular herophili), and higher displacement of the cerebellar hemispheres.

DWM has an incidence of 1 in every 35,000 live births, and it is responsible for 4% of childhood hydrocephalus. The hydrocephalus is not present at birth, and develops by 3 months of age in up to 75% of cases.

DWM is associated with a high incidence of motor dysfunction and mental retardation (40%). Most of the symptoms and signs of DWM are related to the hydrocephalus complications.

Numerous anomalies can be associated with DWM such as agenesis of the corpus callosum, gyral malformation, gyral heterotopias, occipital meningoceles, and cardiac anomalies. DWM can also occur as a part of other syndromes (e.g., PHACE syndrome).

Signs on CT and MRI

- Hypoplasia/aplasia of the cerebellar vermis with marked dilatation of the fourth ventricle causing a "keyhole configuration" (Figs. 1.11.1 and 1.11. 2).
- Partial agenesis or hypoplasia of the cerebellar hemispheres (Fig. 1.11. 3).
- Obstructive hydrocephalus in 80% of cases.
- The confluence of dural venous sinuses (torcular herophili) is elevated, and the straight sinus is horizontally oriented as it approaches the confluence of the sinuses (Fig. 1.11.4).

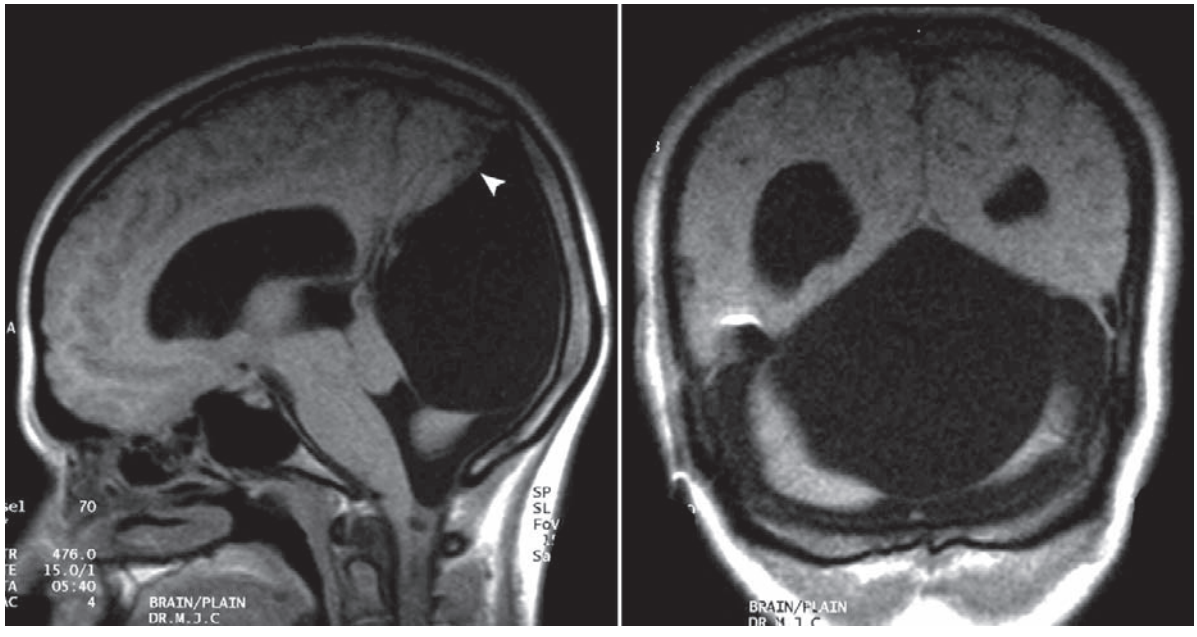

Fig. 1.11.1. Sagittal and coronal T1-weighted MR images of DWM show large posterior fossa cyst communicating with the fourth ventricle. The cerebellar hemispheres are hypoplastic and lifted upward (*arrowhead*). Note also upward displacement of the tentroium

Fig. 1.11.2. Axial CT image of another case of DWM with dolichocephaly. The fourth ventricle communicates with a posterior fossa cyst making a "keyhole configuration"

Fig. 1.11.4. MR venography illustration shows high torcular herophili (*arrowhead*) with ascending straight sinus that becomes horizontal as it joins the torcular herophili (*arrow*)

Fig. 1.11.3. Axial CT image of another case of DWM shows posterior fossa cyst that communicates with a dilated fourth ventricle (*open arrow*) via a hypoplastic/aplastic cerebellar vermis (*white arrowhead*). Note the small cerebellar right hemisphere (*white arrow*)

Dandy-Walker Variants and Mimickers

A Dandy-Walker variant (DWV) is a term reserved for posterior fossa malformations that do not fulfill the classical description of DWM. DWVs include mega cisterna magna and retrocerebellar arachnoid cyst.

- **Mega cisterna magna:** It is a big cisterna magna located behind the cerebellum. The cerebellum has a normal configuration and can be small (Fig. 1.11.5). A characteristic criterion of the mega cisterna magna is an absent hydrocephalus, which is part of the DWM triad.

Fig. 1.11.5. Axial CT image of a patient with mega cisterna magna. Note the intact cerebellar vermis (*white arrowhead*) and the normally configured small cerebellum. The fourth ventricle is not dilated (*open arrowhead*), and there is absence of hydrocephalus in the temporal horns (*white arrow*)

- **Retrocerebellar arachnoid cyst:** It is a cyst that is located in the subarachnoid space and does not communicate with the fourth ventricle. The cerebellum and its vermis are normal. It causes hydrocephalus by pressing over the fourth ventricle.

For Further Reading

1. Adamsbaum C et al. MRI of the fetal posterior fossa. Pediatr Radiol 2005;35:124–140
2. Niesen CE. Malformations of the posterior fossa: Current perspectives. Semin Pediatr Neurol 2002;9(4):320–334
3. Klein O et al. Dandy-Walker malformation: prenatal diagnosis and prognosis. Childs Nerv Syst 2003;19:484–489
4. Raj Kumar et al. Dandy-Walker syndrome: Different modalities of treatment and outcome in 42 cases. Childs Nerv Syst 2001;17:348–352
5. Serlo W et al. Ante- and postnatal evaluation of the Dandy-Walker syndrome. Childs Nerv Syst 1985;1:148–151
6. Joy HM et al. Trans-sphenoidal encephalocele in association with Dandy-Walker complex and cardiovascular anomalies. Neuroradiology 2001;43:45–48
7. Cure JK et al. Congenital and acquired abnormalities of the dural venous sinuses. Semin Ultrasound CT MRI 1994; 15(6):520–539

1.12

Cavum Septum Pellucidum and Cavum Vergae

Cavum septum pellucidum and cavum vergae are normal variants that result from separation of the two leaflets of the septum pellucidum.

Cavum septum pellucidum (Fig. 1.12.1) is an anterior separation of the two leaflets of the septum pellucidum with filling of the resulting space in between by cerebrospinal fluid. It is found at birth in more than 80% of individuals, and is obliterated by the age of 3–6 months. The normal septum pellucidum is 1–3 mm thick, and supplied by medial lenticulostriate arteries arising from the anterior cerebral arteries.

Cavum vergae (Figs. 1.12.2 and 1.12.3) is the posterior continuation of the cavum septum pellucidum beneath the splenium of the corpus callosum. Like cavum septum pellucidum, it is found in the brain of all neonates but rapidly closes with age.

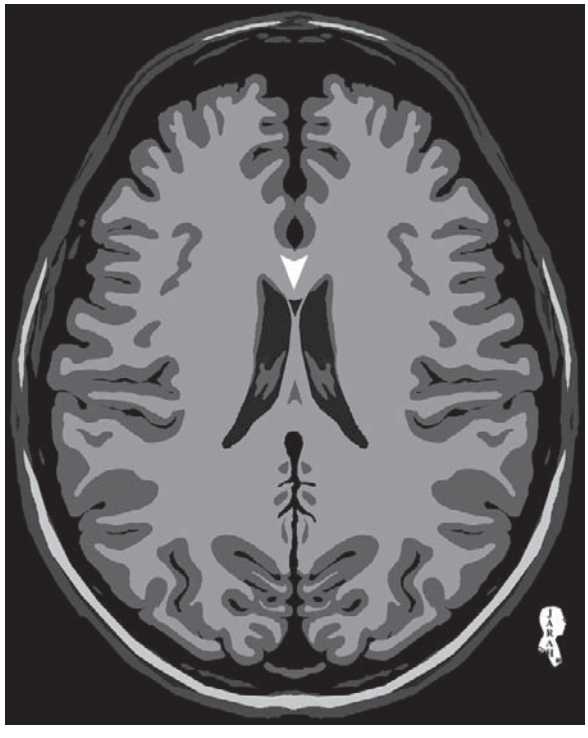

Fig. 1.12.1. Axial T1-weighted MR illustration shows small anterior cavum septum pellucidum (*arrowhead*)

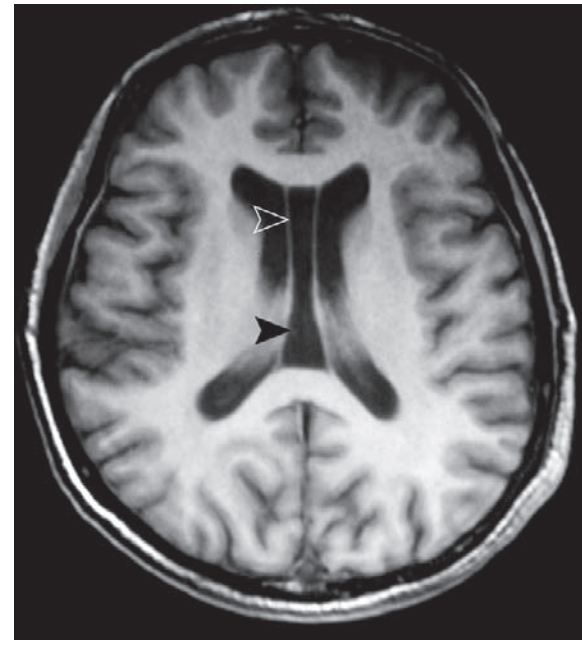

Fig. 1.12.2. Axial T1-weighted MR image shows anterior cavum septum pellucidum (*open arrowhead*) with its posterior continuation cavum vergae (*black arrowhead*)

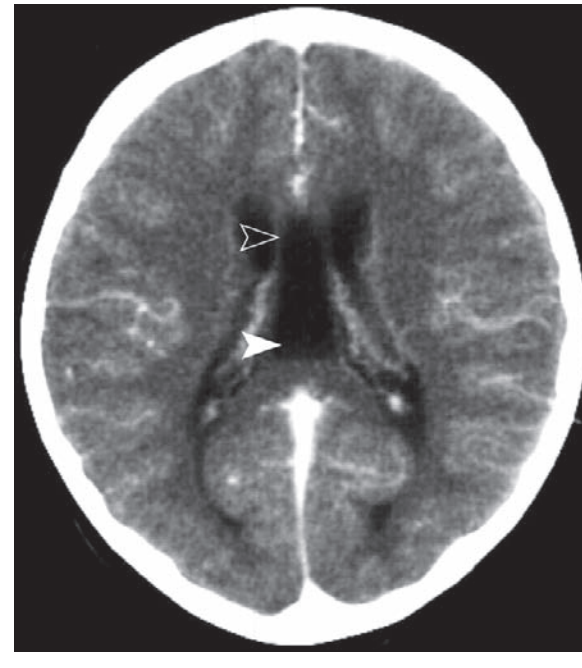

Fig. 1.12.3. Axial CT postcontrast image in another patient shows anterior cavum septum pellucidum (*open arrowhead*) with its posterior continuation cavum vergae (*white arrowhead*)

For Further Reading

1. Scoffings DJ et al. Congenital and acquired lesions of the septum pellucidum. Clin Radiol 2008;63:210–219
2. Sayama CM et al. Spontaneous regression of a cystic cavum septum pellucidum. Acta Neurochir (Wien) 2006;148: 1209–1211
3. Born CM et al. The septum pellucidum and its variants. An MRI study. Eur Arch Psychiatry Clin Neurosci 2004;254: 295–302

1.13

Fahr Disease

Fahr disease is an idiopathic nonatherosclerotic disease characterized by symmetric calcification of the basal ganglia, thalami, and the cerebellar dentate nuclei. Fahr disease has both an autosomal dominant and a recessive mode of inheritance. Sporadic cases have also been reported. The disease manifests itself in the form of impairment of the early cerebral cognitive functions and dementia. It is known to be associated with cases of pseudohyperparathroidism.

Signs on CT

- The CT scan shows diffuse bilateral symmetrical cerebral calcification, with calcification of the basal ganglia, thalami, pons, and the cerebellar dentate nuclei (Figure 1.13.1).
- Mild cerebral atrophy can be found.

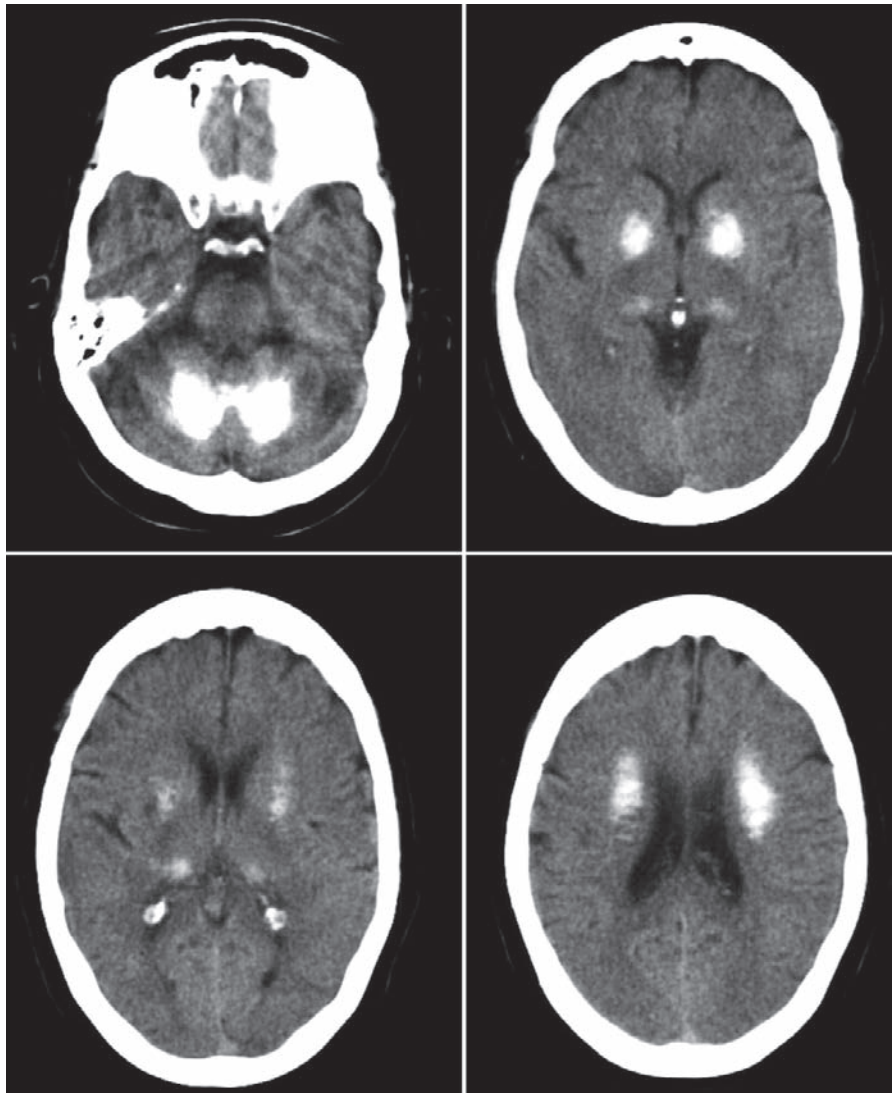

Fig. 1.13.1. Multiple sequential axial nonenhanced CT images show bilateral symmetrical calcifications of the thalami, basal ganglia, cerebellar, and dentate nuclei (Fahr disease)

Signs on MRI

Bilateral, almost symmetrical hypointense lesions are seen on both T1- and T2-weighted images in the basal ganglia, thalami, dentate nuclei, and the cerebral hemispheres representing calcifications.

For Further Reading

1. Chalkias SM et al. Fahr disease: Significance and predictive value of CT and MR findings. Eur Radiol 1992;2:570–575
2. Modrego PJ et al. Fahr's syndrome presenting with pure and progressive presenile dementia. Neurol Sci 2005;26: 367–369
3. Eleopra R et al. Unusual case of Fahr syndrome with motoneuron disease. Ital J Neurol Sci 1991;12:597–600

1.14

Menkes and Wilson Diseases

Menkes and Wilson diseases are diseases of abnormal copper metabolism within the body. Although both diseases occur due to abnormal copper metabolism, they have different clinical presentations.

Menkes Disease (Kinky Hair Disease)

Menkes disease is a progressive, neurodegenerative, X-linked disease characterized by defective copper metabolism that results from poor or no absorption of copper from the intestine, with maldistribution of the copper within the body organs. This maldistribution causes defects in the functions of the numerous copper-containing enzymes in different organs. The disease has an incidence of 2 per 100,000 live male births.

The abnormalities and clinical picture of Menkes disease can be linked to the low activities of the various copper-containing enzymes. Loss of the copper-containing enzymes results in:

- Defective elastin and collagen cross-linking, causing abnormal, elongated, and tortuous vessels with bleeding tendency.
- Abnormal hair with abnormal pigmentation (e.g., pili torti). Pili torti is a term used to describe an abnormal hair shaft, where the hair shaft is flattened at certain intervals and twisted 180° along its axis, causing its fragility. Pili torti is also called "corkscrew hair."
- Impaired brain myelination.
- Skeletal abnormalities including osteoporosis, metaphyseal spurs, and posterior scalloping of the vertebral bodies.

Neonates with Menkes disease are usually normal at birth, and the disease manifestations start to appear during the first 2–3 months of life. Hypotonia, seizures, hypothermia, failure to thrive, poor feeding, and multiple bone fractures are common symptoms. The disease does not affect the liver. In contrast, the main target of Wilson disease is the liver.

The face has a characteristic cherubic (cherubism) appearance with a depressed nasal bridge.

Hydronephorsis, hydroureter, and pale optic discs are other manifestations. Recurrent infections, sepsis, and meningitis are common due to impaired T-cell function.

Diagnosis is confirmed by detecting low serum copper and ceruloplasmin levels. The diagnosis should be made after 2 months of age, because in normal-term newborns the serum copper is low. The newborn serum level does not reach the normal adult level until 1–2 months of life. An abnormal low serum level beyond 2 months of age is significant. Moreover, the serum copper level tends to be higher during childhood than during adult life.

Signs on Brain MRI

- Brain atrophy, abnormal signal on T2-weighted images representing dysmyelination, and unilateral or bilateral subdural hemorrhage.
- On MR angiography, tortuous intracranial vessels can be seen.

Wilson Disease (Hepatolenticular Degeneration)

Wilson disease is a progressive, autosomal recessive disorder characterized by deposition of copper within the liver due to a deficiency in its carrier ceruloplasmin. Copper accumulates in the hepatocytes due to their inability to secrete the copper–ceruloplasmin complex into plasma and free copper into bile.

The disease affects mainly the liver and the basal ganglia, and manifests itself between 10 and 20 years of age.

Clinical manifestations of the disease include liver cirrhosis, seizures, ataxia, and psychogenic disturbance. The early signs are related to difficulties in swallowing and indistinct speech.

Deposition of the copper within the cornea results in a pathognomonic yellowish corneal pigmented ring (Kayser-Fleischer ring).

Signs on Brain and Liver CT

- The CT scan of the brain is often normal. Hypodensities within the caudate nucleus may be seen.
- On liver CT scans, liver contour irregularity with multiple hyperdense nodules seen on noncontrast-enhanced scans are common features (Fig. 1.14.1).

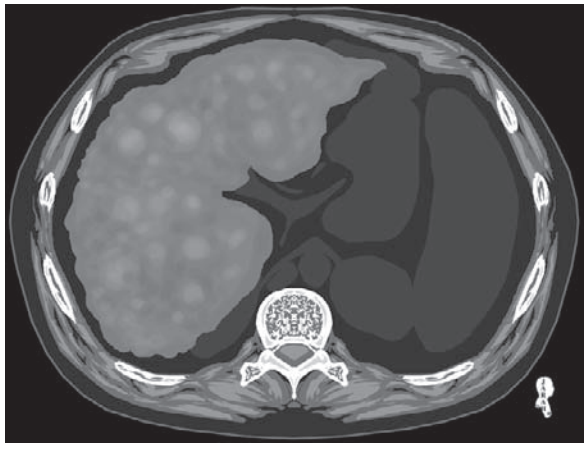

Fig. 1.14.1. Axial abdominal noncontrast-enhanced CT illustration shows liver contour irregularity, with multiple hyperdense nodules. These are common radiological features seen in Wilson disease

Signs on Brain MRI

- Bilateral high-signal lesions on T2-weighted images in the basal ganglia (most common), thalamus, dentate nucleus, and subcortical white matter (Fig. 1.14.2).
- Other causes of bilateral basal ganglia hyperintense signals on T2-weighted images include: chronic liver failure for any cause of hepatic encephalopathy and calcium metabolism disorders (hyperparathyroidism and hypoparathyroidism).

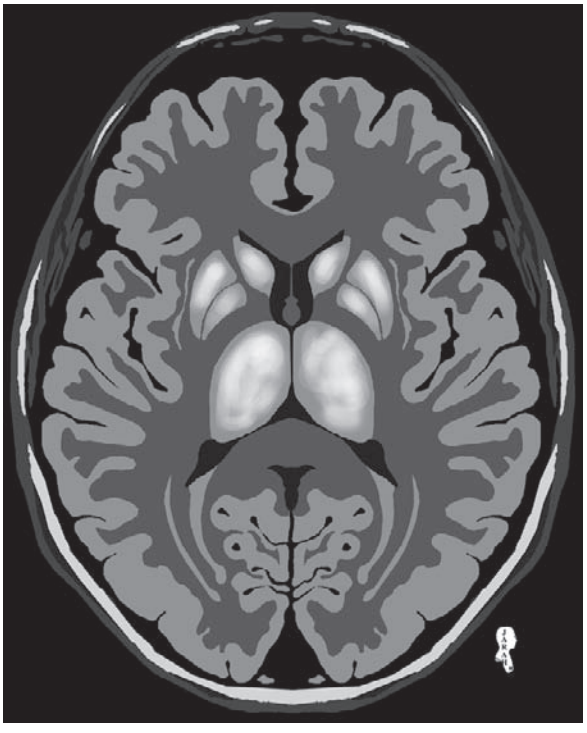

Fig. 1.14.2. Axial FLAIR MR illustration shows bilateral high-signal-intensity lesions affecting both thalami and the caudate and lentiform nuclei

For Further Reading

1. Menkes JH. Menkes disease and Wilson disease: Two sides of the same copper coin. Part I: Menkes disease. Eur J Paediatr Neurol 1999;3:147–158
2. Menkes JH. Menkes disease and Wilson disease: Two sides of the same copper coin. Part II: Wilson disease. Eur J Paediatr Neurol 1999;3:245–253
3. Akhan O et al. Imaging findings of liver involvement of Wilson's disease. Eur J Radiol 2007. doi:10.1016/j.ejrad.2007.09.029
4. Yamada H et al. Menke's kinky hair disease: Report of a case and distribution of sulfhydrl residues and disulfide bonds in kinky hair. J Eur Acad Dermatol Venerol 1996;6:240–245
5. Kodama H et al. Biochemical indicator for evaluation of connective tissue abnormalities in Menkes' disease. J pediatr 2003;142:726–728
6. Jayawnt S et al. Menkes kinky hair disease: An unusual case. Eur J Paediatr Neurol 2000;4:131–134
7. Pinto F et al. Radiological findings in a case of Menkes' disease. Child's Nerv Syst 1995;11:112–114
8. Kim OH et al. Intracranial and extracranial MR angiography in Menkes disease. Pediatr Radiol 1997;27:782–784
9. Bekiesinska-Figatowska M et al. Menke's disease with Dandy-Walker variant: Case report. Neuroradiology 2001; 43:948–950

1.15

Cerebellar Anomalies

Anomalies of the cerebellum are usually associated with other lesions of the posterior fossa. Cerebellar diseases are usually associated with ataxias and motor coordination disorders. Rhombencephalosynapsis and Joubert syndrome (JS) are two congenital disorders affecting mainly the cerebellum.

Rhombencephalosynapsis

Rhombencephalosynapsis is a congenital disease characterized by agenesis or hypoplasia of the cerebellar vermis with fusion of the cerebellar hemispheres, cerebellar peduncles, and dentate nuclei. The disease is thought to be caused by insult to the hindbrain (rhombencephalon) between the fourth and sixth weeks of gestation.

Thalamic fusion, third ventricle deficiency, gray matter heterotopia, hypertelorism, and partial or total absence of the septum pellucidum are common brain malformations associated with rhombencephalosynapsis.

Signs on MRI

- Absence or severely hypoplastic cerebellar vermis, with fusion of both cerebellar hemispheres.
- The fourth ventricle has a characteristic "keyhole appearance" due to the fusion of the cerebellar peduncles and inferior colliculi (Fig. 1.15.1).

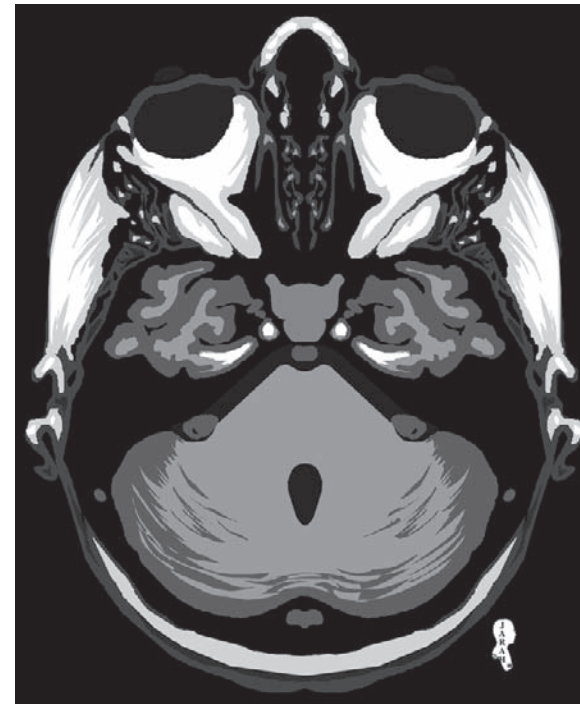

Fig. 1.15.1. Axial T1-weighted MR illustration shows rhombencephalosynapsis. Note the absence of the cerebellar vermis with fusion of both cerebellar hemispheres, with the "keyhole-shaped" fourth ventricle

Joubert Syndrome

Joubert syndrome (JS) is a neuronal migration disorder of the cerebellum characterized by hypoplasia or agenesis of the superior cerebellar vermis, enlargement of the fourth ventricle, and cystic lesions of the viscera.

JS is inherited as an autosomal recessive disorder. JS is essentially a clinical diagnosis. The infant with JS typically presents with episodes of rapid breathing

(hyperpnea) followed by episodes of absence of breathing (apnea), and jerky eye movements. The disease can be associated with optic disc colobomas, multicystic kidney disease, polydactyly, agenesis of the corpus callosum, mental retardation, and cerebellar ataxia.

The neonatal breathing abnormalities are considered the hallmark of this disease, and they occur in 44% of cases. The respiratory abnormalities are normally seen during sleep, particularly during non-REM (rapid eye movement) sleep. These respiratory abnormalities are thought to be caused by dysfunction of the respiratory centers in the medulla oblongata. JS is the only posterior fossa anomaly associated with respiratory abnormalities.

Signs on MRI

- Enlargement of the fourth ventricle.
- Horizontally oriented superior cerebellar peduncles seen on axial images, giving a diagnostic "molar tooth sign" (Fig. 1.15.2).
- Mega cisterna magna or Dandy-Walker malformation may be seen.

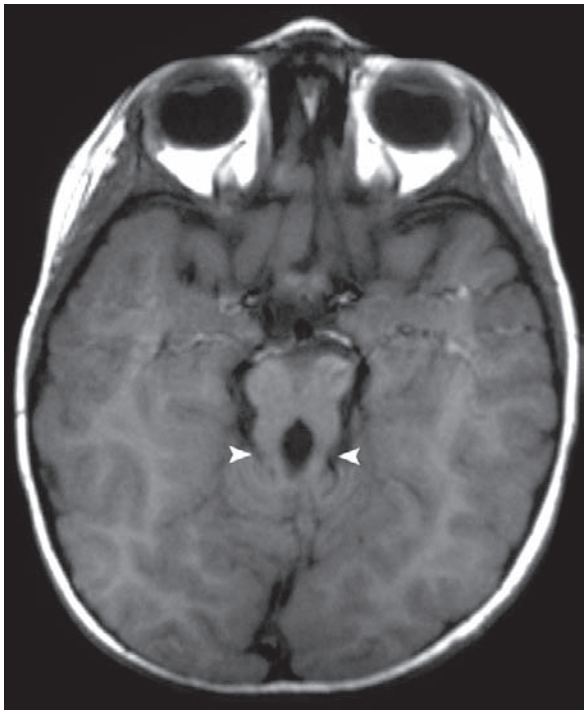

Fig. 1.15.2. Axial T1-weighted MR image shows elongated superior cerebellar peduncles with absence of the superior vermis causing the midbrain to have a "molar tooth sign" (*arrowheads*)

For Further Reading

1. Montull C et al. Neuroradiological and clinical findings in rhombencephalosynapsis. Neuroradiology 2000;42:272–274
2. Demaerel P et al. Uncommon posterior cranial fossa anomalies: MRI with clinical correlation. Neuroradiology 1995;37:72–76
3. Cakirer S. Joubert syndrome vs rhombencephalosynapsis: Differentiation on the basis of MRI findings. Clin Radiol Extra 2003;58:13–17
4. Kendall B et al. Joubert syndrome: A clinico-radiological study. Neuroradiology 1990;31:502–506
5. Silverstein DM et al. Joubert syndrome associated with multicystic disease and hepatic fibrosis. Pediatr Nephrol 1997;11:746–749
6. Suzuki T et al. A case cranial meningocele associated with Joubert syndrome. Child's Nerv Syst 1996;12:280–282
7. Adamsbaum C et al. MRI of the fetal posterior fossa. Pediatr Radiol 2005;35:124–140

"*This page left intentionally blank.*"

Chapter 2

The Head and Neck

CONTENTS

J. A. Al-Tubaikh, M. F. Reiser: *Congenital Diseases and Syndromes* – An Illustrated Radiological Guide
DOI: 10.1007/978-3-642-00160-4_2, © Springer-Verlag Berlin Heidelberg 2009

2.1

Eagle Syndrome

Eagle syndrome (ES) is a disease characterized by cervicofacial pain caused by elongation of the styloid process, which occurs due to extensive ossification of the stylohyoid ligament (Fig. 2.1.1). ES is noted to occur in some patients with a previous history of tonsillectomy.

The disease has an incidence of 4% in the general population, with a female predominance. The typical ES patient is female between 30 and 50 years of age with an elongated styloid process and cervicofacial pain.

ES can be asymptomatic, while some patients present with cervicofacial pain in the distribution of the carotid artery, neuralgia of the pharynx, dysphagia, and alteration in taste. Other patients present with chronic headaches with pain in the ophthalmic and the occipital regions when they turn their heads. This pain is classically seen due to bilateral internal carotid artery compression.

The key diagnostic presentations of ES according to otolaryngologists include a patient with throat pain radiating to the ear post tonsillectomy and a patient with a throbbing pain through either the external or the internal carotid artery distribution.

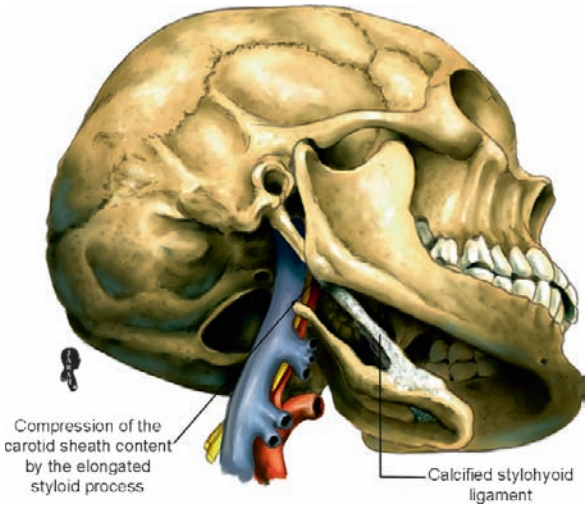

Fig. 2.1.1. Illustration of a calcified stylohyoid ligament with elongation of the temporal styloid process. The calcified ligament presses over the vascular and neural contents of the carotid sheath

Symptoms are believed to be caused by compression of the external carotid artery, internal jugular vein, or cranial nerves (9, 10, and 11) by the deviated, calcified stylohyoid ligament, or by a fibrous tissue scar post tonsillectomy.

Signs on Radiographs

Lateral plain radiographs of the skull and neck show elongation of the temporal styloid process until it reaches the hyoid bone (classic sign) (Fig. 2.1.2).

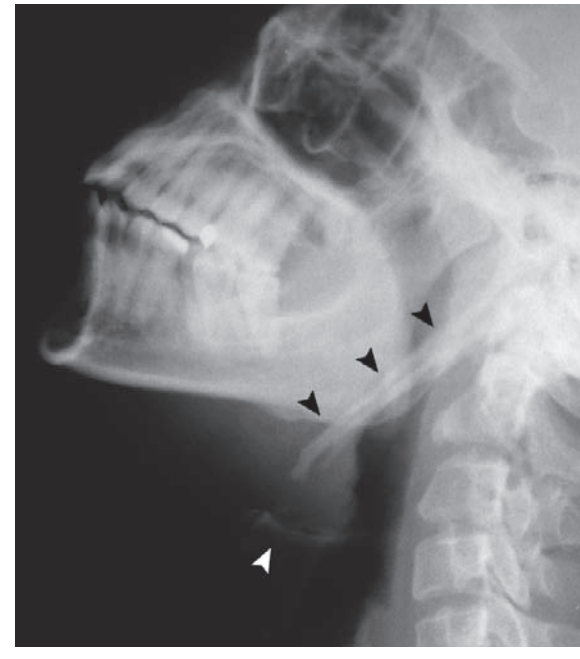

Fig. 2.1.2. Lateral plain radiograph of the neck showing the elongated temporal styloid process with the calcified stylohyoid ligament (*black arrowheads*) reaching up to the hyoid pone (*white arrowhead*)

For Further Reading

1. Gustavo M et al. Three-dimensional identification of vascular compression in eagle's syndrome using computer tomography: Case report. J Oral Maxillofac Surg 2008;66:169–176
2. Beder E et al. Current diagnosis and transoral surgical treatment if eagle's syndrome. J Oral Maxillofac Surg 2005; 63:1742–1745
3. Mendelson AH et al. Heterogeneity in the clinical presentation of eagle's syndrome. Otolarngol Head Neck Surg 2006; 134:389–393

2.2

Hyperostosis Frontalis Interna

Hyperostosis frontalis interna (HFI) is a benign normal variant of unknown cause characterized by increased thickness of the trabecular bone of the inner vault of the skull affecting the frontal bone. HFI is a progressive and symmetrical process. It has an incidence of 4–5% in the general population. HFI affects women more than men (up to 40% of cases are seen in postmenopausal women).

Patients with HFI may suffer from headache and neuropsychiatric diseases like epilepsy and dementia. Additionally, HFI has been linked to various endocrinopathies such as diabetes mellitus, toxic goiter, and acromegaly.

Morgagni syndrome: a syndrome characterized by obesity, hirsutism (abnormally excessive hair growth), and HFI.

Signs on Plain Skull Radiographs

There is increased thickening of the inner frontal bone (Fig. 2.2.1).

Fig. 2.2.1. A lateral plain radiograph of the skull shows increased bone thickness in the inner surface of the frontal bone (*arrowheads*)

Signs on CT

Bilateral, almost symmetrical increased thickening of the inner surface of the frontal bone (Fig. 2.2.2).

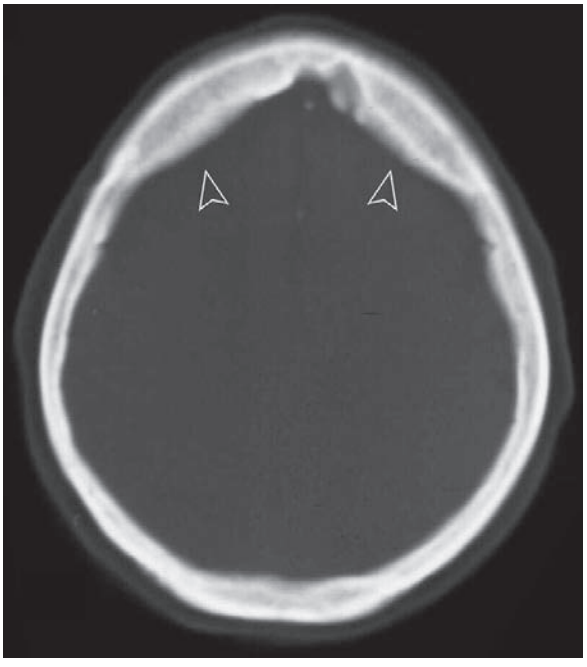

Fig. 2.2.2. Axial bone-window CT of the skull shows bilateral increase in the thickness of the inner surface of the frontal bone (*arrowheads*)

For Further Reading

1. Kocabas H et al. Hyperostosis frontalis interna in a patient with giant cell arteritis. Mod Rheumatol 2008;18:181–183
2. Chaljub G et al. Unusually exuberant hyperostosis frontalis interna: MRI. Neuroradiology 1999;41:44–45
3. Harding FE. Endocrinopathies associated with hyperostosis frontalis interna. Am J Med 1949;6(3):329–335

2.3

Craniofacial Fibrous Dysplasia and Its Anomalies

Craniofacial fibrous dysplasia (CFD) is a disease of unknown origin characterized by replacement of the normal bone and bone marrow by fibrous tissues; it affects any bone in the body.

The disease may affect a single bone (called monostotic fibrous dysplasia) or multiple bones (called polyostotic fibrous dysplasia). CFD occurs in 20% of the general population and is commonly associated with the polyostotic form of the disease. The peak incidence is in children and teenagers (before 30 years of age).

The common presentation is a young child brought in by the parents due to facial swelling and asymmetry. Other clinical presentations involve unilateral proptosis due to orbital bone involvement. Visual disturbance may occur as a result of optic nerve compression secondary to optic foramen stenosis by the expanded, sclerotic bones.

Leontiasis ossea: is a rare form of CFD with extensive maxillary involvement leading to maxillary encroachment on the orbital cavities, mouth, and paranasal sinuses, which produces a wide facial appearance likened to a lion's face (Fig. 2.3.1, 2.3.4, and 2.3.5).

McCune-Albright syndrome: is a rare disease affecting young female subjects characterized by polyostotic fibrous dysplasia, precocious puberty, and skin hyperpigmentation.

Cherubism: is a term used to describe symmetrical involvement of the maxilla and mandible producing bilateral, progressive swelling of the cheeks (Fig. 2.3.2). It can be caused by CFD and giant cell lesions (Fig. 2.3.3). Cherubism is a benign condition with an autosomal dominant mode of inheritance. Typically, it presents around the age of 7 years and tends to regress after adolescence.

Mazabraud syndrome: is a rare disease characterized by the association of polyostotic fibrous dysplasia with intramuscular myxoma.

Signs on Plain Radiographs

Diffuse thickening and sclerosis of the affected facial bones with classic "ground glass" appearance due to the fibrous matrix nature of the disease.

Fig. 2.3.1. Illustration of a patient with bilateral leontiasis ossea. Note the wide face that looks like the characteristic face of a lion. Also, note the hypertelorism resulting from distension of the facial bones

Fig. 2.3.2. Illustration of a young girl with bilateral full cheeks (cherubism). Cherubism is a term used to describe bible drawings of children with full cheeks

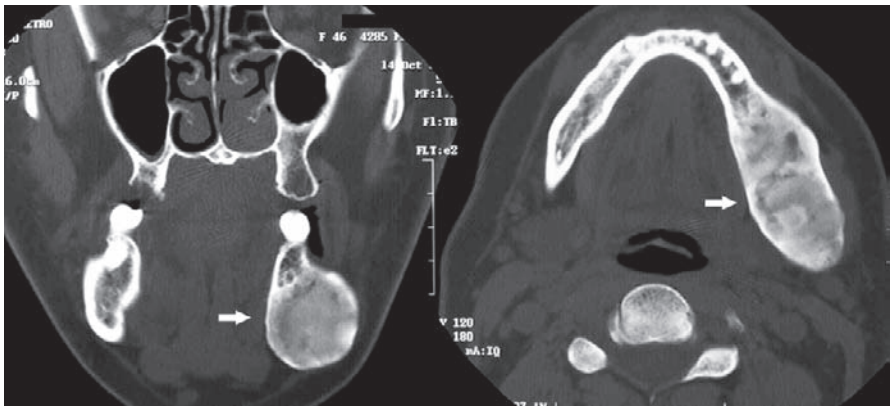

Fig. 2.3.3. Axial and coronal bone-window CT scan of a patient with unilateral fibrous dysplasia of the mandible (*arrows*). Bilateral involvement of the mandible by fibrous dysplasia is termed cherubism

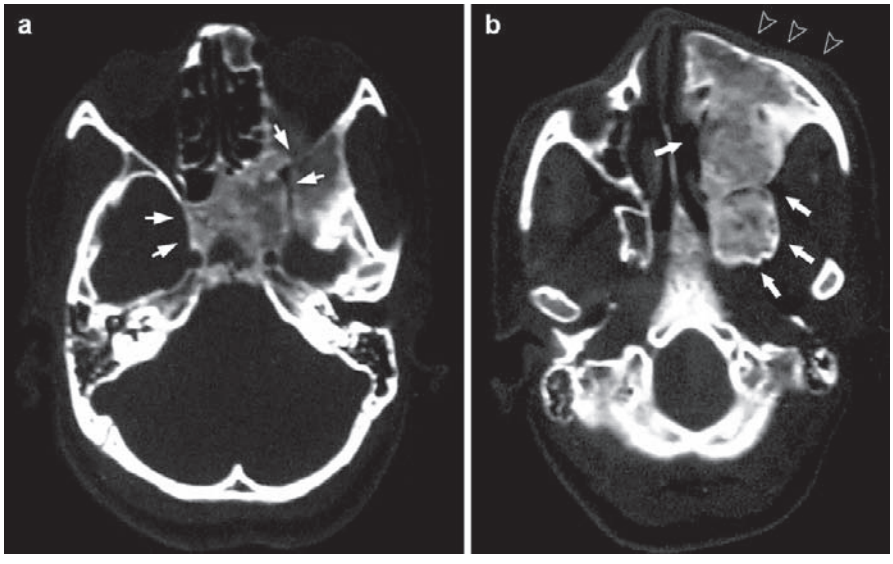

Fig. 2.3.4. Axial bone-window CT images of a patient with leontiasis ossea. **a** Note the extensive involvement of the left foramen rotundum, greater wings of the sphenoid, petrygopalatine fossa and its canal, basisphenoid bone, posterior ethmoid air cells, and clivus by fibrous dysplasia (*arrows*). The lesion has a classic "ground glass" appearance. **b** Extensive involvement of the left maxillary sinus, zygomatic bone, and the petrygoid plates is clearly seen (*arrows*). Note the left facial distension (*open arrowheads*) caused by the lesion compared with the normal right side

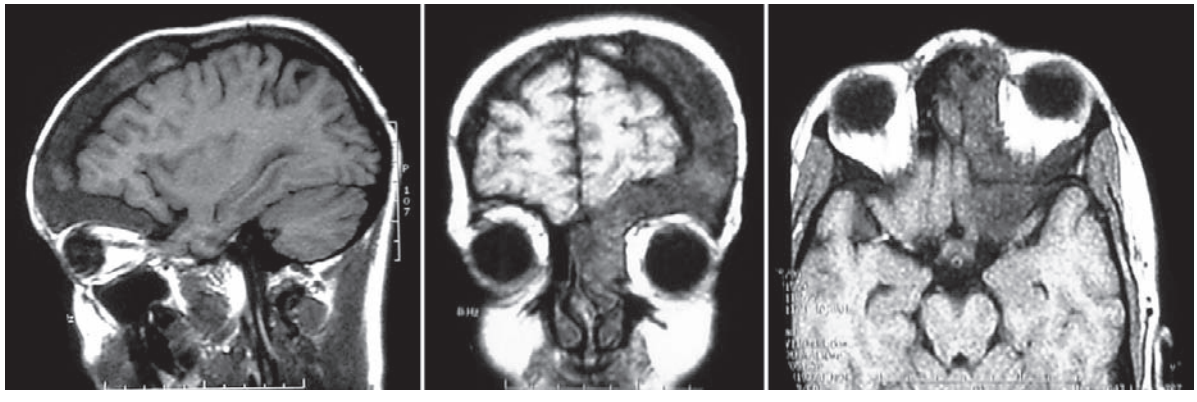

Fig. 2.3.5. Sagittal, coronal, and axial T1-weighted MR images show extensive fibrous dysplasia involving the left clavarium and the left paranasal sinuses in another patient with CFD. Note the hypointense signal of the lesion due to its fibrous content

Signs on CT

- The involved bones appear expanded with intact inner and outer surfaces (Fig. 2.3.4).
- The bone may show osteolytic features or sclerotic features depending on the matrix calcification rate.
- **Small orbit sign:** a decrease in the size of the orbit due to bony orbit expansion.

Signs on MRI

The bones show expansion with low signal intensity in T1-weighted sequence with inhomogeneous gadolinium enhancement due to the fibrous nature of the lesion (Fig. 2.3.5).

Differential diagnosis:

- **Ossifying fibroma of the head and neck** (localized to one bone and rarely crosses to another bone. It also has a female predominance, with age of presentation in the third to fourth decade).
- **Paget disease of the skull** (found in older age-group and affects both the facial bones and the clavarium extensively, in contrast to fibrous dysplasia which can extensively affect the facial bones without affecting the clavarium).

For Further Reading

1. Jain V et al. Radiographic, CT and MRI features of cherubism. Pediatr Radiol 2006;36:1099–1104
2. Carbral CEL et al. Polyostotic fibrous dysplasia associated with intramuscular myxoma: Mazabraud's syndrome. Skeletal Radiol 1998;27:278–282
3. Yüceer N et al. Polyostotic fibrous dysplasia with craniofacial localization presenting with frontal lobe compression in a 14-year-old Girl. Acta Neurochir (Wien) 1999;141:203–207
4. Mendonca JJ et al. Fibrous dysplasia of the mandible: Surgical treatment with platelet-rich plasma and a cortico-cancellous iliac crest graft-report of a case. Oral Surg Oral Med Oral Pathol Oral Radiol Endod 2008;105: e12–e18
5. Sherman NH et al. Fibrous dysplasia of the facial bones and mandible. Skeletal Radiol 1982;8:141–143
6. Maramatton BV. Leontiasis ossea and post traumatic cervical cord contusion in polyostotic fibrous dysplasia. Head Face Med 2006;2:24. doi 10.1186/1746–160x-2–24

2.4

Gardner Syndrome

Gardner syndrome is a rare, hereditary disease characterized by intestinal polyposis (made of adenomas), multiple osteomas (mainly in the jaw), and multiple cutaneous and subcutaneous lesions (epidermoid cysts and desmoid tumor).

The intestinal polyposis is hereditary with a 100% chance of malignant transformation if not treated.

Osteoma is a benign bony island that can be made up of compact (ivory) or trabecular bone. In Gardner syndrome, osteomas are commonly found in the jaw and the skull. In the jaw, the most characteristic and diagnostic locations for Gardner syndrome osteomas are the mandibular angle or its inferior surface (Fig. 2.4.1). Mandibular osteomas can be the initial sign and symptom of Gardner syndrome.

The disease commonly presents with dental abnormalities (30%) such as dental hypoplasia, supernumerary teeth, and compound odontomas.

Epidermoid cysts present in the face, scalp, and extremities in around 50% of cases.

Fig. 2.4.1. Illustration of the classic locations of Gardner syndrome osteomas, at the angle of the mandible and its inferior surface

Desmoid tumor is a benign fibrous soft-tissue proliferation that occurs in the skin or inside the abdomen. It has no malignant tendency; however, it has an aggressive infiltration of the adjacent tissues and tends to reoccur after surgical excision. It is seen in 8.9% of cases.

Congenital hypertrophy of the retinal pigment epithelium (CHRPE) can be seen in up to 85% of cases.

Signs on Plain Radiographs

- Osteomas of the skull, angle of the mandible, or its inferior surface (Fig. 2.4.2).
- Dental anomalies, hypoplasia, and unruptured teeth.
- Cortical thickening (hyperostosis) in the long bones.

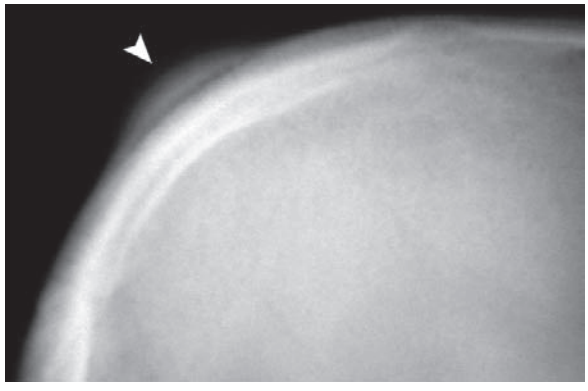

Fig. 2.4.2. Plain radiograph of the skull shows ivory osteoma of the clavarium (*arrowhead*)

For Further Reading

1. Baykul T et al. Multiple huge osteomas of the mandible causing disfigurement related with Gardner's syndrome: Case report. Auris Nauses Larynx 2003;30:447–445
2. Butler J et al. Gardner syndrome-review and report of a case. Oral Oncology EXTRA 2005;41: 89–92
3. Parks ET et al. Gardner syndrome. J Am Acad Dermatol 2001;45:940–942

2.5

Choanal Atresia

Choanal atresia is an uncommon sinusoidal malformation characterized by unilateral or bilateral closure of the communication between the posterior nasal choana and the nasopharynx. The closing ridge is bony in 90% of cases and membranous in 10% of cases.

Up to 50% of neonates with choanal atresia have craniofacial, cardiovascular, or visceral congenital malformations (e.g., CHARGE association). *CHARGE association* is a congenital syndrome characterized by *c*oloboma, *h*eart disease, *a*tresia of the choanae, *r*etarded mental development, *g*enital hypoplasia, and *e*ar anomalies and deafness.

Neonates with bilateral choanal atresia present with respiratory distress in the immediate newborn period. In contrast, unilateral choanal atresia may be diagnosed later in life.

Signs on Plain Radiographs

- Lateral radiographs demonstrate a discrete separation between the air in the nasopharynx and the air in the posterior nasal cavity.
- Contrast material instilled into the nasal cavity in supine position will collect against the obstruction (Fig. 2.5.1).

Fig. 2.5.1. Plain radiograph of the skull base shows contrast material instilled into the nose with collection of the contrast material against an obstructed posterior choana in a patient with bony choanal atresia

Signs on Paranasal Sinus CT

- Axial CT images demonstrate thickening and medial bowing of the lateral wall of the nasal cavity with atresia of the posterior choana. Fusion between the vomer and the palatine bones obstructing the opening to the nasopharynx is usually seen.
- Membranous atresia is seen as an isodense soft-tissue mass closing the passage between the posterior choana and the nasopharynx (Fig. 2.5.2).

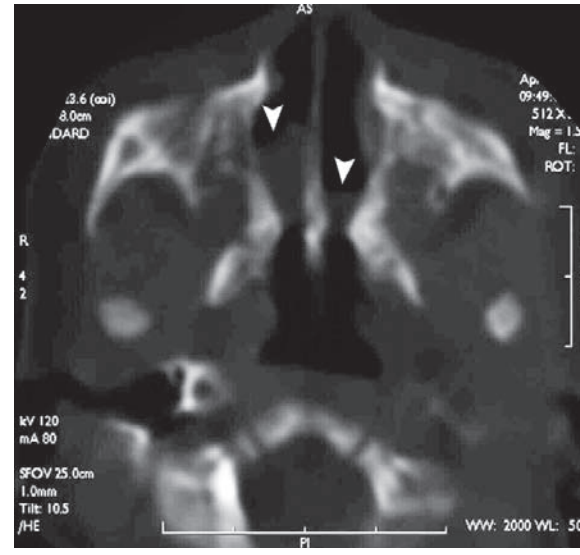

Fig. 2.5.2. Axial bone-window CT of the paranasal sinuses shows bilateral soft-tissue density masses blocking the passage of the posterior choana in a patient with soft-tissue choanal atresia (*arrowheads*)

For Further Reading

1. El-Sawy H et al. Bilateral choanal atresia and paranasal sinus hypoplasia in an adult patient with hypogammaglobulinaemia. Eur Arch Otorhinolaryngol 2006;263:1136–1138
2. Koletzko B and Majewski F. Congenital anomalies in patients with choanal atresia: CHARGE-association. Eur J Pediatr 1984;142:271–275

2.6

Congenital Cystic Lesions of the Head and Neck

Cystic lesions of the head and neck are usually either congenital or acquired in origin. Acquired lesions are a result of inflammatory conditions or, rarely, neoplastic (e.g., Warthin tumor). Most of the cystic lesions are seen in children, and are diagnosed according to their location.

The Pharyngeal Bursa of Luschka

The pharyngeal bursa of Luschka is a median formation that projects in the midline of the nasopharynx between the longus capitis muscles. It is seen in 7% of the population as an incidental, asymptomatic finding. When the bursa becomes infected, it is called "Thornwaldt cyst."

Signs on CT and MRI

The scan shows a median recess that contains air between the longus capitis muscles (Fig. 2.6.1).

Fig. 2.6.1. Axial head CT illustration shows a median recess located between the longus capitis muscles representing the pharyngeal bursa of Luschka (*arrowhead*)

Thornwaldt Cyst (Pharyngeal Bursitis)

Thornwaldt cyst results from obstruction of the pharyngeal bursa due to inflammation or trauma. The cyst is typically located midline in the posterosuperior wall of the nasopharynx.

Signs on CT

- A hyperdense cyst located at the midline between the longus capitis muscles and the posterior wall of the nasopharynx. The cyst does not enhance after contrast material administration (Fig. 2.6.2).
- Occasional calcifications may occur.

Fig. 2.6.2. Axial noncontrast-enhanced head CT illustration shows a round, hyperdense mass located between the longus capitis muscles representing a Thornwaldt cyst (*arrowhead*)

Signs on MRI

- The cyst is located in the mid-posterior wall of the nasopharynx with high T1 and high T2 signal intensities (the high signal in T1 depends on the protein content of the cyst).
- The cyst wall may enhance after injection of contrast material.

Differential Diagnosis

- Mucosal cyst (exhibits low T1 signal intensity on MR images and is usually located in the lateral recess).
- Branchial cleft cysts (by their location).

Thyroglossal Duct Cyst

The thyroid gland develops medially at the base of the tongue and then descends anterior to the hyoid bone along the thyroglossal duct to its normal position. When the thyroglossal duct fails to obliterate, it results in the formation of a median or paramedian cyst. The normal thyroglossal duct extends from the foramen cecum at the base of the tongue to the lower neck region where the thyroid bed is. It is obliterated between the fifth and sixth weeks of gestation.

Thyroglossal duct cysts account for up to 70% of all cystic malformations in the neck. Up to 50% are located at the hyoid bone, 25% below the hyoid and 25% above it.

Signs on CT

- Typically, the scan shows a median–paramedian cyst located at the level of the hyoid bone with no contrast enhancement (Fig. 2.6.3).
- The cyst typically splits the two anterior bellies of the diagastric muscles.
- Ring contrast enhancement may be seen in cases of infected cyst.

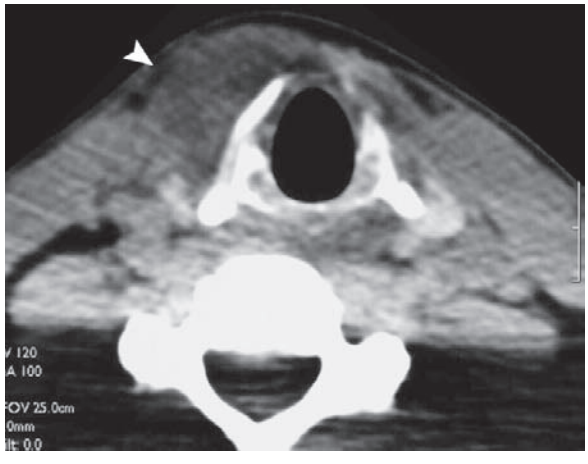

Fig. 2.6.3. Axial postcontrast neck CT shows a right paramedian hypodense cystic lesion at the level of the larynx representing a thyroglossal duct cyst (*arrowhead*)

Cystic Hygroma (Lymphangiomatosis)

Lymphangiomatosis is a rare disorder of unknown origin characterized by diffuse proliferation of the lymphatic channels in the body with obstruction of lymphatic drainage. It involves lymphatic proliferation in the bones and viscera. The disease affects children and young adults.

There are three forms of lymphangiomatosis:

- **Cystic form:** this form is known as "cystic hygroma," and most commonly occurs in the neck or the axilla in children.
- **Capillary form:** this form affects the skin.
- **Cavernous form:** this form affects the bone, soft tissues, and the viscera.

Cystic hygroma is usually diagnosed before 2 years of life. Typically, the cyst grows in size as the child grows.

Cystic hygroma can be associated with genetic syndromes such as Turner syndrome, trisomy 21, 13, and 18.

Signs on CT and MRI

- Cystic hygroma appears as a cyst with a thin wall, and a water-dense mass with multiple lobules that do not enhance after injection of contrast material. The mass may show fluid–fluid levels due to intracystic hemorrhage (Fig. 2.6.4).
- The cyst shows ring contrast enhancement if superimposed by infection.
- Hypertrophy of the adjacent bony structures (e.g., mandible) may occur occasionally.

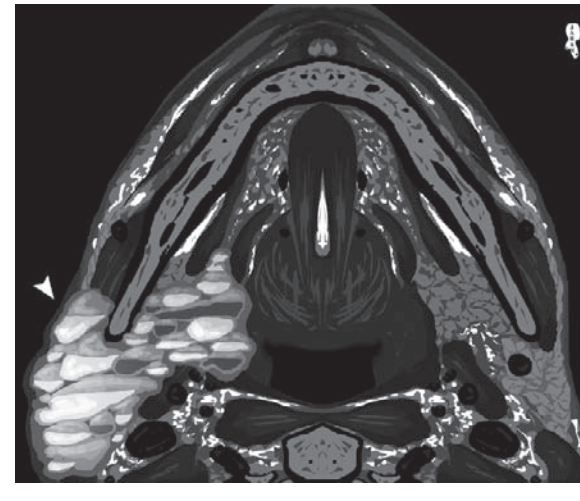

Fig. 2.6.4. Axial T1-weighted MR illustration shows cystic hygroma on the right side with typical fluid–fluid appearance within the cyst, and different intensities due to the cyst content (*arrowhead*)

Dermoid and Epidermoid Cysts

These lesions are commonly located medially within the neck, and characteristically have thick walls. They are typically midline lesions arising from the floor of the mouth deep to the myelohyoid muscle. Dermoid cysts contain skin, sebaceous glands, and hair follicles. In contrast, epidermoid cysts contain fluid but not fatty material.

Signs on CT and MRI

- These lesions are commonly located medially within the neck, and have thick walls (Fig. 2.6.5).
- On MRI, globules of floating fat within the lesion can produce a characteristic "sack of marbles" appearance or fat–fluid levels (Fig. 2.6.6).
- They can be mistaken for thyroglossal cyst.

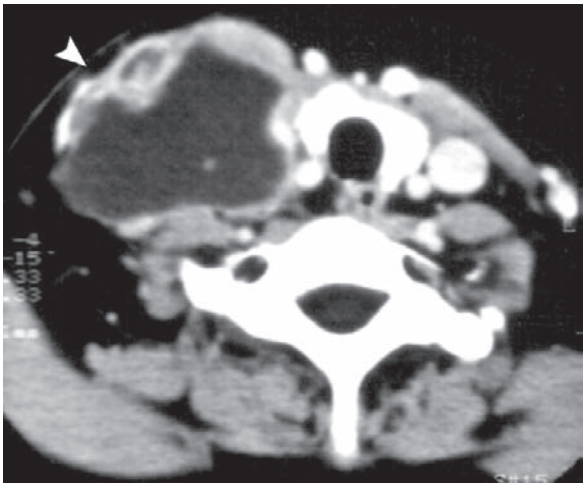

Fig. 2.6.5. Axial postcontrast neck CT shows large paramedian mass with hypodense center and very thick walls. The mass proved to be a malignant epidermoid cyst after biopsy (*arrowhead*)

Branchial Cleft Cysts

The branchial apparatus comprises structures composed of six pairs of mesodermal arches separated by five pairs of endodermal pharyngeal pouches internally and five pairs of ectodermal branchial clefts externally. They develop between the fourth and fifth weeks of gestation. Branchial cysts are malformations that usually arise from the first four branchial apparatuses.

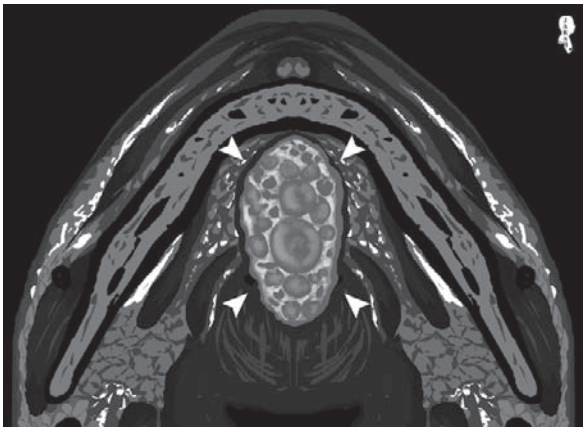

Fig. 2.6.6. Axial T1-weighted MR illustration shows a medial isointense cystic mass containing multiple mildly hyperintense small masses. This appearance is typically seen in dermoid and epidermoid cysts resulting in a "sack of marbles" appearance (*arrowheads*)

- **First Branchial Cleft Cyst:** This cyst occurs near the external auditory canal or the parotid gland (Fig. 2.6.7). It accounts for 8% of all branchial cleft cysts. Patients present with a mass near the ear with or without recurrent infections.
- **Second Branchial Cleft Cyst:** This cyst occurs anterior to the sternocleidomastoid muscle, lateral to the carotid sheath, and posterior to the submandibular gland and the mandibular edge (Fig. 2.6.8). It accounts for 95% of all branchial cleft cysts. Patients typically present with a nontender lateral neck mass.

Fig. 2.6.7. Axial postcontrast head CT illustration shows a cyst located near the right external auditory canal and the parotid gland, a typical site for first branchial cleft cyst

Fig. 2.6.8. Axial postcontrast head CT image shows typical location of the second branchial cleft cyst (*arrowhead*)

- **Third Branchial Cleft Cyst**: This cyst occurs posterior to the internal carotid artery in the upper neck; in the lower neck it can be found in the anterior triangle.

Signs on CT

The cysts appear as hypodense lesions that do not enhance after contrast medium administration. The origin of the cyst is determined according to its location.

Thymic Cysts

Normally, the thymus originates from the third branchial pouch during the fifth week of gestation. It detaches from the pharynx and migrates caudally and medially via the thymopharyngeal duct to reach its normal position in the upper mediastinum. The track of the thymopharyngeal duct extends from the angle of the mandible to the upper mediastinum. Thymic cysts occur due to persistence of remnants of the thymopharyngeal duct (like the thyroglossal duct cyst).

Patients present before 20 years of age complaining of hoarseness, dysphagia, and respiratory distress.

Signs on CT

- The scan shows a hypodense, cystic mass in the upper mediastinum or the lower neck causing tracheal deviation, or exerting mass effect over the adjacent structures.
- The cyst is closely related to the carotid sheath.

Dentigerous (Follicular) Cysts

A dentigerous cyst is one that arises from a tooth after calcification of its crown, and is usually located at the mandibular or the maxillary third molar tooth. The cyst can be large enough to occupy half of the mandible. The peak incidence is between 40 and 60 years of age.

Dentigerous cysts can be associated with mucopolysaccharidosis.

Signs on Radiograph or CT

A cystic lesion of the mandible with an eccentrically placed tooth crown (Fig. 2.6.9).

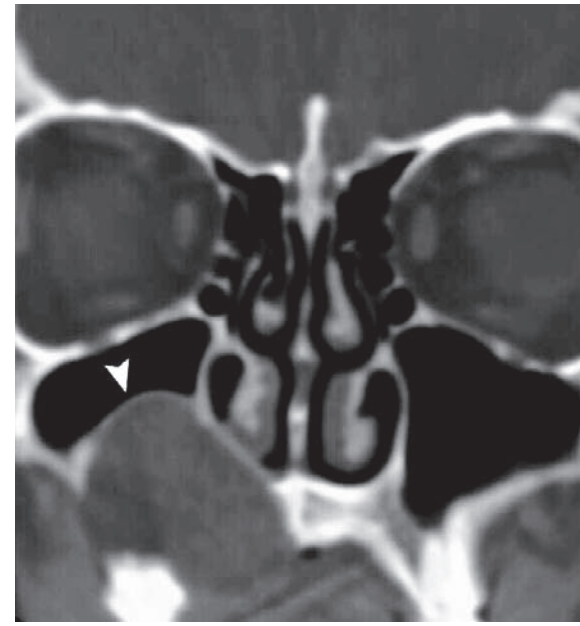

Fig. 2.6.9. Coronal CT of the paranasal sinuses shows a large cyst that arises from the third maxillary molar tooth (dentigerous cyst). The cyst is expanding into more than half the space of the right maxillary sinus (*arrowhead*)

Ranula

The sublingual glands have 8–20 excretory ducts that open below the tongue posterior to the opening of the subamndibular duct (of Warton). Ranula is a retention cyst of the minor salivary gland or the sublingual glands occurring most commonly after trauma or inflammation of the mouth; congenital ranulas are rare.

Typically, the patient is between 25 and 30 years of age with 50% having a history of previous trauma to the mandible.

Ranulas are divided into two types:

- **Simple ranula:** occurs due to obstruction of the salivary gland duct without rupturing. It does not cross the boundaries of the submandibular space.
- **Complicated (diving) ranula:** results from rupture of the gland within the sublingual space with formation of a pseudocyst that can extend into the submandibular space.

Patients often present with painless swelling of the sublingual glands with bluish discoloration (Fig. 2.6.10).

Fig. 2.6.10. Illustration showing the clinical finding in a patient with ranula. Typically, there is a bluish mass found below the tongue, where the sublingual ducts open

Signs on CT

- Simple ranula: the scan shows a hypodense mass located in the sublingual space with a ring enhancement after contrast material injection.
- Complicated ranula appears as a "comet-tail-shaped mass." The tail is located in the sublingual space and the head is in the submandibular space (Fig. 2.6.11).

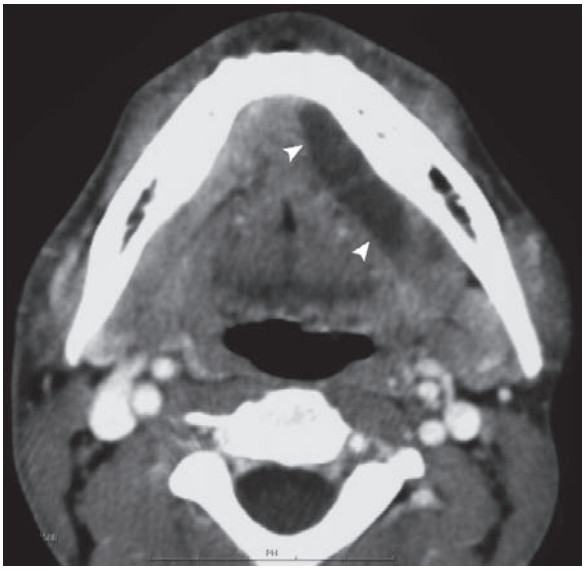

Fig. 2.6.11. Axial postcontrast CT of the floor of the mouth shows complicated (diving) ranula (*arrowheads*)

Signs on MRI

- The cyst has low T1/high T2 signal intensities with a homogeneous internal architecture. An inhomogeneous internal architecture excludes the diagnosis of ranula.
- The comet-tail sign is seen as a high fluid signal on T2-weighted images within the sublingual space (Figs. 2.6.12 and 2.6.13).
- Extension of the ranula may reach the submandibular space, or further upward into the parapharyngeal space. This free extension occurs because there are no fascial boundaries between the sublingual, submandibular, and parapharyngeal spaces.

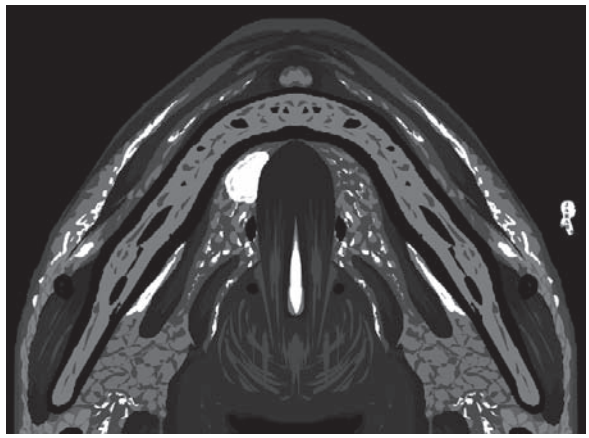

Fig. 2.6.12. Axial T2-weighted MR illustration of the floor of the mouth shows simple ranula seen as a homogeneous mass with defined boundaries

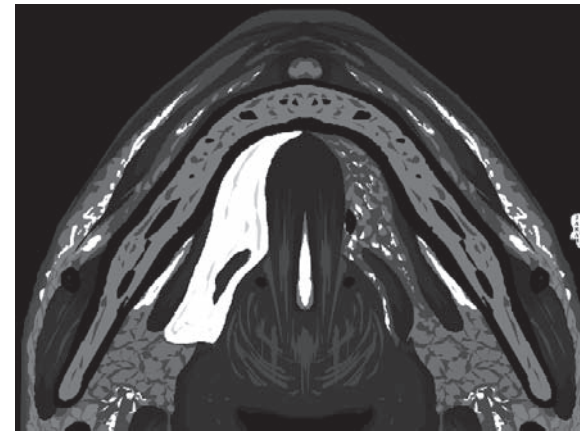

Fig. 2.6.13. Axial T2-weighted MR illustration of the floor of the mouth shows complicated ranula with its "comet tail sign"

For Further Reading

1. Wong KT et al. Imaging of cystic or cyst-like neck masses. Clin Radiol 2008;63:613–622
2. Koch BL. Cystic malformations of the neck in children. Pediatr Radiol 2005;35:463–477
3. Kurabayashi T et al. MRI of ranulas. Neuroradiology 2000; 42:917–922
4. Chong VFH et al. Radiology of the nasopharynx: Pictorial essay. Australas Radiol 2000;44: 5–13

2.7

External Auditory Canal Atresia

Signs on Petrous Bone CT

There is absence of the external ear auditory canal, or blockage of the canal by a bone or soft tissue (Figs. 2.7.2 and 2.7.3).

The external and the middle ear arise from the second and the first branchial arches, and the first branchial cleft in the embryo. External auditory canal (EAC) atresia is characterized by underdevelopment of the external auditory canal.

EAC atresia is often associated with small, deformed pinna (microtia), and deformities in the mandible or the temporomandibular joint (Fig. 2.7.1). EAC atresia is usually bilateral, but unilateral malformation may occur. EAC atresia can be associated with middle ear anomalies (e.g., contracted middle ear cavity) or facial anomalies (e.g., Goldenhar syndrome).

Petrous bone CT is performed to assess bony or soft-tissue blockage and associated middle ear abnormalities (e.g., fused ossicles). A contracted middle ear cavity below 3 mm is incompatible with reconstruction surgery.

Fig. 2.7.1. Illustration shows absence of the entrance of the external auditory canal in a patient with EAC atresia

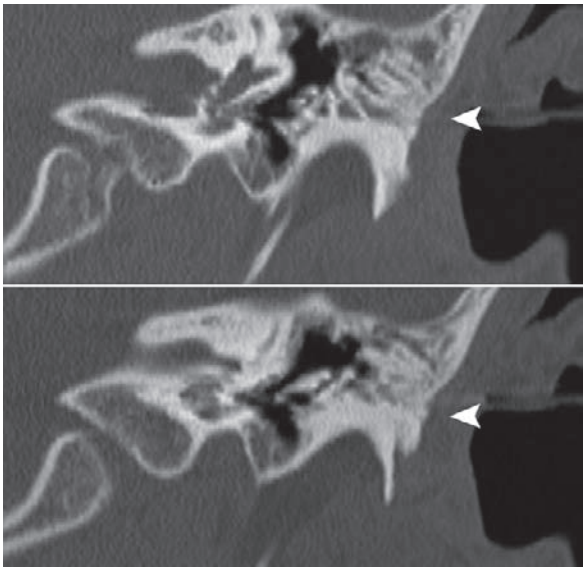

Fig. 2.7.3. Coronal bone-window CT images show absence of the external auditory canal passage on the left ear. The middle ear cavity is blocked by bone with no sign of EAC formation (*arrowheads*)

For Further Reading

1. Ada M et al. Unusual extension of the first branchial cleft anomaly. Eur Arch Otorhinolaryngol 2006;263:263–266
2. Sheykholeslami K et al. Bone-conducted vestibular evoked myogenic potentials in patient with congenital atresia of the external auditory canal. Int J Pediatr Otorhinolaryngol 2001;57:25–29

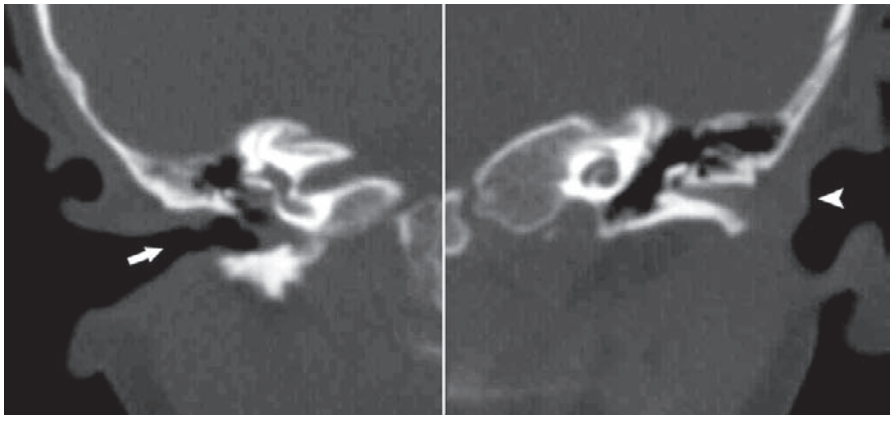

Fig. 2.7.2. Coronal bone-window CT images show soft-tissue blockage of the EAC on the left ear (*arrowhead*). Note the normal EAC passage on the right ear (*arrow*)

2.8

Congenital Anomalies of the Internal Ear (Congenital Hearing Loss)

In normal embryological development of the ear, the bony labyrinth evolves between the 4th and 8th week of gestation, grows between from the 8th to the 16th week, and ossifies from the 16th to 24th week. Development of the sensory epithelium occurs after the 25th week. Congenital malformation arises when an insult (e.g., intrauterine infection) occurs between the fourth and eighth weeks of gestation.

Up to 50% of cases of congenital anomalies of the inner ear are due to genetic defects, and the remainder of cases are attributed to intrauterine infections (TORCH), fetal drug ototoxicity, and trauma. Cytomegalovirus is a common infection that causes inner ear anomalies and congenial deafness. Ingestion of ototoxic drugs by pregnant women can lead to congenital hearing loss; examples are alcohol (fetal alcohol syndrome), aminoglycosides, aspirin, erythromycin, and furosamide.

Up to 70% of genetic congenital hearing losses occur as isolated cases, the rest of the genetic cases occur as parts of syndromes.

Presbycusis: is bilateral sensorineural hearing loss due to age. The CT scan shows a normal temporal structure. Malformations that only involve the membranous labyrinth are classified as Alexander and Scheibe deformities. The CT examination of these deformities is normal.

Michel Dysplasia

Michel dysplasia is a term used to describe complete absence of the entire middle ear, including the cochlea, vestibule, and all semicircular canals. The medial wall of the inner ear and the promontory are flat due to inner ear aplasia.

It is a very rare anomaly, and its main differential diagnosis is postmeningitic labyrinthine ossification.

Signs on Petrous Bone CT

The scan shows complete absence of the inner ear (Fig. 2.8.1).

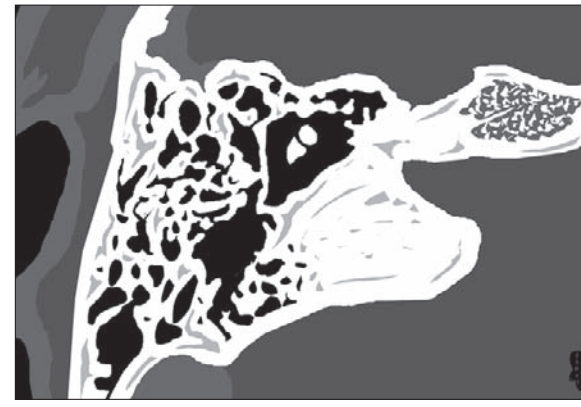

Fig. 2.8.1. Axial petrous bone CT illustration shows complete absence of the cochlea, vestibule, and semicircular canals (Michel anomaly)

Mondini Anomaly

Mondini anomaly is a term used to describe fusion of the apical and the middle cochlear turns making up one cavity, while the basal turn is present.

Up to 20% of patients with Mondini anomaly have other malformations of the vestibule, endolymphatic duct, or semicircular canals.

Patients with Mondini anomaly present with low-frequency hearing deficit, due to fusion of the apical and the middle cochlear turns. In contrast, high-frequency hearing persists due to presence of the basal turn.

Signs on Petrous Bone CT

The scan shows fused apical and middle cochlear turns with loss of the cochlear modiolus (Fig. 2.8.2).

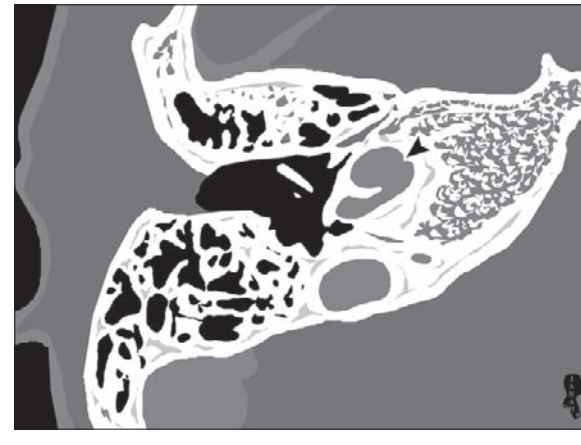

Fig. 2.8.2. Axial petrous bone CT illustration shows Mondini anomaly. Note the fusion between the apical and the middle cochlear turns with absence of the cochlear modiolus (*arrowhead*)

Common Cavity Deformity

Common cavity deformity is characterized by replacement of the cochlea and the vestibule by a single hollow cavity without internal architecture. It occurs due to inner ear developmental arrest between the fourth and fifth week of gestation.

Signs on Petrous Bone CT

The scan shows one cavity occupying the area of the vestibule and the cochlea (Fig. 2.8.3).

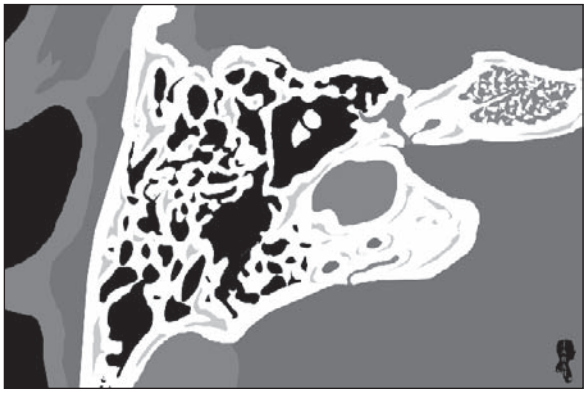

Fig. 2.8.3. Axial petrous bone CT illustration shows the common cavity anomaly. Note the complete fusion between the vestibule and the cochlea to form a single hollow cavity

Semicircular Canal Aplasia/Hypoplasia

Aplasia or hypoplasia of the semicircular canal is an anomaly that arises due to developmental interruption of the semicircular canals during embryogenesis between the sixth and eighth week of gestation. There will be underdevelopment or complete abscence of one or more of the semicircular canals; the lateral semicircular canal is the most commonly affected.

Semicircular aplasia can be associated with syndromes such as Goldenhar syndrome and CHARGE association.

Signs on Petrous Bone CT

The scan shows agenesis or underdevelopment of one or more of the semicircular canals.

Semicircular Canal Dehiscence

Semicircular canal dehiscence is a condition characterized by loss of the bony overlay of the posterior or superior semicircular canals. The area of the bony defect is covered only by dura separating the semicircular canal from the cerebrospinal fluid in the cranial fossa. Changes in the pressure within the intracranial space can be transmitted through this defect into the labyrinth resulting in vertigo.

Signs on Petrous Bone CT

The scan shows a bony defect over the superior or the posterior semicircular canal (Fig. 2.8.4).

Fig. 2.8.4. Axial petrous bone CT illustration shows loss of the bony covering over the superior semicircular canal, representing semicircular canal dehiscence (*arrowhead*)

Large Vestibular Aqueduct Syndrome

The vestibular (endolymphatic) aqueduct is a J-shaped bony canal that extends from the medial wall of the vestibule to the posterior surface of the petrous temporal bone. The normal vestibular aqueduct diameter measures

up to 1.5 mm. Congenital enlargement of the vestibular aqueduct beyond this diameter results in progressive, bilateral, sensorineural hearing loss and vertigo, commonly in the younger population.

The vertigo and the sensorineural hearing loss are attributed to damage of the hair cells within the labyrinth due to cerebrospinal fluid pressure fluctuation, which is delivered by the enlarged vestibular aqueduct.

Signs on Petrous Bone CT

The scan shows enlargement of the vestibular aqueduct beyond 1.5 mm in diameter (Fig. 2.8.5).

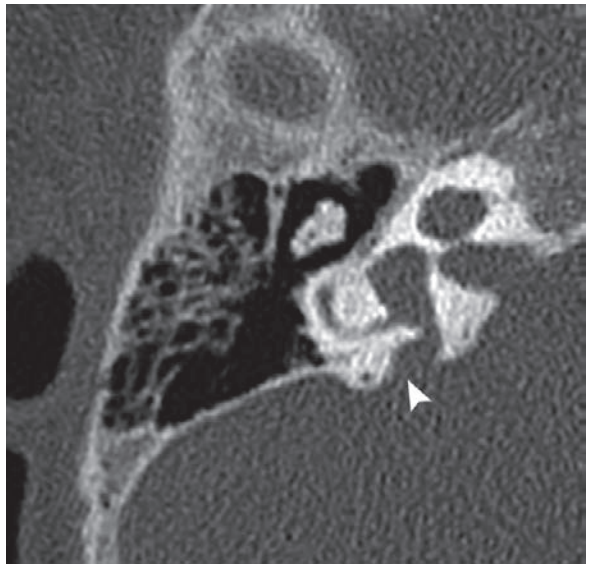

Fig. 2.8.5. Axial petrous bone CT image shows an enlarged vestibular aqueduct (*arrowhead*)

Signs on MRI

The scan shows enlargement of the vestibular aqueduct on T2-weighted images with fluid signal intensity (Fig. 2.8.6).

Fig. 2.8.6. Axial T2-weighted MR image in another patient shows markedly enlarged vestibular aqueduct (*arrowhead*)

For Further Reading

1. Kavanagh KT and Magill HL. Michel dysplasia, Common cavity inner ear deformity. Pediatr Radiol 1989;19:343–345
2. Davidson HC. Imaging of the temporal bone. Neuroimag Clin N Am 2004;14:721–760
3. Naganawa S et al. Serial MR imaging studies in enlarged endolymphatic duct and sac syndrome. Eur Radiol 2002; 112:S114–S117
4. Krombach GA. Imaging of congenital anomalies and acquired lesions of the inner ear. Eur Radiol 2008;18(2): 319–330

2.9

Hearing Loss Syndromes

Hearing loss can occur due to aging, trauma, as well as drug-related and congenital causes. Congenital hearing loss is divided into "syndromic" and "nonsyndromic" types. In the syndromic type, hearing loss occurs as part of a syndrome with other manifestations within the body. There are many syndromes that cause hearing loss as one of their manifestations. Only four of the most common hearing loss syndromes are discussed here.

Waardenburg Syndrome

Waardenburg syndrome is a rare congenital disorder distinguished by characteristic facial features, pigmented abnormalities, and profound, congenital, sensorineural hearing loss (up to 75% of cases).

The disease has an autosomal dominant mode of inheritance, with an incidence of 1:40,000 live births. It accounts for 2% of all congenital hearing loss cases.

Waardenburg syndrome is characterized by (Fig. 2.9.1):

- **Dystopia canthorum** (lateral displacement of the inner canthi, or inner angles of the eyes, plus lateral displacement of the lacrimal puncta).
- Prominent broad nasal root.
- **Synophrys** (the eyebrows grow together).
- **White forelock** (whitish or grayish hair in the front of the head).
- **Heterochromia irides** (two eyes with different colors, or one eye with two different colors in the iris).
- Congenital bilateral sensorineural hearing loss.

Fig. 2.9.1. Illustration shows the typical facial features of Waardenburg syndrome. Note the lateral displacement of the medial angles of the eye (*dystopia canthorum*), the prominent broad nasal root, the adjacent eyebrows (*synophrys*), the white forelock, and the two different colors of the iris (*heterochromia irides*)

The disease has four subtypes

- **Waardenburg syndrome type 1:** it is the classic form, and the patient presents with the above-mentioned features.
- **Waardenburg syndrome type 2:** this disease has the same features as type 1 but lacks the dystopia canthorum.
- **Waardenburg syndrome type 3 (Waardenburg-Klein syndrome):** it is a combination of type 1 with upper limb anomalies (e.g., syndactyly).
- **Waardenburg syndrome type 4 (Waardenburg-Shah syndrome):** it is a combination of type 2 with Hirschprung disease.

ABCD syndrome: is a rare variant expression of Waardenburg-Shah syndrome characterized by *a*lbinism, *b*lack lock, *c*ell migration disorder of the gut neurocytes, and *d*eafness. The disease has an autosomal recessive mode of inheritance.

Signs on Petrous Bone CT

Abnormalities of the petrous bone are present in 17% of cases, and include aplasia of the semicircular canals and the vestibule.

Pendred Syndrome

Pendred syndrome is an autosomal recessive disease characterized by severe congenital sensorineural hearing loss with iodine organification defect that causes developmental thyroid goiter in infants. The disease accounts for almost 10% of all cases of congenital hearing loss syndromes.

In Pendred syndrome, up to 80% of the thyroid-accumulated iodide is discharged on administration of a substance called "perchlorate". The perchlorate test is the gold standard test for diagnosing this disease.

The sensorineural hearing loss is often caused by Mondini anomaly or bilateral enlarged vestibular aqueduct syndrome.

Goldenhar Syndrome (Oculo-Auriculo-Vertebral Syndrome)

Goldenhar syndrome is a congenital disorder related to a group of congenital diseases known as "the hemifacial microsomia spectrum." These diseases are characterized by unilateral or bilateral and often asymmetrical abnormalities of the first and second branchial arch derivatives with facial asymmetry.

Most cases are sporadic and affect one side of the face only.

Goldenhar syndrome is characterized by the following facial features (Fig. 2.9.2):

- Unilateral or bilateral external ear atresia (microtia).
- Unilateral or bilateral mandibular hypoplasia.
- Unilateral or bilateral maxillary flattening.
- **Epibulbar dermoid:** is a benign, white–yellow, or pinkish tumor located on the cornea and the sclera in the temporal quadrants of the eye (characteristic and specific feature of this disease).

Fig. 2.9.2. Illustration shows the typical facial features of Goldenhar syndrome. Note the right unilateral hypoplasia of the mandible, the small right maxilla compared to the left one (unilateral hypoplasia), the small deformed ear on the right side, and the soft-tissue lesion seen in the right eye (*epibulbar dermoid*)

Signs on Petrous Bone CT

- The scan reveals unilateral or bilateral external auditory canal atresia.
- Contracted tympanic cavity and oval window atresia may be seen.

Cogan Syndrome

Cogan syndrome is a rare disease of unknown origin characterized by nonsyphilitic interstitial keratitis with cochleovestibular defects causing sensorineural hearing loss. Interstitial keratitis is an infectious, chronic, nonulcerative inflammation of the cornea with neovascularization.

The disorder is considered to be an autoimmune disease. The autoimmune origin theory is supported by the development of generalized vasculitis affecting the heart coronaries, aorta, and brain vessels in chronic stages of the disease that respond to steroid therapy.

The disease affects adults between 20 and 40 years of age, although it can also affect children in rare cases.

Patients with Cogan syndrome present with bilateral, rapidly progressing hearing loss with tinnitus often combined with vertigo, dizziness, or ataxia. The diagnosis is made based on the clinical combination of eye abnormalities and cochleovestibular disease.

Cogan syndrome is classified according to its ocular manifestations into two types:

- Typical Cogan syndrome: the disease causes nonsyphilitic interstitial keratitis (affects the cornea only).
- Atypical Cogan syndrome: the disease affects the whole globe, presenting with episcleritis, uveitis, and conjunctivitis.

Systemic manifestations of the disease occur in up to 70% of the patients and include fever, malaise, arthralgias, and weight loss.

Cogan syndrome causes acute autoimmune labyrinthitis, which later leads to diffuse fibrosis, cochlear atrophy, and calcifications causing permanent hearing loss. The patient may need cochlear implantation.

Signs on Petrous Bone CT

The cochlea may show signs of thickening, internal soft-tissue density (fibrosis), and in advanced stages cochlear sclerosis (Fig. 2.9.3).

Fig. 2.9.3. Coronal petrous bone CT illustration shows thickening and sclerosis of the cochlea (*arrowhead*), an advanced stage of Cogan syndrome

Signs on MRI

- In active stage of the disease, the membranous labyrinth shows enhancement and high signal intensity on postcontrast T1-weighted images due to inflammation (labyrinthitis) (Fig. 2.9.4a).
- In advanced stages, a hypointense signal is seen in the membranous labyrinth on both T2- and T1-weighted postcontrast images due to calcification and fibrosis (Fig. 2.9.4b).

For Further Reading

1. Lee D et al. Waardenburg syndrome, clinical photographs. Otolaryngol Head Neck Surg 1996;114:166–167
2. Rarey KE et al. Intralabyrinthine osteogenesis in Cogan's syndrome. Am J Otolaryngol 1986;4:387–390
3. Oysu C et al. Temporal bone imaging findings in Waardenburg's syndrome. Int J Pediatr Otorhinolaryngol 2001;58:215–221
4. Robson CD. Congenital hearing impairment. Pediatr Radiol 2006;36: 309–324
5. Espeso A et al. The diagnosis of hearing loss in children: Common presentations and investigations. Curr Paediatr 2006;16:484–488
6. Phelps PD et al. Radiological malformations of the ear in Pendred syndrome. Clin Radiol 1998;53:268–273
7. Ozluk A et al. Carcinomas of the thyroid and breast associated with Pendred's syndrome: Report of a case. Surg Today, Jpn J Surg 1998;28:673–674
8. Thomas P. Goldenhar syndrome and hemifacial microsomia: Observations on three patients. Eur J Pediatr 1980;133: 287–292
9. Reddy MVV et al. Facio-auricular vertebral syndrome – A case report. Indian J Hum Genet 2005;11(3):156–158
10. Olfat M et al. Cogan's syndrome in childhood. Rheumatol Int 2001;20:246–249
11. Baumann A et al. Cogan's syndrome: Clinical evolution of deafness and vertigo in three patients. Eur Arch Otorhinolaryngol 2005;262:45–49
12. Im GJ et al. Side selection for cochlear implantation in a case of Cogan's syndrome. J Laryngol Otology, 2008;122(3): 310–313
13. Kothari PR et al. ABCD syndrome revisited. Indian J Hum Genet 2006;12(3):144–145

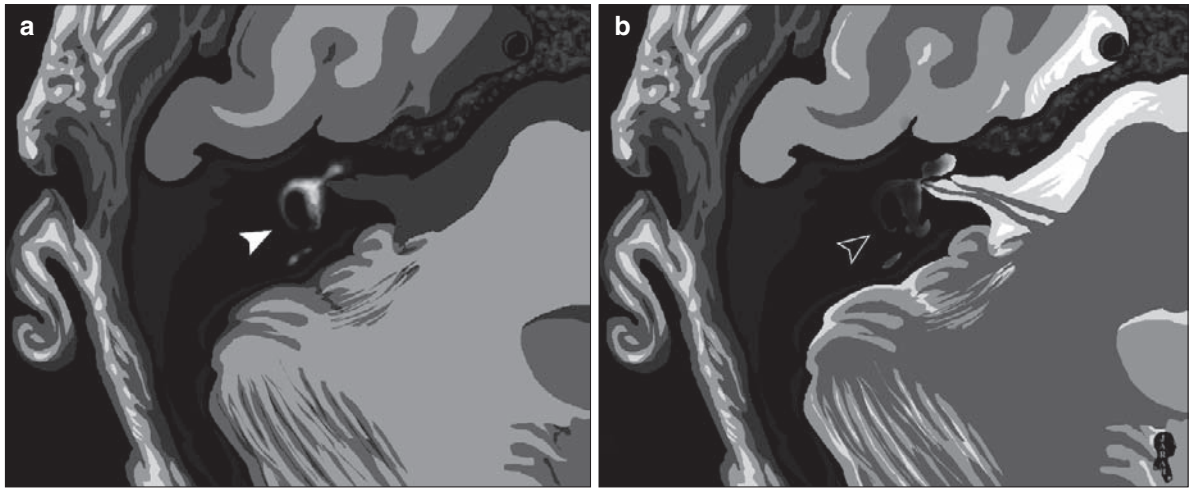

Fig. 2.9.4. Axial T1- and T2-weighted MR illustrations show different stages of the vestibular changes in Cogan syndrome. **a** Illustration representing a postcontrast T1-weighted image showing enhanced vestibule due to labyrinthitis (*arrowhead*). **b** Illustration representing a noncontrast-enhanced T2-weighted image showing loss of the normal fluid signal within the vestibule due to fibrosis and sclerosis (*open arrowhead*)

2.10

Petrous Bone Vascular Anomalies

Congenital vascular anomalies affecting the petrous bone can be asymptomatic or can result in pulsatile tinnitus. Tinnitus is an auditory sensation perceived in the absence of external stimuli. It is described as buzzing, ringing, or humming. Pulsatle tinnitus is defined as tinnitus that follows the patient's pulse. The most common petrous bone vascular anomalies causing pulsatile tinnitus are the aberrant internal carotid artery, high jugular bulb, and persistent stapedial artery.

Aberrant Internal Carotid Artery

The normal carotid artery courses inside the petrous bone in its carotid canal before entering the middle cranial fossa. Aberrant internal carotid artery (ICA) is a rare condition characterized by presence of the ICA inside the middle (tympanic) ear cavity (Fig. 2.10.1). The condition is explained by two theories:

- **The Alternate Blood Flow Theory:** Normally, the ICA inside its canal is separated from the middle ear cavity via the carotid plate, a bony covering that is less than 0.5 mm in thickness. This plate is perforated by a small branch of the ICA called the "caroticotympanic artery," which is a remnant of the embryologic "hyoid artery." The caroticotympanic artery anastomoses over the cochlear promontory with another artery called the "inferior tympanic artery," a branch of the ascending pharyngeal artery. Both arteries supply portions of the medial wall of the tympanic cavity. Aberrant ICA represents an enlarged inferior tympanic artery anastomosing with an enlarged caroticotympanic artery (persistent hyoid artery) with underdevelopment of the cervical portion of the ICA.
- **The Bony Dehiscence Theory:** This is a rare situation characterized by dehiscence of the carotid plate causing the ICA to herniate inside the middle ear cavity. It is seen on MRI or angiography as a "laterally displaced" ICA.

Clinically, the lesion can be asymptomatic or accompanied by pulsatile tinnitus and conductive hearing loss. It can be mistaken with glomus tympanicum or high jugular bulb on otoscopic examination.

Signs on Petrous Bone CT

The ICA is seen inside the middle ear cavity with no bony plate separating it from the middle ear cavity (Fig. 2.10.2).

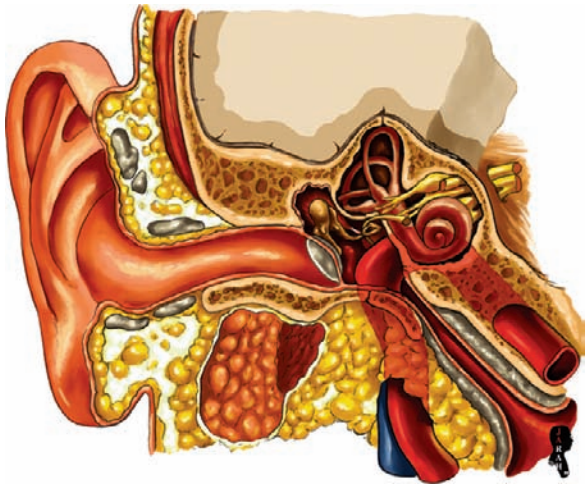

Fig. 2.10.1. Illustration shows aberrant course of the internal carotid artery inside the middle ear cavity

High Jugular Bulb

The jugular bulb is the continuation link between the sigmoid sinus and the internal jugular vein. It lies in the jugular fossa, an oval hollowed area at the internal and inferior surface of the petrous pyramid. The dome of the jugular bulb lies at the floor of the middle ear cavity, at the level of the hypotympanum.

High jugular bulb is a condition characterized by protrusion of the jugular bulb inside the middle ear cavity, commonly due to hypotympanum bone dehiscence (Fig. 2.10.3). The jugular bulb is said to be high if it projects above the bony annulus or the basal turn of the cochlea.

The incidence of high jugular bulb is 5% of the general population; bilateral incidence is found in up to 16% of cases.

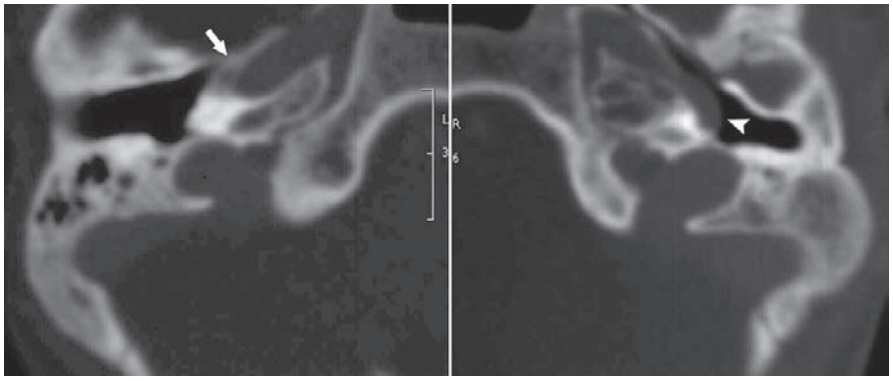

Fig. 2.10.2. Axial bone-window petrous bone CT shows aberrant internal carotid artery inside the middle ear cavity on the left side (*arrowhead*). Note the intact carotid bony plate on the right side (*arrow*) and compare it with the left side

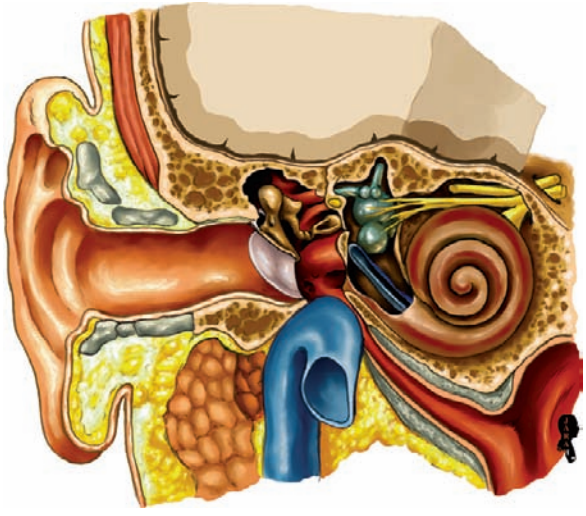

Fig. 2.10.3. Illustration shows bone deficiency (dehiscence) of the hypotympanum with projection of the jugular bulb inside the middle ear cavity at the level of the basal turn of the cochlea (high jugular bulb)

Clinically, it can be asymptomatic in most cases, or accompanied by pulastile tinnitus. Conductive hearing loss can occur if the bulb encroaches over the tympanic membrane or the ossicles. On otoscopic examination, it is difficult to differentiate high jugular bulb from glomus tympanicum or aberrant ICA.

Signs on Petrous Bone CT

The scan shows a mass with a fluid density projecting inside the middle ear cavity with hypotympanum bone dehiscence (Fig. 2.10.4).

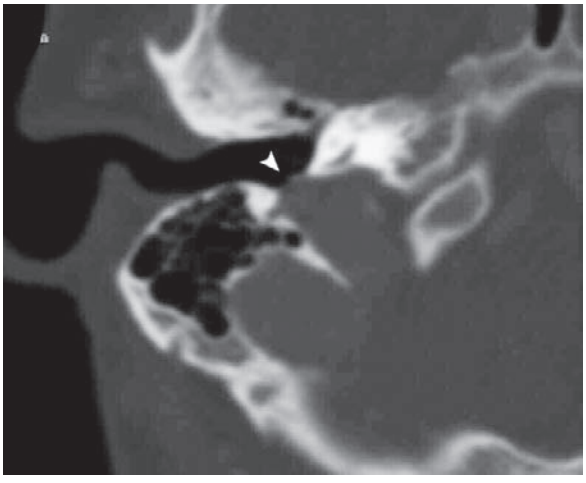

Fig. 2.10.4. Axial bone-window petrous bone CT shows bone dehiscence over the jugular bulb (*arrowhead*)

Persistent Stapedial Artery

Persistent stapedial artery is a rare vascular anomaly that can present in adulthood with pulsatile tinnitus. The stapedial artery is part of the embryonic fetal circulation of the head and neck region. If the fetal artery persists after birth, the middle meningeal artery will not develop, and its arterial territory will be supplied by the stapedial and the ophthalmic arteries.

Persistence of the stapedial artery after birth can be an isolated anomaly or accompanied by an aberrant ICA. It can be seen in cases of trisomy 13, 15, and 21 as well as Paget's disease of the bone.

Signs on Petrous Bone CT

- A mass in the mesotympanum lying near the stapes, which enhances in an arterial fashion after contrast material injection. The key for diagnosis is the relationship of the artery to the stapes (Fig. 2.10.5).
- Foramen spinosum will be absent due to the absence of the middle meningeal artery (Fig. 2.10.6).

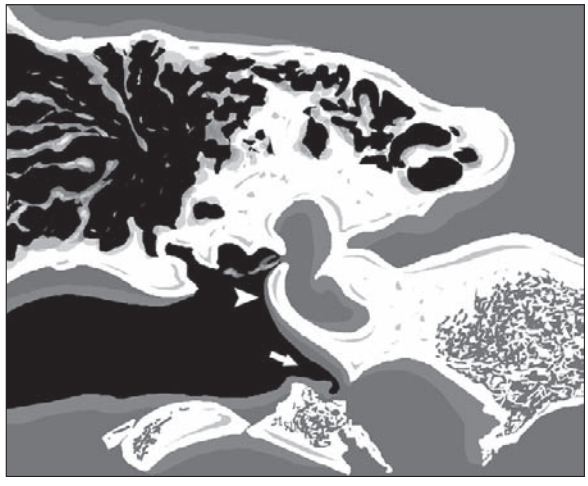

Fig. 2.10.5. Coronal noncontrast-enhanced petrous bone CT illustration shows the persistent stapedial artery with its close relationship to the stapes (*arrowhead*). Note the origin of the artery from the carotid canal (*arrow*)

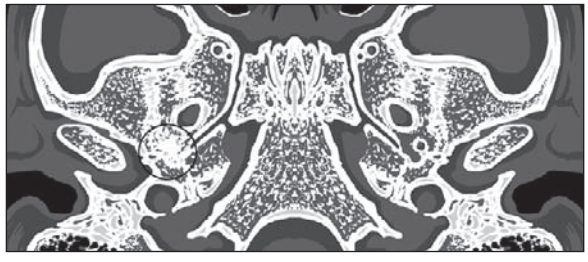

Fig. 2.10.6. Axial base of the skull CT illustration shows absence of the foramen spinosum on the right side (*circle*), a typical finding with persistent stapedial artery

For Further Reading

1. Schwartz JD et al. Aberrant internal carotid artery lying within the middle ear, High resolution CT diagnosis and differential diagnosis. Neuroradiology 1985;27:322–326
2. Sauvaget E et al. Aberrant internal carotid artery in the temporal bone, imaging findings and management. Arch Otolaryngol Head neck Surg 2006;132(1):86–91
3. Lo WWM. Aberrant carotid artery: Radiologic diagnosis with emphasis on high-resolution computed tomography. Radiographics 1985;5(6):985–993
4. Davidson HC. Imaging of the temporal bone. Neuroimag Clin N Am 2004;14:721–760
5. Roche PH et al. High jugular bulb in the translabryrinthine approach to the cerebellopontine angle: Anatomical considerations and surgical management. Acta Neurochir (Wien) 2006;148:415–420
6. Ozturkcan S et al. Surgical treatment of the high jugular bulb by compressing sinus sigmoideus: Two cases. Eur Arch Otorhinolaryngol 2008;265(8):987–991. doi 10.1007/s00405-007-0545-0
7. Lo WWM et al. High-Resolution CT of the jugular foramen: Anatomy and vascular variants and anomalies. Radiology 1984;150:743–747
8. Thiers FA et al. Persistent stapedial artery: CT findings. Am J Neuroradiol 2000;21:1551–1554
9. Branstetter BF IV. The radiologic evaluation of tinnitus. Eur Radiol 2006;16:2792–2802

2.11

Orbital Anomalies

Orbital anomalies are usually seen in infants and children, and are generally rare. Children usually present early in life with visual field disturbance and sometimes with blindness.

Coloboma

Coloboma is a rare congenital orbital anomaly characterized by herniation of the retina through a choroidal defect, creating a cystic pouch within the eye. Another definition for coloboma is absence of some ocular tissue, usually due to malclosure of the fetal intraocular fissure.

The disease has an autosomal dominant mode of inheritance.

Three types of colobomas are found:

- **Optic disc coloboma (morning glory syndrome):** The defect occurs at the optic disc. On fundoscopy, there is enlargement and excavation of the optic disc, which has pale glial tissue in its floor, and is surrounded by an annulus of pigmented choroidal tissue. This appearance is typical for optic disc coloboma (Fig. 2.11.1). The rest of the eye can be normal or microphthalmic.

  The disease is diagnosed in the first year of life due to strabismus (the eyes are not properly aligned with each others) and poor vision.

Fig. 2.11.1 Illustration shows the typical fundoscopic appearance of the optic disc coloboma "morning glory syndrome"

Optic nerve coloboma is usually associated with other anomalies such as optic nerve atrophy, frontosphenoidal encephalocele, and craniosynostosis.

Differential diagnosis of optic nerve coloboma

- **Staphyloma:** a localized, inflammatory expansion (ectasia) of the globe. It lacks the fundoscopic characteristic feature of the optic nerve coloboma.
- **Microphthalmos with cyst:** is a condition characterized by severe malformation of the globe with gross scleral dilatation forming a cyst that can exceed the size of the globe. An important feature on CT is that the cyst neck is smaller than the cyst itself (not as wide as the coloboma).

Signs on Orbital CT

- There is cystic expansion of the optic nerve, which is isodense and is continuous with the vitreous humor (Fig. 2.11.2).
- Calcification of the optic nerve can be seen in cases of nerve atrophy.
- Microphthalmia may or may not be found.

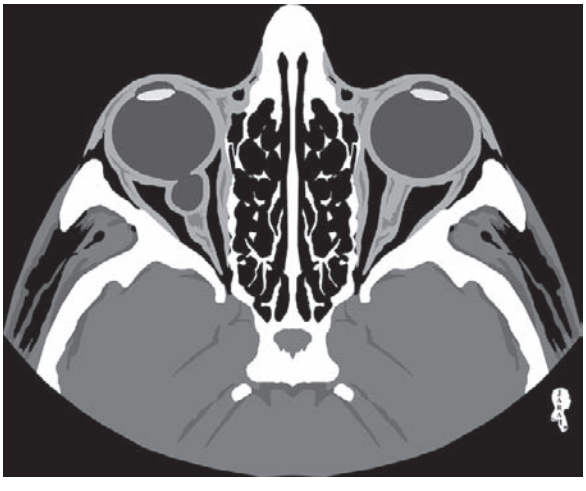

Fig. 2.11.2. Axial orbital CT illustration shows cystic expansion of the right optic disc (optic disc coloboma)

- **Megarbane syndrome:** is a syndrome characterized by microcephaly, coloboma of the iris and optic disc, strabismus, and mental retardation.
- **Retinochoroidal coloboma:** Retinochoroidal coloboma occurs in the inferior aspect of the eye near the optic disc. It is bilateral in up to 60% of cases.

Signs on Orbital CT

The scan shows a small globe (microphthalmia) with a retroocular cyst that is connected to the vitreous humor inferiorly.

Fuch's coloboma (tilted disc syndrome) Fuch's coloboma is a rare congenital malformation characterized by tilting of the optic disc in any direction, with myopia, and minor dilatation of the inferionasal area of the globe due to scleral thinning.

The disease is bilateral in 80% of patients.

There is an association between Fuch's coloboma and craniopharyngioma and craniosynostosis.

Signs on Orbital CT

- Moderate to severe hypoplasia of the choroids, retina, and sclera.
- Focal dilatation of the inferionasal posterior wall of the globe, with oblique insertion of the optic nerve and the retinal arteries (Fig. 2.11.3).

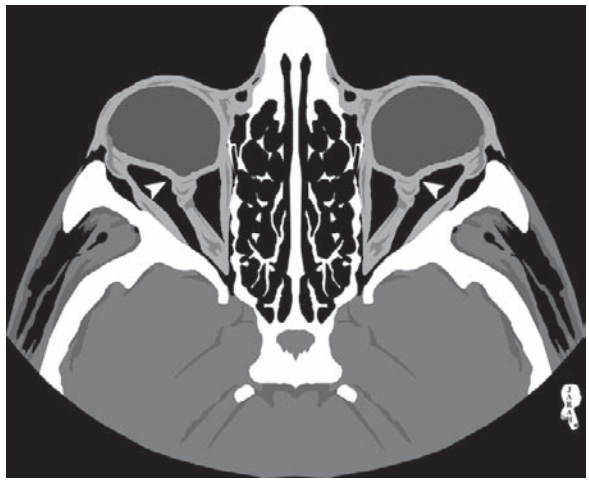

Fig. 2.11.3. Axial orbital CT illustration shows bilateral, abnormal, tilted insertion of the optic nerves into the orbit, a typical sign of "tilted disc syndrome" (*arrowheads*)

Staphyloma

Staphyloma is a condition characterized by bulging of the uvea into a thinned and stretched sclera. It commonly occurs in the posterior aspect of the globe at the temporal side of the optic disc.

Staphyloma is commonly associated with congenital myopia, a condition characterized by painless bulging eye and amblyopia (poor vision in a physically normal eye).

Signs on Orbital CT

The scan shows a focal posterior or anterior bulge within the eye, and an area of thinning or absence of the scleral–uveal rim (Fig. 2.11.4). There is no contrast enhancement after contrast material injection.

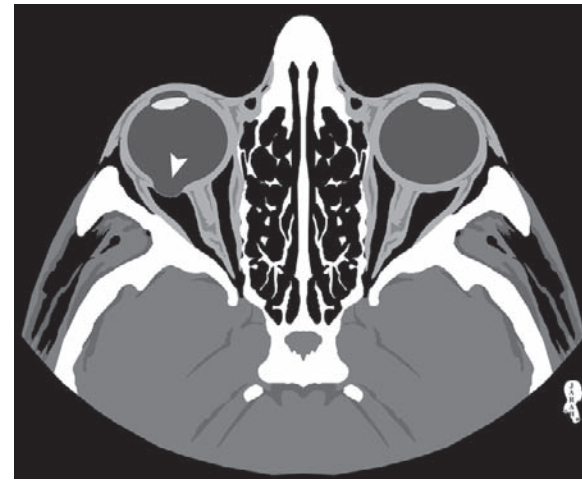

Fig. 2.11.4. Axial orbital CT illustration shows thinning of the scleral-uveal region of the right globe, representing a classic sign of staphyloma (*arrowhead*)

Coats Disease

Coats disease is a rare congenital, idiopathic, nonfamilial disease characterized by an abnormal blood–retinal barrier of the retinal arteries, resulting in leakage of yellowish exudates rich in cholesterol crystals into the vessel wall. Weakening of the blood vessel wall causes the formation of telangiectases (chronic dilatation of groups of capillaries), aneurysms, and subretinal leakage (Fig. 2.11.5), all of which lead to retinal detachment.

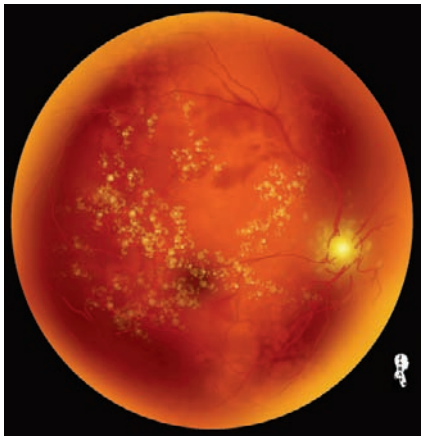

Fig. 2.11.5. Illustration shows the typical fundoscopic appearance of Coats disease. Note the intravitreous hemorrhage and yellowish exodates, which result in a hyperdense and hyperintense appearance of the globe on both CT and MR images

The mean age of presentation is between 3 and 9 years of age.

The disease is unilateral in 80% of cases, and affects men in 70% of cases.

The main signs of the disease are strabismus and leukokoria (white pupillary reflex when one shines a bright light on the pupil; it normally appears red).

The main indication for orbital CT is to differentiate retinoblastoma from chronic Coats disease by searching for intraocular calcifications (very commonly seen in retinoblastoma).

Signs on CT and MRI

- The vitreous humor in the affected eye is homogeneously hyperdense on CT, and hyperintense on T1-weighted and T2-weighted MR images due to exudates and hemorrhage (Fig. 2.11.6).
- Absence of intraocular mass (retinoblastoma presents as intraocular mass).
- Absence of intraocular calcification (calcification in retinoblastoma is very common).
- Partial or incomplete retinal detachment in advanced stages.

Optic Disc Drusen

Optic disc drusen is a rare disease characterized by deposition of hyaline-like material on or near the surface of the optic disc, subsequently resulting in optic disc calcification. It occurs in about 1% of the population.

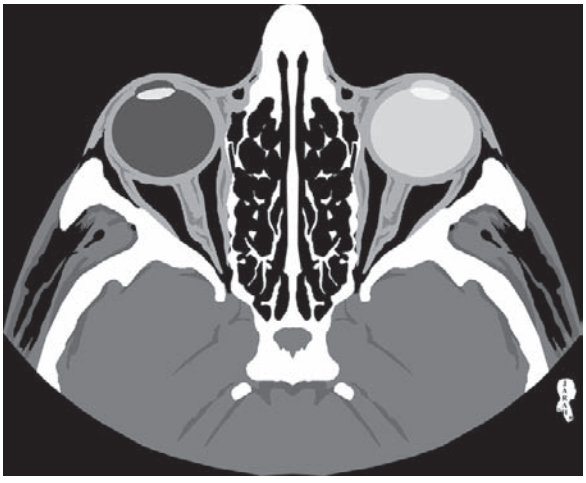

Fig. 2.11.6. Axial orbital CT illustration shows homogeneously hyperdense left globe with absence of a mass lesion, a typical finding in Coats disease

The mean age of presentation is about 12 years of age (hyaline proteins take time to deposit and calcify). The disease is familial, and sometimes discovered accidentally on ophthalmoscopic or CT examinations. Up to 70% of cases are bilateral. Patients present with visual field defects in 80% of cases and with migraine-like headache in up to 30% of cases.

Signs on CT

The scan shows bilateral calcification of the optic disc (Fig. 2.11.7).

Fig. 2.11.7. Axial orbital CT illustration shows bilateral calcification of the optic nerves in optic disc Drusen disease (*arrowheads*)

Persistent Hyperplastic Primary Vitreous

In the embryo, the primary vitreous occupies the space between the lens and the retina, and it is supplied by a branch from the posterior ophthalmic artery called "the hyaloid artery" in the third week of gestation. Later in life, the primary vitreous is replaced by a secondary vitreous and the hyaloid artery regresses by the third trimester. Persistent hyperplastic primary vitreous (PHPV) represents a condition characterized by persistent proliferation of the primary vitreous due to persistence of the hyaloid artery supplying it (Fig. 2.11.8).

PHPV is a disease of infants, and occurs in a unilateral eye. The infant presents with micropthalmia and leukokoria (white papillary reflex). PHPV is the second most common cause of leukokoria after retinoblastoma.

Signs on Orbital CT

- The affected eye is microphthalmic (Fig. 2.11.9).
- Generalized increase in the vitreous density in the affected eye (Fig. 2.11.9).
- An irregular mass with posterior vitreous extensions present at the area of the lens (Fig. 2.11.9).
- The lens is deformed and misshaped, with no signs of calcification. The lens may be replaced by fat (Fig. 2.11.8).
- Retinal detachment may be present.
- Enhancement of the abnormal vitreous mass after contrast material administration.
- Triangular, cylindrical, or tubular intraventral densities representing remnant of the primary vitreous (Fig. 2.11.9).

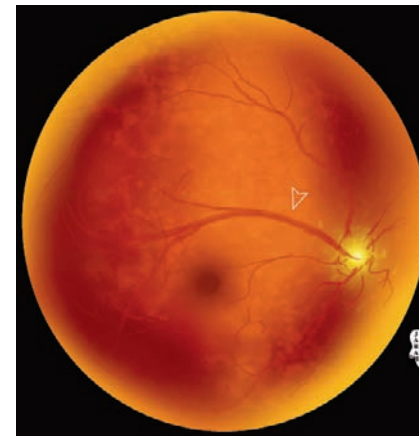

Fig. 2.11.8. Illustration shows the fundoscopic appearance of the persistent hyaloids artery in PHPV (*open arrowhead*)

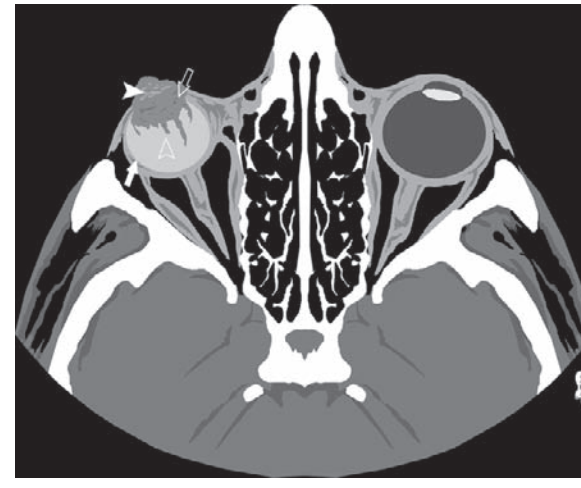

Fig. 2.11.9. Axial orbital CT illustration shows the typical findings in PHPV. Note the small size of the eye (*white arrow*), the irregular mass with posterior vitreous extensions present at the area of the lens (*open arrow*), the deformed lens (*white arrowhead*), and the tubular intraventral densities representing remnants of the primary vitreous (*open arrowhead*). Also, note the hyperdense vitreous humor of the affected right globe compared to the normal left globe

Retinopathy of Prematurity (Retrolental Fibroplasias)

Retinopathy of prematurity is a disease that occurs in premature babies due to abnormal growth of blood vessels within the retina, and fibroblastic overgrowth of a persistent vascular sheath behind the lens as a consequence of premature birth. The disease can progress rapidly within a few weeks resulting in complete blindness.

The disease has similar manifestations and radiological findings to PHPV, but characteristically affects both eyes bilaterally and symmetrically (whereas PHPV affects a single globe). When PHPV occurs in both globes, the only criterion with which to differentiate it from retinopathy of prematurity is the history of the patient.

The disease has a correlation with high oxygen therapy due to prematurity.

Diagnostic criteria:

- History of prematurity with admission to intensive care unit and oxygen therapy.
- Bilateral disease with small globe (Fig. 2.11.10).

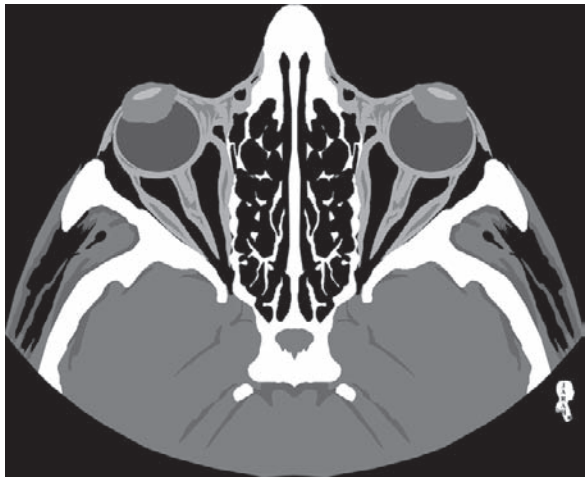

Fig. 2.11.10. Axial orbital CT illustration shows bilateral microphthalmia with masses seen around the lens in the same pattern as PHPV. These findings plus history of prematurity and oxygen therapy are diagnostic criteria for retinopathy of prematurity

For Further Reading

1. Mafee MF et al. Computed tomography of optic nerve colobomas, morning glory anomaly, and colobomatous cyst. Radiol Clin North Am 1987;25(4):693–699
2. Manfre L et al. Bitemporal pseudohemianopia related to the "tilted disk" syndrome: CT, MR, and fundoscopic findings. Am J Neuroradiol 1999;20:1750–1751
3. Chen CS et al. Morning glory syndrome and basal encephalocele. Child Nerv Syst 2004;20:87–90
4. Doglietto F et al. Micropthalmia and colobomatous cyst of the orbit. Acta Neurochir (Wien) 2006;148:1123–1125
5. Murphy BL et al. Optic nerve coloboma (morning glory syndrome): CT findings. Radiology 1994;191:59–61
6. Belden CJ. MR imaging of the globe and optic nerve. Neuroimag Clin N Am 2004;14:809–825
7. Galluzzi P et al. Coats disease: Smaller volume of the affected globe. Radiology 2001;221:64–69
8. Ramirez H et al. Computed tomographic identification of calcified optic nerve drusen. Radiology 1983;148:137
9. Mafee MF et al. Persistent hyperplastic primary vitreous (PHPV): Role of computed tomography and magnetic resonance. Radiol Clin North Am 1987;25(4):683–692
10. Okay CA et al. Megarbane syndrome. Indian J Hum Genet 2008;14(1):27–29

2.12

Congenital Cholesteatoma

Cholesteatoma is a mass of abnormal squamous epithelium (ectopic skin) found inside the middle ear cavity. When cholesteatoma occurs inside the brain, it is referred to as "epidermoid cyst."

Up to 98% of cholesteatomas are acquired, only 2% are congenital.

Acquired cholesteatoma arises as a complication of recurrent, chronic otitis media. It originates commonly from the sinus tympani, or Prussak's space, which is the lateral space between the scutum and the ossicles. Cholesteatoma commonly erodes the scutum first, affecting the integrity of the tympanic membrane. It can also erode the tegmen tympani (roof of the middle ear cavity) causing intracranial extension of the lesion. Patients with acquired cholesteatoma usually present with conductive hearing loss and ear discharge. In contrast, patients with congenital cholesteatoma present with conductive hearing loss and a whitish mass behind an intact tympanic membrane (seen with an otoscope).

Congenital cholesteatoma has the same pathological and radiological features as acquired cholesteatoma, except that it usually occurs in young patients with no history of ear infections.

Congenital cholesteatoma can arise anywhere within the petrous bone, but it is commonly found at the cerebellopontine angle, the petrous apex, the geniculate ganglion region, and the tympanic mastoid cavity.

Congenital cholesteatoma can be mistaken with "cholesterol granuloma" when it affects the petrous apex; differentiation between both lesions can be achieved by MRI.

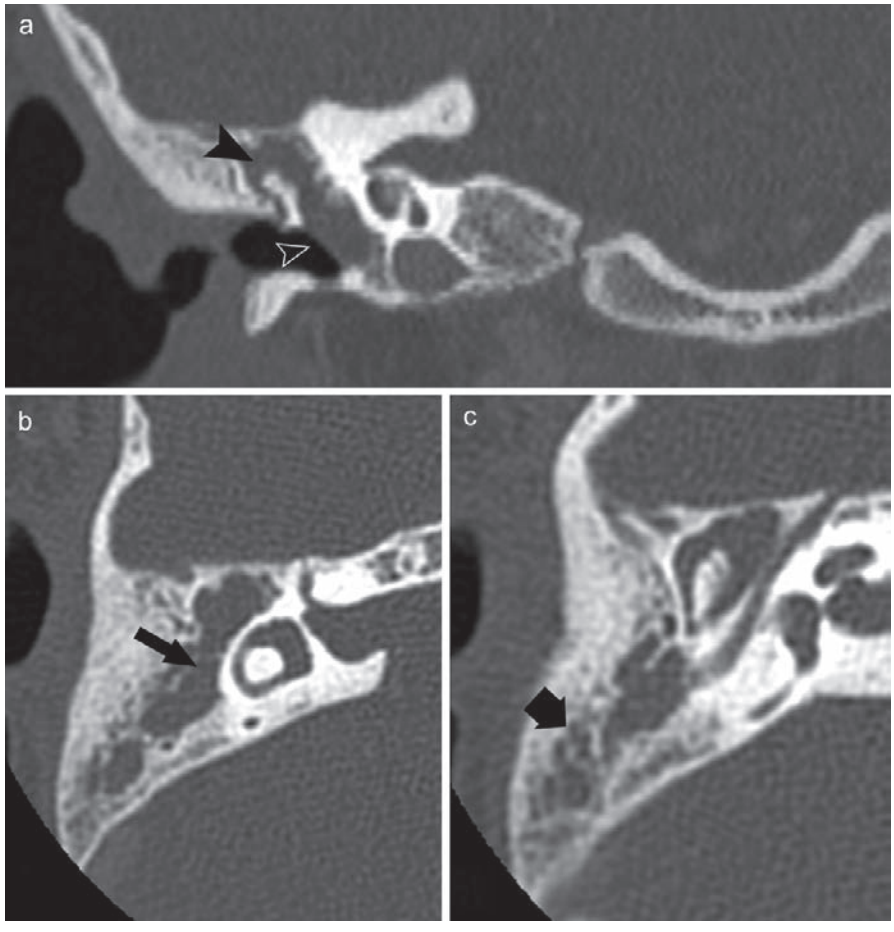

Fig. 2.12.1. Coronal and axial postcontrast petrous CT sections in a 9-year-old patient with congenital cholesteatoma. In **a**, there is an isodense opacity filling the middle ear cavity (black arrowhead), with an intact tympanic membrane (*open arrowhead*). In **b**, the cholesteatoma is seen filling the adetus ad antrum and the mastoid antrum (*black arrow*). In **c**, the middle ear cavity and the mastoid air cells are fully filled by the cholesteatoma (*thick black arrow*). Notice lack of enhancement and bone erosions in all sections

Signs on Petrous Bone CT and MR

- An isodense, nondependent soft-tissue opacity seen within the middle ear cavity with opacified mastoid air cells (Fig. 2.12.1).
- The lesions do not enhance after contrast material administration (diagnostic).
- Signs of bone destruction may be seen (e.g., scutum erosions) (Figs. 2.12.2 and 2.12.3).
- Cholesterol granuloma is an inflammatory mass with fatty and hemorrhagic material commonly found at the petrous apex. Cholesteatoma gives low T1 and high T2 signal intensities, while cholesterol granuloma gives high signal intensity in all sequences due to its mix of hemorrhagic–fatty content.

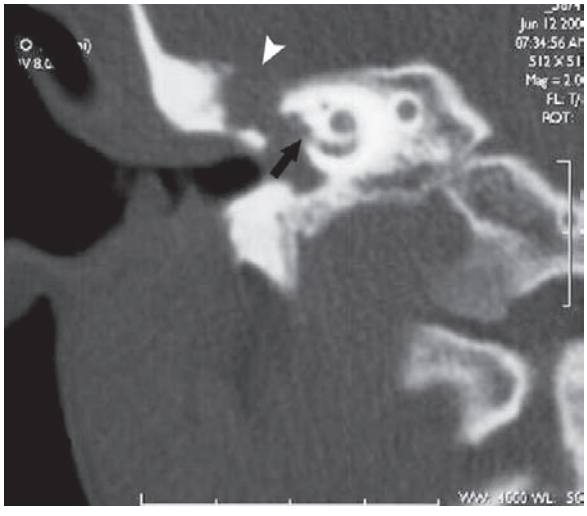

Fig. 2.12.2. Coronal postcontrast petrous CT section in a patient with acquired cholesteatoma. Notice the bony erosion of the tegmen tympani with extension of the cholesteatoma into the middle intracranial fossa (white arrowhead). Notice the lack of enhancement and sever destruction of the ossicles. The cholesteatoma also invades the cochlea forming "labyrinthine fistula" (*black arrow*)

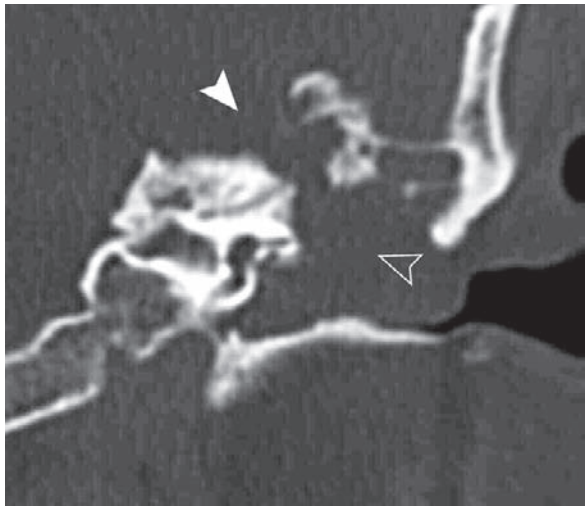

Fig. 2.12.3. Coronal postcontrast petrous CT section in another patient with acquired cholesteatoma. Notice the large cholesteatoma filling the middle ear cavity, eroding the tegmen tympani (white arrowhead), violating the integrity of the tympanic membrane (*open arrowhead*), and completely destroying the ossicles (vanished within the mass)

For Further Reading

1. Gok A et al. Congenital cholesteatoma with spontaneous epidural abscess, sinus thrombosis and cavernous fistula. Neurosurg Rev 1996;19:189–191
2. Davidson CH. Imaging of the temporal bone. Neuroimag Clin N Am 2004;14:721–727

"*This page left intentionally blank.*"

Chapter 3

The Chest and Heart

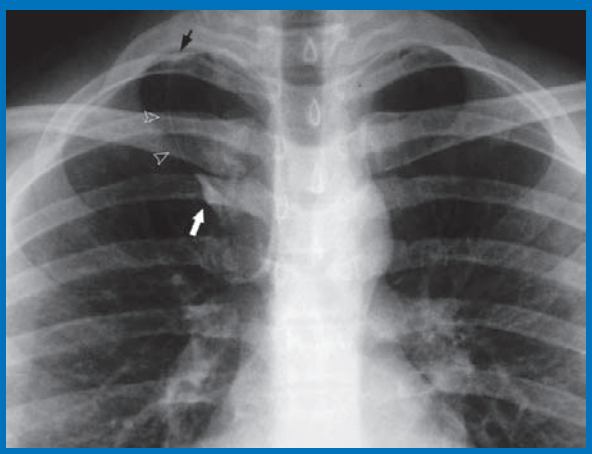

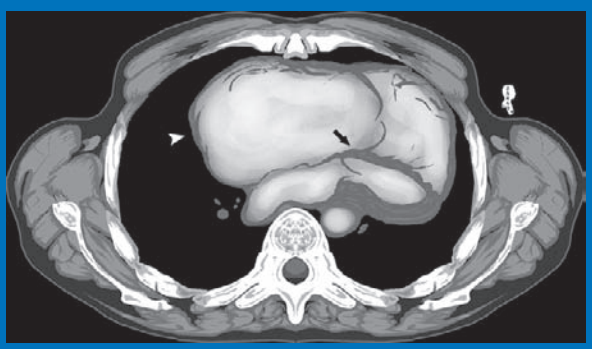

CONTENTS

J. A. Al-Tubaikh, M. F. Reiser: *Congenital Diseases and Syndromes* – An Illustrated Radiological Guide
DOI: 10.1007/978-3-642-00160-4_3, © Springer-Verlag Berlin Heidelberg 2009

3.1

Azygos Fissure

The azygos fissure (AF) is a normal variant that forms when the right posterior cardinal vein fails to migrate over the apex of the right lung to its normal position in the mediastinum. The right posterior cardinal vein, which is a precursor to the upper segment of the azygos vein, carries along pleural layers that entrap a portion of the right upper lobe resulting in "azygos lobe" (Fig. 3.1.1). The AF has four layers of pleura (two parietal and two visceral).

The incidence of azygos lobe on chest radiographs is about 0.4%, with an incidence of 1% in anatomical specimens.

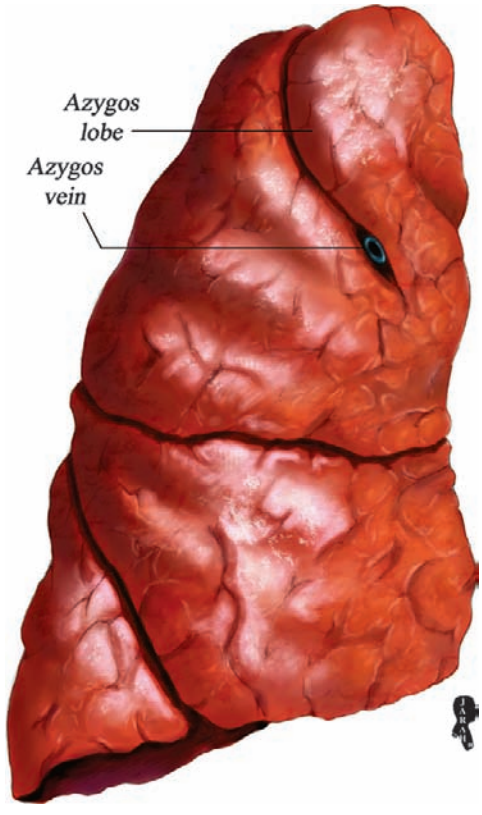

Fig. 3.1.1. Illustration showing the gross anatomy of a lung with azygos fissure. Note the accessory azygos fissure with the new azygos lobe formed

AF is symptomless, and usually discovered incidentally on chest radiographs. It may be mistaken for an intrapulmonary nodal lesion by the examiner who is unaware of its existence.

Signs on Chest Radiographs

The azygos lobe is seen at the right lung apex with the azygos vein lying on its lowermost part forming a "tear-shaped" radio-opaque shadow. A fine convex line crosses the apex of the right lung to merge with a triangular-shaped upper part of the azygos lobe (trigonum parietale). The triangular-shaped area corresponds to a small amount of extrapleural areolar tissue between the parietal layers of the pleura (Fig. 3.1.2).

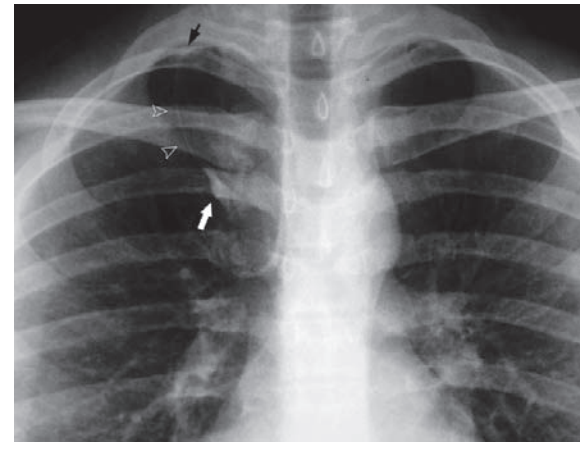

Fig. 3.1.2. Plain chest radiograph shows the azygos fissure components. Note the azygos vein (*white arrow*), the azygos fissure (*open arrowheads*), and the trigonum parietale (*black arrow*)

For Further Reading

1. Caceres J et al. The azygos lobe: Normal variants that may simulate disease. Eur J Radiol 1998;27:15–20
2. Felson B. The azygos lobe: Its variations in health and disease. Semin Roentgenol 1989;24:56–66
3. Arslan G et al. Intrapulmonary right brachiocephalic vein associated with azygos lobe. J Clin Imaging 2000;24:84–85

3.2

Scimitar Syndrome (Hypogenic Lung Syndrome)

Scimitar syndrome is a rare congenital anomaly characterized by complete or partial unilateral pulmonary venous return from the right lung to the inferior vena cava via an anomalous vein. The disease is characterized by:

- Right lung hypoplasia.
- Right pulmonary artery hypoplasia.
- The right upper lobe or the whole right lung has an anomalous arterial supply from the abdominal aorta and venous drainage of the right lower lobe to the inferior vena cava (scimitar vein) (Fig. 3.2.1).

The characteristic appearance of the anomalous vein resembles a short, curved Turkish sword, or "scimitar".

The anomaly almost always occurs on the right side.

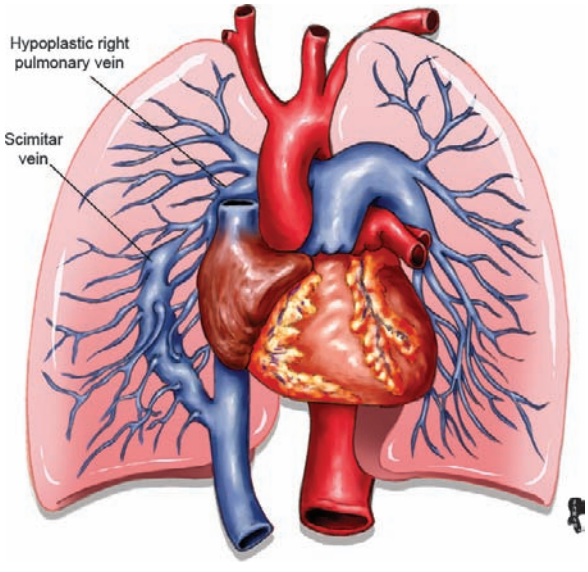

Fig. 3.2.1. Illustration showing the gross anatomical components of the heart and the great vessels in a patient with scimitar syndrome. The right pulmonary vein is hypoplastic and an anomalous, crescent, scimitar-shaped vein drains the right lung to join the inferior vena cava

Scimitar syndrome is an asymptomatic disease in adults. In newborns, the disease may result in pulmonary hypertension, cyanosis, and heart failure, while in children, the disease can present with recurrent chest infections.

Signs on Radiographs

The radiograph shows the anomalous vein that courses from the hilum to the diaphragm creating the shape of a scimitar in the right lung field (Fig. 3.2.2).

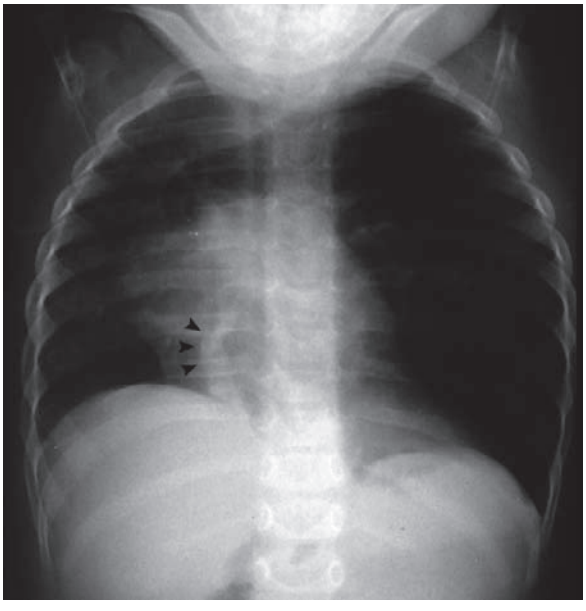

Fig. 3.2.2. Plain chest radiograph of a child shows an anomalous scimitar-like vessel in the lower field of the right lung (*arrowheads*)

Signs on Chest CT

The anomalous vein is seen on the right lung as an intensely enhanced nodule on postcontrast images. Following the vein along the examination will show its connection to the inferior vena cava. Coronal images and volume-rendered 3D reconstruction images are better in illustrating this connection (Fig. 3.2.3).

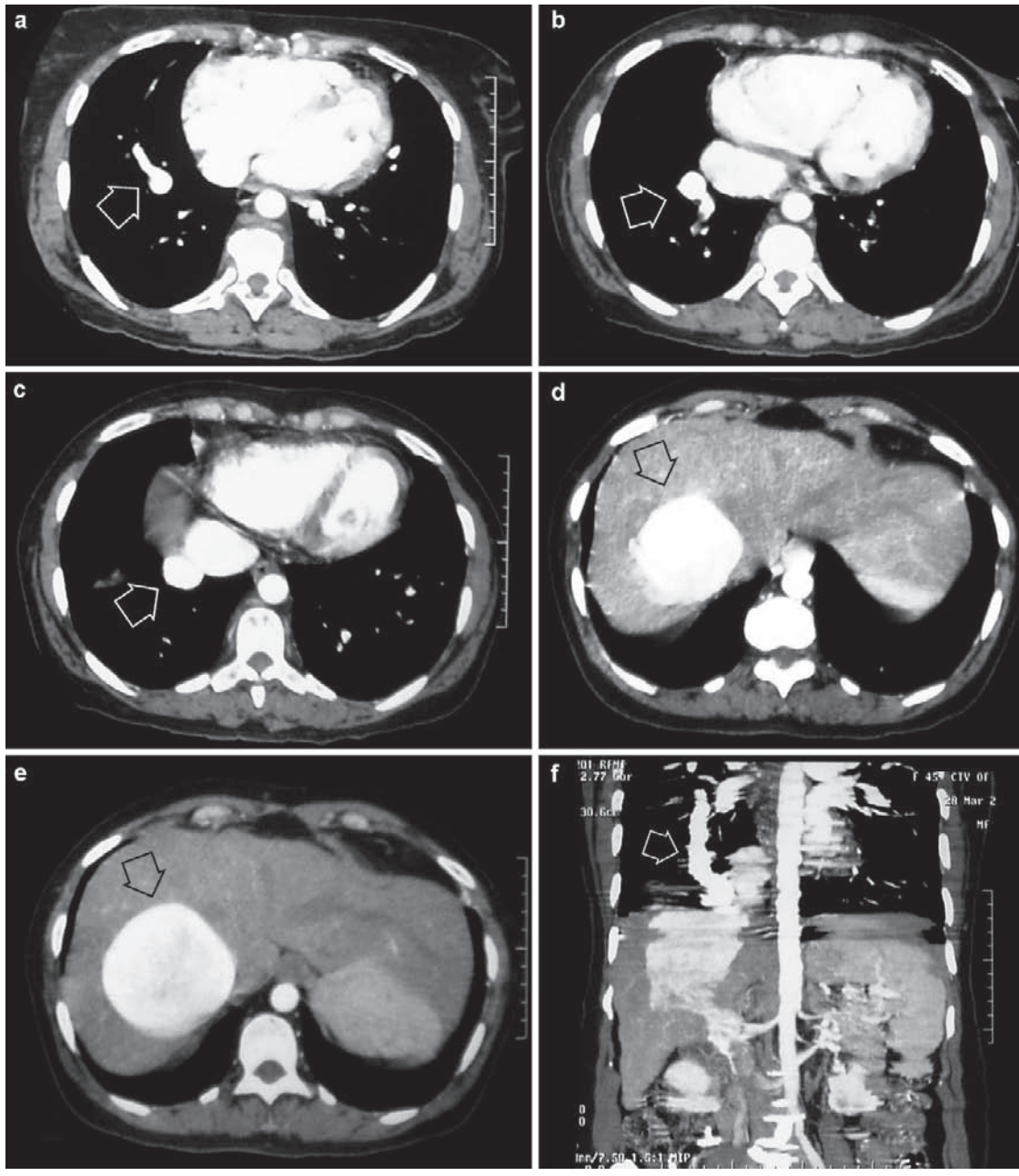

Fig. 3.2.3. Serial axial chest CT with contrast of another patient with scimitar syndrome. If you follow the anomalous vein (*open white arrow*) detected in **a**, you can see how it is related to the inferior vena cava (*open white arrows*) and how it joins it in **b** and **c**. The inferior vena cava is massively dilated (*open black arrows*) in **d** and **e**. **f** Coronal CT image showing the full course of the anomalous scimitar vein (*open white arrow*)

For Further Reading

1. Kramer U et al. Scimitar syndrome: Morphological diagnosis and assessment of hemodynamic significance by magnetic resonance imaging. Eur Radiol 2003;13:L147–L150
2. Gikonyo DK et al. Scimitar syndrome in neonates: Report of four cases and review of the literature. Pediatr Cardiol 1986;6:193–197
3. Wang CC et al. Scimitar syndrome: Incidence, treatment, and prognosis. Eur J Pediatr 2008;167:155–160
4. Christopher B. Ho. Scimitar syndrome. J Emerg Med 2001;21(3): 279–281

3.3

Horseshoe Lung

Horseshoe lung is a rare congenital malformation characterized by fusion of the two lungs by a lung isthmus that connects the right lower lobe to the left lower lobe across the midline. This pulmonary isthmus is located posterior to the heart and anterior to the esophagus and the descending aorta (Fig. 3.3.1).

Typically, the pulmonary isthmus is covered by a layer of parietal pleura that is continuous with the normal parietal pleural covering of both lungs (Fig. 3.3.2).

The fused pulmonary segment is supplied by an anomalous branch of the right pulmonary artery (pulmonary sling).

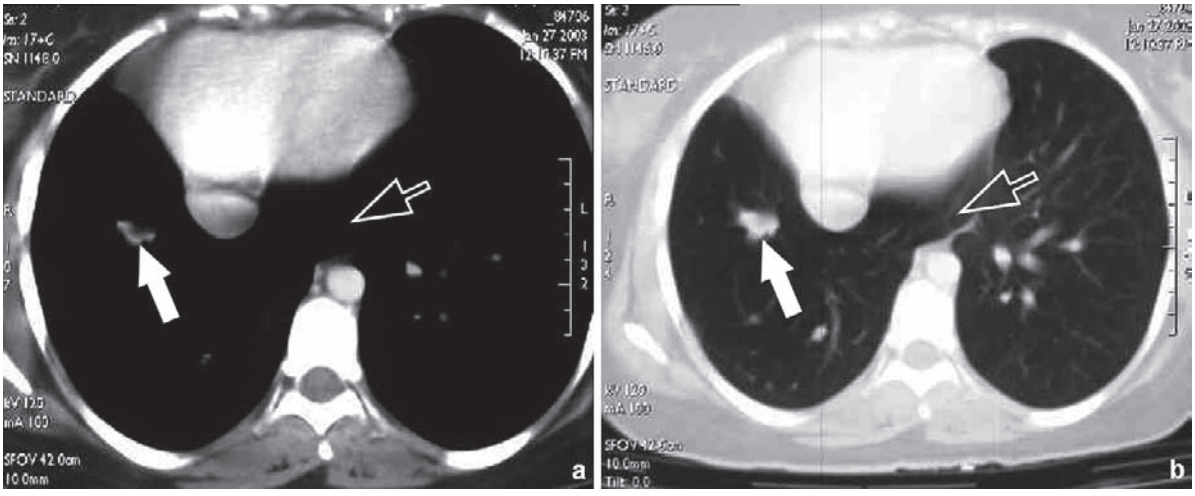

Fig. 3.3.1. Axial chest CT with contrast on mediastinal **a** and lung **b** windows shows an abnormal connection between the lower lung lobes by an isthmus (*open arrow*). An anomalous scimitar vein is seen within the right lung field (*white arrow*)

Fig. 3.3.2. Multiple multislice CT volumetric 3D reconstruction images showing the horseshoe lung in different angles illustrating the abnormal lung isthmus. A continuous pleural covering of the isthmus can be clearly demonstrated (*open arrow*)

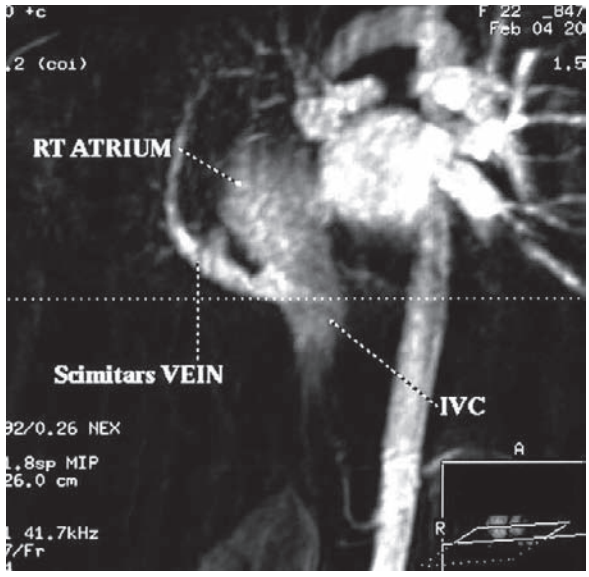

Fig. 3.3.3. Magnetic resonant angiography of the great vessels clearly demonstrates the scimitar vein with its connection to the inferior vena cava

Horseshoe lung is associated with scimitar syndrome in up to 85% of cases (Figs. 3.3.1 and 3.3.3).

For Further Reading

1. Paterson A et al. Imaging evaluation of congenital lung abnormalities in infants and children. Radiol Clin N Am 2005;42:303–323
2. Figa FH et al. Horseshoe lung-a case report with unusual bronchial and pleural anomalies and a proposed new classification. Pediatr Radiol 1993;23:44–47
3. Akay HO et al. Horseshoe lung associated with rare bilateral variant of scimitar syndrome: Demonstration by 64-slice MDCT angiography. Pediatr Radiol 2008;38:563–566. doi 10.1007/s00247–0722–8
4. Hawass ND et al. Horseshoe lung: Differential diagnosis. Pediatr Radiol 1990;20:580–584

3.4

Poland Syndrome

Poland syndrome (PS) is a congenital disease characterized by unilateral hypoplasia of the anterior chest wall components and by ipsilateral upper limb anomalies (Fig. 3.4.1).

In PS, there is unilateral absence of the nipple and the pectoralis major, serratus anterior, and latissimus dorsi muscles. Moreover, the ipsilateral arm is hypoplastic and associated with a small hand, syndactyly, or brachydactyly.

The disease is thought to be caused by intrauterine embryonic insult in the sixth to seventh week of gestation.

Hypomastia (small breast) or amastia (absence of the breast) is found in up to 30% of female patients with PS.

Rib cage depression, scoliosis, and rib aplasia affecting the first five upper ribs are also common features.

The diagnostic criteria for PS include absence of the pectoralis major muscle and breast hypoplasia.

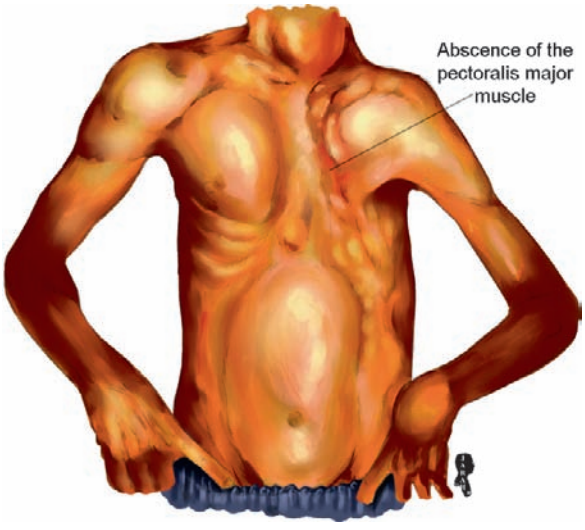

Fig. 3.4.1. Illustration of a patient with left-sided pectoralis major absence (Poland syndrome)

Signs on Chest and Hand Radiographs

- Unilateral radiolucent lung on chest radiographs on both inspiratory and expiratory films due to pectoralis muscle absence or hypoplasia (Fig. 3.4.2).
- Rib, sternal, and scapular deformities.
- Syndactyly or brachydactyly of the ipsilateral hand.

For Further Reading

1. Beer GM et al. Poland's syndrome and vascular malformation. Br J Plast Surg 1996; 49:482–484
2. Renato da Silva Freitas et al. Poland's syndrome: Differential clinical presentations and surgical reconstructions in 18 Cases. Aesth Plast Surg 2007;31:140–146
3. Avci G et al. Mild degree of Poland's syndrome reconstruction with customized silicone prosthesis. Aesth Plast Surg 2003;27:112–115
4. Hönig JF. Correction of Poland's syndrome in a male solid chest wall implants. Eur J Plast Surg 1999;22:128–131

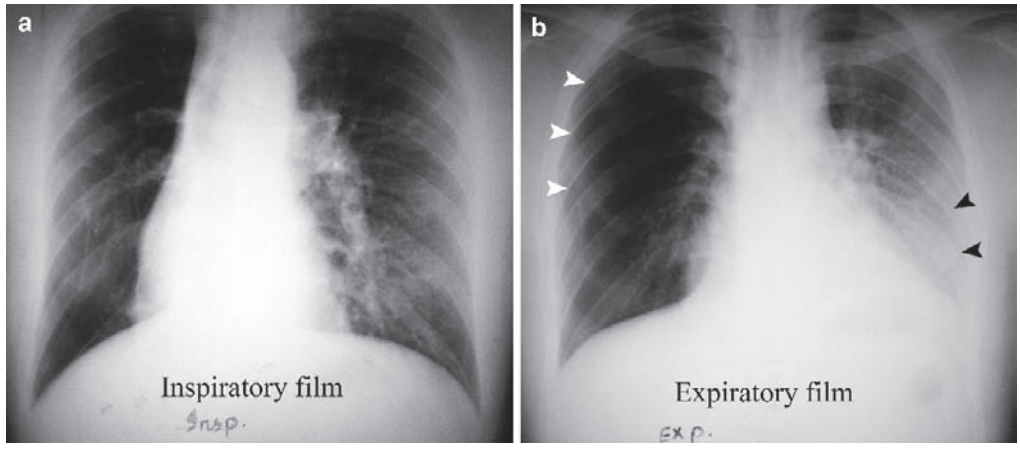

Fig. 3.4.2. Plain chest radiographs of a patient with right-sided absent pectoralis major (Poland syndrome). In the inspiratory film **a**, both lungs appear radiolucent. However, in the expiratory film **b**, the right lung remains radiolucent (*white arrowheads*) while the left lung becomes radio-opaque due to the overshadowing effect from the intact left pectoralis major muscle (*black arrowheads*)

3.5

Bronchiectasis

Bronchiectasis is defined as diffuse or focal irreversible dilatation of the bronchi, usually as a consequence of chronic inflammation and damage to the bronchial wall.

Bronchiectasis starts by cylindrical dilatation of the bronchi as an early stage, which is not visible on chest radiographs. Later, the dilatation progresses until it reaches the form of cystic dilatation in the last stages of the disease, which is visible on plain radiographs and high-resolution CT (HRCT).

Signs on Chest Radiograph

- Cystic interstitial pattern: multiple cysts arranged in bundles forming a "honeycomb appearance."
- Tram line shadow: it is seen in the lung periphery as two thick, white, parallel lines separated by a black line representing dilated bronchial walls.

Signs on HRCT

- Dilatation of the peripheral bronchi (they are usually very small and not seen).
- The bronchi are greater than the accompanied pulmonary artery.

Bronchiectasis can be part of syndromes such as:

- **Right Middle Lobe Syndrome:** Right middle lobe syndrome is a disease characterized by a spectrum of conditions affecting mostly the right middle lobe and the lingula. These conditions range from atelectasis, pneumonia, and bronchiectasis (Figs. 3.5.1 and 3.5.2).

  Most of these patients have had asthma or a history of familial atopic diseases.
- **Swyer–James Syndrome/Macleod Syndrome:** Swyer–James syndrome is a rare disorder characterized by hyperlucent lung due to air trapping with normal or reduced volume in one lung only (small and hyperlucent lung); the disorder is commonly associated with pulmonary artery hypoplasia. Reduction in the pulmonary vessels later leads to bronchitis and bronchiolitis obliterans. Bronchiectasis develops later in life as a complication to the previous bronchiolitis obliterans infection.

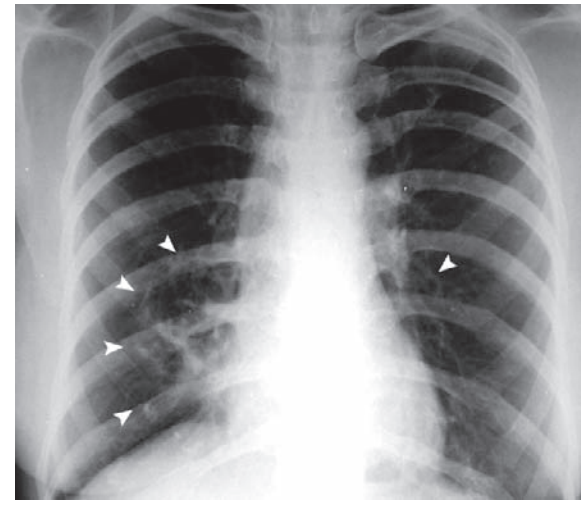

Fig. 3.5.1. A posteroanterior plain chest radiograph shows honeycomb appearance affecting mainly the right middle lobe, and to a lesser extent the lingula (*arrowheads*). These are classic findings in right middle lobe syndrome

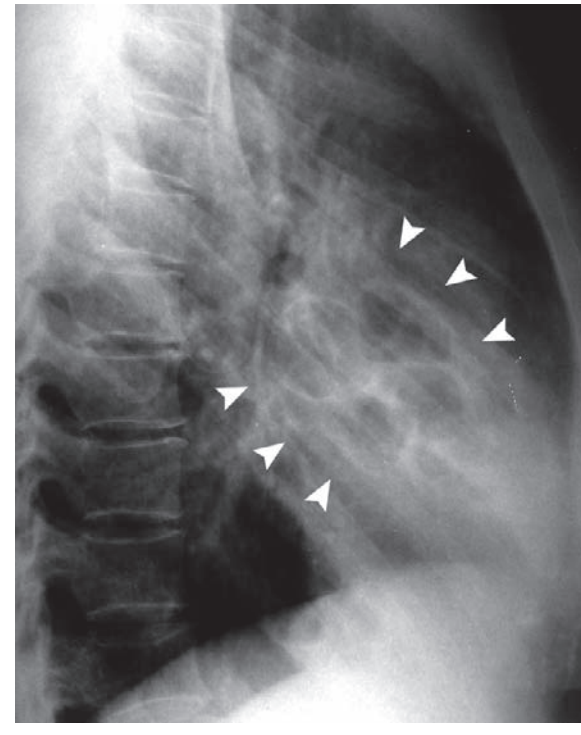

Fig. 3.5.2. A lateral plain chest radiograph of the same patient shows the honeycomb appearance affecting the right middle lobe in a better view (*arrowheads*). Note the massive cystic dilatation of the bronchi

Signs on HRCT

The scan shows a small and hyperlucent lung, associated with reduction in the vasculature of the pulmonary arteries in the affected lung (diagnostic).

- **Kartagener Syndrome:** Kartagener syndrome is a disease characterized by chronic sinusitis, bronchiectasis, and dextrocardia (Figs. 3.5.3 and 3.5.4).

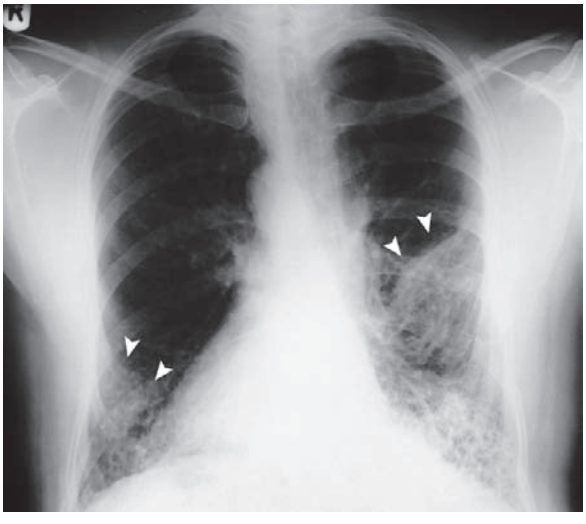

Fig. 3.5.3. A posteroanterior plain chest radiograph shows a case of Kartagener syndrome. Note the multiple bronchiectatic lung changes with superimposed pneumonia (*arrowheads*). Also, note the right-sided heart position (dextrocardia)

Fig. 3.5.4. Lung-window HRCT image shows the findings in Kartagener syndrome. Note the dextrocardia with bilateral, scattered, dilated bronchi with thick walls (*arrowheads*)

The disease has an autosomal recessive mode of inheritance.

- **Mounier-Kuhn Syndrome:** Mounier-Kuhn syndrome is a rare disease characterized by bronchiectasis associated with tracheobronchomegaly. The trachea and its main branches are dilated due to atrophy or absence of the elastic fibers and smooth muscle cells.
- **Cystic Fibrosis:** Cystic fibrosis is a multisystemic disease characterized by production of thick mucus in the respiratory system with failure of respiratory ciliary function, leading to blockage of the bronchi. Mucus stasis and recurrent chest infections cause the development of bronchiectasis later in life, mainly affecting the upper lobes (Fig. 3.5.5). The disease has an autosomal recessive mode of inheritance.

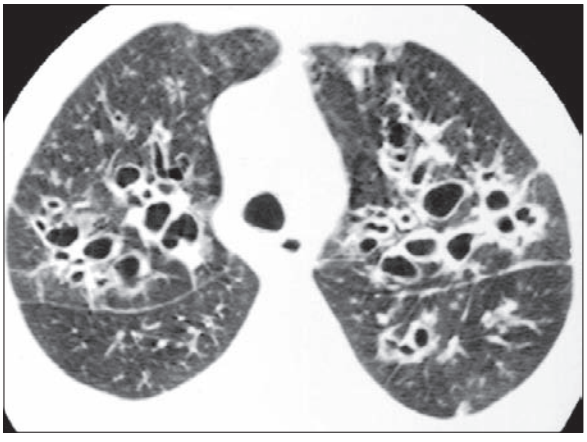

Fig. 3.5.5 Lung-window HRCT image shows bilateral, severe, cystic dilatation of the bronchi in a patient with cystic fibrosis

For Further Reading

1. Livingston GL et al. Right middle lobe syndrome in children. Int J Pediatr Otorhinolaryngol 1987;13:11–23
2. Yikilmaz A et al. Swyer-James syndrome with pulmonary vein hypoplasia detected by multislice CT. Eur J Radiol Extra 2005;56:79–81
3. Peters ME et al. Swyer-James-Macleod syndrome: A case with baseline normal chest radiograph. Pediatr Radiol 1982;12:211–213
4. Tek I et al. Kartagner's syndrome with dextrocardia and corrected transposition of the great arteries. Int J Cardiol 2000;75:305–308
5. Ghanei M et al. Mounier-Kuhn syndrome: A rare cause of severe bronchial dilatation with normal pulmonary function test: A case report. Respir Med 2007;101:1836–1839
6. Robinson TE. Imaging of the chest in cystic fibrosis. Clin Chest Med 2007;28:405–421

3.6

Osler-Weber-Rendu Syndrome (Hereditary Hemorrhagic Telangiectasia)

Osler-Weber-Rendu syndrome (OWRS) is a rare disease characterized by abnormal vascular development ranging from small mucocutaneous telangiectasias to large arteriovenous malformations (AVMs). Telangiectasias are small, linear, dilated blood vessels located near the surface of the skin and the mucosa.

The disease has an incidence of 1 in 10,000 in the general population, and has an autosomal dominant mode of inheritance.

The diagnosis of OWRS requires at least two out of four major criteria (Curacao criteria)

- Sneezing blood (epistaxis).
- Cutaneous and mucosal telangiectasias.
- Visceral AVMs.
- Family history of OWRS, or a first-degree relative affected by the disease.

Patients present clinically with recurrent attacks of epistaxis, which is the first and the most common feature of the disease. Epistaxis is caused by rupture of the telangiectatic blood vessels in the nasal mucosa.

Clinical examination reveals multiple telangiectasias found on the tongue, palate, arm, trunk, and fingertips (50–80%).

Formation of AVMs in different regions in the body is another crucial manifestation of the disease. AVMs can be found in the lungs, brain, and gastrointestinal tract. Cerebral AVMs occur in 15% of cases and produce multiple symptoms like headache, migraine, seizures, strokes, and subarachnoid hemorrhage when ruptured. Pulmonary AVMs occur in 15–30% of cases, while gastrointestinal AVMs are seen in 13–45% of cases. Pulmonary AVMs can result in coughing blood (hemoptysis) or paradoxical embolism resulting in stroke. Gastrointestinal AVMs may result in microcytic hypochromic anemia due to acute or chronic gastrointestinal bleeding.

Signs on CT

- In the lungs, AVMs are seen as multiple nodules with typical feeding vessels. The nodules enhance intensely after contrast material injection (Figs. 3.6.1 and 3.6.2).
- In the gastrointestinal tract, AVMs show the same picture as the pulmonary AVMs (Fig. 3.6.3).
- In the brain, an unruptured AVM appears as an enhancing lesion related to the arterial tree and the circle of Willis, typically at the areas of vascular union between the cerebral arteries. In contrast, a ruptured AVM appears as an intraparenchymal or subarachnoid hemorrhage. Subarachnoid hemorrhage is identified when the blood fills the intracranial cisterns and the sylvian fissures.
- Brain abscess may occur in 10% of cases when pulmonary AVMs are present. Recurrent cerebral abscesses should raise suspicion of OWRS.

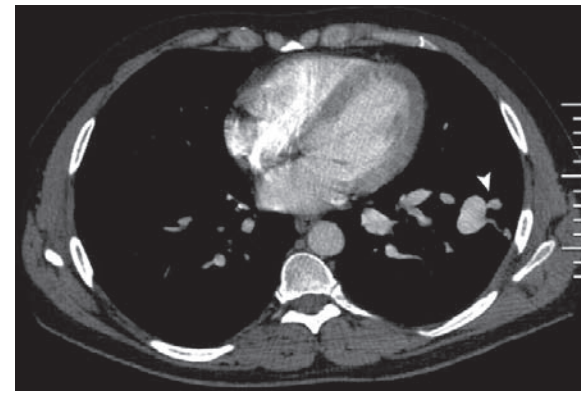

Fig. 3.6.1. Axial chest CT image shows bilateral multiple nodules affecting the left lung more than the right one in a patient with OWRS. Note the feeding vessels of the nodule, which is a typical sign of AVMs (*arrowhead*)

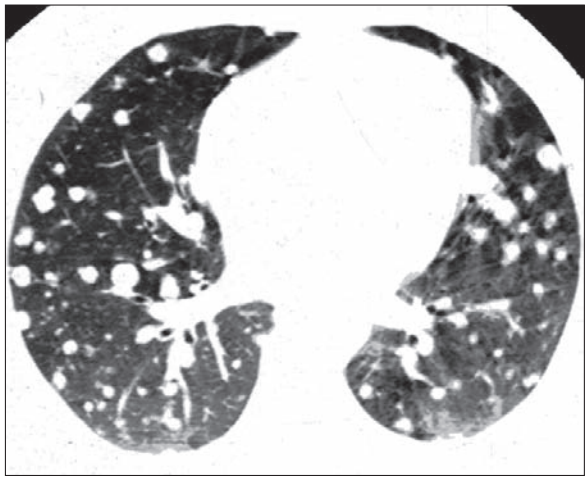

Fig. 3.6.2. Axial lung-window chest CT image shows bilateral extensive AVMs in another patient with OWRS

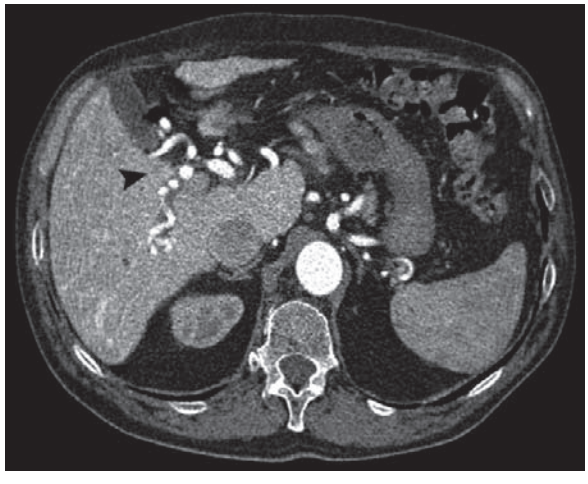

Fig. 3.6.3. Axial abdominal CT shows liver AVMs in another patient with OWRS (*arrowhead*)

For Further Reading

1. te Veldhius EC et al. Rendu-Osler-Weber disease: Update of medical and dental considerations. Oral Surg Oral Med Oral Pathol Oral Radiol Endon 2008;105:e38–e41
2. McDonald MJ et al. Rendu-Osler-Weber syndrome: A current perspective on cerebral manifestations. J Clin Neurosci 1998;5(3):345–350

3.7

Aortic Arch Anomalies

Anomalies of the aortic arch range from simple valvular, asymptomatic anomalies to anomalies associated with dyspnea and recurrent chest infections due to the direct relationship of the aortic arch to the trachea. This section discusses the main aortic arch anomalies commonly encountered during radiological examinations.

Right-Sided Aortic Arch

Right-sided aortic arch (RAA) is an uncommon congenital anomaly where the aortic arch is located on the right side, while the heart is normally positioned (left side).

The anomaly has an incidence about 0.14% of the general population, and patients may present with tracheal obstruction, dysphagia, or recurrent chest infections.

In the embryological development of the aorta, a ventral aorta gives rise to two aortic arches on each side of the trachea; both arches fuse together posteriorly to form a common descending aorta. Each arch has its own ductus arteriosus, common carotid artery, and subclavian artery (Fig. 3.7.1). Normally, the right arch regresses after the right subclavian artery conducts its normal branches. Interruption of the left arch at different levels causes persistence of the right aortic arch.

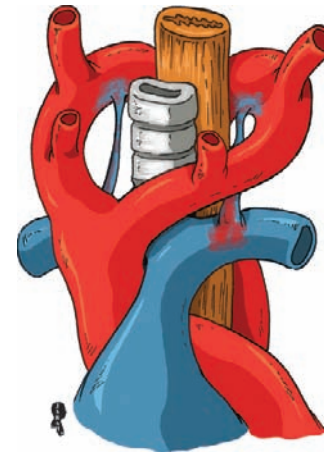

Fig. 3.7.1. Illustration showing the primitive common aortic arch giving rise to the right and left aortic arches on each side of the trachea. Each arch has its own ductus arteriosus, common carotid artery, and subclavian artery

There are three main types of left aortic arch interruptions:

- **Right aortic arch with aberrant left subclavian artery:** this anomaly arises due to regression of the left aortic arch between the left common carotid artery and the left subclavian artery (Fig. 3.7.2).
- **Right aortic arch with isolated subclavian artery:** this anomaly arises due to regression of the left aortic arch before and after the left subclavian artery. The artery is connected to the aorta via a patent ductus arteriosus (Fig. 3.7.3).

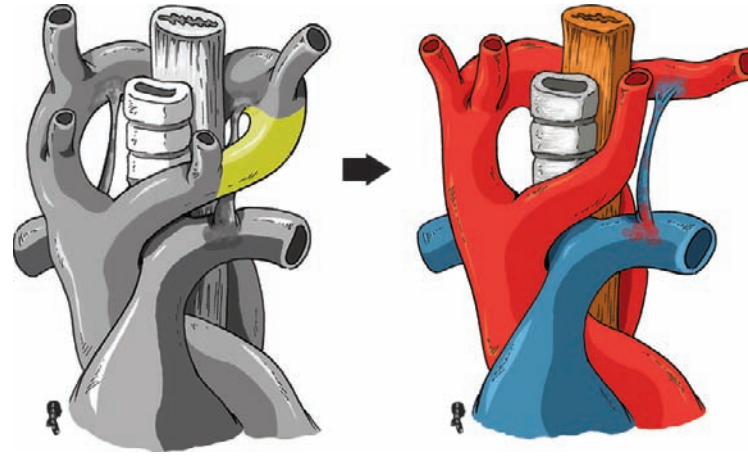

Fig. 3.7.2. Illustration showing the origin of the right aortic arch with the left aberrant subclavian artery

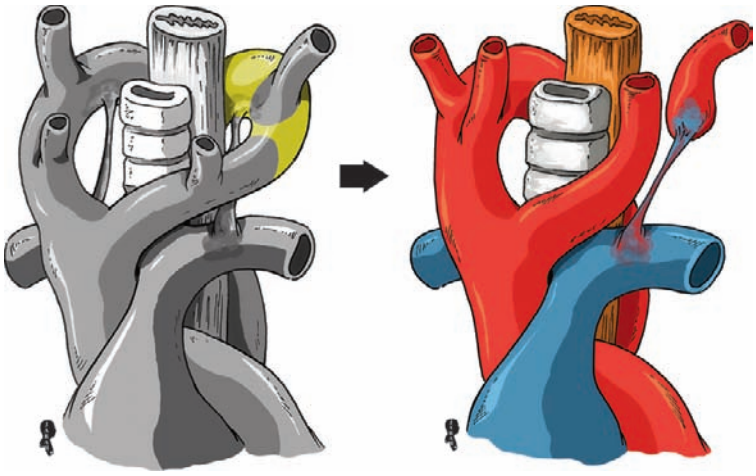

Fig. 3.7.3. Illustration showing the origin of the right aortic arch with the isolated left subclavian artery

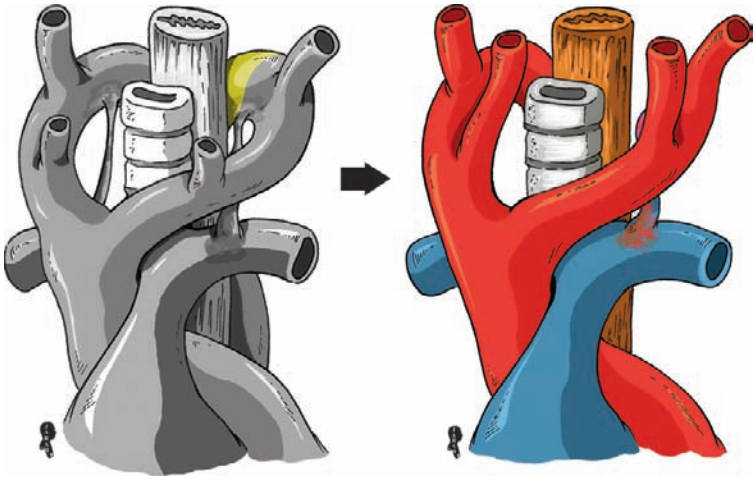

Fig. 3.7.4. Illustration showing the origin of the mirror-image right aortic arch

- **Mirror-image right aortic arch:** this arch has exactly the same branches as the left arch but is located on the right side. It arises due to regression of the left aortic arch segment behind the left subclavian artery (Fig. 3.7.4).

RAA can be associated with other cardiovascular anomalies such as tetralogy of Fallot, complete transposition of the great arteries, and Kommerell diverticulum.

Signs on Chest Radiographs, CT, and MRI

- On chest radiographs, MRI, and CT, the aortic arch is located on the right side (Figs. 3.7.5 and 3.7.6).
- An aberrant left subclavian artery may be seen running posterior to the esophagus.

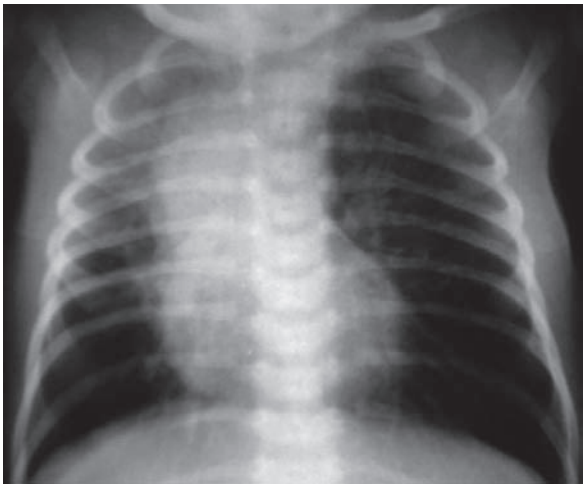

Fig. 3.7.5. Anteroposterior chest radiograph of a baby shows right-sided aortic arch

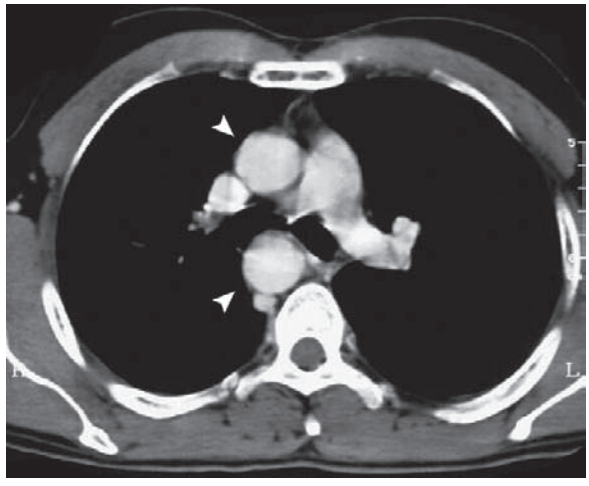

Fig. 3.7.6. Axial postcontrast chest CT image shows right-sided aortic arch in a patient with mirror-image type (*arrowheads*)

Double Aortic Arch (Aortic Ring)

Aortic ring is a congenital anomaly that arises due to persistence of the right and left fourth branchial arches between the sixth and eighth week of gestation, resulting in the formation of double aortic arch around the trachea (Fig. 3.7.7).

Babies and young children with aortic ring commonly present with stridor, swallowing problems, and recurrent chest infections due to vascular compression over the trachea and esophagus.

Symptoms are usually present at birth, and become obvious in early childhood starting from 3 weeks to 2 years of age.

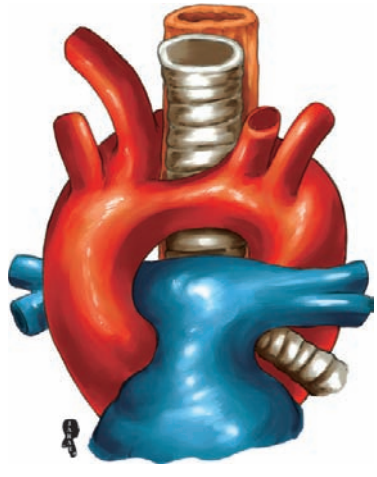

Fig. 3.7.7. Illustration showing aortic ring anomaly

Signs on Chest Radiographs and CT

- The plain radiograph might be normal or show widening of the upper mediastinum (Fig. 3.7.8).
- On CT, the trachea is seen surrounded by two aortae, with the second arch located between the trachea and the vertebral body (Fig. 3.7.9).

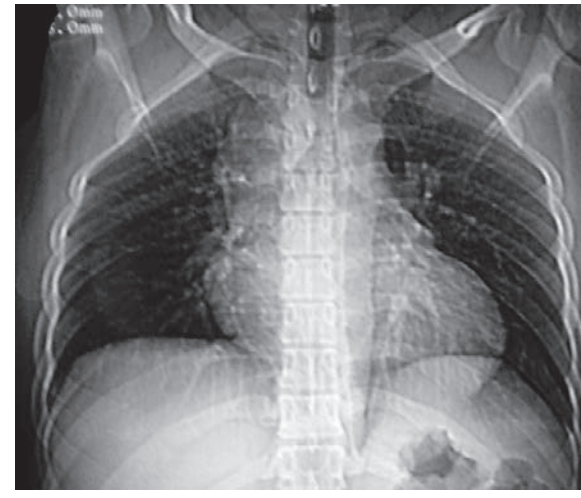

Fig. 3.7.8. Plain chest radiograph shows widening of the mediastinum in a patient with aortic ring

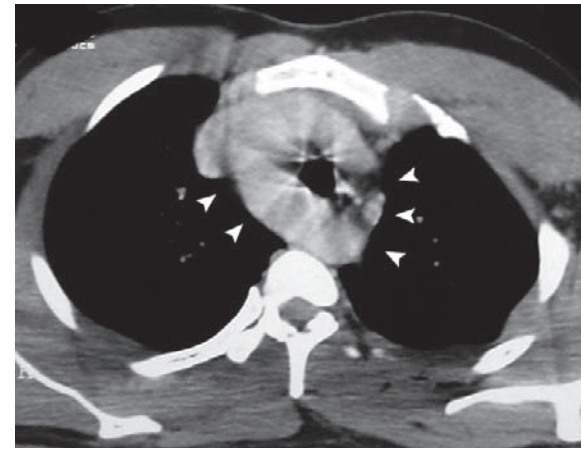

Fig. 3.7.9. Axial chest CT image shows the aortic ring. Note how the trachea is completely surrounded by the aortic arches in all directions (*arrowheads*)

Kommerell Diverticulum

Left-sided aortic arch with aberrant right subclavian artery is a rare anomaly of the great vessels with an incidence of 0.5–2% of the general population. Kommerell diverticulum (KD) is a rare condition characterized by

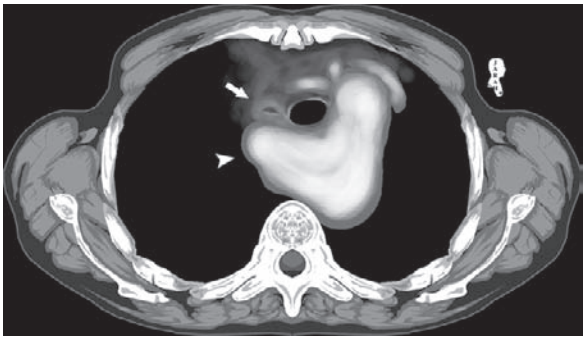

Fig. 3.7.10. Axial postcontrast chest CT illustration shows Kommerell diverticulum (*arrowhead*). Note the location of the diverticulum behind the esophagus (*arrow*), where the aberrant right subclavian artery passes

aneurysmal dilatation of the origin of the aberrant right subclavian artery from the descending aorta (Fig. 3.7.10). Most KD patients are asymptomatic.

Bicuspid Aortic Valve

The normal aortic valve is composed of an annulus, three cusps, and commissures. When the aortic valve has only two cusps (anterior and posterior), it is called "bicuspid aortic valve." The anomaly is thought to be caused by congenital fusion of the cusps with a fibrous raphe.

Bicuspid aortic valve (BAV) is the most common cardiac anomaly seen in adults with a prevalence of 2% of the general population.

Patients may be asymptomatic, or complain of symptoms caused by the coarctation of the aorta, which is commonly associated with BAV. BAV is one of the common causes of early aortic insufficiency or stenosis (at 40 years).

Signs on CT and MRI

- CT or MRI shows an aortic valve with two leaflets clearly seen on systole and diastole (Fig. 3.7.11).
- Coarctation of the aorta with its "inverted 3 sign" may be present.

Aortic Nipple

Aortic nipple is a radiographic term used to describe a focal bulge of the aortic knuckle classically seen on chest radiographs. Aortic nipple represents a lateral projection of the left superior intercostal vein over the aortic arch (Fig. 3.7.12).

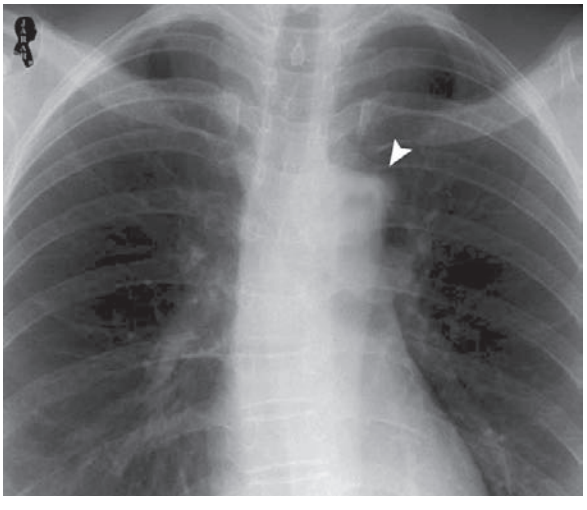

Fig. 3.7.12. Posteroanterior digitally manipulated chest radiograph illustrates the aortic nipple as focal bulging over the aortic arch (*arrowhead*)

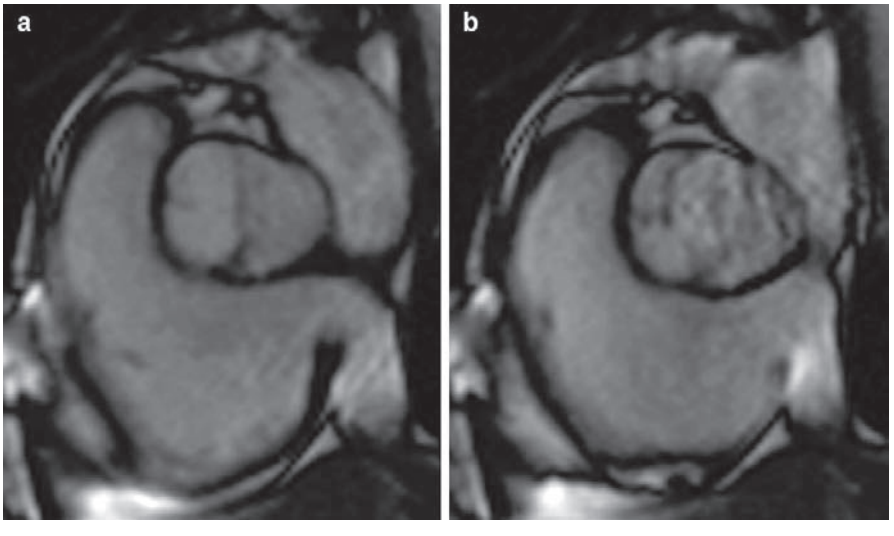

Fig. 3.7.11. MR image of the aortic valve shows bicuspid aortic valve. Note the two leaflet configuration during diastole **a**, and systole **b**

For Further Reading

1. D'Souza VJ et al. Mirror-image right aortic arch: A proposed mechanism in symptomatic vascular ring. Cardiovasc Intervent Radiol 1985;8:134–136
2. Knight L et al. Right aortic arch: Types and associated cardiac anomalies. Circulations 1974;50:1047–1051
3. Sakalihassan N et al. Right aortic arch with aberrant left subclavian artery. Report of two cases. Surg Radiol Anat 1991;13:327–331
4. Saito R et al. Esophageal cancer associated with right aortic arc: Report of two cases. Jpn J Surg 1999;29:1164–1167
5. Cina CS et al. Kommerell's diverticulum and right-sided aortic arc: A cohort study and review of the literature. J Vasc Surg 2004;39:131–139
6. Ota T et al. Surgical treatment of Kommerell's diverticulum. J Thorac Cardiovasc Surg 2006;131:574–578
7. Garti IJ et al. Type C double aortic arch. Cardiovasc Radiol 1978;1:143–145
8. Machiels F et al. A Functioning double aortic arch in an infant: A case report. Pediatr Radiol 1994;24:76–77
9. Ciotti GR et al. Morphology and function of the bicuspid aortic valve with and without coarctation of the aorta in young. Am J Cardiol 2006;98:1096–1102

3.8

Coronary Artery Anomalies

Anomalies of the coronary arteries are usually asymptomatic and clinically insignificant unless they cause clinical manifestations. They occur in 0.5–1% of the population in total.

Some coronary anomalies carry the risk of sudden cardiac death in young athletes, from where the importance of recognizing such anomalies in coronary CT angiography comes into play. Coronary CT angiography is considered the method of choice for investigating angina in young patients and athletes.

Anomalous Aortic Origins of the Coronary Arteries

In these anomalies, the left coronary artery (LCA) arises from the right coronary artery (RCA) or vice versa.

The danger of this anomaly arises when the anomalous artery runs between the aorta and the pulmonary trunk (interarterial groove) making it susceptible to compression between these two large vessels in cases of hypertension and muscular activity. Running of the anomalous coronary artery in the interarterial groove is the second most common cause of sudden cardiac death in young people.

Single Coronary Artery

In single coronary artery, all the coronary arteries arise from a single ostium, usually the RCA (Fig. 3.8.1). The incidence is 0.04% of the general population.

In 41% of cases, single coronary artery is associated with other cardiac anomalies including bicuspid aortic valve, tetralogy of Fallot, and transposition of the great vessels.

Clinical manifestations are usually absent. Possible manifestations include angina pectoris and cardiomyopathy.

Inverted Coronary Sinuses

Inverted coronary sinuses is an anomaly where the RCA arises from the left ostium and sinus, and the LCA arises from the right ostium and sinus.

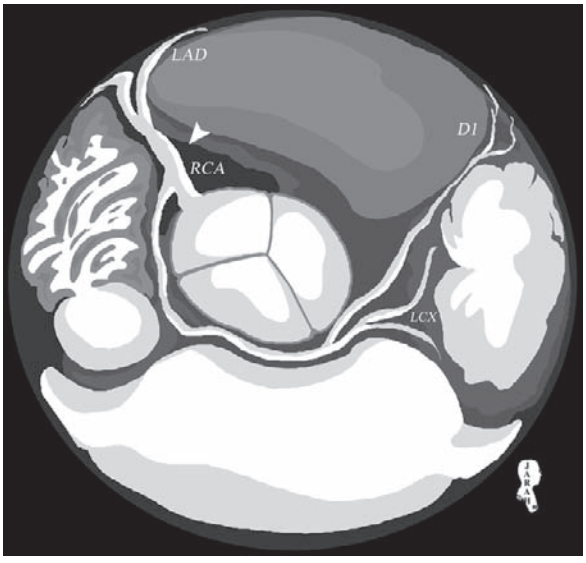

Fig. 3.8.1. Maximum intensity projection (MIP) CT angiography (CTA) illustration shows a single ostium of the right coronary artery (*arrowhead*), with all other arteries that supply the heart originating from it: *LAD* (left anterior descending artery), *LCX* (left circumflex artery), and *D1* (first diagonal branch)

Multiple Ostia

Multiple ostia occurs when some of the coronary branches arise separately from the aortic sinuses with their own ostia. An example is absence of the LCA, with the left circumflex artery (LCX) and the left anterior descending artery (LAD) arising separately from the left aortic sinus (Fig. 3.8.2). Another example is seen when the conal artery arises separately from the right aortic sinus (Fig. 3.8.3).

High Coronary Origins (High Take-Off)

This anomaly is characterized by the RCA originating directly from the ascending aorta and not from the right aortic sinus (e.g., 1 cm above the aortic sinuses) (Fig. 3.8.4).

Coronary Arteriovenous Fistulae

Coronary arteriovenous fistula (CAF) is a rare anomaly characterized by the abnormal communication between a coronary artery and any of the cardiac chambers, coronary sinus, superior vena cava, pulmonary arteries, or pulmonary veins (Fig. 3.8.5).

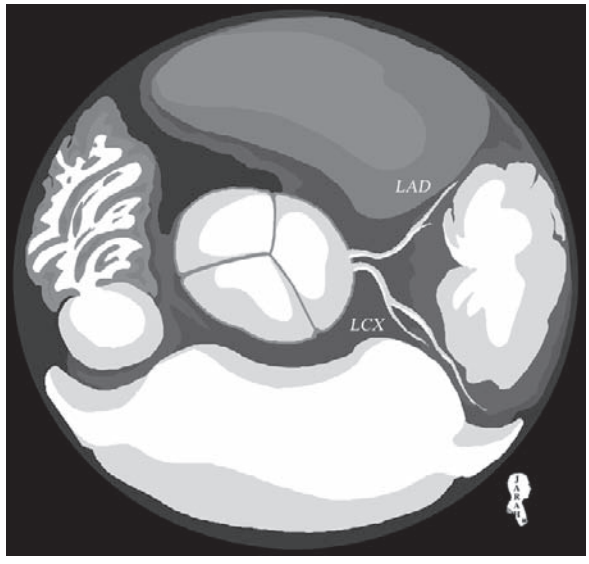

Fig. 3.8.2. MIP CTA illustration shows separate origin of the LAD and LCX with absence of the LCA

Fig. 3.8.3. MIP CTA illustration shows separate origin of the conal artery from the right aortic sinus (*white arrowhead*). The sinoatrial nodal artery (SA) arises from the RCA as its first branch (*black arrowhead*)

The incidence of CAF is 0.02% of the general population, and it can be associated with other cardiac anomalies including tetralogy of Fallot and hypoplastic left heart syndrome.

Fig. 3.8.4. Multiplanar reconstruction CTA shows the high origin of the RCA. The RCA arises directly from the aorta, not from the right sinus of Valsalva

Fig. 3.8.5. MIP CTA illustration shows an RCA fistula with the right ventricle. Note dilatation of the arterial segments before and after the fistula (type B)

Two types of fistulae are found:

- **Type A:** only the arterial segment proximal to the fistula is dilated.
- **Type B:** both proximal and distal arterial segments of the coronary artery are dilated.

Coronary Artery Bridging

Coronary artery bridging is an anomaly characterized by an intramyocardial course of a normally subepicardial coronary artery (part of the coronary artery runs inside the myocardium and then exits to complete its course normally) (Fig. 3.8.6).

The prevalence ranges between 5 and 85% of the population, and it commonly affects the middle segment of the LAD.

Symptoms include angina, myocardial infarction, and sudden death, especially in young athletes. Strenuous activity in young athletes causes stenosis of the coronary segment inside the myocardium during, which leads to angina during strenuous activities.

Coronary Artery Aneurysm

Coronary artery aneurysm is defined as dilatation of the artery more than 1.5–2 times the diameter of the adjacent normal segment. It can be saccular, fusiform, or tubular.

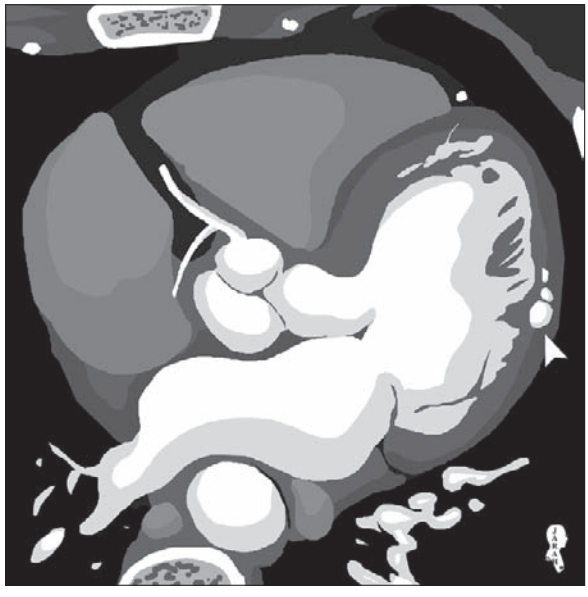

Fig. 3.8.6. Axial cardiac CT shows arterial bridging inside the myocardium (*arrowhead*)

Up to 30% of congenital coronary artery aneurysm are due to Kawasaki syndrome, Takayasu arteritis, and polycystic kidney disease. In contrast, atherosclerosis is the most common cause of acquired coronary aneurysms.

It has a male predominance, and can occur in up to 4.9% of the population.

The RCA is mostly involved (68%), followed by the LCA (39%).

Bland-White-Garland Syndrome

Bland-White-Garland syndrome is a rare congenital disease (1 in every 300,000 births) characterized by an anomalous origin of the LCA from the pulmonary artery (ALCAPA). The area of the left ventricle supplied by the anomalous coronary artery shows signs of myocardial ischemia a few weeks or months after birth when the pressure in the pulmonary artery starts to decline and the patent ductus arteriosus closes (Fig. 3.8.7).

Up to 90% of infants die in the first year of life due to myocardial ischemia and heart failure. Symptoms range from failure to thrive, dyspnea, to heart failure.

Survival depends on formation of collateral vessels between the anomalous LCA and the RCA.

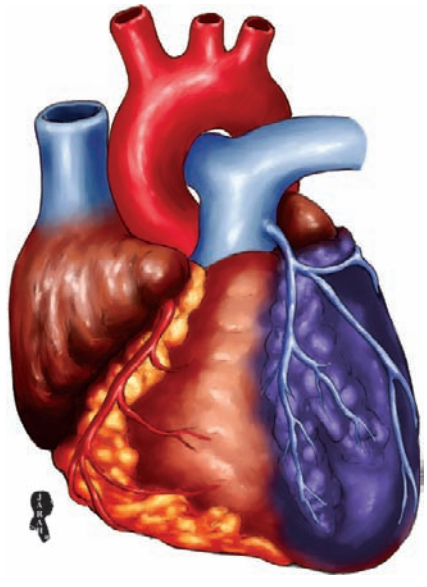

Fig. 3.8.7. Illustration of Bland-White-Garland syndrome with the anomalous origin of the LCA from the pulmonary artery. The area supplied by the LAD and the LCX is colored in blue to demonstrate areas of deoxygenated blood supply

Signs on CT and MRI

Both CT and the MRI show an anomalous origin of the LCA from the pulmonary artery.

Kawasaki Syndrome

Kawasaki syndrome is a pediatric disease characterized by self-limiting vasculitis involving the skin, mucous membranes, lymph nodes, and later the heart. The cause of the disease is unknown, but it is presumed to be caused by infectious agents.

Eighty percent of cases occur in children younger than 5 years.

The child presents with fever that does not respond to antipyretic medications. The fever may last for a week or two, with erythematous rash over the skin and mucus membrane. A catastrophic complication of the disease includes aneurysms of the coronary vessels (25% of cases).

To diagnose Kawasaki syndrome, the patient must have five out of six clinical criteria during the acute phase of the disease:

- Fever that lasts more than 5 days.
- Bilateral conjunctivitis.
- Strawberry tongue and erythema of the oral cavity and lips.
- Erythema of the palms and sole of the feet.
- Diffuse erythematous rash in the body.
- Enlarged lymph nodes: >1.5 cm.

Signs on CT and MRI

Both scans show multiple aneurysms of the coronary vessels, which may show partial or complete thrombosis (Fig. 3.8.8).

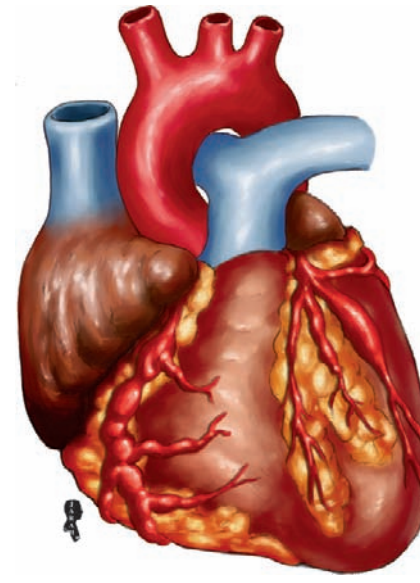

Fig. 3.8.8. Illustration of Kawasaki syndrome. Note the multiple aneurysmal changes affecting both coronary arteries and their branches

Ramus Intermedius

Ramus intermedius is an occasional normal variant of the accessory coronary artery that arises from the LCA (Fig. 3.8.9).

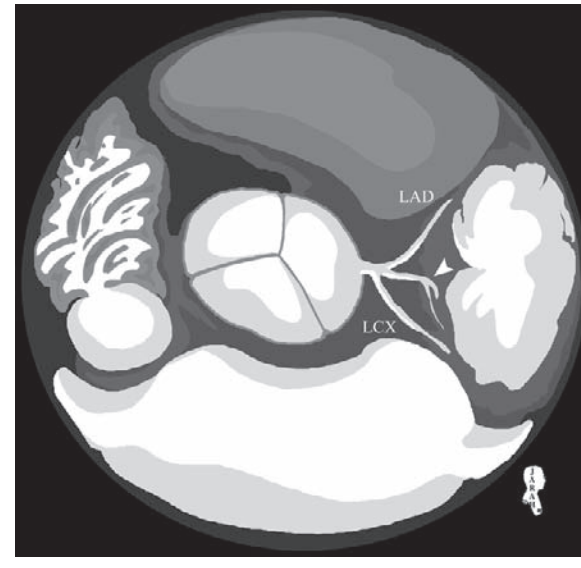

Fig. 3.8.9. MIP CTA illustration shows trifurcation of the LCA giving rise to the ramus intermedius artery (*arrowhead*)

For Further Reading

1. Kantarci M et al. Congenitally corrected transposition of the great arteries: MDCT angiography findings and interpretation of complex coronary anatomy. Int J Cardiovasc Imaging 2007;23:405–410
2. Lee BY et al. Myocardial infarction in a young female with reninoma induced hypertension and myocardial bridging. Int J Cardiovasc Imaging 2007;23:639–643
3. Rychter K et al. Multifocal coronary artery myocardial bridging involving the right coronary and the left anterior descending arteries detected bt ECG-gated 64 slice multidetector CT coronary angiography. Int J Cardiovasc Imaging 2007;22: 713–717
4. Lemburg SP et al. Detection of a double right coronary artery with 16-row multidetector computer tomography. Int J Cardiovasc Imaging 2007;23:293–297
5. Montaudon M et al. Congenital coronary arteries anomalies: review of the literature and multidetector computed tomography (MDCT)-appearance. Surg Radiol Anat 2007; 29:343–355
6. van Ooijen PMA et al. Detection, visualization and evaluation of anomalous coronary anatomy on 16-slice multidetector-row CT. Eur Radiol 2004;14:2163–2171
7. Schneider T et al. Bland-White-Garland syndrome and atrial septal defect-rare association and diagnostic challenge. Clin Res Cardiol 2006;95:295–300
8. Cowles RA et al. Bland-White-Garland syndrome of anomalous left coronary artery arising from the pulmonary artery (ALCAPA): A historical review. Pediatr Radiol 2007;37:890–895
9. Reller M et al. Coronary aneurysms in a patient with atypical Kawasaki syndrome and a streptococcal infection. Pediatr Cardiol 1984;5:205–208
10. Watanabe T et al. Hyponatremia in Kawasaki disease. Pediatr Nephol 2006;21:778–781

3.9

Rare Congenital Heart Anomalies

This section discusses most of the complex congenital and rare heart diseases and syndromes. The following diseases are rare in general.

Signs on Chest Radiographs and Cardiac CT or MRI

- Cardiomegaly in the first few days of life.
- Prominent right heart shadow or "globular-shaped heart."
- On cardiac CT or MRI, the tricuspid valve is seen located abnormally into the right ventricle with a dilated right atrium (Fig. 3.9.2).

Ebstein Anomaly

Ebstein anomaly (EA) is an uncommon cardiac anomaly characterized by displacement of the tricuspid valve inferior into the right ventricle (Fig. 3.9.1). Part of the right ventricle will be "arterialized."

EA constitutes less than 1% of cardiac anomalies, and it is one of the most common causes of cyanotic heart diseases.

Atrioventricular septal defect (ASD) or patent ductus arteriosus (PDA) is associated with EA in up to 50% of cases.

EA infants commonly present with cyanosis, failure to thrive, hepatomegaly, first-degree heart block, and syncopal attacks.

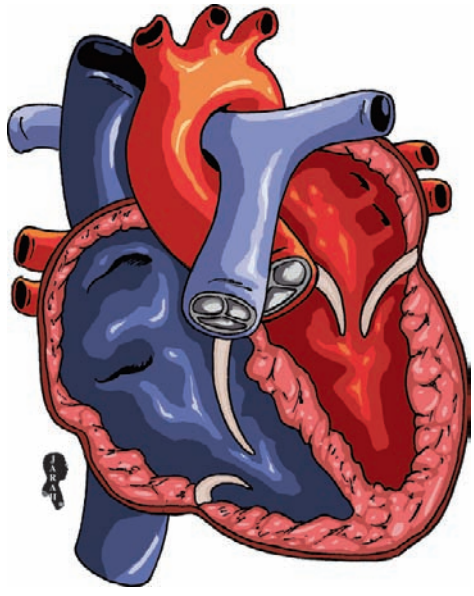

Fig. 3.9.1. Illustration shows abnormally low displacement of the tricuspid valve into the right ventricle (Ebstein anomaly)

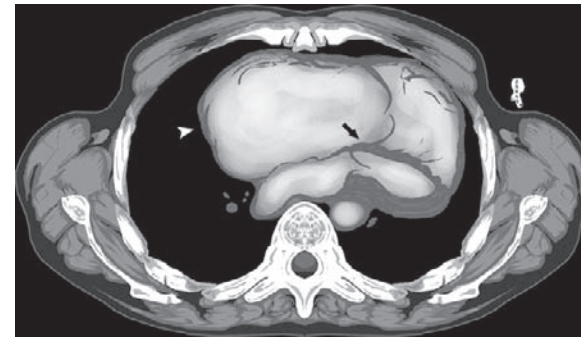

Fig. 3.9.2. Axial cardiac CT illustration shows Ebstein anomaly. Note the cardiomegaly, dilated right atrium (*arrowhead*), and the low-positioned tricuspid valve (*arrow*)

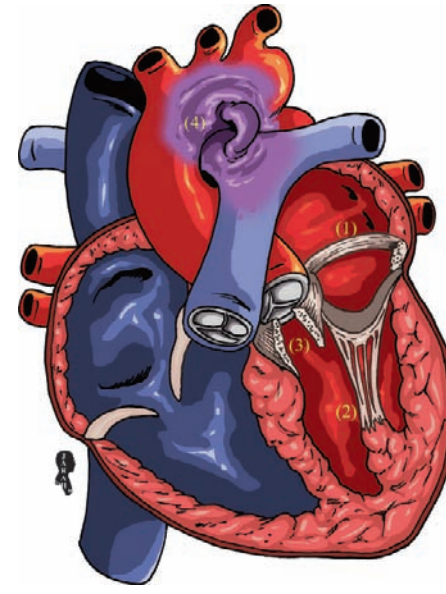

Fig. 3.9.3. Illustration showing Shone complex. Note the supravalvular mitral fibrous ring (1), solitary posterior papillary muscle with the parachute mitral valve (2), subaortic fibrous band (3), and PDA (4). The purple color indicates mixed oxygenated and deoxygenated blood

Shone Syndrome

Shone syndrome (SS), also known as "Shone complex," is a rare congenital cardiac disease characterized by (Fig. 3.9.3):

- Supravalvular mitral fibrous ring.
- Absent anterior papillary muscle with all the choardae tendineae attached to the solitary posterior papillary muscle. Attachment of all the choardae tendineae to a solitary papillary muscle gives the mitral valve the shape of a "parachute."
- Subaortic fibrous band causes aortic valve stenosis.
- Aortic coarctation.

SS constitutes 0.6% of all cardiac anomalies, and it may be associated with PDA.

Without surgical correction, the mortality rate is high within the first 5 years of life.

Truncus Arteriosus

Truncus arteriosus (TA) is a rare cardiac anomaly that arises due to failure of the primitive common truncus arteriosus to divide into the aorta and pulmonary artery.

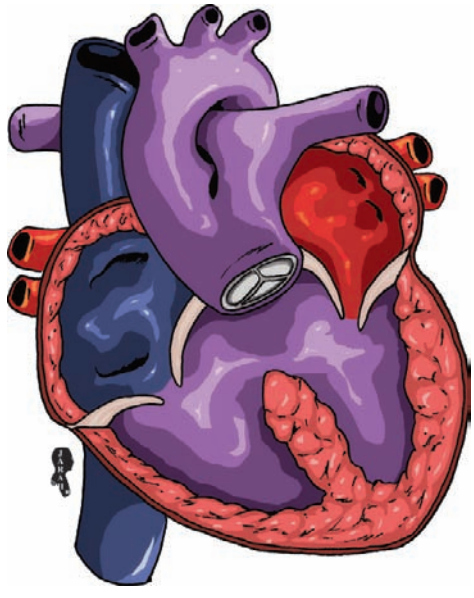

Fig. 3.9.4. Illustration showing truncus arteriosus. Note the common origin of the aorta and the pulmonary trunk. Also, note the ventricular septal defect connecting both ventricles together. The purple color indicates mixed oxygenated and deoxygenated blood

The aorta and the pulmonary trunk share a common origin with one valve (Fig. 3.9.4).

TA accounts for 0.4–1% of all cardiac anomalies, and it is a fatal disease (most infants die at the age of 6 months due to congestive heart failure).

Types of truncus arteriosus

- **Type 1:** the pulmonary trunk arises from the left side of the aorta and then divides into the right and left pulmonary arteries.
- **Type 2:** both pulmonary arteries arise from the posterior aspect of the aorta.
- **Type 3:** both pulmonary arteries arise from the lateral sides of the aorta.
- **Type 4:** it is composed of tetralogy of Fallot plus tricuspid atresia.

Signs on Chest Radiographs

- The common truncus arteriosus is seen as a widening of the mediastinum (Fig. 3.9.5).
- Cardiomegaly with left atrial enlargement (Fig. 3.9.5).
- Right-sided aortic arch is seen in 33% of cases.

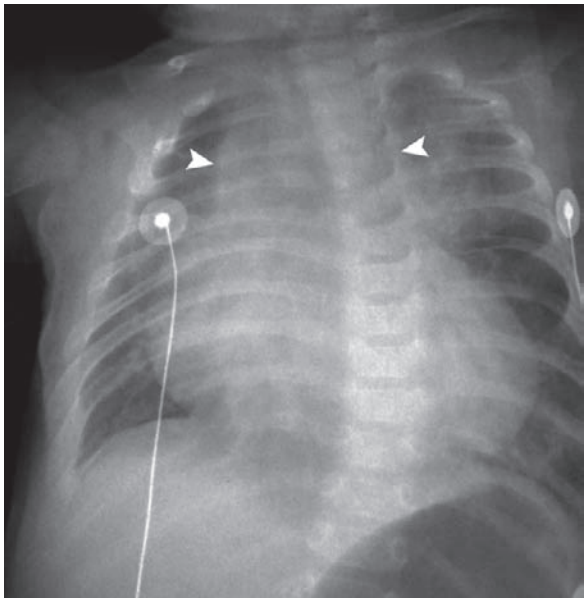

Fig. 3.9.5. Anteroposterior plain chest radiograph of a child with truncus arteriosus shows massive cardiomegaly, with the common truncus arteriosus seen as widening of the mediastinum (*arrowheads*). (*The radiograph is slightly deviated to the left side due to the patient position*)

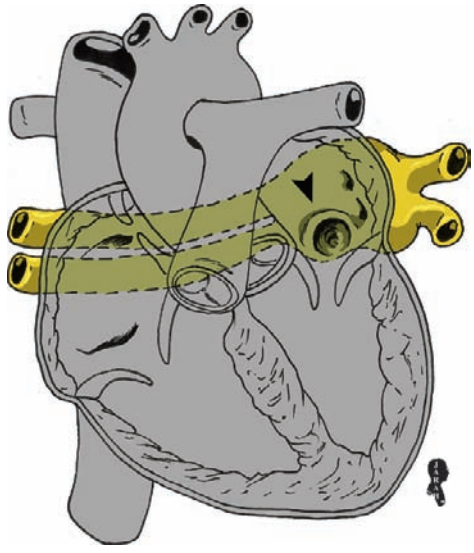

Fig. 3.9.6. Illustration shows cor triatriatum. Note how all the pulmonary veins are drained into an accessory posterior chamber behind the left atrium (*yellow shaded*). The posterior accessory chamber is linked to the left atrium via a septal opening (*arrowhead*)

Cor Triatriatum

Cor triatriaum is a very rare form of congenital heart disease (0.1%) characterized by draining of part of or all the pulmonary veins into an accessory chamber that is linked to the distal portion of the left atrium (Fig. 3.9.6). This disease presents in infancy and is rarely seen in adults.

Cor triatriaum radiographically, hemodynamically, and clinically resembles mitral stenosis, but in infantile form.

Signs on Chest Radiographs and Cardiac CT or MRI

- Chest radiographs show the signs of mitral stenosis (e.g., left atrial enlargement) with mild to moderate cardiomegaly.
- On cardiac MRI or CT, the left atrium is seen divided into two anterior and posterior halves by a fibrous septum. The pulmonary veins drain into the posterior half (Fig. 3.9.7).

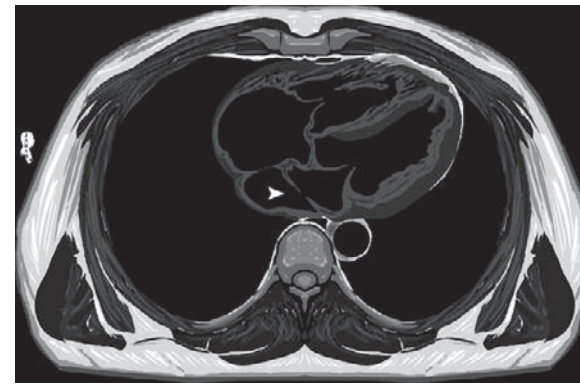

Fig. 3.9.7. Axial dark-blood MR illustration shows cor triatriatum. The left atrium is divided into an anterior and posterior segment via a membrane that transverses the left atrium from the interatrial septum to the left atrial appendage. Note the membranous opening connecting the two chambers (*arrowhead*)

Apical Ballooning Syndrome (Takotsubo Cardiomyopathy)

Apical ballooning syndrome (ABS) is a rare disease characterized by transient reversible left ventricular apical dilatation making its shape resemble a Japanese octopus trap, a "takotsubo."

ABS mimics ventricular dilatation that is seen after myocardial infarction, with absence of coronary artery obstruction.

ABS is mostly seen in postmenopausal women between 62 and 75 years of age.

Possible etiologies include endocrine disturbance (e.g., thyrotoxicosis), nutritional deficiency (e.g., thiamine), and cardio-toxins (e.g., excessive alcohol).

Patients present with sudden angina-like chest pain that can be mistaken with myocardial infarction. Moreover, an electrocardiogram study (ECG) classically demonstrates ST elevation with T-wave inversion. The main difference between this disease and true myocardial infarction is the absence of coronary artery obstruction or stenosis on angiography. Ventricular systolic functions are restored amazingly rapidly after the sudden onset, which is not seen in a true myocardial infarction.

ABS represents 1% of cases of suspected myocardial infarction admissions.

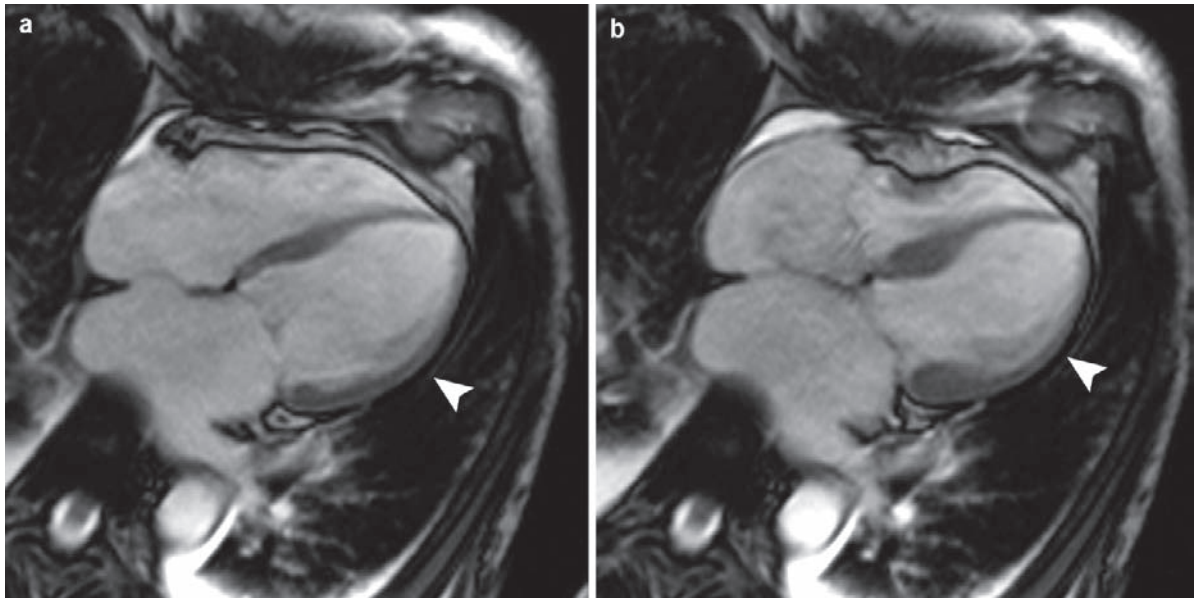

Fig. 3.9.8. Axial white-blood MRI shows apical ballooning syndrome. Note the shape and the apical dilatation of the left ventricle during diastole **a**. After systole **b**, the left ventricle is not contracting properly, and shows very mild contraction compared with the right ventricle (*arrowheads*)

Signs on Cardiac MRI

- Striking dilatation of the left ventricle apex with akinesia during systole and diastole (Fig. 3.9.8).
- No cardiac edema on T2-weighted images.
- After contrast material administration, no delayed myocardial contrast enhancement (sign of true myocardial infarction).

Williams Syndrome

Williams syndrome (WS) is a rare disease characterized by "elfin-like" facial features (facial features of an elf), hypercalcemia, mental retardation, and supravalvular aortic stenosis.

WS is mostly sporadic, although a few families showed an autosomal dominant inheritance.

The elfin-like features include: periorbital fullness, short up-turned nose, epicanthal folds, long philtrum, and hypoplastic malar region (Fig. 3.9.9). Other features include strabismus (abnormal eye deviation to one side).

Fig. 3.9.9. Illustration showing the elfin-like facial features seen in patients with William syndrome

Up to 41% of patients have supravalvular aortic stenosis with some degree of aortic hypoplasia.

Signs on Brain MRI

Some studies showed decreased gray matter concentration in the parieto-occipital areas in patients with Williams syndrome (Fig. 3.9.10).

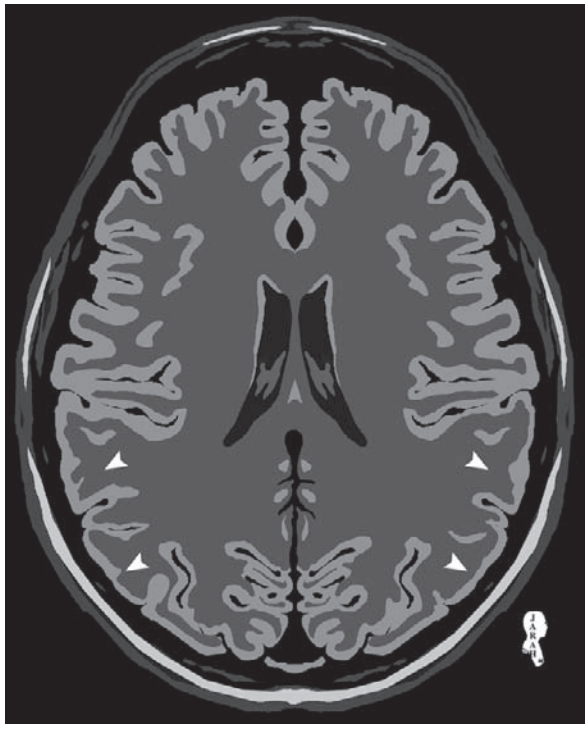

Fig. 3.9.10. Axial FLAIR brain MR illustration shows bilateral decrease in the gray matter substance in the parieto-occipital areas. This finding is seen in some patients with William syndrome and it is thought to be one of the causes of mental retardation in these patients (*arrowheads*)

Pulmonary Artery Sling

Pulmonary artery sling (PS) is a rare congenital anomaly in which the left pulmonary artery arises from the right pulmonary artery. The left pulmonary artery then passes behind the trachea and anterior to the esophagus forming a sling around the trachea that causes tracheal compression (Fig. 3.9.11).

Infants with PS present at birth (50%) or early in life (65%) with signs of severe airway obstruction, with inspiratory or expiratory stridor.

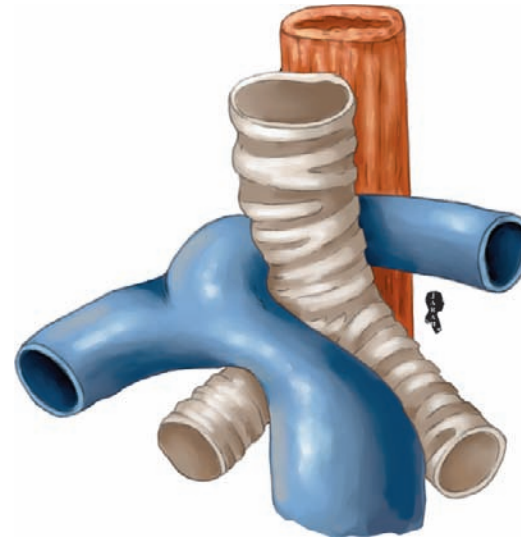

Fig. 3.9.11. Illustration showing pulmonary sling anomaly

PS is commonly associated with complete cartilaginous rings in the distal trachea, which will further increase in tracheal stenosis. The complete tracheal ring anomaly is called "chicken trachea."

PS can be seen in patients with trisomies 18 and 21.

Signs on CT or MRI

The left pulmonary artery arises from the right pulmonary artery and passes behind the trachea and anterior to the esophagus making a sling (Fig. 3.9.12).

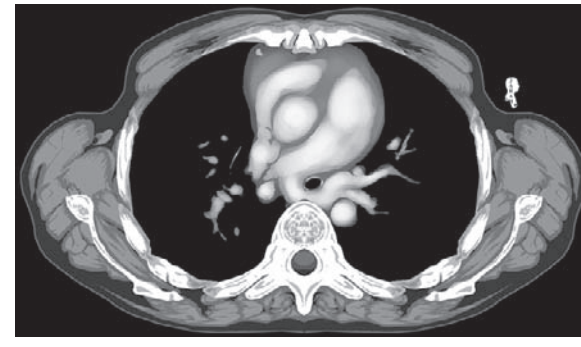

Fig. 3.9.12. Axial postcontrast thoracic CT illustration shows pulmonary sling anomaly

Congenital Absence of the Pericardium

Complete or partial absence of the pericardium is a rare anomaly. Up to 30% of cases are associated with other congenital cardiac diseases.

Patients are usually asymptomatic when the defect is small. However, medium-sized defects may result in cardiac herniation and even strangulation at the site of the defect.

Signs on Plain Radiographs

There is loss of definition of the left heart border, with deviation of the heart to the left side of the chest.

Signs on CT or MRI

The heart appears enlarged, and is shifted to the left side of the chest and posteriorly (Fig. 3.9.13).

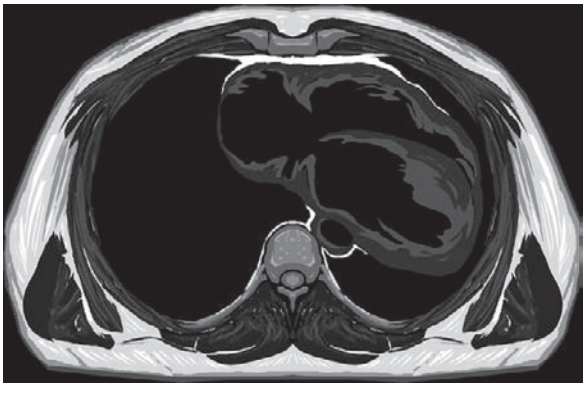

Fig. 3.9.13. Axial dark-blood MR illustration shows displacement of the heart to the left and posteriorly, plus enlargement due to almost complete loss of the pericardium

Uhl Anomaly

Uhl anomaly (UA) is characterized by complete or partial absence of the right ventricular myocardium; the free right ventricular wall is composed only of surfaces of endocardium and epicardium.

The anomaly is very rare with an unknown incidence rate, and it has a male predominance (56% of cases). The majority of cases are sporadic.

Patients with UA are typically young male subjects who present with severe congestive heart failure, syncopal attacks, and ventricular tachycardia that may lead to sudden cardiac death.

UA can be mistaken with arrhythmogenic right ventricular dysplasia (ARVD), another rare progressive cardiomyopathy that has almost the same clinical presentation. ARVD is a disease characterized by infiltration and replacement of the right ventricular-free wall myocardium with fibrofatty tissue. This fibrofatty tissue replacement impedes the contractility of the ventricle and causes electrical instability, leading to ventricular arrhythmias and sudden cardiac death.

Signs on MRI

- The right ventricle is markedly dilated, with an extremely thin right ventricle wall, owing to the complete or partial absence of the myocardium. Absence of the myocardium differentiates UA from ARVD, which is characterized by fibrofatty infiltration of the right ventricular myocardium, seen as areas of hyperintense signal within the myocardium on T1-weighted images (Fig. 3.9.14).
- The right atrium may be enlarged, with its tricuspid valve seen in its normal position. A normal position of the tricuspid valve differentiates UA from Ebstein anomaly causing a dilated right atrium and ventricle.

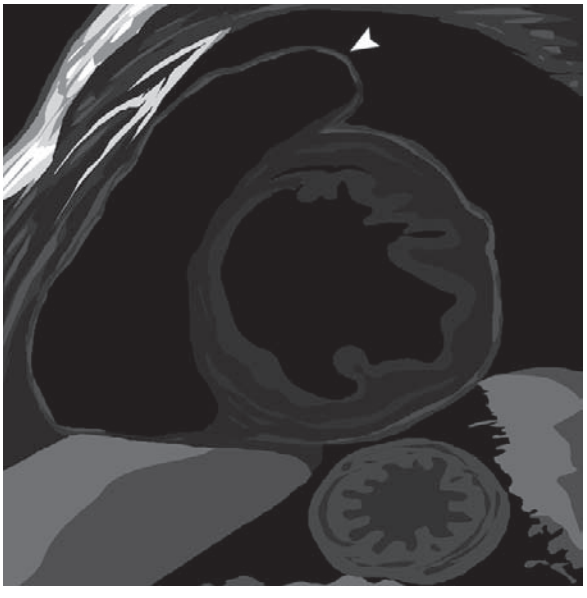

Fig. 3.9.14. Short-axis dark-blood MR illustration shows dilatation and almost complete absence of the myocardium in the right ventricle representing Uhl anomaly (*arrowhead*)

For Further Reading

1. Ohta M et al. Pseudo-Meigs' syndrome caused by retroperitoneal tumor in a patient with Ebstein anomaly. Int J Clin Oncol 2005;10:269–271
2. Uyan C et al. Ebstein's anomaly in siblings: An original observation. Int J Cardiovasc Imaging 2002;18:435–438
3. Sekhar KC et al. Anesthetic management of a case of Shone's syndrome. Indian J. Anesth. 2004;48(3):212–214
4. Mühler MR et al. Truncus arteriosus communis in a midtrimester fetus: Comparison of prenatal ultrasound and MRI with postmortem MRI and autopsy. Eur Radiol 2004;14: 2120–2124
5. Godoy I et al. Cor Triatriatum. Circulation 1998;98;2781
6. Williams G. Recognition of the apical ballooning syndrome in the United States. Circulations 2005;111;388–390
7. Chandrasegaram MD et al. Apical ballooning syndrome complicated by acute sever mitral regurgitation with left ventricular outflow obstruction – Case report. J Cardiothorac Surg 2007;2:14
8. Dichtl W et al. Apical ballooning syndrome. Wien Klin Wochenschr 2005;117(13–14): 456
9. Boddaert N et al. Pareito-occipital grey matter abnormalities in children with Williams syndrome. NeuroImage 2006;30: 721–725
10. Park JH et al. Demonstration of peripheral pulmonary stenosis and supravalvular aortic stenosis by different cardiac imaging modalities in a patient with Williams syndrome-usefulness of noninvasive imaging studies. Int J Cardiol 2007;128(3): e95–e97
11. Pierpont MEM. Genetic etiology of cardiac syndromes. Prog Pediatr Cardiol 1996;6:29–41
12. Cobo J et al. Williams syndrome, report of a case. Oral Surg Oral Med Oral Pathol 1992;74:756–759
13. Chen SJ et al. Left pulmonary artery sling complex: computed tomography and hypothesis of embryogenesis. Ann Thorac Surg 2007;84:1645–1650
14. Calcagni G et al. CT demonstration of "chicken trachea" resulting from complete cartilaginous rings of the trachea in ring-sling complex. Pediatr Radiol 2008;38:798–800
15. Döhlemann C et al. Pulmonary sling: Morphological findings. Pre- and postoperative course. Eur J Pediatr 1995;154:2–14
16. Glockner JF. Imaging of pericardial diseases. Magn Reson Imaging Clin N Am 2003;11:149–162
17. Greer ML et al. MRI of Uhl's anomaly. Circulations 2000;101;e230–e232
18. Ikari NM et al. Uhl's anomaly. Differential diagnosis and indication for cardiac transplantation in an infant. Arq Bras Cardiol 2001;77:73–76

Chapter 4

The Abdomen and Pelvis

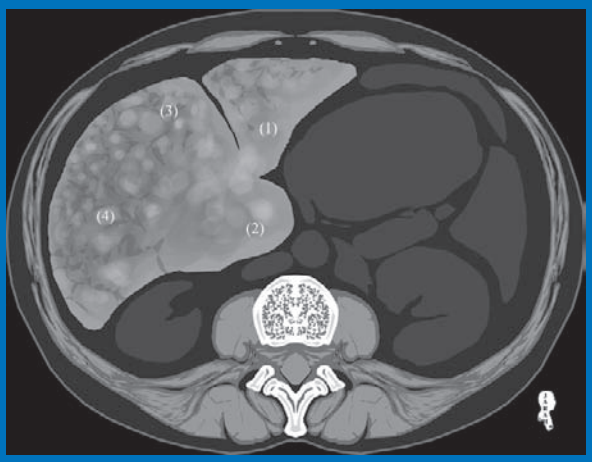

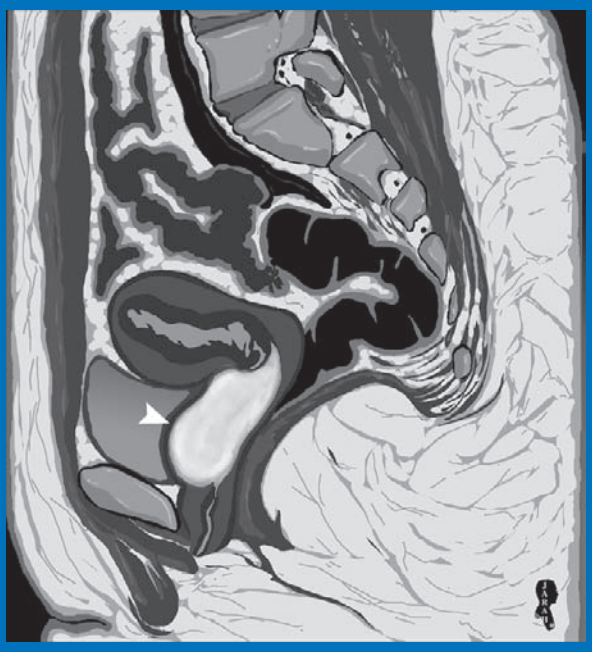

CONTENTS

J. A. Al-Tubaikh, M. F. Reiser: *Congenital Diseases and Syndromes* – An Illustrated Radiological Guide
DOI: 10.1007/978-3-642-00160-4, © Springer-Verlag Berlin Heidelberg 2009

4.1

Heterotaxy Syndromes

Heterotaxy syndromes describe a group of diseases characterized by abnormal arrangement of the visceral organs, abnormal venous system, and cardiac anomalies. It accounts for 1–3% of cardiac anomalies. There are two types of heterotaxy syndrome: asplenia syndrome and polysplenia syndrome.

Polysplenia Syndrome

Polysplenia syndrome is a complex congenital anomaly characterized by situs ambiguous (partial visceral heterotaxia) and levoisomerism (bilateral left-sidedness). The disease has a female predominance.

Situs ambiguous is a situation characterized by abnormal positions of the viscera, while *levoisomerism* is a situation where the right-side body organs assume the morphology of the left-side body organs (e.g., both lungs have two lobes instead of a trilobed right lung and bilobed left lung).

The syndrome is usually diagnosed in early childhood because of the various cardiac anomalies that accompany it, which can lead to death of the child by the age of 5 years. Only 40% of patients survive the second year of life, usually due to cardiovascular failure.

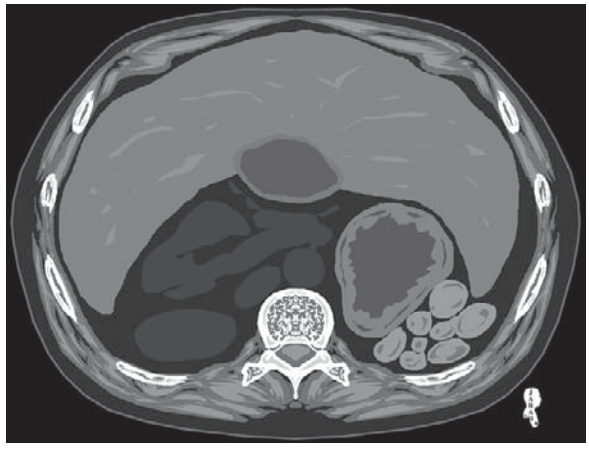

Fig. 4.1.1. Axial CT illustration of some of the abdominal manifestations of polysplenia syndrome. Note the symmetrically extending liver with the centered gallbladder, the right-sided stomach with the polysplenia on the stomach side and aligned along its greater curvature

Anomalies of polysplenia syndrome can by summarized as follows (Fig. 4.1.1):

- **Spleen:** is composed of many small splenules and always found on the same side of the stomach, either on the right or the left side. Also, it is always found along the greater curvature of the stomach.
- **Liver, gallbladder, and biliary tree:** the liver is situated on the midline extending symmetrically to both sides of the upper abdomen, with the gallbladder located centrally. Biliary atresia can be found in 20% of cases.
- **Pancreas and stomach:** the pancreas is usually short, and the stomach is often located on the right side.
- **Genitourinary system:** renal agenesis or double ureters (Fig. 4.1.2) can be found.
- **Cardiovascular system:** atrial septal defect, dextrocardia, and persistent left side superior vena cava are common anomalies.

Fig. 4.1.2. An intravenous urography image shows right double ureters. This anomaly can be found with polysplenia syndrome

- **Venous system:** in up to 80% of cases there is continuation of the inferior vena cava as the azygos or hemiazygos veins.

Asplenia Syndrome

Asplenia syndrome is a congenital disease characterized by situs ambiguous, cardiac anomalies, and absence of the spleen. The disease has a male predominance.

Cardiac anomalies occur in 99–100% of cases (e.g., transposition of the great vessels).

For Further Reading

1. Ito H et al. Heterotaxy syndrome with pancreatic malrotation: CT features. Abdom Imaging 2003;28:856–858
2. Gagner M et al. Hepatobiliary anomalies associated with polysplenia syndrome. Gastrointest Radiol 1991;16:-167–171
3. Vossen PG. Computed tomography of the polysplenia syndrome in the adult. Gastrointest Radiol 1987;12:209–211
4. Gayer G et al. Polysplenia syndrome detected in adulthood: Report of eight cases and review of the literature. Abdom imaging 1999;24:178–184
5. Gayer G et al. Congenital anomalies of the spleen. Semin Ultrasound CT MRI 2006;27:358–369

4.2

Chilaiditi Syndrome

Chilaiditi syndrome (CS) is a condition characterized by interposition of the colon or small intestine temporarily or permanently between the liver and the diaphragm.

CS is usually asymptomatic, and is discovered as an incidental finding on chest or abdominal radiographs (called Chilaiditi sign). Only when there are abdominal problems, ranging from abdominal pain to intestinal obstruction, is the term "Chilaiditi syndrome" used.

The incidence of CS is lower than 0.3% in the general population.

Many factors can cause CS, including:

- **Colonic causes:** mega colon and abnormal colonic motility.
- **Diaphragmatic causes:** diaphragmatic eventration or paralysis due to phrenic nerve injury.
- **Liver causes:** small liver (cirrhosis) and relaxation of the hepatic suspensory ligaments.

Signs on Chest Radiographs

Fake air under the right diaphragm represents hepatodiaphragmatic interposition of the colon, with elevation of the right hemidiaphragm usually seen (Figs. 4.2.1 and 4.2.2).

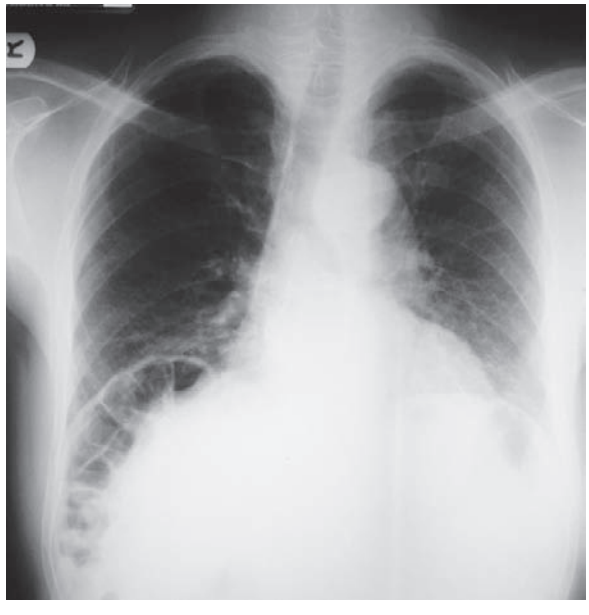

Fig. 4.2.1. Posteroanterior plain chest radiograph shows hepatodiaphragmatic interposition of the colonic hepatic flexure (Chilaiditi sign). The patient was asymptomatic

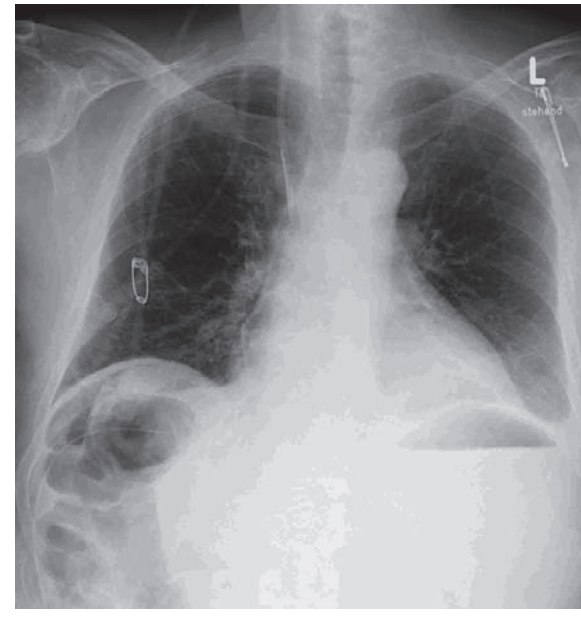

Fig. 4.2.2. Posteroanterior plain radiograph of another patient shows Chilaiditi sign

Signs on CT

A colon or small intestine is abnormally located between the liver and the diaphragm.

For Further Reading

1. Keles S et al. Chilaiditi syndrome as a cause of respiratory distress. Eur J Pediatr 2006;165:367–369
2. Oh SN et al. Chilaiditi syndrome caused by Fity-Hugh-Curtis syndrome: Multidetector CT findings. Abdom Imaging 2006;31:45–47
3. Sato M et al. Chilaiditi syndrome: Sonographic findings. Abdom Imaging 2000;25:397–399
4. Kurt Y et al. Colonic volvulus associated with chilaiditi syndrome: Report of a case. Surg Today 2004;34:613–615

4.3

Meckel Diverticulum

Meckel diverticulum (MD) is a gastrointestinal congenital anomaly that arises due to incomplete closure of the intestinal omphalomesenteric (vitelline) duct.

MD has the shape of the finger of a glove, and it is supplied by a vitelline artery that arises from the ileal branch of the superior mesenteric artery.

The diverticulum arises either from the cecum or the ileum, and its main features can be summarized by the "rule of two":

- It is located about 2 feet from the ileocecal valve.
- It is often 2 in. in length.
- It occurs in 2% of the population.
- It is twice as common in men.
- It can contain two heterotopic tissues (e.g., gastric).
- It is often asymptomatic before 2 years of age.
- Two percent of cases are symptomatic.

MD may contain gastric, liver, or pancreatic tissue (5–20% of cases). Patients may present with melena secondary to intestinal wall ulceration due to the ectopic gastric mucosa.

Although most cases are asymptomatic, symptomatic patients commonly present with complications like gastrointestinal hemorrhage, perforation, obstruction, and inflammation. Inflamed MD is very difficult to distinguish from appendicitis preoperatively.

MD can be diagnosed by nuclear medicine scan if the diverticulum contains gastric mucosa.

Malignancy may occur in 4–5% of complicated MD cases. The tumor most commonly is a leiomyosarcoma.

Reiter hernia: is MD herniated indirectly through the inguinal canal.

Signs on Barium Enema

MD is identified as a blind-ending intestinal diverticulum arising from the antimesenteric border of the distal ileum near the ileocecal valve (Figs. 4.3.1–4.3.3).

Fig. 4.3.1. Normal double-contrast barium enema

Fig. 4.3.2. Single-contrast barium enema shows Meckel diverticulum (*arrowhead*). Compare this image with the normal barium enema examination in Fig. 4.3.1

Fig. 4.3.3. Another double-contrast barium enema shows Meckel diverticulum (*arrowhead*)

For Further Reading

1. You JS et al. A case of strangulated small bowel obstruction caused by Meckel's diverticulum in an adult. J Emerg Med 2007;33(2):133–135
2. Ko SF et al. Internal hernia associated with Meckel's diverticulum in 2 pediatric patients. Am J Emerg Med 2008; 26:86–90
3. Giusti S et al. Ileal invaginated Meckel's diverticulum: imaging diagnosis (2004:9b). Eur Radiol 2004;14:2368–2371
4. Dixon PM et al. The diagnosis of Meckel's diverticulum: A continuing challenge. Clin Radiol 1987;38:615–619

4.4

Duodenal and Jejunoileal Atresias

Duodenal atresia (DA) means congenital closure of the whole or part of the duodenum, usually due to mucosal transverse septum. The most common site for DA is the second part of the duodenum, distal to the duodenal papilla (85%). The incidence of DA is about 1:10,000 live births, and it affects males more than females.

DA is commonly associated with other problems like Down syndrome (30%), prematurity (45%), and other congenital anomalies (e.g., tracheoesophageal fistula). Mothers with neonates affected by DA have a history of polyhydramnios in up to 50% of cases. DA can be caused rarely by annular pancreas, where the head of the pancreas totally surrounds the second part of the duodenum.

Jejunoileal atresia (JA) is another congenital anomaly characterized by closure of the jejunum. The site of the atresia can be anywhere from the ligament of Treitz to the cecum.

JA is more common than DA and it has an incidence of about 1:1,000 live births.

Abdominal distension and bilious vomiting within the first 24 h of birth are common features of both DA and JA.

Fig. 4.4.1. Erect babygram shows the classic double-bubble appearance with air–fluid levels in an infant with duodenal atresia

Feingold syndrome (oculodigitoesophageoduodenal syndrome): is a rare disease characterized by microcephaly, short middle phalanges of the second and fifth fingers with clinodactyly, esophageal atresia, and DA. The disease has an autosomal dominant mode of inheritance.

Signs on Plain Abdominal Radiographs

- DA radiographs classically show distension of both the stomach and the first part of the duodenum with air giving a "double-bubble appearance" (Fig. 4.4.1).
- JA radiographs show "triple-bubble appearance," where the third bubble is caused by filling of the first part of the jejunum by air (Fig. 4.4.2).

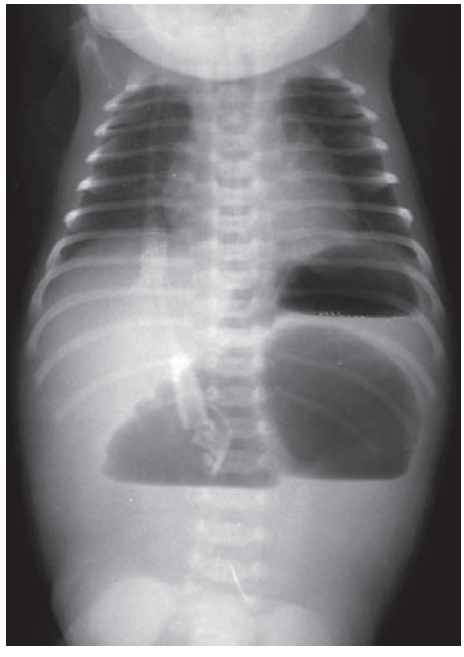

Fig. 4.4.2. Erect babygram shows the triple-bubble appearance with air–fluid levels of jejunoileal atresia

For Further Reading

1. Sajja SBS et al. A duodenal atresia associated with proximal jejunal perforation: A case report and review of the literature. J Pediatr Surg 2003;38(9):1396–1398
2. Downard CD et al. Esophageal atresia, duodenal atresia, and unilateral lung agenesis: A case report. J pediatr Surg 2004;39:1283–1285
3. Layman-Pleet L et al. Feingold syndrome: A rare but important cause of syndromic tracheoesophageal fistula. J Pediatr Surg 2007;42:E1–E3
4. Aslam M et al. End-stage renal failure, reflux nephropathy and Feingold's syndrome. Pediatr Nephrol 2008;23:159–161

4.5

Budd-Chiari Syndrome

Budd-Chiari syndrome (BCS) is an uncommon disease characterized by thrombotic or nonthrombotic hepatic venous outflow obstruction. BCS causes severe hepatic parenchymal congestion, atrophy, and necrosis.

Causes of BCS include hepatocellular carcinoma (most common), pregnancy, oral contraceptives, polycythemia rubra vera, and paroxysmal nocturnal hemoglobinurea. All these predisposing conditions are accompanied by an increased risk of intravascular thrombosis. In contrast, nonthrombotic causes include inferior vena cava (IVC) webs (most common), radiation injury, trauma, and Behcet disease.

Patients with BCS classically present with a triad of abdominal pain, ascites, and hepatomegaly. The disease is typically associated with peripheral hepatic atrophy as a consequence of the liver congestion.

Signs on US

- Absence of flow in the hepatic vein is a pathognomonic finding. The veins usually show persistent monophasic flow waves on Doppler scanning (Fig. 4.5.1).
- Enlargement of the caudate lobe (Fig. 4.5.2). The caudate lobe is spared from cirrhosis because it has a separate drainage to the IVC.
- Ascites (Fig. 4.5.3).

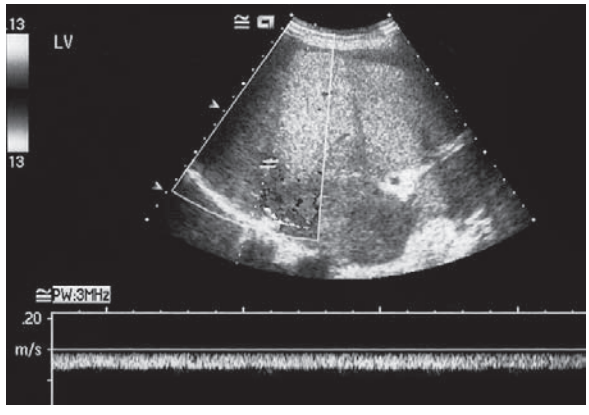

Fig. 4.5.1. Doppler wave spectrum of the hepatic veins shows flattened monophasic blood flow in a patient with BCS

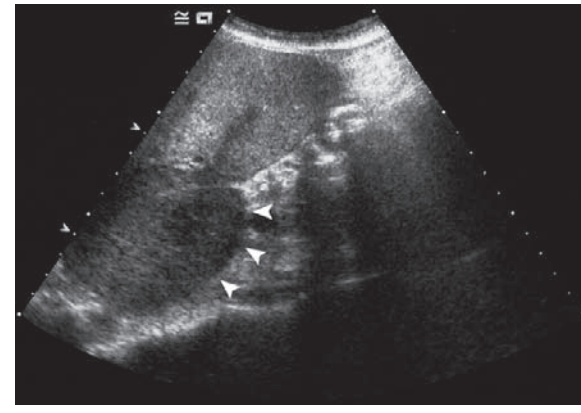

Fig. 4.5.2. US image of the same patient shows enlargement of the caudate lobe (*arrowheads*)

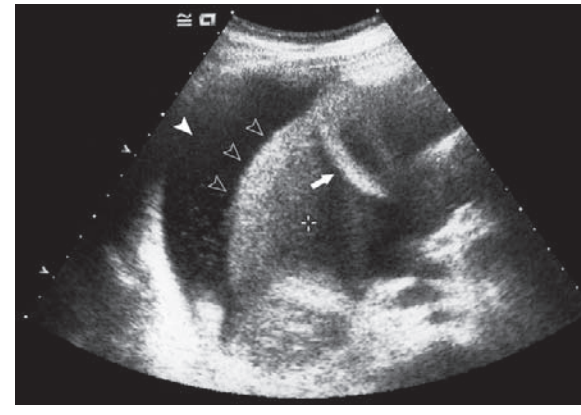

Fig. 4.5.3. US image of the same patient shows perihepatic ascetic collection (*solid arrowhead*), shrunken liver (*open arrowheads*), and thickening of the gallbladder wall as a sign of cholecystitis (*arrow*)

Signs on CT

- The liver texture is inhomogeneous and mottled on contrast imaging. The center of the liver enhances early and the periphery enhances late (Fig. 4.5.4).
- Signs of liver atrophy, except in the caudate lobe, are a common finding in chronic cases.
- The hepatic veins and the IVC are narrowed or not seen.
- Presence of multifocal, large, regenerative nodules ranging between 0.5 and 2 cm in size. These nodules enhance in the arterial phase of the liver scan due to their hypervascularity (Fig. 4.5.5).

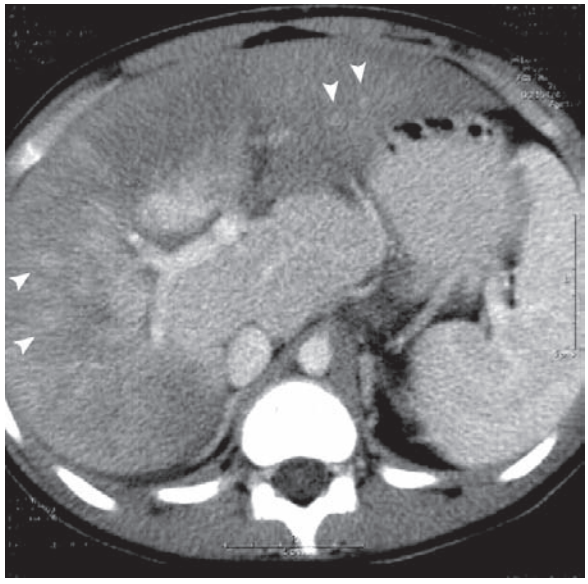

Fig. 4.5.4. Axial postcontrast abdominal CT image shows signs of BCS. Periphery of the liver does not enhance, while the center does. The caudate lobe is enhancing, the liver veins are not identified, and small scattered regenerative nodules are noted (*arrowheads*)

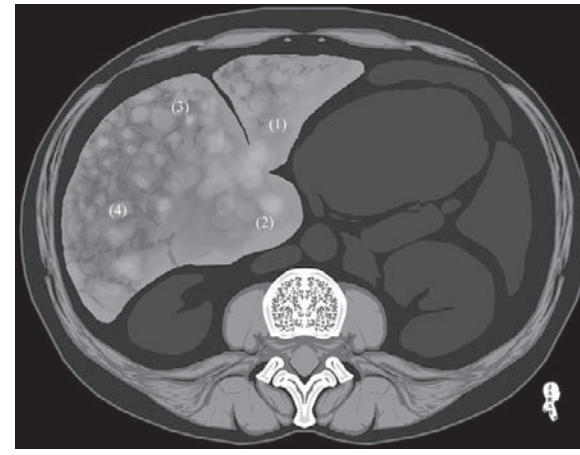

Fig. 4.5.5. Axial postcontrast abdominal CT illustration sums up the CT characteristics of BCS. The liver veins are not identifiable (*1*), enlargement of the caudate lobe (*2*), congested liver periphery with inhomogeneous texture (*3*), and multiple regenerative nodules (*4*)

For Further Reading

1. Buckley O et al. Imaging of Budd-Chiari syndrome. Eur Radiol 2007;17:2071–2078
2. Soler R et al. Benign regenerative nodules with copper accumulation in a case of chronic Budd-Chiari syndrome: CT and MR findings. Abdom Imaging 2000;25:486–489

4.6

Cruveilhier-Baumgarten Syndrome

Cruveilhier-Baumgarten syndrome (CBS) is a rare disease characterized by a patent paraumbilical vein as a consequence of portal hypertension due to liver cirrhosis. The patent paraumbilical vein represents a normal portal–systemic venous collateral route between the periumbilical veins of the abdominal wall, the left portal vein, and the superficial and deep inferior epigastric veins reaching the external iliac veins. These portosystemic collaterals can be reopened in cases of portal hypertension.

In CBS, the umbilical portion of the left portal vein feeds a paraumbilical vein which runs through the ligamentum teres toward the umbilicus.

In normal situations, the portal system has no communication with the systemic venous system. However, in cases of portal hypertension, a communication between the two systems arises (portocaval anastomosis) via four anastomoses:

- **With the azygos vein** via the coronary vein and its esophageal veins forming esophageal varices.
- **With the rectum** via the superior, inferior, and middle rectal veins.
- **With the umbilicus** via the umbilical veins. The patent paraumbilical vein supplies the liver segments (2, 3, and 4b).
- **With the retroperitoneum** via the retroperitoneal venous plexus.

Other manifestations of this syndrome are all related to liver cirrhosis and portal hypertension such as splenomegaly, esophageal varices, prominent abdominal wall venous markings (caput medusa), anemia, leukopenia, and thrombocytopenia. The danger of the patent umbilical vein comes from its risk for spontaneous bleeding or hemorrhage after abdominal surgery or paracentesis.

The development of a large paraumbilical vein was found to prevent formation of bleeding esophageal varices, but at the same time it predisposes patients to hepatic encephalopathy.

In one-third of cases, a venous hum can be heard with a stethoscope between the xyphoid process and the umbilicus on clinical examination.

Cruveilhier-Baumgarten disease: is another condition characterized by the same clinical features in the absence of liver cirrhosis.

Signs on CT and MRI

The patent paraumbilical vein is seen as a tubular structure leaving the left portal vein via the falciform ligament toward the anterior abdominal wall at the level of the umbilicus (Fig. 4.6.1).

Signs on Doppler US

- The patent umbilical vein is seen as a patent vessel running from the umbilicus through the ligamentum teres to join the portal vein inside the liver (Figs. 4.6.2–4.6.6).
- Enlargement of the vein from 1 to 3 mm on sonography has been suggested as a sign of portal hypertension.

For Further Reading

1. Cerra FB et al. Cruveilhier-Baumgarten disease with associated splenic artery aneurysm. Dig Dis 1977;22(6):559–564
2. Ohkubo H et al. Cruveilhier-Baumgarten syndrome presenting with precordial murmer and thrill. Report of a case diagnosed by percutaneous transhepatic portography. Diseases 1978;23(5 Suppl):S65–S68
3. Cheng TO et al. Cruveilhier-Baumgarten syndrome, review of the literature and report of a case. Am J Med 1954;17:143–150
4. Saddenki S et al. The sonographic patent umbilical vein in portal hypertension. Radiology 1982;145:441–443
5. Singla V et al. Cruveilhier Baumgarten syndrome with giant paraumbilical vein. J Postrgrad Med 2008;54:328–9
6. Sodhi JS et al. Cruveilhier-Baumgarten syndrome revisited. Indian J Gastroenterol 2007;26(4):173

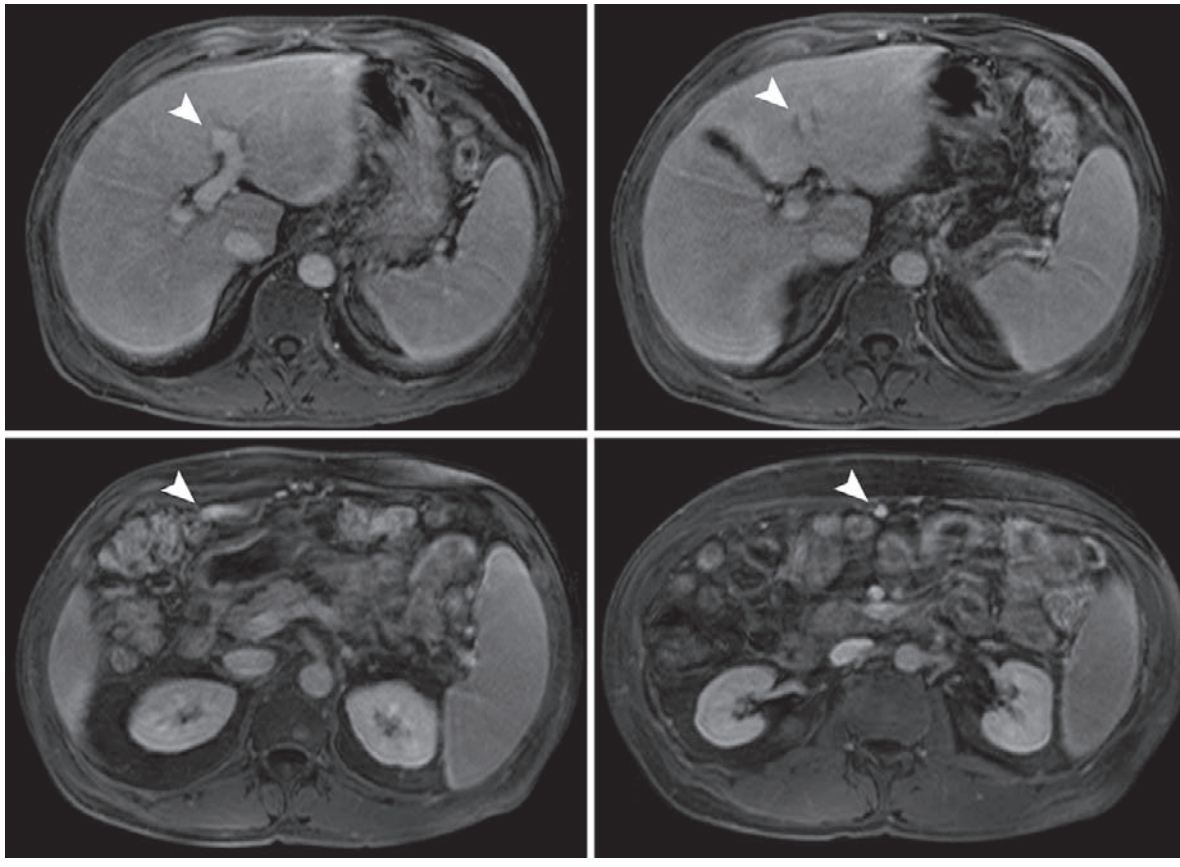

Fig. 4.6.1. Serial axial abdominal MR images show the route of the patent paraumbilical vein from the left portal vein to the anterior abdominal wall (*arrowheads*)

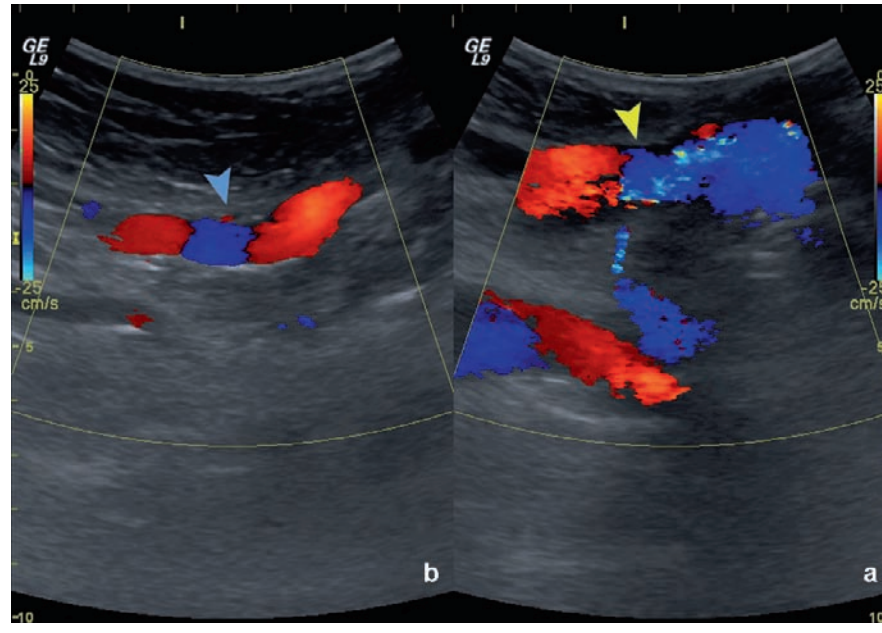

Fig. 4.6.2. Double-window color-coded Doppler image of the same patient shows the beginning of the patent paraumbilical vein (*yellow arrowhead*) at the level of the umbilicus in **a**. In **b**, the vein shows different blood color signal due to its tortuosity (*blue arrowhead*)

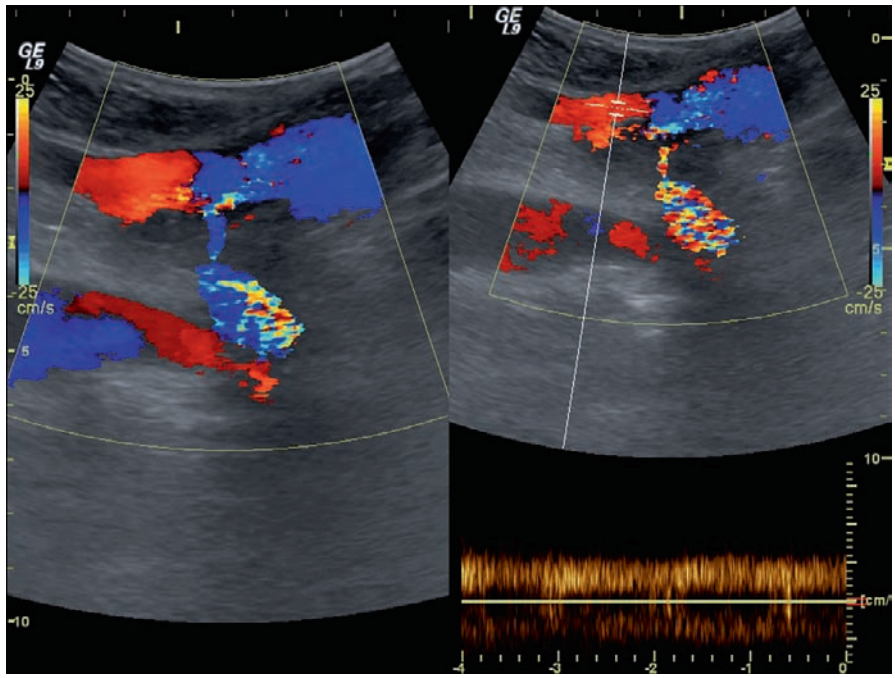

Fig. 4.6.3. Double-window color-coded Doppler image with pulsed Doppler showing a typical venous waveform of the paraumbilical vein

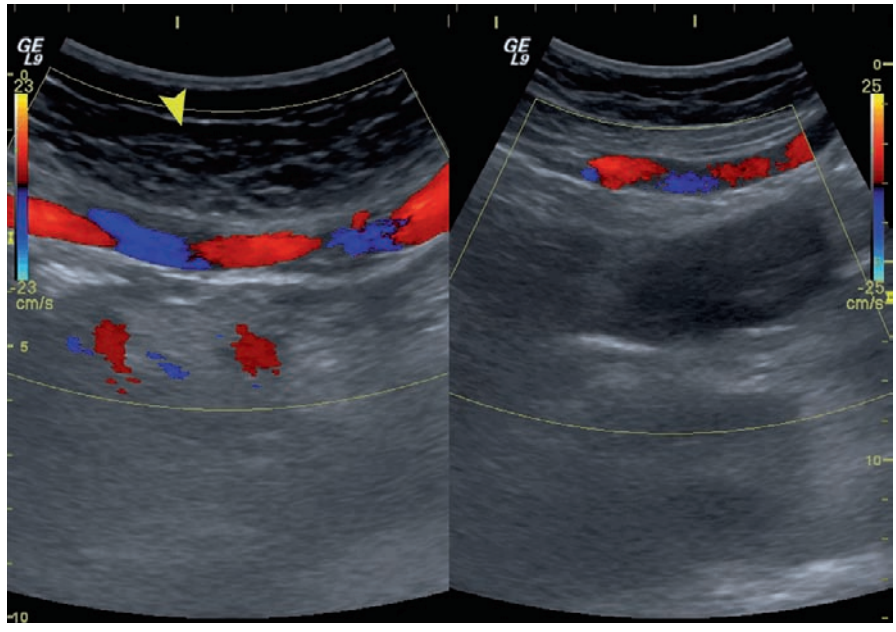

Fig. 4.6.4. Double-window color-coded Doppler image follows the route of the paraumbilical vein below the anterior abdominal wall. Note the superficial position of the vein in relation to the abdominal wall (*yellow arrowhead*)

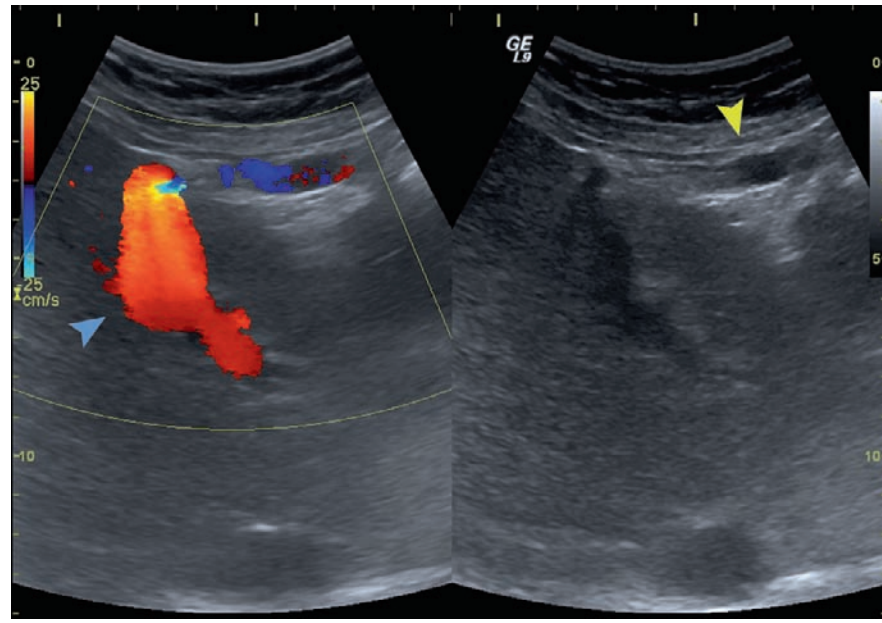

Fig. 4.6.5. Double-window color-coded Doppler image shows the paraumbilical vein within the ligamentum teres (*yellow arrowhead*) heading into the liver to join the left portal vein (*blue arrowhead*)

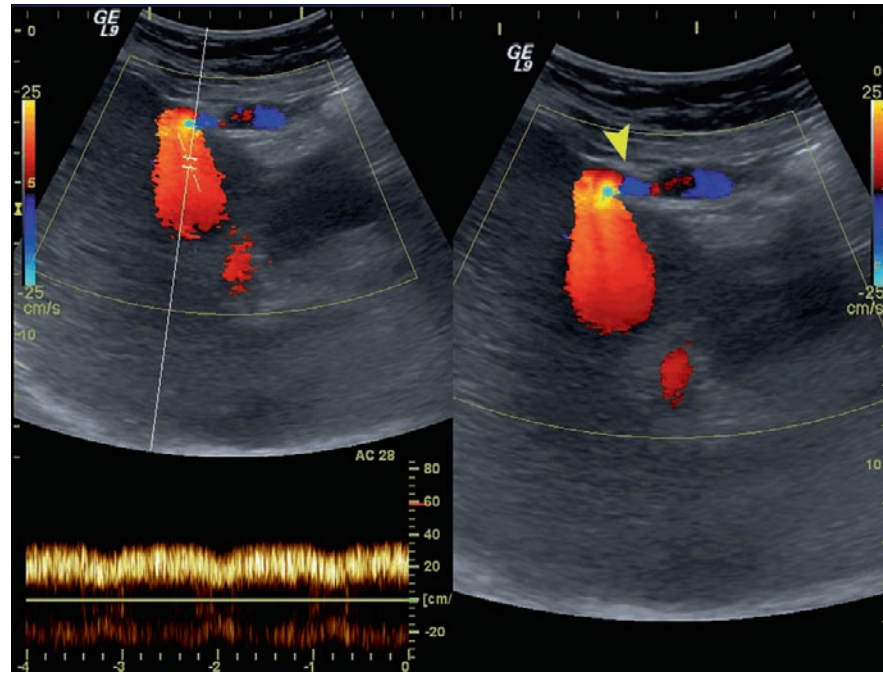

Fig. 4.6.6. Double-window color-coded Doppler image shows the paraumbilical vein within the ligamentum teres with its connection to the portal vein (*yellow arrowhead*). Pulsed Doppler window shows the normal portal vein waveform

4.7

Choledochal Cyst and Caroli Disease

Choledochal cyst is a congenital anomaly characterized by focal cystic dilatation of the extrahepatic bile ducts (the common bile duct or the common hepatic duct). In contrast, Caroli disease is an uncommon congenital disease characterized by cystic dilatation of the intrahepatic biliary ducts with stone formation in the absence of cirrhosis or portal hypertension.

Choledochal cyst is divided into four types:

Type I: is classically characterized by cystic dilatation of the common bile duct. It is the most common type, and presents in infancy or childhood. Up to 60% of cases are diagnosed before the age of 10 years. It has a female predominance.

Type II: is characterized by a diverticulum that arises from the common bile duct or the common hepatic duct.

Type III: is characterized by intramural dilatation of a distal part of the common bile duct that protrudes into the second part of the duodenum. This type is commonly referred to as "choledochocele" (similar to ureterocele when it occurs at the vesicoureteric junction).

Type IV: Caroli disease, the cystic dilatation can occur in one lobe (segmental) or all over the liver (diffuse).

There are two forms of Caroli disease:

- **Caroli syndrome**: is a cystic dilatation of the intrahepatic biliary radicals associated with congenital hepatic fibrosis and portal hypertension.
- **Caroli disease**: is characterized by cystic dilatation of the intrahepatic biliary radicals only. It may be associated with autosomal recessive polycystic kidney disease in up to 70% of cases. It usually presents in a child with intermittent abdominal pain, fever, and hepatomegaly. It has a high risk of malignant transformation. Cholangitis, liver cirrhosis, and septicemia are other possible complications.

Signs on Cholangiography

- Choledochal cyst is diagnosed when a focal cystic dilatation of the common bile duct or the common hepatic duct is found.
- The diagnosis of Caroli disease is based on the identification of the cystic dilatation of the intrahepatic bile ducts (Fig. 4.7.1).

Fig. 4.7.1. Endoscopic retrograde cholangiography shows multifocal saccular dilatation of the intrahepatic biliary ducts mostly affecting the right lobe of the liver (Caroli disease)

Signs on CT

- Choledochal cyst is usually seen as a focal, iso-/hypodense cyst located at the porta hepatis, in the absence of intrahepatic bile duct dilatation (Fig. 4.7.2).
- Caroli disease is diagnosed by identification of multiple, diffuse, or focal dilatations of the intrahepatic bile ducts (Fig. 4.7.3). Polycystic kidney disease may be seen in up to 70% of cases.

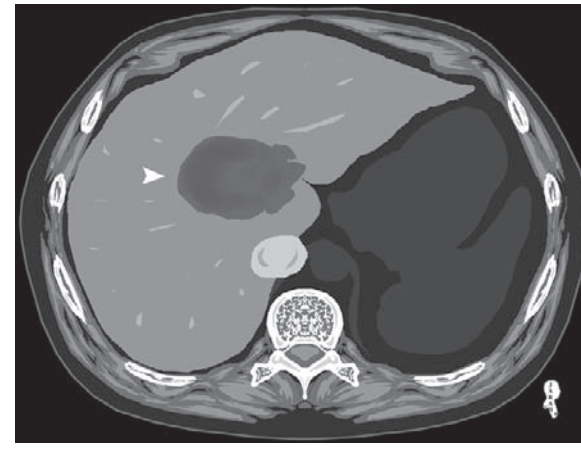

Fig. 4.7.2. Axial abdominal CT illustration shows the typical sign of choledochal cyst (*arrowhead*)

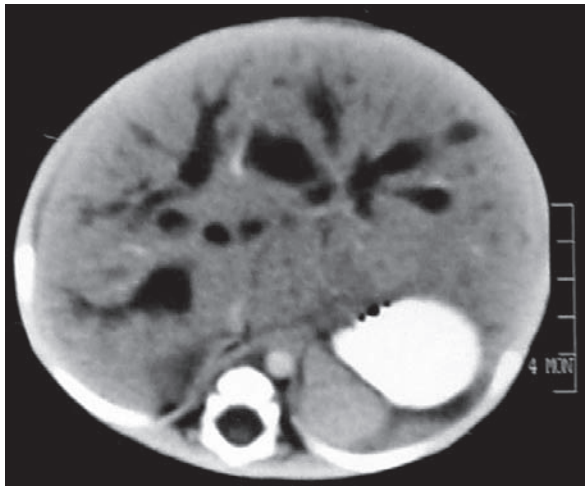

Fig. 4.7.3. Axial postcontrast abdominal CT shows multiple cystic dilatations of the intrahepatic biliary radicals (Caroli disease)

For Further Reading

1. Asselah T et al. Caroli's disease: A magnetic resonance cholangiography diagnosis. Am J Gasteroenterol 1998;93: 109–110
2. Sood GK et al. Caroli disease: Computed tomographic diagnosis. Gastroiintest Radiol 1991;16:243–244
3. Pinto RB et al. Caroli's disease: Report of 10 cases in children and adolescents in southern Brazil. J Pediatr Surg 1998;33:1531–1535
4. Satya R et al. Type IV-a choledocal cyst – a rare adolescent presentation as acute abdomen. Emerg Radiol 2006;13: 39–41

4.8

Mirizzi Syndrome

Mirizzi syndrome is a rare complication of chronic gallbladder stones characterized by obstruction of the common hepatic duct due to impaction of a stone in the cystic duct, resulting in obstructive jaundice.

The disease is rarely identified preoperatively, and it is thought to be caused by long-standing gallbladder stones and parallel orientation of the common bile duct. The patient presents with signs of chronic cholecystitis. Formation of biliobiliary fistula occurs in 1–6% of cases.

MR cholangiography (MRCP) is the method of choice for diagnosing this syndrome, because it demonstrates the whole biliary tree showing the source of obstruction.

Signs on MRCP

The scan shows dilatation of the intrahepatic biliary radicals with obstruction of the common hepatic duct by a cystic duct stone impaction (Figs. 4.8.1 and 4.8.2).

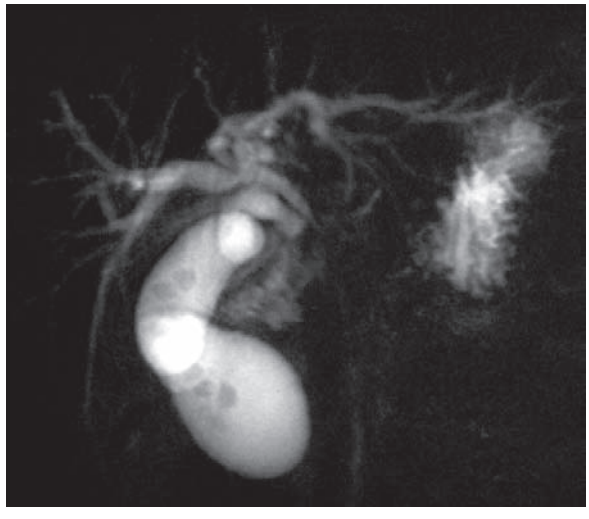

Fig. 4.8.1. MR cholangiography shows dilatation of the intrahepatic biliary radicals with stenosis of the common hepatic duct

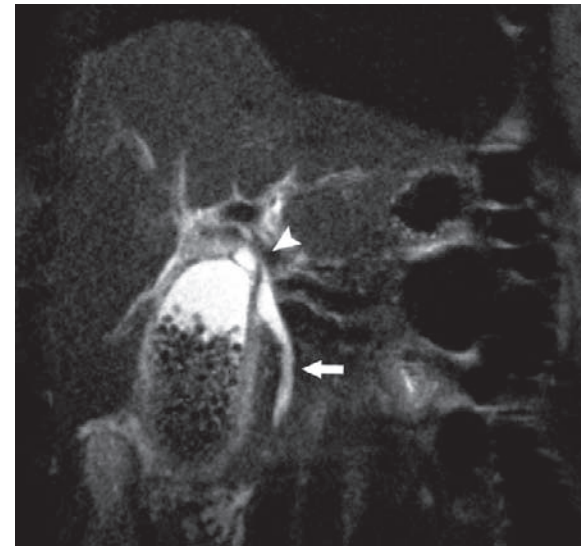

Fig. 4.8.2. MR cholangiography shows the cystic duct abutting the common hepatic duct causing its collapse (*arrowhead*). Note the normal-sized common bile duct (*arrow*) and the large amount of gallbladder stones within the gallbladder cavity

Signs on CT

- Dilatation of the intrahepatic biliary radicals with dilated proximal common bile duct.
- Stone presence in cystic duct may be identified.

For Further Reading

1. Cornud F et al. Mirizzi syndrome and biliobiliary fistulas: Roentgenologic appearance. Gastrointest Radiol 1981;6: 265–268
2. Kaya D et al. MRCP diagnosis of Mirizzi syndrome in a paediatric patient: importance of T1-weighted gradient echo images for diagnosis. Pediatr Radiol 2006;36:980–982

4.9

Congenital Anomalies of the Spleen

Most congenital anomalies of the spleen are asymptomatic and clinically insignificant. However, it is important to recognize these anomalies so as to differentiate them from tumors or other true pathological conditions of the spleen.

Splenic Clefts

Clefts are occasionally seen within the spleen. They are a remnant of the grooves that separates the fetal lobules. These clefts can be deep and sharp in some cases (Fig. 4.9.1).

Splenic clefts are asymptomatic, and it is important to recognize them so as to differentiate them from splenic lacerations.

Accessory Spleen (Supernumerary Spleen)

Accessory spleen (splenule) is a congenital focus of healthy splenic tissue separated from the main body of the spleen due to failure of fusion during embryogenesis.

Accessory spleen is the most common congenital anomaly of the spleen and it is seen in 10–30% of patients at autopsy.

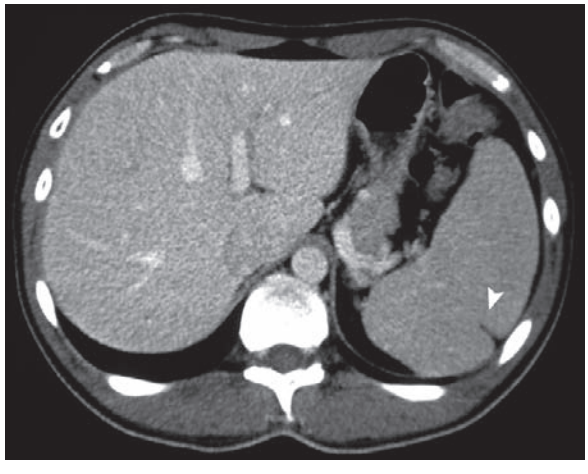

Fig. 4.9.1. Axial abdominal postcontrast CT image shows small splenic cleft as an incidental finding (*arrowhead*)

Accessory splenules can be found commonly at the hilum (Fig. 4.9.2) or the inferior pole of the spleen (Fig. 4.9.3); they can be mistaken for enlarged lymphadenopathy, and they enhance with a similar density as the normal healthy spleen.

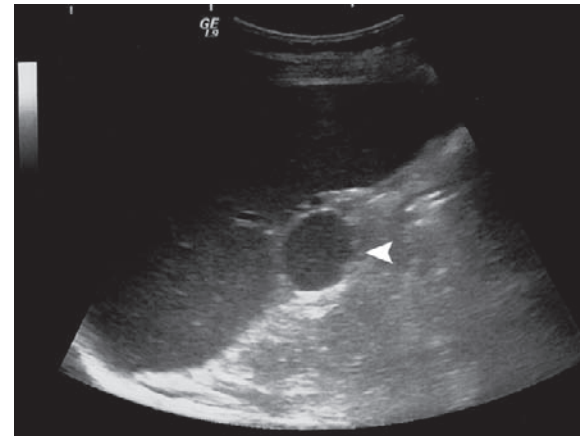

Fig. 4.9.2. US image of the spleen shows a rounded, sharply defined mass with similar echogenicity as the spleen and located at the hilum, representing an accessory spleen (*arrowhead*)

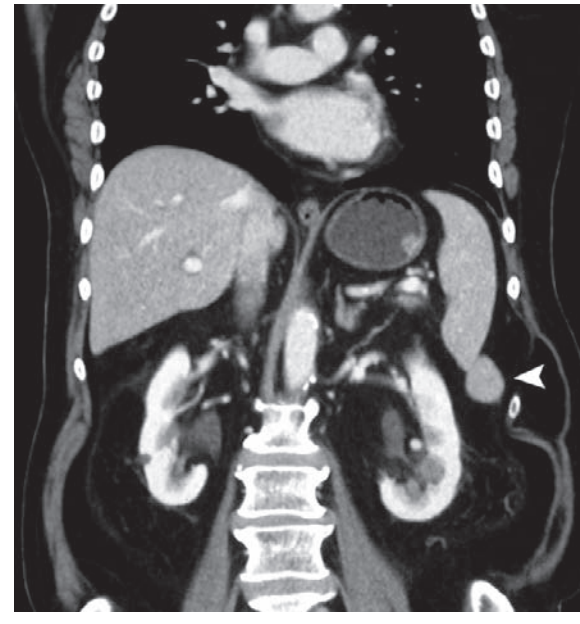

Fig. 4.9.3. Coronal abdominal postcontrast CT image shows a round mass with similar density and degree of enhancement as the spleen and located at its inferior pole, representing an accessory spleen (*arrowhead*)

Fig. 4.9.4. Axial abdominal postcontrast CT image shows mottled appearance of the spleen during the arterial phase of a contrast-enhanced CT examination of the abdomen, representing wild spleen (*arrows*)

Fig. 4.9.5. Axial abdominal CT illustration shows abnormally high location of the spleen with its hilum facing down (wandering spleen)

Wild Spleen (Moiré Spleen)

Wild spleen is a term that describes the mottled appearance of the spleen in the arterial phase of contrast-enhanced CT examination of the abdomen. The spleen enhances in a mottled fashion creating a fake appearance of pseudomasses (Fig. 4.9.4). It is caused by differential enhancement of the red and white pulp. It is a normal finding and should not be mistaken for a pathological process.

Wandering Spleen

Wandering spleen is a condition characterized by movement of the spleen from its normal position. It occurs due to laxity of the splenic ligaments (the gastrosplenic and the splenorenal ligaments), usually as a result of aging and pregnancy. Congenital wandering spleen occurs due to a deficiency of one of its ligaments. It is a rare condition and accounts for 0.2% of congenital anomalies of the spleen.

Wandering spleen can be suspected when the hilum of the spleen is seen facing the aorta instead of facing the stomach (Fig. 4.9.5).

Patients are usually asymptomatic or they present with a mobile abdominal mass with acute or chronic abdominal pain due to torsion of the splenic artery.

For Further Reading

1. Gayer G et al. Congenital anomalies of the spleen. Semin Ultrasound CT MRI 2006;27:358–369
2. Sels JPJE et al. Pitfall of the accessory spleen. Neth J Med 2000;56:153–158
3. Corsi A et al. Acute abdomen in torsion of accessory spleen. Eur J Radiol Extra 2007;64:15–17

4.10

Anomalies of the Inferior Vena Cava

The inferior vena cava (IVC) arises due to the formation and regression of several anastomoses of three pairs of venous channels (posterior, subcardinal, and supracardinal veins). The posterior cardinal vein usually disappears to give rise, on the right, to the common iliac vein and the caval fork. The right subcardinal vein gives rise to the right hepatic vein and the suprarenal IVC segment. The right supracardinal vein gives rise to the infrarenal IVC, and the anastomoses between the supracardinal vein and the subcardinal vein on the right side give rise to the renal IVC segment (Fig. 4.10.1).

Congenital anomalies of the IVC are explained by abnormal regression or persistence of parts of these embryonic veins:

- **Double Inferior Vena Cava:** A double IVC is defined as the presence of double infrarenal IVCs, one on the right in the normal position, and an accessory left infrarenal IVC segment that ends at the left renal vein (Fig. 4.10.2). It arises due to persistence of the right and left supracardinal veins. It has a prevalence of 2–3% in the general population (Fig. 4.10.3).
- **Left-Sided Inferior Vena Cava:** In left-sided IVC, the right infrarenal IVC is absent and there is presence of the left infrarenal IVC. The left infrarenal IVC typically ends at the left renal vein, which then crosses anterior to the aorta to join the right IVC via a renal cava segment (Fig. 4.10.4). It arises due to persistence of the left supracardinal vein and regression of the right supracardinal vein. It has a prevalence of 0.5% in the general population. Left-sided IVC is a common anomaly in heterotaxy syndromes (Fig. 4.10.5).
- **Double Right Inferior Vena Cava:** Double right IVC is defined as the presence of two infrarenal IVCs lying

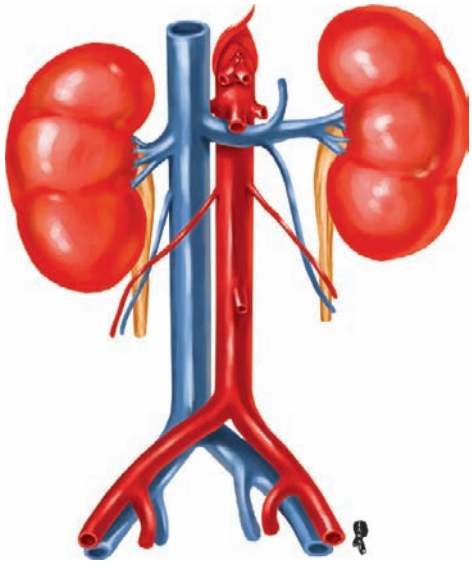

Fig. 4.10.1. Illustration showing the normal IVC with its normal branches and relationship to the adjacent structures

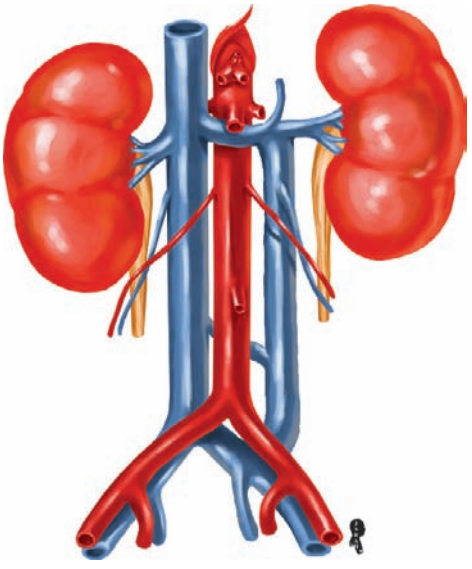

Fig. 4.10.2. Illustration showing the double IVCs. Note the accessory IVC on the left side of the aorta, which opens into the left renal vein

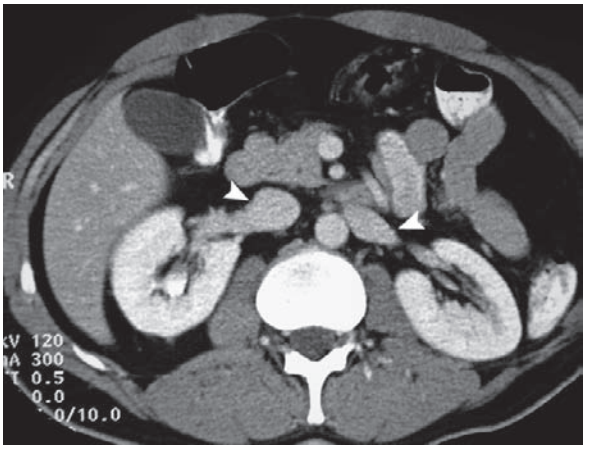

Fig. 4.10.3. Axial postcontrast CT image shows double IVCs, one located on the right side of the aorta and the other located on the left side (*arrowheads*)

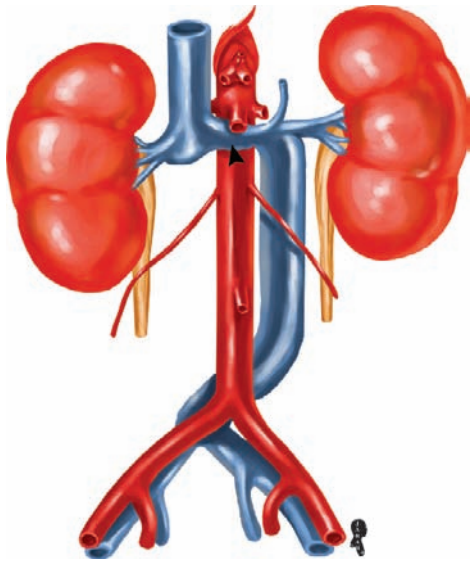

Fig. 4.10.4. Illustration showing left-sided IVC. Note absence of the IVC continuation on the right side, and connection of the right suprarenal IVC segment to the left-sided infrarenal IVC segment via a renal cava segment (*arrowhead*)

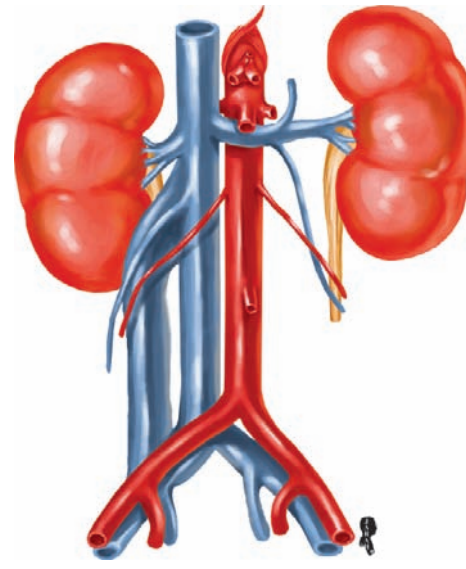

Fig. 4.10.6. Illustration showing double right IVC. Note the accessory IVC originating from the infrarenal IVC and opening into the right common iliac vein

Fig. 4.10.5. Axial postcontrast CT image shows left-sided IVCs (*white arrowhead*). Note the pancreas in its normal position (*open arrowhead*)

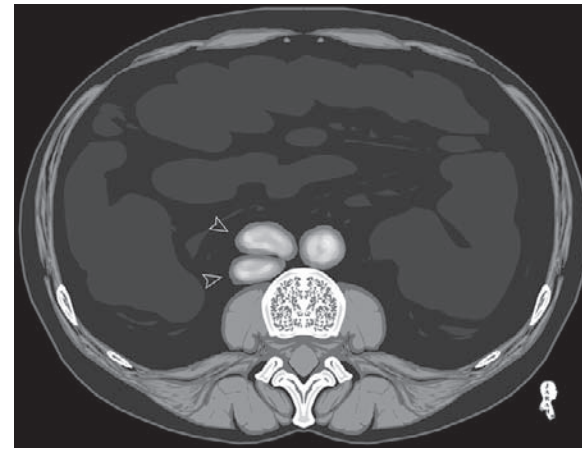

Fig. 4.10.7. Axial CT illustration shows the appearance of the double right IVC. Note the presence of two IVCs on the right side of the aorta (*open arrowheads*)

on the right side of the aorta (Fig. 4.10.6). It is a very rare anomaly and usually asymptomatic (Fig. 4.10.7).

- **Azygos Continuation of the Inferior Vena Cava:** In azygos continuation of the IVC, the IVC passes posterior to the diaphragmatic crura to enter the thorax as the azygos vein (Fig. 4.10.8). The azygos vein joins the superior vena cava (SVC) at the usual location (at the level of T4 posteriorly).
- **Hemiazygos Continuation of the Inferior Vena Cava:** In hemiazygos continuation of the IVC, the IVC crosses posterior to the aorta in the abdomen to continue cephalad to the thorax as the hemiazygos vein (Fig. 4.10.9). In the thorax, the hemiazygos vein crosses posterior to the descending thoracic aorta at the level of T8 or T9 to join the azygos vein as normal.

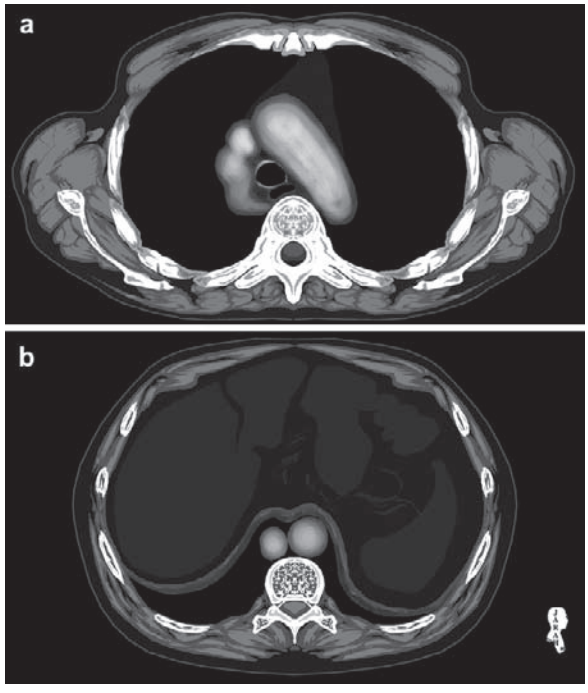

Fig. 4.10.8. Axial thoracic and abdominal CT illustrations show azygos continuation of the IVC. In **a**, the azygos vein is dilated (*white arrowhead*) and occupies the position of the IVC (*open arrowhead*). In **b**, the dilated azygos vein can be seen in its normal position running posterior to the diaphragmatic crura (*open arrow*), with absence of the IVC near the liver (*white arrow*)

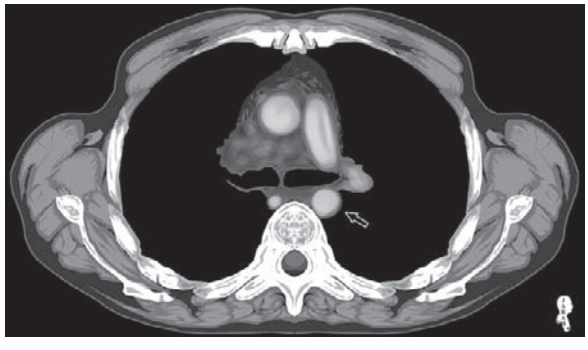

Fig. 4.10.9. Axial thoracic postcontrast CT illustration shows dilated hemiazygos vein (*open arrow*)

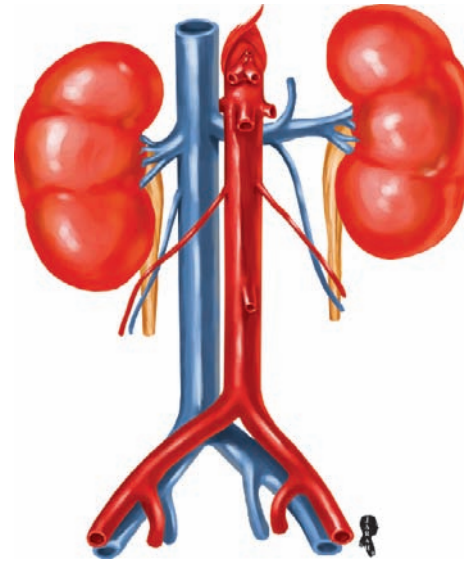

Fig. 4.10.10. Illustration showing the retroaortic left renal vein

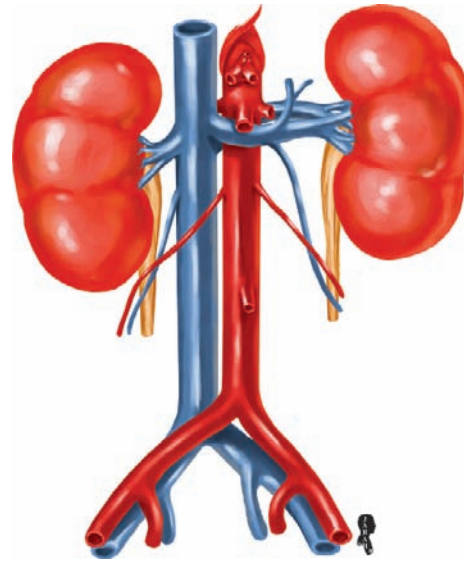

Fig. 4.10.11. Illustration showing the circumaortic left renal vein

- **Retroaortic Left Renal Vein:** *The left renal vein* passes posterior to the aorta (Fig. 4.10.10). It has a prevalence of 2% in the population.
  Posterior nutcracker syndrome is an unusual cause of unexplained episodes of microscopic or macroscopic hematouria with or without flank pain in the absence of glomerular disease. The disease arises due to compression of a retroaortic left renal vein between the aorta and the vertebral body, causing venous hypertension, hematouria, and left gonadal vein varicocele.
- **Circumaortic Left Renal Vein (Renal Collar):** In circumaortic left renal vein, two left renal veins are present. The superior renal vein crosses anterior to the aorta, and the inferior renal vein crosses posterior to the aorta (Fig. 4.10.11). It has a prevalence of 8% in the population.

- **Persistent Left Superior Vena Cava:** In persistent left SVC, two SVCs are found due to persistence of the anterior left cardinal vein. It has a prevalence of 0.5% in the population. On plain chest radiographs, the left SVC causes widening of the mediastinum giving the heart a "figure of 8" shape.

For Further Reading

1. Tagliafico A et al. Double inferior vena cava associated with an anomalous venous ring encircling the right common iliac artery: Report of one case with CT and US. Eur J Radiol Extra 2007;64:111–115
2. Kumar S et al. Rare case of renal cell carcinoma with double inferior vena cava with venous thrombosis. Urology 72: 461.e7–461.e10
3. Shindo S et al. Anomalies of the inferior vena cava and left renal vein: Risks in aortic surgery. Ann Vasc Surg 2000; 14:393–396
4. Gil RJ et al. Left-sided inferior vena cava and aortoiliac surgery. EJVES Extra 2008;15:9–11
5. Kim HJ et al. Hemiazygos continuation of a left inferior vena cava draining into the right atrium via persistent left superior vena cava: Demonstration by helical computed tomography. Cardiovasc Intervent Radiol 1995;18:65–67
6. Sanchez FW et al. Hemiazygos continuation of a left inferior vena cava: Misleading radiographic finding in chest trauma. Cardiovasc Intervent Radiol 1985;8:140–142
7. Artico M et al. Radiological evidence of anatomical variation of the inferior vena cava: Report of two cases. Surg Radiol Anat 2004;26:153–156
8. Jang YB et al. Posterior nutcracker phenomenon. Nephrol Dial Transplant 2005;20:2573–2574

4.11

Congenital Anomalies of the Kidneys

Congenital renal anomalies are the most common urinary anomalies encountered via the use of imaging modalities compared to other organs. Some of these anomalies are normal variants without clinical significance, and some anomalies cause significant clinical symptoms.

Persistent Fetal Lobulation

Persistent fetal lobulation is a normal variant characterized by renal indentations between the spaces of the renal pyramids (Fig. 4.11.1). These lobulations may be mistaken for renal scars from chronic infection. Fetal lobulations can be differentiated from renal scarring simply by looking at the renal parenchyma, which is normal in fetal lobulation, and abnormal in renal scarring.

Junctional Parenchymal Defect

Junctional parenchymal defect (JPD) is a normal variant characterized by an area of defect in the renal cortex that reaches the central sinus. The area of defect is typically triangular and filled with fatty tissue from the perinephric fat. On US, JPD is identified as a linear or triangular echogenic area in the posteroinferior or anterosuperior aspect of the kidney (Fig. 4.11.2). On CT, JPD is identified as an area of cortical defect with fat-density (Fig. 4.11.3).

Fig. 4.11.1. Axial postcontrast abdominal CT shows fetal lobulation of the right kidney (*arrowheads*)

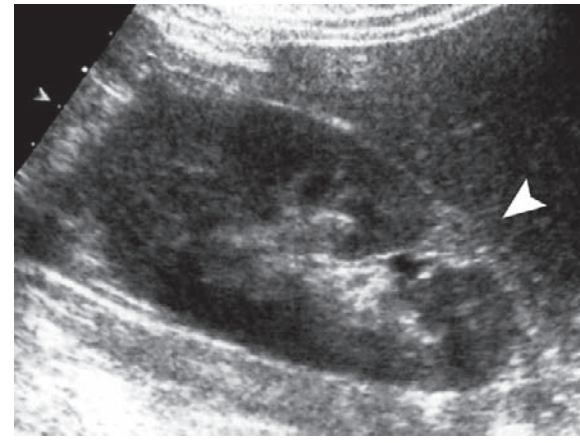

Fig. 4.11.2. Sagittal US image shows typical hyperechoic area located at the anterosuperior surface of the kidney representing junctional parenchymal defect that reaches the central sinus (*arrowhead*)

Dromedary Hump (Renal Hump)

Dromedary hump is a normal variant characterized by focal bulging of the lateral border of the left kidney as a surface adaptation to the adjacent spleen (Fig. 4.11.4).

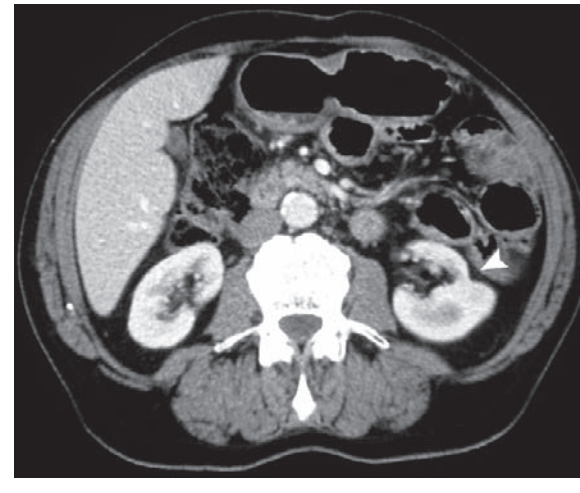

Fig. 4.11.3. Axial postcontrast abdominal CT image of another patient shows the junctional parenchymal defect as an area of fat-density defect in the left renal cortex (*arrowhead*)

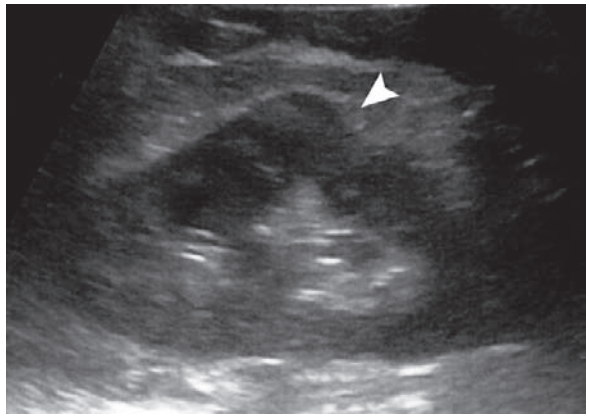

Fig. 4.11.4. Sagittal US image shows dromedary hump (*arrowhead*)

Hypertrophy of the Column of Bertin

Column of Bertin is a term used to describe the normal cortical tissue located between the pyramids that project into the renal sinus. Hypertrophy of these columns may occur as a normal variant that can be mistaken for a mass lesion. Columns of Bertin are typically seen in the middle third of the left kidney (Fig. 4.11.5).

Duplex Kidney and Renal Duplication

Duplication of the kidney is the most common anomaly in the genitourinary (GU) system. *Duplex kidney* is defined as one kidney that is drained by two separate renal pelves. In contrast, *renal duplication* is a term used to describe two ureters draining a duplex kidney (Fig. 4.11.6). The ureters can join together above the bladder in a "Y" or "V" shape.

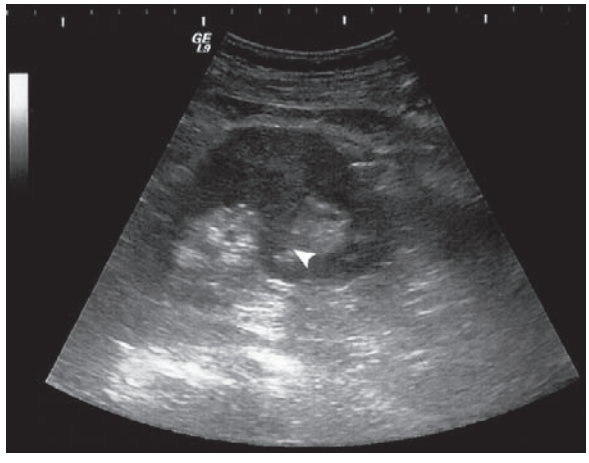

Fig. 4.11.5. Sagittal US image shows hypertrophic column of Bertin in the middle third of the kidney (*arrowhead*)

Fig. 4.11.6. Intravenous urography image shows left duplex kidney with two renal pelves joining together into one ureter (*arrowhead*), and a right renal duplication with two hydronephrotic ureters (*open arrowhead*)

Crossed Renal Ectopia

Crossed renal ectopia is a congenital anomaly characterized by a kidney located on the opposite side from which its ureter inserts into the urinary bladder (Fig. 4.11.7).

Pelvic Kidney

Pelvic kidney, when it occurs naturally, represents a congenital ectopic kidney (Fig. 4.11.8). However, pelvic kidney can be due to kidney transplant. Differentiation is based on the clinical history.

Renal Fusion Anomalies

Fusion anomalies are characterized by two kidneys that are fused together to become one. The resulting fused kidney has several shapes, including:

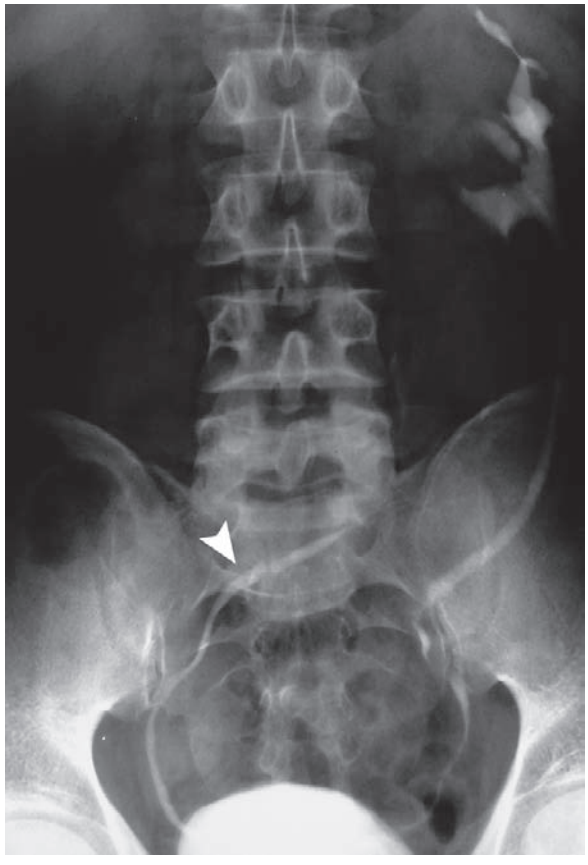

Fig. 4.11.7. Intravenous urography image shows crossed renal ectopia. Both kidneys are fused on the left side and the right kidney's ureter is crossing to the other side to join the urinary bladder in its normal location (*arrowhead*)

- **Horseshoe kidney:** results from fusion of both inferior poles together (Figs. 4.11.9 and 4.11.10). Both renal pelves and the ureters are typically anteriorly displaced.
- **S-shaped or sigmoid kidney:** results from fusion of both kidneys together by a midline isthmus (Fig. 4.11.11).
- **Pancake (disc) kidney:** results from fusion of both kidneys at their renal pelvis side together with displacement of the renal pelves (Fig. 4.11.12).

Fig. 4.11.8. Intravenous urography image shows congenital ectopic right kidney

Fig. 4.11.9. Intravenous urography image shows horseshoe kidney (*arrowheads*)

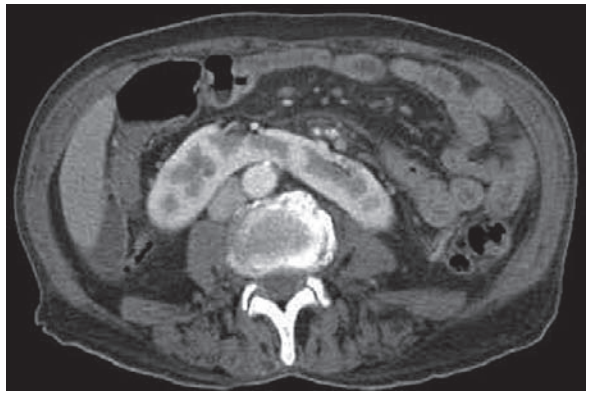

Fig. 4.11.10. Axial postcontrast abdominal CT image of another patient shows horseshoe kidney

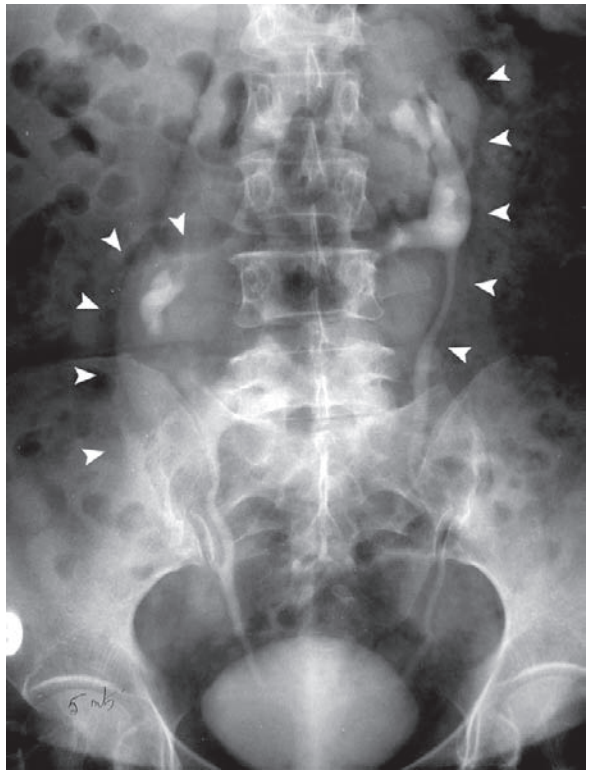

Fig. 4.11.11. Intravenous urography image shows S-shaped or sigmoid kidney (*arrowheads*)

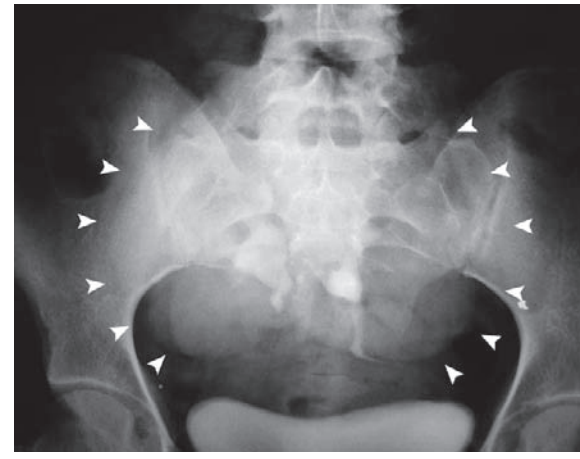

Fig. 4.11.12. Intravenous urography image shows pelvic pancake kidney (*arrowheads*)

For Further Reading

1. Paspulati RM et al. Sonography in benign and malignant renal masses. Radiol Clin N Am 2006;44:787–803
2. Carter AR et al. The junctional parenchymal defect: A sonographic variant of renal anatomy. Radiology 1985;154: 499–502
3. Kehagias DT et al. Horseshoe kidney associated with anomalous inferior vena cava. Eur Radiol 1990;9:935–936
4. Eze AR et al. "Pancake kidney": A renal anomaly complicating aortic reconstruction. Ann Vasc Surg 1998;12:278–281
5. Hartman GW et al. The duplex kidney and related abnormalities. Clin Radiol 1969;20:387–400

4.12

Congenital Uterine Malformations

Congenital uterine malformations, also known as Müllerian duct anomalies, are rare in the general population (2–3%), and usually seen in women with infertility. Infertility is defined as "failure to conceive after 1 year of unprotected intercourse."

In the normal embryo, the uterus is formed by fusion of two Müllerian (paramesonephric) ducts that must meet in the midline. Due to the fusion of the two ducts, an internal midline septum forms. Resorption of the midline septum with maturation of the fused Müllerian ducts results later in the formation of the normal uterus (Fig. 4.12.1).

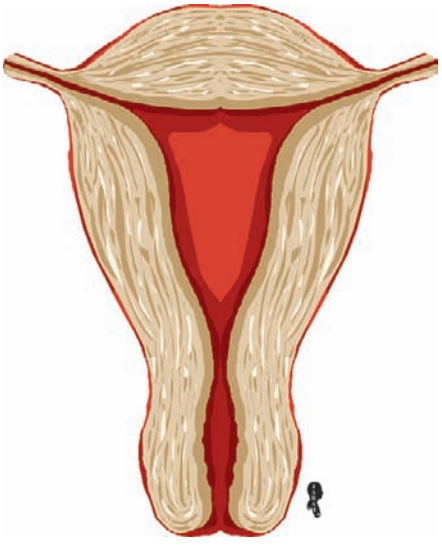

Fig. 4.12.1. Illustration showing the normal shape of the uterus

Congenital uterine anomalies are classified into five major classes

- **Class 1 anomalies:** arise due to failure of both Müllerian ducts to form properly, resulting in agenesis or hypoplasia of the uterus.
- **Class 2 anomalies:** arise due to failure of one Müllerian duct to form, resulting in unilateral uterus or unicornuate uterus.
- **Class 3 anomalies:** arise due to failure of both Müllerian ducts to fuse, resulting in two unilateral uteri or didelphys uterus.
- **Class 4 anomalies:** arise due to failure of the internal midline septum to resorb completely, resulting in septate uterus.
- **Class 5 anomalies:** arise due to exposure to diethylstilbestrol (DES) during pregnancy.

Fig. 4.12.2. Illustration showing the unicornuate uterus

- **Segmental Agenesis or Hypoplasia:** Agenesis or hypoplasia anomalies depend on which portion of the female genital organ fails to form: the vagina, the cervix, or the uterine fundus. These anomalies present with primary amenorrhea, and they constitute 5% of uterine anomalies.
- **Mayer-Rokitansky-Kuster-Hauser syndrome:** is a rare disease characterized by agenesis of the vagina.
- **Unicornuate Uterus:** Unicornuate uterus, or the single horn uterus, arises due to failure of one of the paramesonephric ducts to form. The resulting uterus is described as "banana-shaped" uterus with a single fallopian tube (Figs. 4.12.2 and 4.12.3). This type of uterine anomaly can go unnoticed because some women can have a normal pregnancy with it; others might suffer from recurrent miscarriages, ectopic pregnancy, and fetal malpresentation.

Unicornuate uterus has a high incidence of contralateral renal agenesis to the side of the missing uterus.

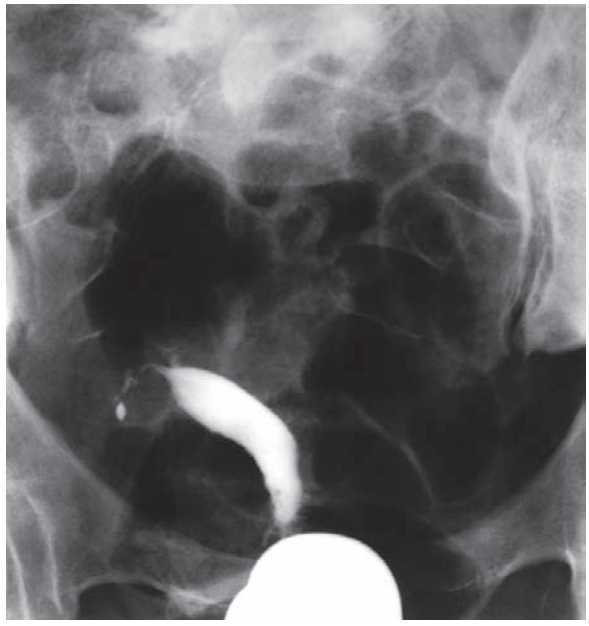

Fig. 4.12.3. Hysterosalpingography image showing the unicornuate uterus

- **Uterus Didelphys:** Uterus didelphys results from failure of the two paramesonephric ducts to fuse. The resulting uterus is made of two separated uterine horns, each with its own cervix and its own vagina (Figs. 4.12.4 and 4.12.5). A vaginal septum is commonly associated with uterus didelphys, creating two separate vaginas. When the vaginal septum is longitudinally oriented, it usually has no clinical significance, although some patients may complain of dyspareunia. When the vaginal septum is horizontally located, it can result in hematocolpos.

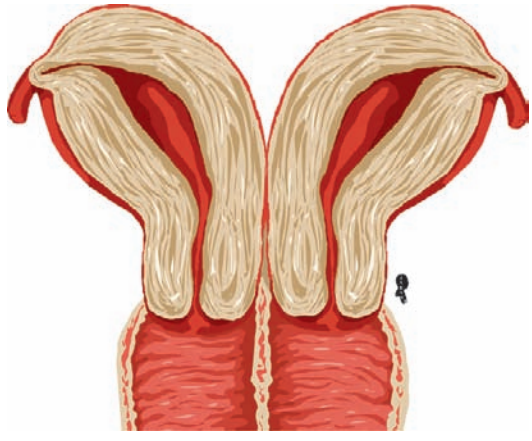

Fig. 4.12.4. Illustration showing the didelphys uterus with vaginal septum

Fig. 4.12.5. Hysterosalpingography image showing the didelphys uterus

- **Bicornuate Uterus:** Bicornuate uterus results from partial fusion of the paramesonephric ducts, with the resulting uterus described as "heart-shaped" or concave. When the duplication of the uterus is accompanied by a single cervix, it is called "*uterus bicornis unicollis*" (Figs. 4.12.6 and 4.12.7). In contrast, when there is duplication of the uterus and the cervix, the uterus is called "*uterus bicornis bicollis*" (Fig. 4.12.8).

  The main obstetrical complication of this uterine anomaly is related to the abnormal fetal position and premature labor. Spontaneous abortion occurs in up to 35% of cases.
- **Septated Uterus:** Septated uterus results from complete fusion of the paramesonephric ducts, with failure of the septum between them to resorb. The septum is composed of myometrium, fibrous tissue,

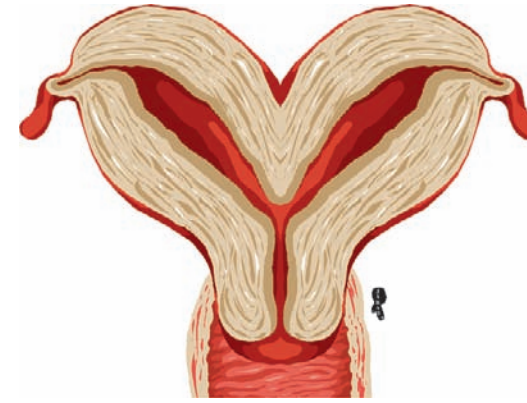

Fig. 4.12.6. Illustration showing the bicornis unicollis uterus

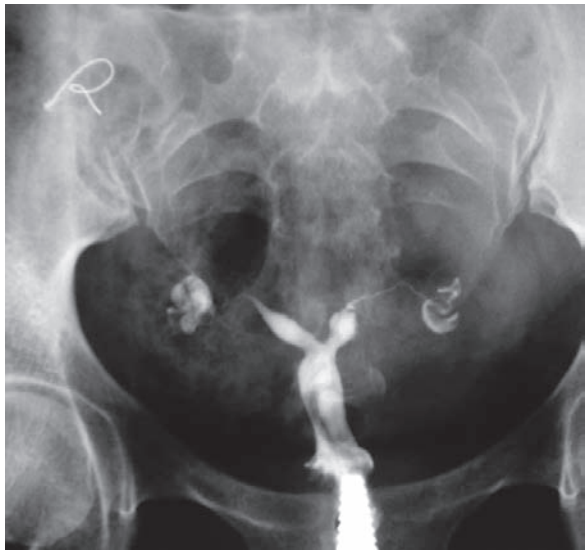

Fig. 4.12.7. Hysterosalpingography image showing the bicornis unicollis uterus

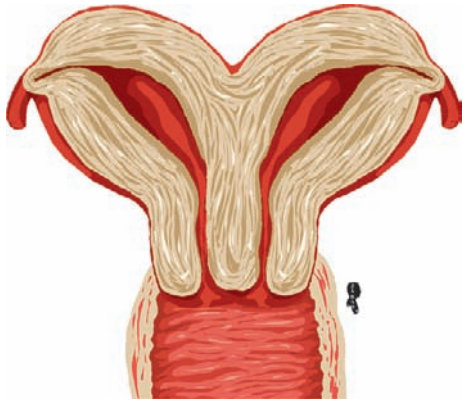

Fig. 4.12.8. Illustration showing the bicornis bicollis uterus

or a combination of the two. The septum can be partial or complete. A complete septum may be long enough to reach the vagina (Fig. 4.12.9).

This anomaly has the highest rate of spontaneous abortion among all the other anomalies (up to 67% of cases). It is thought that decreased blood supply to the septum results in this high rate of spontaneous abortions.

Fig. 4.12.9. Illustration showing complete septated uterus

Q: How can you differentiate between septated uterus and bicornuate uterus on imaging modalities like hysterosalpingography?

If the angle between the two endometrial cavities is acute (<75°), then the diagnosis is a septated uterus; if the angle is wide (>105°), the diagnosis is a bicornuate uterus.

- **DES-Related Anomalies:** DES is an old drug that was used between the late 1940s and 1970s as a helpful medication in cases of threatened abortion, recurrent miscarriages, and diabetes. Daughters of the women who used the drug had variable patterns of uterine anomalies. The most characteristic uterine anomaly related to this drug is a "T-shaped uterus" (Fig. 4.12.10). Moreover, DES exposure increases the risk of vaginal and cervical malignancies.
- **Uterus Arcuatus:** Uterus arcuatus is a mild form of uterine anomaly characterized by slight myometrial indentation in the center of the uterine fundus (Fig. 4.12.11).

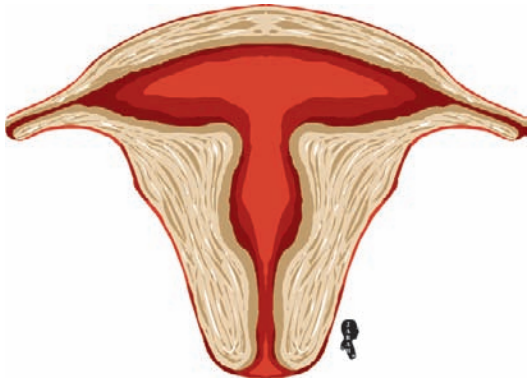

Fig. 4.12.10. Illustration showing DES-related uterus

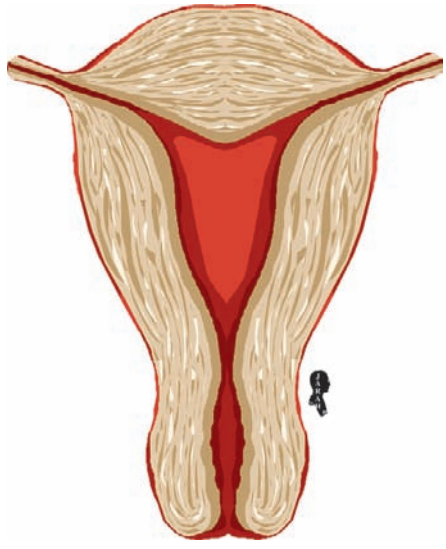

Fig. 4.12.11. Illustration showing the arcuate uterus

For Further Reading

1. Lin PC et al. Female genital anomalies affecting reproduction. Fertil Steril 2002;78:899–915
2. Kumar S et al. Bicornuate uterine horns with complete cervical-vaginal agenesis and congenital vesicouterine fistula. Int Urogynecol J 2008;19:739–741
3. Growdon WB et al. Uterine didelphys with duplicated upper vagina and bilateral lower vaginal agenesis: a novel Müllerian anomaly with options for surgical management. Fertil Steril 2008;89:693–698
4. Baramki TA. Hysterosalpingography. Fertil Steril 2005;83: 1595–1606

4.13

Retrocaval Ureter

Retrocaval ureter (RU) is a rare condition characterized by passage of the right ureter posterior to the inferior vena cava (IVC) at the level of the third and fourth lumbar vertebrae; the ureter then turns anteriorly to complete its normal course and position (Fig. 4.13.1).

RU arises due to persistence of the ventral intrarenal subcardinal vein, one of the components of the embryological IVC.

RU is often asymptomatic; symptomatic patients present with right flank pain due to urinary tract obstruction, hydronephrosis, or infection. There is often hematuria of varying degrees.

There are two types of RU:

- **Type 1 (low loop):** the ureter is obstructed, dilated, with a characteristic feature on intravenous urography (IVU).
- **Type 2 (high loop):** the ureter passes behind the IVC before or at the level of the pelvic–ureteric junction. This type is usually not obstructed.

Signs on IVU

RU presents typically as dilatation of the upper third of the ureter, proximal to the point where the ureter passes behind the IVC. The shape of the dilated proximal third of the ureter plus its renal pelvis is classically described as "reversed J-shaped" or "fish-hook deformity" (Fig. 4.13.2).

Fig. 4.13.1. Illustration showing the abnormal course of the retrocaval ureter

Fig. 4.13.2. Intravenous urography image shows dilatation of the proximal ureter with mild hydronephrosis exhibiting a classic "reversed J-shaped appearance." Note the sudden cut-off of the ureter at the level of the fourth lumbar vertebra (*arrowhead*)

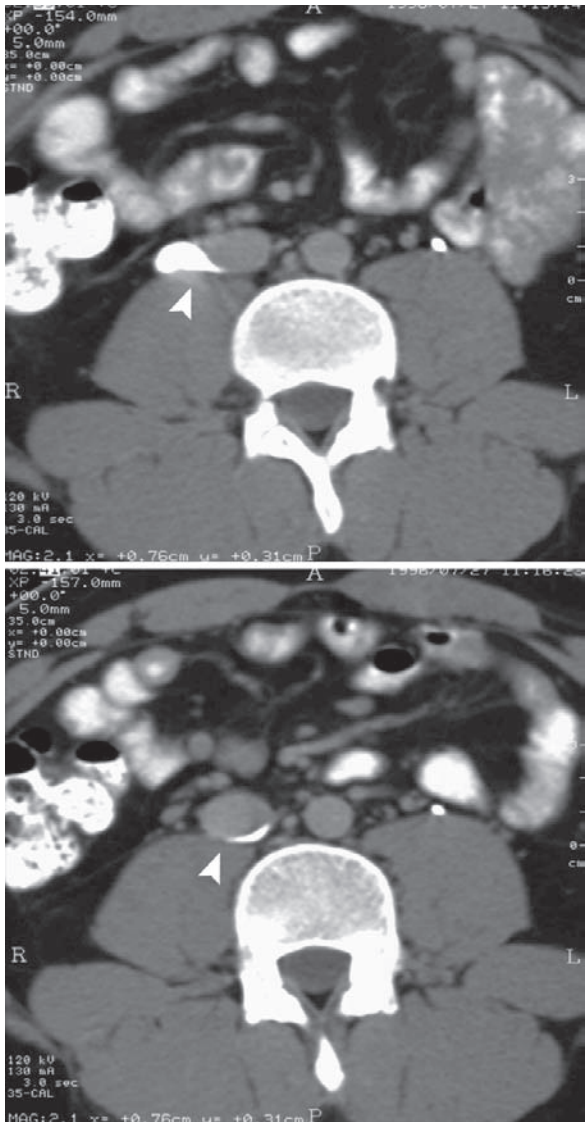

Fig. 4.13.3. Sequential CT urography images show the right ureter passing behind the IVC (*arrowheads*)

Signs on CT

CT demonstrates the abnormal course of the right ureter wrapping around the IVC (Fig. 4.13.3).

For Further Reading

1. Perimenis P et al. Retrocaval ureter and associated anomalies. Int Urol Nephrol 2002;33:19–22
2. Rao J et al. Right retrocaval ureter and left nutcracker syndrome: A case report. Urology 2008;71:1226.e9–1126.e11
3. Uthappa MC et al. Retrocaval ureter-magnetic resonance appearance. Eur Urol Suppl 2006;5:463–465

4.14

Hematocolpos

Hematocolpos is a term used to describe a rare condition characterized by retention of menstrual blood and cellular debris within the vagina (Fig. 4.14.1). Hematocolpos can be caused by imperforated hymen, another very rare condition with an estimated incidence of 0.014% of the population. The hymen is an embryological remnant of mesodermal tissue that is normally perforated. Hematocolpos is sporadic, although familial cases have been reported.

The condition is often diagnosed at puberty, where patients present with vague chronic abdominal pain, amenorrhea, constipation, urinary obstruction, and abdominal mass. On clinical vaginal examination, a bulging imperforated hymen is usually found.

Hematocolpometra: is another rare condition characterized by retention of menstrual blood within both the vagina and the uterus.

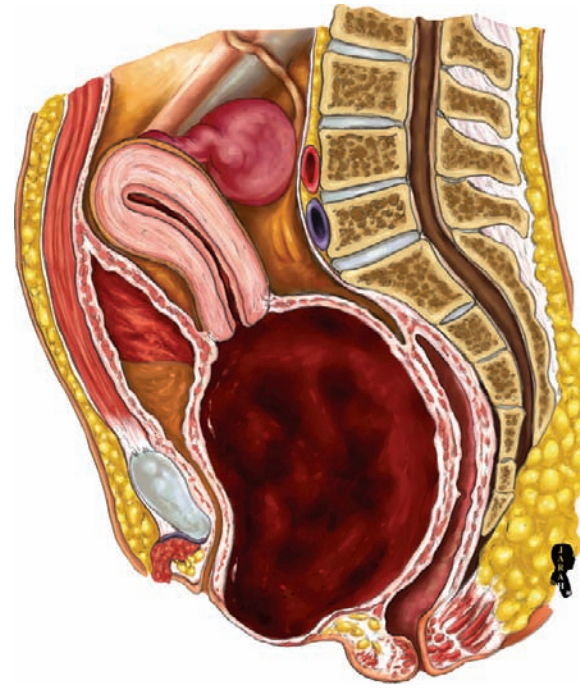

Fig. 4.14.1. Illustration showing the pathological image of hematocolpos, where the vagina is fully distended with blood

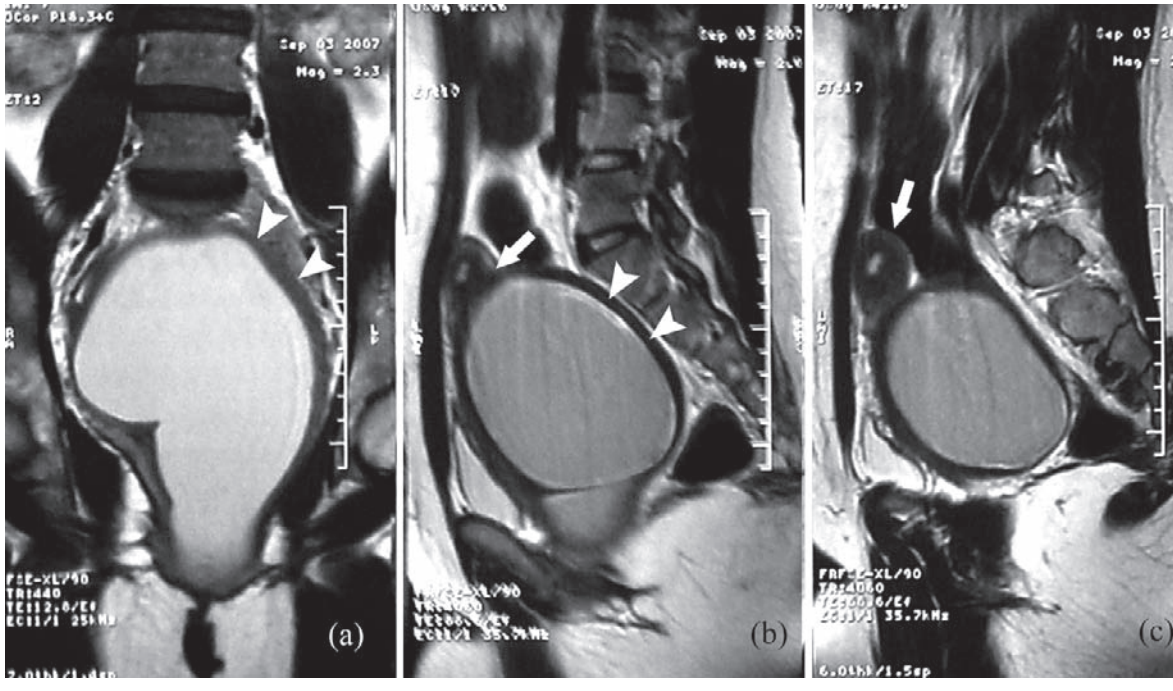

Fig. 4.14.2. Coronal (**a**) and sagittal (**b**, **c**) pelvic T2-weighted MR images show hematocolpos in a young girl who presented with abdominal pain. Note distention of the vagina with menstrual blood of hyperintense signal intensity (*arrowheads*). The uterus can be identified (*arrow*), and it is relatively small compared to the huge mass of vaginal distention

Signs on MRI

Hematocolpos is seen as a dilated full vagina, with high-signal intensity fluid on both T1- and T2-weighted images reflecting the blood component (Fig. 4.14.2). The signal intensity of the blood component depends on the hemoglobin age.

Herlyn-Werner-Wünderlich syndrome: is a rare congenital disease characterized by uterus didelphys, obstructed hemivagina with blood (hematocolpos), and ipsilateral renal agenesis (Figs. 4.14.3 and 4.14.4). Patients with this rare condition present with recurrent progressive pelvic pain usually in adulthood, when menarche occurs. Hematocolpometra or hematosalpinx (dilated fallopian tube full with blood) may occur. When hematosalpinx occurs, hemoperitoneum may be seen due to communication of the fallopian tubes with the peritoneal cavity.

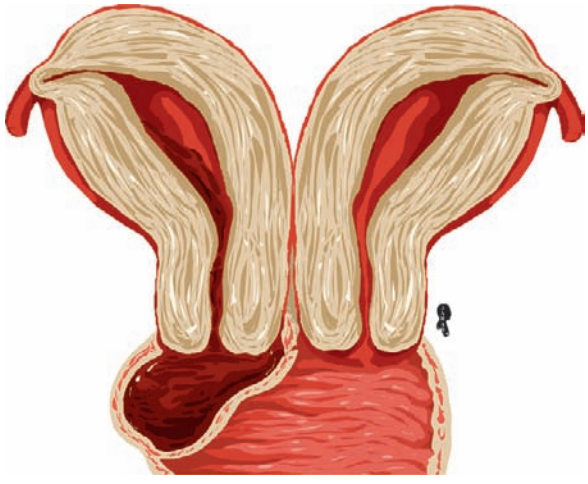

Fig. 4.14.3. Illustration showing the basic uterine anomaly in Herlyn-Werner-Wünderlich syndrome.

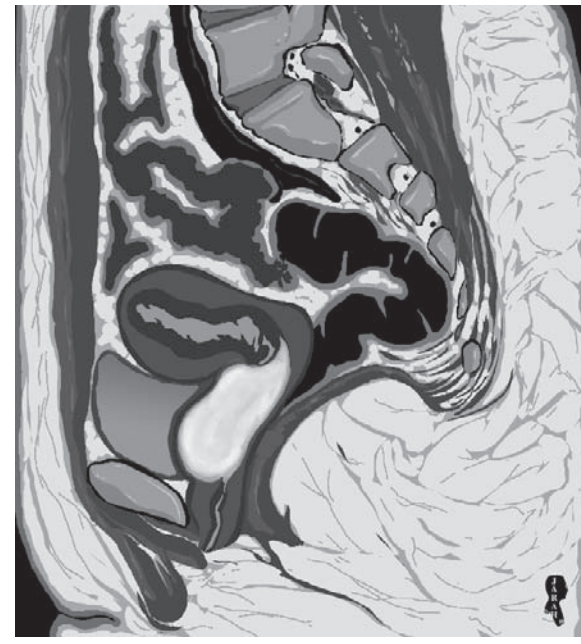

Fig. 4.14.4. Sagittal T1-weighted MR illustration showing the localized hematocolpos in Herlyn-Werner-Wünderlich syndrome

For Further Reading

1. Dickson CA et al. Imperforated hymen with hematocolpos. Ann Emerg Med 1985;14:467–469
2. Ballesio L et al. Hematocolpos in double vagina associated with uterus didelphus: US and MR findings. Eur J Radiol 2003;45:150–153
3. Mirkovic L et al. Magnetic resonance imaging in the evaluation of uterus didelphys with obstructed hemivagina and renal agenesis: A case report. Arch Gynecol Obstet 2006; 274:246–247
4. Anguenot JL et al. Hematocolpos secondary to imperforated hymen, contricution of transrectal echography. Acta Obstet Gynecol Scand 2000;79:614–615
5. Agarwal U et al. Massive hematocolpos mimicking as an ovarian tumor: Atypical presentation of imperfect hymen. J Gynecol Surg 2002;18(3):109–111
6. Orazi C et al. Herlyn-Werner-Wunderlich syndrome: Uterus didelphys, blind hemivagina and ipsilateral renal agenesis. Sonographic and MR findings in 11 cases. Pediatr Radiol 2007;37:657–665

4.15

Alagille Syndrome (Arteriohepatic Dysplasia)

Alagille syndrome (AS) is a rare congenital, autosomal dominant, pediatric disease characterized by congenital intrahepatic biliary tree atresia/hypoplasia, cardiac anomalies, skeletal anomalies, and eye defects.

AS is diagnosed by a histopathology-proven liver biopsy showing intrahepatic bile duct reduction (paucity), in association with three of five major clinical features:

- **Chronic cholestasis:** typically appears during the first 2 years of life and might be severe enough to produce dark urine and acholic stool.
- **Congenital cardiac anomalies:** occur in 85% of cases and include pulmonary artery stenosis with moderate right ventricular enlargement.
- **Skeletal malformations:** include butterfly vertebra (characteristically) and fused vertebra.
- **Ocular posterior embryotoxon:** is defined as abnormal prominence of Schwalbe's lines in the anterior chamber.
- **Characteristic facial features:** include prominent forehead, deep-set eyes with mild hypertelorism, straight nose, and triangular face (Fig. 4.15.1)

Fig. 4.15.1. Illustration showing the facial features of a patient with Alagille syndrome

Minor criteria (not part of the diagnostic scheme) include:

- **Failure to thrive:** seen in up to 80% of cases.
- **Xanthomas (fatty deposition below the skin):** found on the palmar creases, knee, elbow, and extensor surface of the fingers (up to 40% of cases) (Fig. 4.15.2).
- **Endocrinopathies:** the most common endocrine abnormality in AS is hypogonadism.
- **Vascular abnormalities:** include renal artery stenosis and aortic coarctation.

Laboratory findings show increased direct bilirubin, high alkaline phosphatase, and high liver enzymes. The total lipid profile shows increased levels of cholesterol and triglycerides in the blood.

Fig. 4.15.2. Illustration showing the palmar xanthomas, one of the minor signs of Alagille syndrome

Signs on Skeletal Radiographs

- Butterfly vertebra is the most common skeletal abnormality seen in AS.
- Shortening of the distal or the middle phalanges of the hand is a common feature.

Fig. 4.15.3. Sagittal US image of a 10-year-old boy with Alagille syndrome shows splenomegaly with congenital absence of the left kidney.

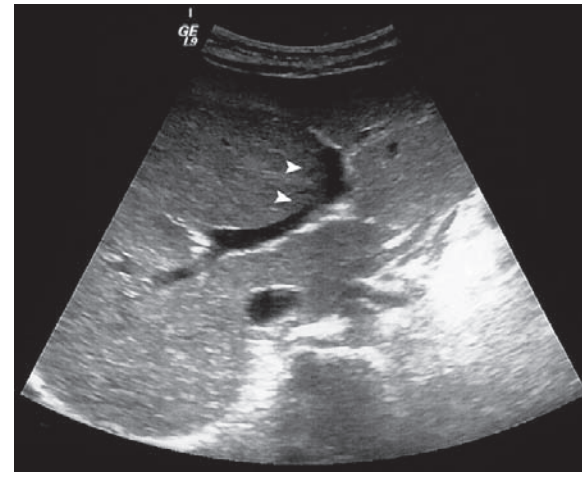

Fig. 4.15.4. Transverse US image of the liver in the same patient shows displacement of the intrahepatic vessels by a rounded mass within the liver (*arrowheads*).

Signs on Abdominal US

- Signs of hepatic cirrhosis such as enlarged caudate lobe and shrunken live with irregular contour.
- Signs of portal hypertension in chronic cases.
- Splenomegaly with or without signs of portal hypertension is seen in up to 50% of cases (Fig. 4.15.3).
- Well-circumscribed round liver masses that distort the liver contour and can be large enough to replace one lobe of the liver. These masses usually cause displacement of the intrahepatic vessels (Fig. 4.15.4). This sign is not specific for Alagille syndrome, as it can be seen in cases of chronic liver cirrhosis.
- Doppler scan may show signs of renal artery stenosis especially if the patient suffers from hypertension.

For Further Reading

1. Schwartz B et al. Intense Pruritus and failure to thrive in Alagille syndrome. J Am Acad Dermatol 2008;58:S9–S11
2. Pierpont MEM. Genetic etiology of cardiac syndromes. Prog Pediatr Cardiol 1996;6:29–41
3. MacMillan JC et al. Arteriohepatic dysplasia (Alagille syndrome; Watson-Alagille syndrome). Baillieres Clin Gastroenterol 1998;12(2):275–291
4. Berrocal T et al. Syndrome of alagille: Radiological and sonographic findings. Eur Radiol 1997;7:115–118
5. Halvorsen RA. Arteriohepatic dysplasia (Alagille's syndrome): Unusual hepatic architecture and function. Abdom Imaging 1995;20:191–196
6. Ghidini A et al. Alagille syndrome: Prenatal sonographic findings. J Clin Ultrasound 2007;35(3):156–158

Chapter 5

The Musculoskeletal System

CONTENTS

5.1

Basic Concepts in Bone Dysplasias

Bone dysplasia means "abnormal bone formation." Bone dysplasias comprise a large group of multiple diseases, with each arising due to certain defects in the basic bone formation or metabolism. Discussing bone dysplasias is beyond the scope of this book. However, several common definitions and anomalies are seen in many congenital bone diseases. The aim of this section is to introduce the radiologist to some of the main basic definitions, terms, and common anomalies that he/she may encounter in bone dysplasia reference textbooks or journals. The following definitions and anomalies are arranged from the head to the toes.

The Skull

Craniosynostosis

Craniosynostosis is a term used to describe premature closure of one or more of the cranial sutures resulting in deformity of the skull shape. The anomalies can be can be primary (sporadic, isolated anomaly) or secondary (occur as a part of metabolic or congenital disease).

Types of Craniosynostosis:

- **Dolichocephaly (scaphocephaly):** occurs due to premature closure of the sagittal suture. The head will be thin and long (Figs. 5.1.1 and 5.1.2).
- **Brachycephaly:** occurs due to premature closure of the coronal suture. The head will be round and short (Fig. 5.1.1).
- **Trigonocephaly:** occurs due to premature closure of the metopic suture. The forehead will be triangular in shape (Fig. 5.1.1). The metopic suture is found in the infant skull separating the frontal bone into two bones. This suture fuses at the age of 5 years, and it persists in less than 10% of the population.
- **Turricephaly (oxycephaly):** results from early synostosis between the parietal and the occipital bones. The skull exhibits a tower or pyramid shape.

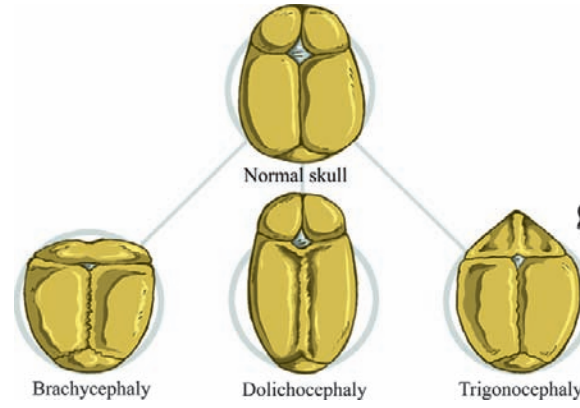

Fig. 5.1.1. Illustration showing different types of skull deformities of craniosynostosis

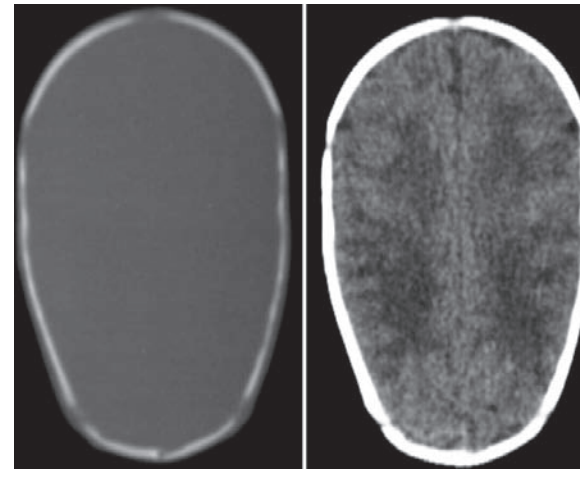

Fig. 5.1.2. Axial bone and soft-tissue window CT images show dolichocephaly. Note how the head is thin and long

Lacunar Skull

Lacunar skull is a congenital skull defect characterized by abnormal, osseous, finger-like impressions seen at the inner vault of the skull separated by dense bony ridges, making a mesh-like structure on plain radiographs (Fig. 5.1.3). Lacunar skull is almost always associated with severe central nervous system anomalies such as meningocele and Arnold-Chiari malformations. It occurs in infants under the age of 3 months, and usually the imaging findings resolve at the age of 6 months.

Fig. 5.1.3. Lateral plain radiograph of the skull shows the imaging findings in lacunar skull. Note the osseous soap-bubble or finger-like impressions at the inner vault of the skull, making mesh-like structures

The Orbital Cavities

- **Hypertelorism:** is a condition characterized by a wide distance between the orbital cavities (increase of the interpupillary distance).
- **Hypotelorism:** is a condition characterized by a narrow distance between the orbital cavities (reduction of the interpupillary distance).

The Mandible

- **Micrognathia:** is a term used to describe a small retracted mandible; it can be seen in cases of Klippel-Feil syndrome.
- **Prognathism:** is a term used to describe mandibular protrusion. Prognathism can be due to mandibular enlargement or maxillary hypoplasia. It can be seen in cases of mucopolysaccharidosis.

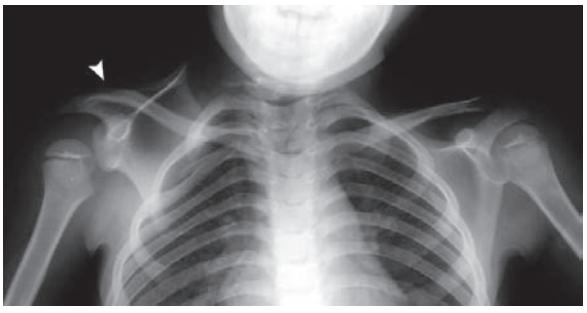

Fig. 5.1.4. Plain radiograph of the upper thorax shows elevated and medially rotated right scapula, representing Sprengel deformity (*arrowhead*)

The Scapula

Sprengel Deformity

Sprengel deformity is an uncommon congenital anomaly characterized by an elevated, medially rotated, and higher than normal scapula (Fig. 5.1.4). In 30% of cases the scapula is attached to the spine by an "*omovertebral bone*," cartilage, or fibrous tissue, which can limit the scapulothoracic motion.

The patient is usually asymptomatic, and the lesion is bilateral in 14% of cases. Sprengel deformity can be associated with scoliosis, cervical rib, and renal anomalies (30%).

The Clavicles and the Thoracic Inlet

Rhomboid Fossa

Rhomboid fossa is a concave osteolytic defect seen along the inferiomedial aspect of the clavicle on plain radiographs (Fig. 5.1.5). This bony defect represents the insertion site of the costoclavicular ligament. It is not a true bony dysplasia and is considered to be a normal variant. It is important to recognize this normal variant

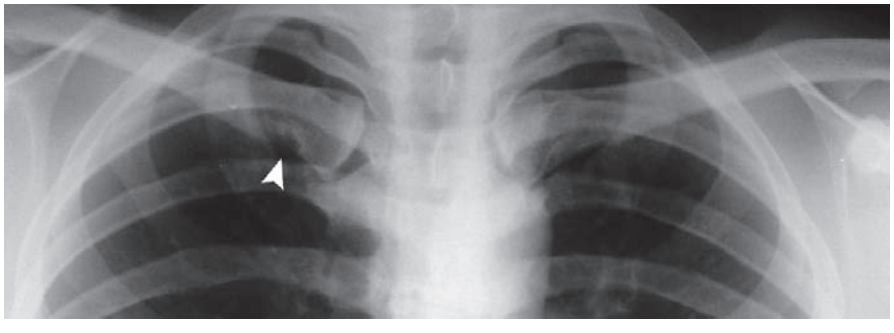

Fig. 5.1.5. Clavicular plain radiograph shows bony defect on the inferiomedial side of the right clavicle (*arrowhead*). This finding and location is typical of rhomboid fossa

so as not to mistake it for a fracture or a neoplastic lesion affecting the clavicle. Patients are typically asymptomatic, and the condition is classically discovered as an incidental finding on plain chest radiographs.

Cervical Rib

Cervical rib is a rare congenital anomaly characterized by an excess small rib that articulates with the seventh cervical vertebra (Fig. 5.1.6). The anomaly is common in females, and it is usually asymptomatic. The brachial plexus is always located above the cervical rib. Compression over the subclavian vessels can occur occasionally (5–10%). The anomaly is bilateral in 50% of cases (Fig. 5.1.7). Cervical rib can be one of the causes of *thoracic outlet syndrome* (neuronal or vascular compression of the arm vessels or nerves as they exit from the thoracic outlet).

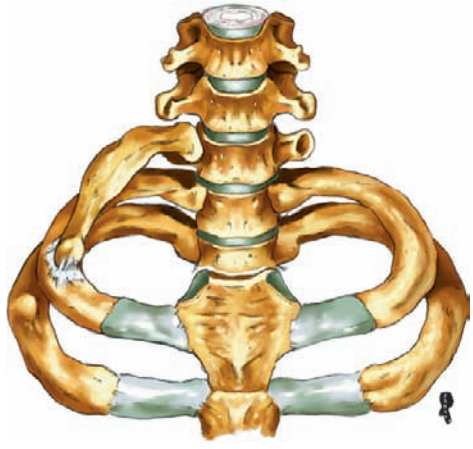

Fig. 5.1.6. Illustration showing a cervical rib on the right side articulating with the seventh cervical vertebra

Fig. 5.1.7. Plain radiograph shows bilateral cervical ribs (*arrowheads*)

The Pelvis

Acetabular-Angle Anomalies

- **Horizontal acetabulum (small angle):** is usually seen due to hypoplastic iliac bones (Fig. 5.1.8). It impedes femoral head growth later in life, resulting in humeral epiphyseal deformities and coxa vara. Horizontal acetabulum can be seen in chondroectodermal dysplasia (Ellis-van Creveld syndrome) and hypothyroidism.
- **Protrusio acetabuli:** is intrapelvic bulging of the medial wall of the acetabulum. It can be seen secondary to diseases like rheumatoid arthritis, osteoarthritis (Fig. 5.1.9), osteoporosis, and Paget disease. When it occurs bilaterally with no defined cause, it is called "*Otto disease*." On plain radiographs, there is typically loss of the pelvic teardrop.
- **Trident acetabulum:** is an acetabulum with three inferior pointing spikes. It is diagnostic of *asphyxiating thoracic atrophy (Jeune syndrome)*.

Femoral Neck Deformities

Deformities of the proximal femur are characterized by abnormalities in the femoral neck angle (normal angle = 120–140°). The following types are found:

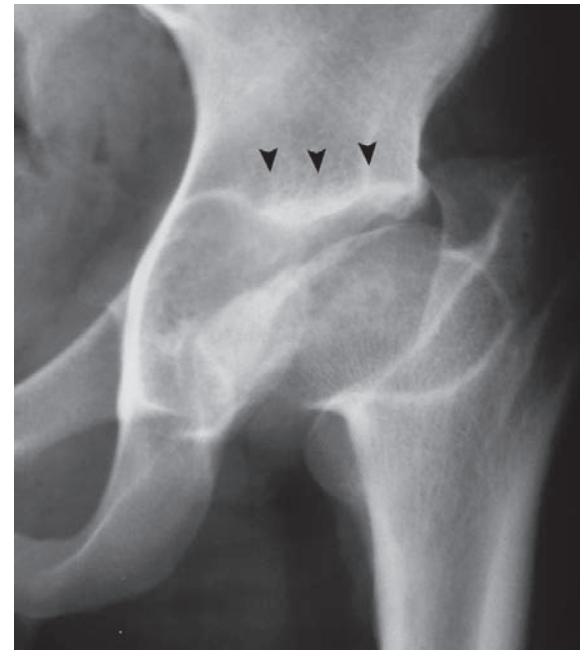

Fig. 5.1.8. Plain radiograph of the left hip shows horizontal acetabulum with coxa vara (*arrowheads*)

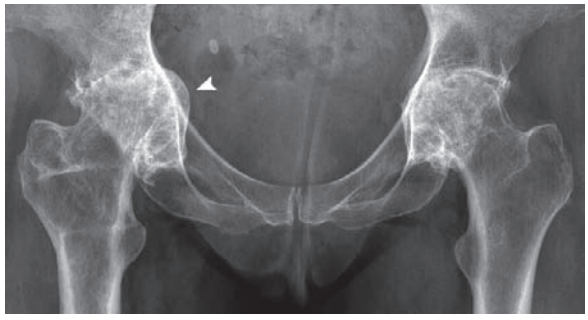

Fig. 5.1.9. Plain hip radiograph shows protrusio acetabuli on the right hip joint due to osteoporosis (*arrowhead*)

Fig. 5.1.10. Plain radiograph shows horizontally oriented femoral neck (coxa vara)

- **Coxa vara:** horizontally oriented femoral neck. It can be seen in *achondroplasia* (dwarfism due to genetic enchondral ossification failure), *Perthes disease* (avascular necrosis of the femoral head), and rickets (Fig. 5.1.10).
- **Coxa valga:** vertically oriented femoral neck. It can be seen in mucopolysaccharidosis, *pyknodysostosis* (lysosomal storage disease characterized by brittle, sclerotic bones), and hereditary multiple exostosis (Fig. 5.1.11).

Fig. 5.1.11. Plain radiograph shows vertically oriented femoral neck (coxa valga)

The Knees

- **Genu varum (bowlegs):** an increase in the distance between the knees with the legs fully extended. It can be seen in achondroplasia, rickets, and Blount disease (osteochondrosis of the medial aspect of the proximal tibial epiphysis).
- **Genu valgum:** a decrease in the distance between the knees with the legs fully extended. It can be seen in achondroplasia, rickets, and fluorosis.

The Upper Limbs

Congenital Limb Shortening

- **Rhizomelic type:** is shortening of the proximal segment of an extremity (humerus or femur). It is seen in achondroplasia and pseudoachondroplasia.
- **Mesomelic type:** is shortening of the middle segment of an extremity (radius, ulna, fibula, or tibia). It is seen in Madelung deformity and Ellis-van Creveld syndrome.

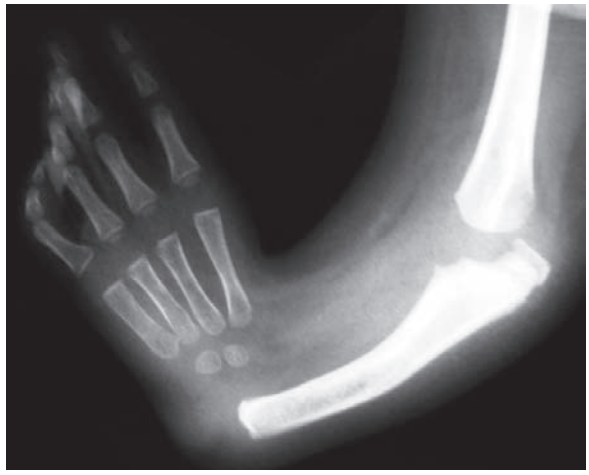

Fig. 5.1.12. Plain radiograph of the hand and arm shows absent thumb, absent ulna, and radially deviated hand (radial ray deficiency anomaly)

- **Acromelic type:** is shortening of the distal segment of an extremity (hand or feet bones). It is seen in Ellis-van Creveld syndrome and asphyxiating thoracic atrophy.
- **Micromelia:** shortening of an entire limb.

Radial Ray Deficiency

Radial ray deficiency is a forearm anomaly characterized by aplastic/hypoplastic radius bone, absent thumb, absent scaphoid and trapezium bones, and radially deviated and clubbed hand (Fig. 5.1.12).

It can be bilateral or unilateral, and often associated with VATER association and Fanconi anemia.

- **Fetal valproate syndrome:** a congenital disease arising due to the use of sodium valproate (anti-epileptic drug) during pregnancy. The infant characteristically has craniosynostosis (often trigonocephaly) and limb anomalies (commonly radial ray deficiency).
- **TAR syndrome:** a congenital disease characterized by thrombocytopenia and absent radii.

The Lower Limbs

Clubfoot

Clubfoot is an anomaly of the talus bone with unknown origin characterized by reduction of the talocalcaneal angle plus flat top of the talus. The foot is inwardly and plantarly flexed (Fig. 5.1.13). Clubfoot is often bilateral, but when it occurs unilaterally, the right foot is affected more than the left.

Fig. 5.1.13. Plain radiograph shows clubfoot deformity

Congenital Vertical Talus

Vertical talus is a congenital deformity characterized by dorsal dislocation of the navicular bone over the talus, forming a rigid talonavicular complex that impedes the normal walking mechanism. The talar head is prominent medially (Figs. 5.1.14 and 5.1.15), while the forefoot is abducted and dorsiflexed. The patient presents with an awkward walking gait described as "peg-leg gait."

Pes Planus

Pes planus is absence or reduction of the medial longitudinal arch of the foot (flatfoot).

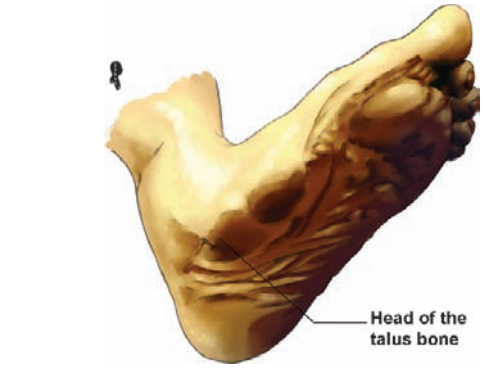

Fig. 5.1.14. Illustration shows a vertical talus deformity. The talus is projecting on the medial side of the foot

Fig. 5.1.15. Lateral plain radiograph of the foot shows vertically oriented talus deformity. Note the angle of the talus (*line*)

Pes Cavovarus

Pes cavovarus is exaggeration of the medial longitudinal arch of the foot (high-arched foot).

Hallux Valgus

Hallux valgus is medial subluxation and bulging of the first metatarsophalangeal joint (Fig. 5.1.16).

Fig. 5.1.16. Plain radiograph of the foot shows hallux valgus (*arrowhead*)

The Digits

- **Brachydactyly:** is short finger.
- **Polydactyly:** is the presence of more than five digits in the hands or feet. It is classified as:
- **Preaxial:** when the accessory digit is in the radial or tibial side.
- **Postaxial:** when the accessory digit is in the ulnar or fibular side (Fig. 5.1.17).
- **Syndactyly:** is fibrous or bony fusion of two or more digits (Fig. 5.1.17).
- **Camptodactyly:** refers to the presence of digit contracture.
- **Clinodactyly:** refers to deviation of a finger, often the fifth finger.
- **Arachnodactyly:** refers to long spider-like fingers; typically seen in Marfan syndrome.

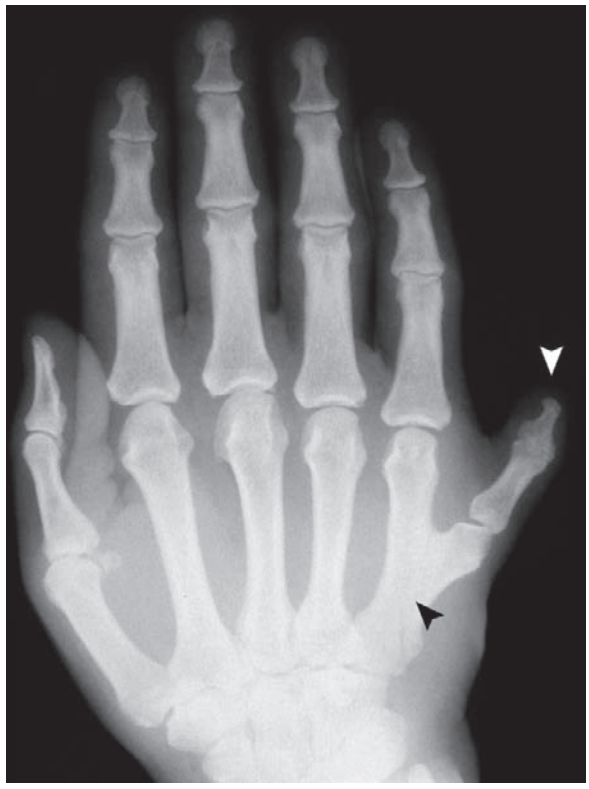

Fig. 5.1.17. Plain hand radiograph shows postaxial polydactyly (*white arrowhead*), with bony syndactyly of the accessory digit with the fifth metatarsal bone (*black arrowhead*)

- **Triphalangeal thumb:** is a rare anomaly of the thumb characterized by the presence of three phalanges instead of two; 90% of cases are bilateral. The anomaly can be sporadic or associated with syndromes.
  - **Aase syndrome:** is a rare congenital disorder characterized by congenital hypoplastic/aplastic anemia and triphalangeal thumb.
  - **Holt-Oram syndrome:** is another rare disorder characterized by triphalangeal thumb and cardiac anomalies.

For Further Reading

1. Castriota-Scanderbeg A et al. Abnormal skeletal phenotypes: From simple signs to complex diagnoses, 1st edn. Springer, Berlin
2. De Wilde V et al. Normal osseous variants presenting as cystic or lucent areas on radiography and CT imaging: A pictorial overview. Eur J Radiol 2004;51:77–84
3. Keeling JW et al. Cervical ribs: Useful marker of monosomy X in fetal hydrops. Pediatr Dev Pathol 1999;2:119–123
4. Kosenak LM et al. Cervical rib variant: Report of a case. Ann Vasc Surg 1992;292–293
5. Nakahara K et al. Lacunar skull deformity and hydrocephalus in infants with myelomeningocele: Is lacunar skull deformity a predictor of hydrocephalus development? Childs Nerv Syst 2007;23:863–865
6. Muis N et al. The Aase syndrome. Eur J Pediatr 1986; 145:153–157

5.2

Congenital Radioulnar Synostosis

Radioulnar synostosis (RS) is a rare congenital malformation characterized by bony or fibrous fusion (synostosis) between the radius and the ulna, usually at their proximal joint. The fusion can be due to thick fibrous ligament distal to the proximal upper ends of the radius and ulna, or by a true bony fusion between the two bones.

RS occurs due to failure of separation between the perichondrium of the proximal ends of the radius and the ulna in the seventh week of gestation, and it has an autosomal dominant mode of inheritance.

Patients complain of inability to rotate their forearm with almost fixed pronation position with difficult supination (Fig. 5.2.1). Up to 60% of cases are bilateral.

The disease has been reported to occur with *Antley-Bixler syndrome*, which is a rare disease characterized by cartilaginous and bony malformations causing craniosynostosis, midfacial hypoplasia, choanal atresia, and radiohumeral synostosis.

Fig. 5.2.1. Illustration demonstrating the fixed pronation position of the forearm in a patient with radioulnar synostosis trying to grasp something. The patient is only able to move his hand in a fixed pronated position with inability to supinate his forearm

Signs on Plain Skeletal Radiographs

The radiograph shows bony fusion between the proximal ends of the ulna and radius (Fig. 5.2.2). CT is better for evaluating and differentiating fibrous from bony synostosis.

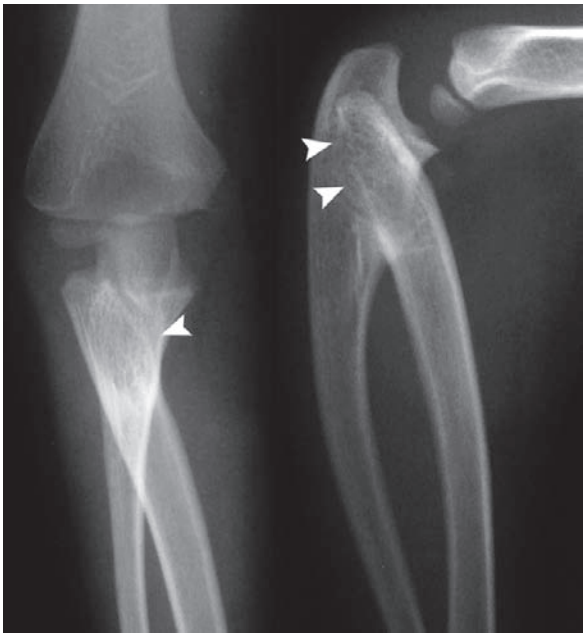

Fig. 5.2.2. Anteroposterior and lateral plain radiographs of the elbow joint showing bony fusion between the proximal ends of the ulna and the radius (*arrowheads*)

For Further Reading

1. Karatosun V et al. Congenital radioulnar synostosis: a case report of a probable subtype. J Orthop Sci 2004;9:314–316
2. Hurley ME et al. Antley-Bixler syndrome with radioulnar synostosis. Pediatr Radiol 2004;34:148–151
3. Castriota-Scanderbeg A et al. Abnormal skeletal phenotypes: From simple signs to complex diagnoses, 1st edn. Springer, Berlin, 2005

5.3

Klippel-Feil Syndrome (Blocked Cervical Vertebrae)

Blocked vertebra is a term used to describe bony fusion between any two vertebrae (synostosis). It can occur due to failure of embryological vertebral segmentation or as a consequence of chronic disease. Klippel-Feil (KF) anomaly is a term used to describe blocked cervical vertebrae.

KF anomaly occurs due to failure of the mesodermal somites to divide during the third to eighth week of gestation. The neural tube closes during the same time that the somites are developing. Dermal elements may be entrapped during the neural tube closure, resulting in the formation of epidermoid and dermoid cysts.

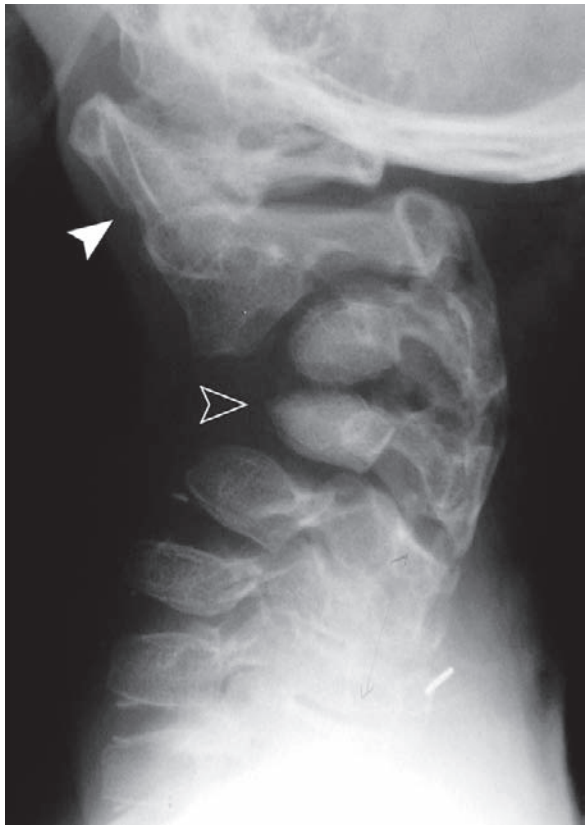

Fig. 5.3.1. Lateral plain radiograph of the neck in a patient with congenital fusion between the atlas and the axis (KF type 1: *white arrowhead*), with mild cervical kyphosis (*open arrowhead*)

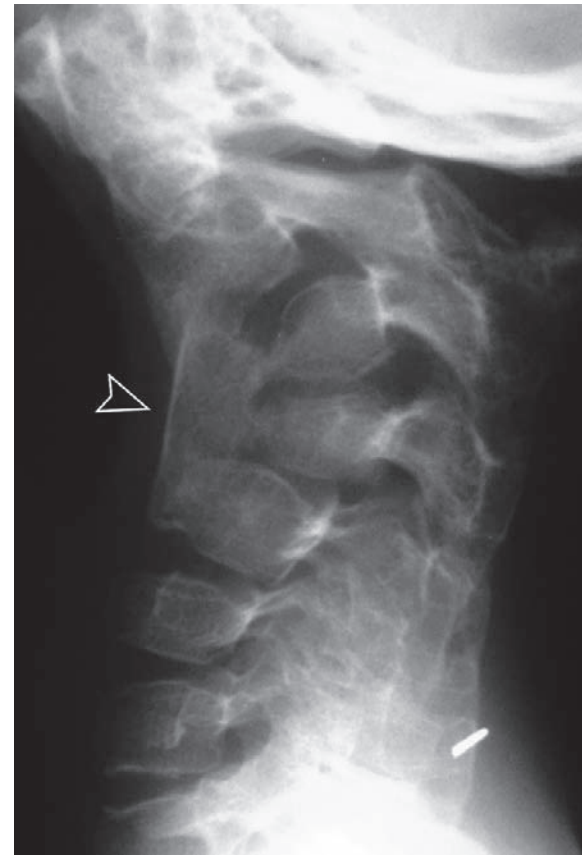

Fig. 5.3.2. Lateral plain radiograph of the neck in another patient with vertebral fusion between C1–C2 with fusion between C3, C4, and C5 by a bony block (KF type 1–2: *open arrowhead*)

The disease occurs most commonly in the cervical spine between C5–C6 and C2–C3, and has an autosomal dominant mode of inheritance.

KF can be associated with Sprengel deformity (30%), deafness (30%), scoliosis (60%), renal anomalies (35%), diastematomyelia, and spina bifida. The patient classically has a triad of short neck, limitation of neck movement, with low posterior hairline. The disease can be seen in *fetal alcohol syndrome* in up to 53% of cases.

- **Wildervanck syndrome:** is a syndrome comprising a combination of anomalies characterized by KF anomaly, deafness, and abnormal ocular motility of *Duane retraction syndrome* (congenital abducens nerve absence with eye abduction/adduction deficits).
- **Congenital bar:** is a term used to describe the fusion between two pedicles (neural arch fusion).

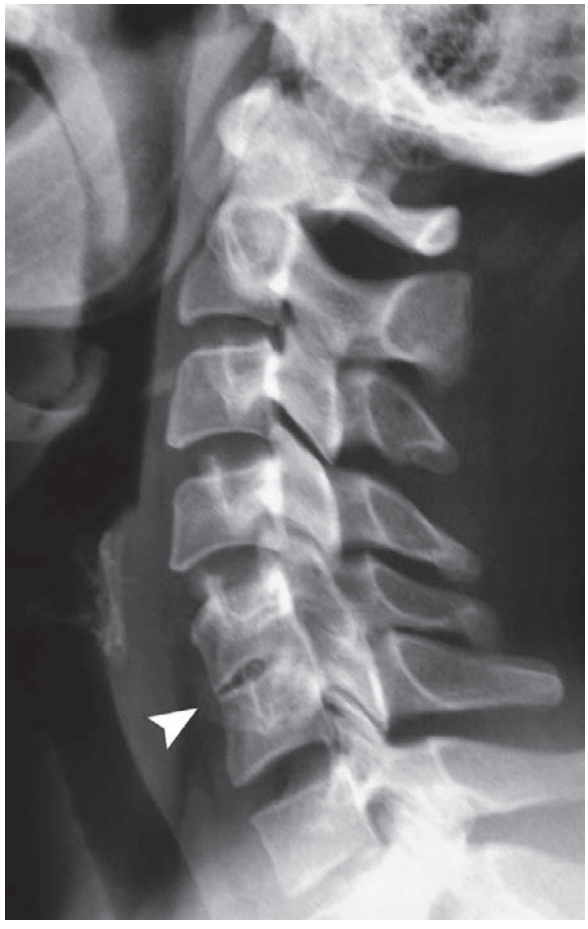

Fig. 5.3.3. Lateral plain radiograph of the neck in a patient with vertebral fusion between C5–C6 (KF type 3: *white arrowhead*)

Classes of KF Anomaly

- **Class 1:** fusion between the atlas (C1) and the axis (C2) (Fig. 5.3.1).
- **Class 2:** fusion between C2–C3 and other vertebrae below (Fig. 5.3.2).
- **Class 3:** fusion of any cervical vertebrae other than C1–C2 (Fig. 5.3.3).

For Further Reading

1. Akosy FG et al. Klippel-Feil syndrome in association with posterior fossa suboccipital dermoid cyst. Eur Radiol 2001; 11:142–144
2. Clarke RA et al. Heterogeneity in Klippel-Feil syndrome: A new classification. Pediatr Radiol 1998;28:967–974
3. Nguyen VD et al. Klippel-Feil syndrome: Pattern of bony fusion and wasp-waist sign. Skeletal Radiol 1993;22: 519–523
4. Schild JA et al. Wildervank syndrome – The external appearance and radiologic findings. Int J Pediatric Otorhinolaryngol 1984;7:305–310

5.4

Spinal Dysraphism

Spinal dysraphism: is a collective term describing the congenital anomalies of the spine. The following types of spinal dysraphism are found:

- **Myelocele:** is herniation of the spinal cord tissue (neural placode) through a spina bifida outside the central canal, but below the skin surface.
- **Myelomeningocele:** is herniation of the spinal cord tissue through a spina bifida outside the central canal within a subarachnoid space extending beyond the skin surface (Fig. 5.4.1).
- **Meningocele:** is a cerebrospinal fluid (CSF)-filled mass, lined by dural and subarachnoid layers, herniating through a spina bifida beyond the skin surface (Fig. 5.4.2).
- **Syringohydromyelia (syrinx):** is a CSF-containing space within the spinal cord representing dilatation of the central canal (Fig. 5.4.3). It can be congenital (primary) or secondary to trauma, tumors, and old spinal cord insult.

Fig. 5.4.1. Sagittal T1-weighted MR illustration showing myelomeningocele. Note herniation of the spinal cord (*open arrowhead*) with its subarachnoid space (*solid arrow*) beyond the skin surface (*solid arrowhead*)

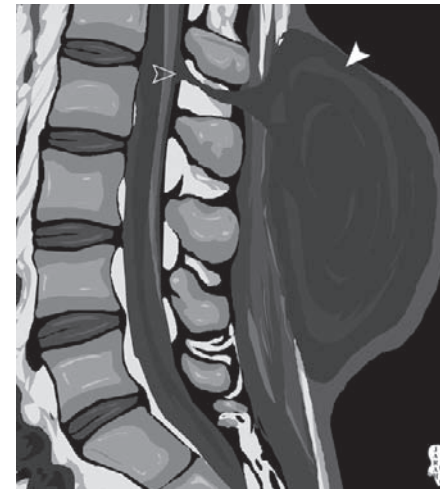

Fig. 5.4.2. Sagittal T1-weighted MR illustration showing meningocele. Note the cerebrospinal fluid-filled mass projecting beyond the skin surface (*solid arrowhead*) with its connection to the spinal subarachnoid space (*open arrowhead*)

Fig. 5.4.3. Sagittal T1-weighted MR illustration showing dilatation of the central canal representing the syrinx (*arrowheads*)

- **Diastematomyelia:** is a condition characterized by sagittal clefting of the spinal cord. There are two types of diastematomyelia:
  - **Type 1 diastematomyelia:** is characterized by cords split by a bony or cartilaginous septum located between the vertebral body and the arch. Each hemicord has its own dural tube and arachnoid space (Fig. 5.4.4).

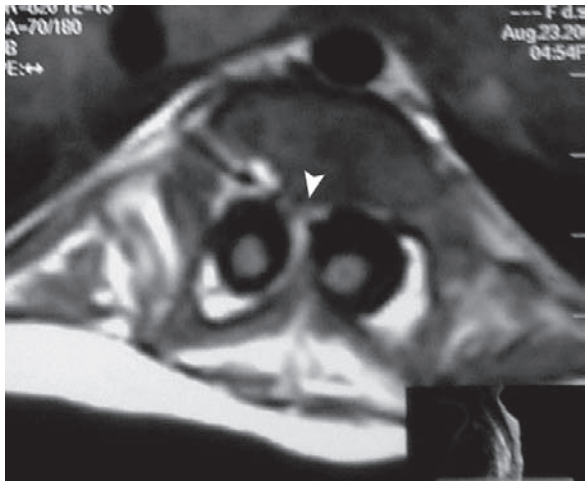

Fig. 5.4.4. Axial T1-weighted MR image shows type 1 diastematomyelia. Note the bony septum separating the two hemicords (*arrowhead*)

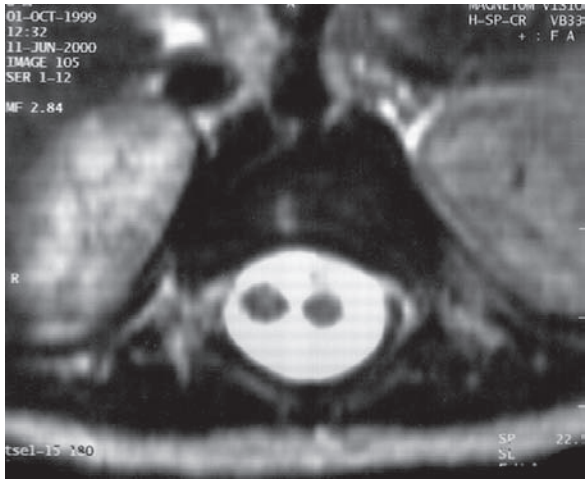

Fig. 5.4.5. Axial T2-weighted MR image shows type 2 diastematomyelia. Note how the two hemicords are contained within one dural sac without the division seen in type 1

- **Type 2 diastematomyelia:** the two hemicords are contained within one dural sheath (Fig. 5.4.5).
- **Hemimyelocele:** is diastematomyelia with one cord herniating through a posterior arch defect (myelocele), while the other is in its normal position.

- **Myelocystocele:** is a rare form of myelomeningocele in which a syrinx and its surrounding subarachnoid space herniate through a spina bifida defect (Fig. 5.4.6).

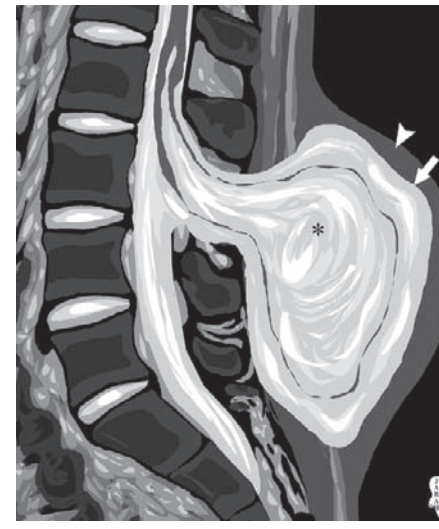

Fig. 5.4.6. Sagittal T2-weighted MR illustration shows myelocystocele. Note how the syrinx (*asterisk*) with its surrounded subarachnoid space (*white arrow*) is herniating through the spina bifida beyond the skin boundary (*white arrowhead*)

Fig. 5.4.7. Sagittal T1-weighted MR illustration shows lipomyelocele. Note herniation of the fatty tissue into the spinal canal (*black arrowhead*) making an interface with the spinal cord (*white arrowhead*)

- **Lipomatous lesions**
  - **Lipomyelocele (lipomyeloschisis):** is a fatty tissue that herniates through a spina bifida into the vertebral canal making a spinal cord–lipoma interface (Fig. 5.4.7).

Fig. 5.4.8. Sagittal T1-weighted MR illustration shows lipomyelomeningocele. Note how the spinal cord with its subarachnoid space is herniating through a lipoma (*arrowhead*) beyond the skin surface

Fig. 5.4.9. Sagittal T1-weighted MR illustration shows lipoma of the filum terminalis (*arrowheads*)

- **Lipomyelomeningocele:** is herniation of the spinal cord and its subarachnoid space into a lipoma that bulges beyond the skin surface (Fig. 5.4.8).
- **Intradural lipoma:** is lipoma located within the dura that presses over the spinal cord.
- **Filar lipoma:** is lipoma located at the filum terminalis (Fig. 5.4.9).

Fig. 5.4.10. Sagittal T2-weighted MR illustration shows the fifth ventricle as a CSF-filled space located within the conus medullaris (*arrowhead*)

- **Tethered cord syndrome:** tethering of the cord means that the spinal cord is stretched and lies below its normal position, usually due to a pathological condition that leads to adherence of the spinal cord to the dura. Tethered cord is characterized clinically by progressive lower extremity sensory deficit, spastic gait, muscle atrophy, and bowel and bladder dysfunction. The age of presentation of this syndrome varies between birth and 15 years.
- **Persistent terminal ventricle (the fifth ventricle):** is a small cavity found within the conus medullaris. It is diagnosed and differentiated from the syrinx by its typical position (Fig. 5.4.10). It is usually asymptomatic, but in some cases can be associated with lower-back and sciatica pains.

For Further Reading

1. Rossi A et al. Imaging in spine and spinal cord malformation. Eur J Radiol 2004;50:177–200
2. Egelhoff JC. MR imaging of congenital anomalies of the pediatric spine. MRI Clin North Am 199;7(3):459–479
3. Roos RAC et al. Magnetic resonance imaging in occult spinal dysraphism. Pediatr Radiol 1986;16:412–416

5.5

Vertebral Clefts

The normal vertebra has three primary ossification centers: one is located in the body and two are located in each pedicle. These centers ossify by enchondral ossification, and fuse together at the age of 7 years. Secondary ossification centers develop later in life and fuse with the vertebra at the age of 25 years.

Vertebral clefts are a set of anomalies within the body of the vertebra (anterior arch) or the posterior elements of the vertebra (posterior neural arch), representing failure of these primary ossification centers to fuse together. Traumatic causes can also result in vertebral clefts (Fig. 5.5.1).

The importance of recognizing these clefts is to distinguish them from traumatic vertebral clefts needing intervention.

Vertebral Body Clefts (Cleft Vertebra)

Cleft vertebra is a congenital anomaly in which there are two ossification centers in the vertebral body instead of one. Failure of these two centers to fuse keeps a cartilaginous cleft in between that will appear as a cleft later in life.

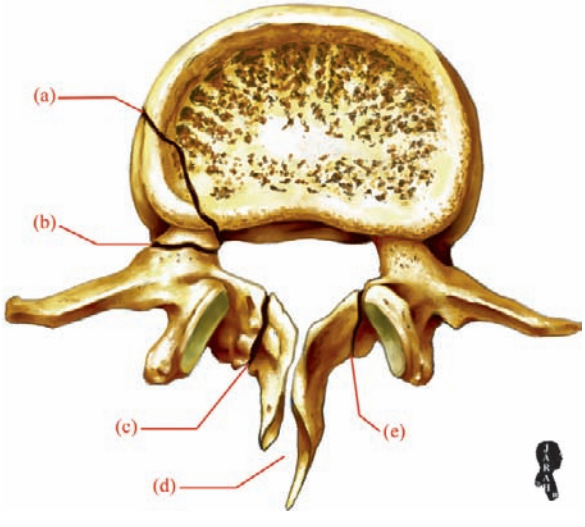

Fig. 5.5.1. Illustration showing different kinds of vertebral clefts. Persistent neurocentral synchondrosis *a*, retrosomatic cleft *b*, retroisthmic cleft with osteophytes *c*, spina bifida *d*, and spondylosis *e*

It most commonly affects the thoracolumbar vertebra, and is commonly seen in congenital diseases like chondrodysplasia punctata (stippled epiphysis).

Cleft vertebrae are divided into two types:

- **Coronal cleft vertebra:** arises when the ossification centers are ventrally and dorsally situated. It is seen on lateral vertebral radiographs as a vertical radiolucent band in the midportion of the vertebra.
- **Sagittal cleft vertebra:** arises when the ossification centers are situated on the right and left side of the vertebral body. It is seen on anteroposterior radiographs as a vertical radiolucent band in the midportion of the vertebra (Fig. 5.5.2).

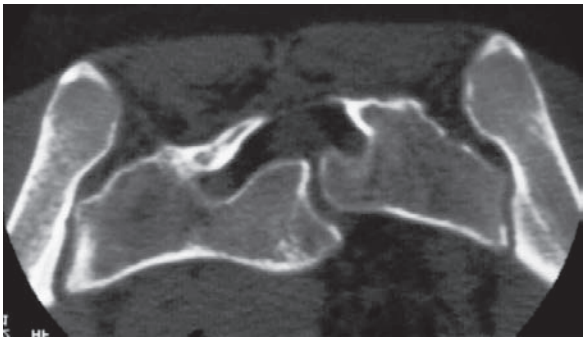

Fig. 5.5.2. Axial spinal CT shows sagittal cleft vertebra

Butterfly Vertebra

Butterfly vertebra results from partial fusion of two sagittal ossification centers of a cleft vertebra at the middle, deforming the shape of the vertebra (Fig. 5.5.3).

Retroisthmic Cleft

Retroisthmic cleft is a rare vertebral cleft that occurs at the laminas (Fig. 5.5.1c). The term retroisthmic means posterior to the pars interarticularis (pars interarticularis is also called vertebral isthmus). It commonly affects the L4 and L5 lumbar vertebrae.

Signs on CT

- A cleft located posterior to the facet joint articulation with regular margins.
- Hypertrophic changes can be found at the site of the cleft (i.e., osteophytes).

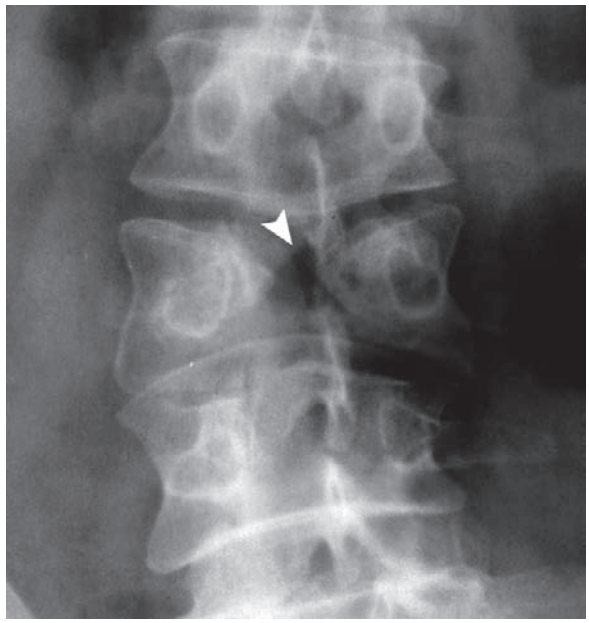

Fig. 5.5.3. Plain vertebral radiograph shows butterfly vertebra with partial fusion between the two vertebral body ossification centers (*arrowhead*)

Retrosomatic Cleft

Retrosomatic cleft is a vertebral cleft that occurs at the pedicles (posterior to the vertebral body) due to hypoplasia or aplasia of the pedicles (Fig. 5.5.1b).

No history of trauma is an important fact supporting the diagnosis. It is most commonly found in women over 30 years of age.

Signs on CT

A cleft with smooth margins is seen within the pedicle with no signs of healing process (callus or osteophytes can be seen occasionally).

Persistent Neurocentral Synchondrosis

Persistent neurocentral synchondrosis is a vertebral cleft that occurs due to failure of the vertebral body growth plates to ossify (Fig. 5.5.1a). They usually fuse at the age of 3–6 years.

Signs on CT

A cleft with smooth margins is seen within the vertebral body, usually at the margins.

Spondylosis

Spondylosis is a vertebral cleft that occurs at the pars interarticularis (Fig. 5.5.1e). It is a traumatic process and not congenital.

Spinous Process Clefts (Spina Bifida)

Spina bifida is a defect in the posterior arch elements of any vertebra. It occurs typically at the spinous process (Fig. 5.5.1d), and is most commonly found at the lumbar vertebra (Fig. 5.5.4). It results from failure of the neural tube to close during embryological development.

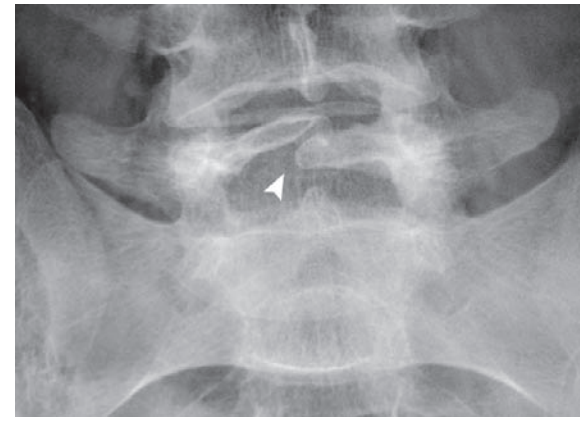

Fig. 5.5.4. Plain vertebral radiograph shows spina bifida (*arrowhead*)

For Further Reading

1. Castriota-Scanderbeg A et al. Abnormal skeletal phenotypes: From simple signs to complex diagnoses, 1st edn. Springer, Berlin, 2005
2. Chen JJ et al. Multiple posterior vertebral fusion abnormalities: A case report and Review of the literature. AJR 2006;186: 1256–1259

5.6

Arcuate Foramen (Kimmerle Anomaly)

Arcuate foramen is a normal variant of the first cervical vertebra (the atlas) characterized by calcification of the ligamentous border of the posterior atlanto-occipital membrane. This calcification makes a bony ring at the area where the vertebral artery travels through the posterior arch of the atlas to enter the foramen magnum (Fig. 5.6.1).

Arcuate foramen is not related to degenerative changes or aging processes and it has an incidence of 1.14–37% of the population.

The anomaly can be associated with *Barré-Lieou syndrome*, which is characterized by headache, vasomotor disturbance, and swallowing and phonation problems due to alteration of blood flow within the vertebral arteries and their periarterial plexus.

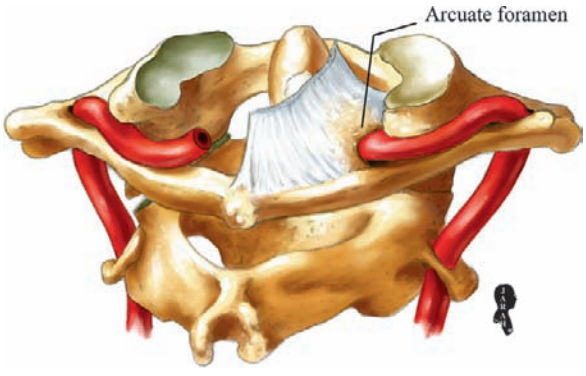

Fig. 5.6.1. Illustration of the atlas shows calcification of the left posterior atlanto-occipital membrane creating the arcuate foramen seen on radiographs

Signs on Radiographs

A bony ring is seen at the posterosuperior border of the atlas on the lateral skull radiographs (Fig. 5.6.2).

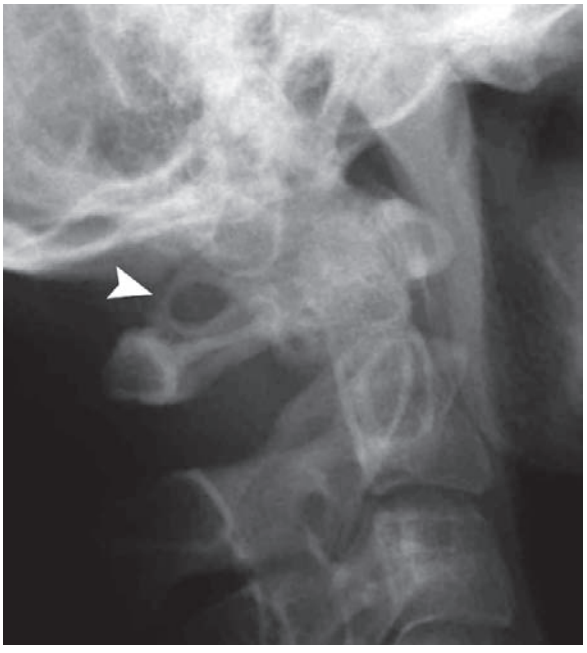

Fig. 5.6.2. Lateral plain radiograph of the neck illustrates the arcuate foramen as a bony ring seen superior to the posterior arch of the atlas (*arrowhead*)

For Further Reading

1. Tubbus RS et al. Foramen arcuate: Anatomical study and review of the literate. J Neurodsurg Spine 2007;6:31–34
2. Tubbus RS et al. Simultaneous lateral and posterior ponticles resulting in the formation of a vertebral artery tunnel of the atlas: Case report and review of the literature. Folia neuropathol 2007;45(1):43–46

5.7

Supracondylar Process of the Humerus

Supracondylar process of the humerus is a peak-like bony process that arises from the anteromedial surface of the distal humerus, approximately 5 cm above the medial epicondyle. The process ranges from 2 to 20 mm in length, and it is seen in 1% of the population.

From the process tip arises a fibrous ligament, called "Struthers ligament," connecting the supracondylar process to the medial humeral epicondyle, and creating a fibrous arch (Fig. 5.7.1). This fibrous arch can compress the median nerve through its course at the elbow joint causing symptoms like carpal tunnel syndrome.

Supracondylar process can be seen in cases of Cornelia de Lange syndrome.

Cornelia de Lange syndrome: is a rare disease characterized by multiple body abnormalities affecting the bones, eyes, ears, heart, gastrointestinal tract, endocrine system, and brain. Severe psychomotor and mental retardation is commonly associated with this syndrome. The patient has a short stature with characteristic facial features including micro-brachycephaly, heavy eyebrows meeting in the midline, low-set ears, and long eyelashes. The facial features, psychomotor retardation, plus the multiple body abnormalities make the diagnosis straightforward.

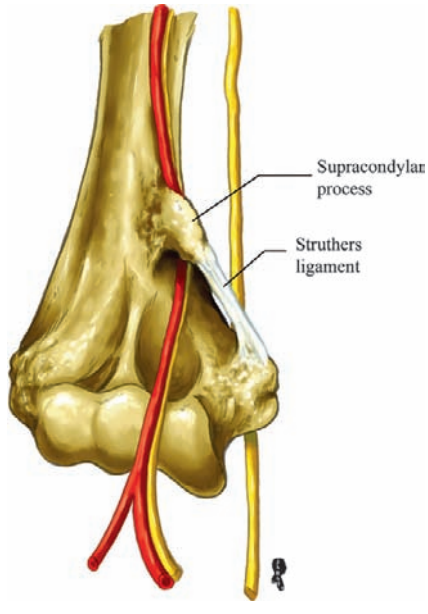

Fig. 5.7.1. Illustration showing the supracondylar process and Struthers ligament. Note the fibrous arch created by the ligament compressing the median nerve and the brachial artery at the elbow joint

Signs on Plain Skeletal Radiographs

A small bony spur is seen at the distal humerus 5 cm above the medial epicondyle (Fig. 5.7.2).

Fig. 5.7.2. Plain radiograph of the elbow shows the supracondylar process (*arrowhead*)

For Further Reading

1. Sener E et al. Supracondylar process syndrome. Arch Orthop Trauma Surg 1998;117:418–419
2. Spinner RJ et al. Fractures of the supracondylar process of the humerus. J Hand Surg 1994;19A:1038–1041
3. Peeters FLM. Radiological manifestations of Cornelia de Lange syndrome. Pediatr Radiol 1975;3:41–46
4. Vuilleumier N et al. Neuropathological analysis of an adult case of Cornelia de Lange syndrome. Acta Neuropathol 2002; 104:327–332

5.8

Tarsal Coalition

Tarsal coalition (TC) is a congenital condition characterized by fibrous or bony fusion of two or more tarsal bones. The most common coalitions are talocalcaneal and calcaneonavicular coalitions (90% of cases).

TC is bilateral in 50% of cases, and it is a common cause of flatfoot in adults. Patients with TC commonly present with pain localized at the lateral or the dorsal aspect of the foot. The pain typically worsens by activity, with occasional episodes of night pain. Later in life, the patient may start to limp due to restricted movement of the tarsus causing a rigid flatfoot. The classical description of the foot deformity due to TC is "peroneal spastic flatfoot" (Fig. 5.8.1).

The clinical presentation usually occurs between 12 and 16 years of age, when the coalition starts to ossify. TC can be osseous (complete) or made up of various amounts of osseous, fibrous, and cartilage tissues (incomplete).

CT is the modality of choice for confirming TC.

Fig. 5.8.1. Illustration shows the pes planovalgus deformity, or the peroneal spastic flatfoot (left foot). This deformity is an advanced stage of TC and not found in every case

Signs on Plain Skeletal Radiographs

- TC is seen as an abnormal connection between two or more tarsal bones by an osseous or partially osseous bridging bone (Fig. 5.8.2).
- In calcaneonavicular coalition, the lateral or the 45° internal oblique ankle radiograph commonly shows the bony bar connecting the anterosuperior aspect of the calcaneus to the midportion of the navicular bone resembling a nose (anteater nose sign) (Fig. 5.8.3).

Fig. 5.8.2. Lateral plain radiograph of the ankle shows small osseous bony bar connecting the calcaneus to the navicular bone (*arrowheads*)

Fig. 5.8.3. A 45-degree internal oblique radiograph of the ankle shows calcaneonavicular coalition with classic "anteater nose" sign" (*arrowheads*)

For Further Reading

1. Solomon LB et al. A dissection and computer tomograph study of tarsal coalition in 100 cadavar feet. J Orthop Res 2003;21:352–358
2. Fopma E et al. Tarsal coalition. Curr Orthop 2002;6:65–73.
3. Emery KH et al. Tarsal coalition: A blinded comparison of MRI and CT. Pediatr Radiol 1998;28:612–616
4. Brown RR et al. The C sign: More specific for flatfoot deformity than tarsal coalition. Skeletal Radiol 2001;30:84–87

5.9

Paget Disease (Ostitis Deformans)

Paget disease (PD) of bone is a progressive chronic disease of unknown origin characterized by abnormal bone remodeling. In PD, there is abnormal activity of the osteoblasts and osteoclasts resulting in phases of bone destruction (osteolytic phase) followed by bone restoration and repair (reparative phase); the net result is a brittle, sclerotic bone.

The disease has an incidence of 3% in the population over 40 years of age. PD commonly affects the axial skeleton. The fibula is the only bone in the body that is rarely affected in PD.

Clinically, PD presents as an incidental finding of abnormally high serum alkaline phosphatase in the absence of liver disease, often in an asymptomatic patient. PD pain is usually localized to an area of a bone currently undergoing metabolic changes. When the pain is localized to a joint that worsens by movement, it is against the typical features of PD.

Complications of PD are related to the phases of osteolytic and sclerotic bone changes (Fig. 5.9.1). They include nerve compression syndrome, hearing loss when it affects the petrous bone, pathological fractures, and spinal canal stenosis.

Fig. 5.9.1. Illustration showing extensive bony deformity of the skull and the facial bones due to multiple osteolytic and sclerotic phases of bone remodeling

Signs on Radiographs

- Thickening of the iliopectineal line in the pelvis (Fig. 5.9.2).
- Thickening of the skull base, with pathognomonic "cotton wool appearance" of the skull due to mixed lytic/sclerotic activities in the flat bones.
- PD in the long bones always starts from the ends (subcortical bone) to the center (diaphysis); an exception to this rule occurs in the tibia. If the lesion is only located in the midshaft, then it is not PD (Fig. 5.9.3).
- **Osteoporosis circumscripta:** is a term describing the osteolytic phase of PD when it affects the skull. It affects mostly the frontal and occipital bones (Fig. 5.9.4).
- **Ivory vertebra:** is a term used to describe complete sclerosis of the vertebral body. It is typically seen in PD, metastasis, and lymphoma (Fig. 5.9.5).

Fig. 5.9.2. Plain pelvic radiograph shows thickening of the left iliopectineal line in a patient with PD (*arrowhead*). Note the sclerotic changes in the left acetabulum, pubic bone, ischium, and iliac wing compared to the right side

Fig. 5.9.3. Plain radiograph of the right hip joint in a patient with PD shows mixed mosaic pattern of osteolytic and sclerotic changes affecting the proximal femur

Fig. 5.9.4. Lateral skull radiograph shows extensive multiple levels of osteolytic changes in the skull of a patient with PD (osteoporosis circumscripta)

Fig. 5.9.5. Plain radiograph of the spine shows ivory vertebra

For Further Reading

1. Bender IB. Paget's disease. J Endod 2003;29(11):720–723
2. Wang WC et al. Paget's disease of bone in a Chinese patient: A case report and review of the literature. Oral Surg Oral Med Oral Pathol Oral Radiol Endod 2005;99:727–733
3. Pratt H et al. Paget's disease of bone presenting as chest pain and shoulder immobility. Clin Radiol 2005;60:407–409
4. Whitten CR et al. MRI of Paget's disease of bone. Clin Radiol 2003;58:763–769
5. Hullar TE et al. Paget's disease and fibrous dysplasia. Otolaryngol Clin N Am 2003;36:707–732

5.10

Osteopetrosis (Albers-Schönburg Disease/Marble Bone Disease)

Osteopetrosis comprises a group of diseases characterized by increased bone density and abnormal modeling due to severely reduced osteoclastic bone activity. The reduction in osteoclast activity results in almost no trabecular bone remodeling or resorption.

Patients affected by osteopetrosis have densely sclerotic bones that are easily fractured along the transverse axis. This bone fragility is due to thinning of the cortical bone with sclerosis of the trabecular bone. In addition, patients are often anemic due to poor development of the bone marrow.

There are two types of osteopetrosis:

- **Autosomal Recessive Osteopetrosis:** Autosomal recessive osteopetrosis is characterized by bone marrow obliteration and hepatosplenomegaly.

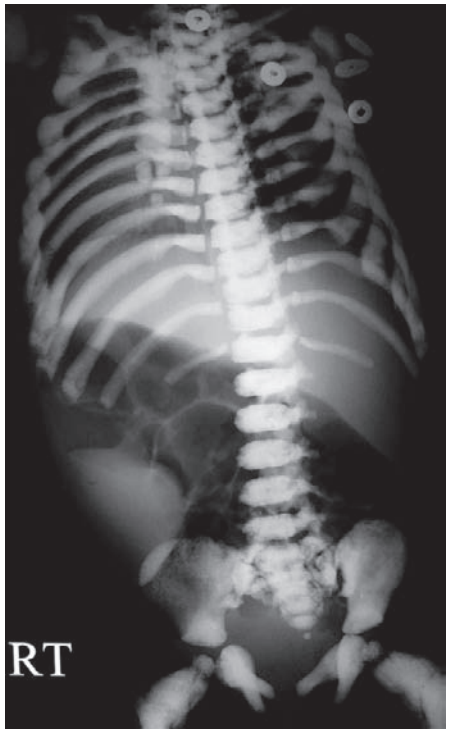

Fig. 5.10.1. Plain babygram of an infant with autosomal recessive osteopetrosis shows generalized increased bone density in a diffuse, bilateral fashion. Note also the liver size and position (situs invertus)

Signs on Plain Skeletal Radiographs

- Diffuse symmetrical increased bone density and metaphyseal flaring due to abnormal bone modeling (Fig. 5.10.1).
- Club-like metaphysis (Erlenmeyer flask deformity): commonly seen affecting the distal femur or proximal humerus (Figs. 5.10.2 and 5.10.3).
- Intracranial calcifications (marble brain): seen in the autosomal recessive osteopetrosis with tubular acidosis. The brain contains multiple calcifications centered mainly in the basal ganglia and the periventricular area.
- Sandwich vertebra (rugger-jersey spine): uniform increased density of the vertebra with greater density seen at both end plates (Fig. 5.10.4).

Fig. 5.10.2. Plain skeletal radiograph of the left knee in a patient with osteopetrosis shows the club-like femoral metaphysis (Erlenmeyer flask deformity)

Fig. 5.10.3. Illustration showing an Erlenmeyer flask

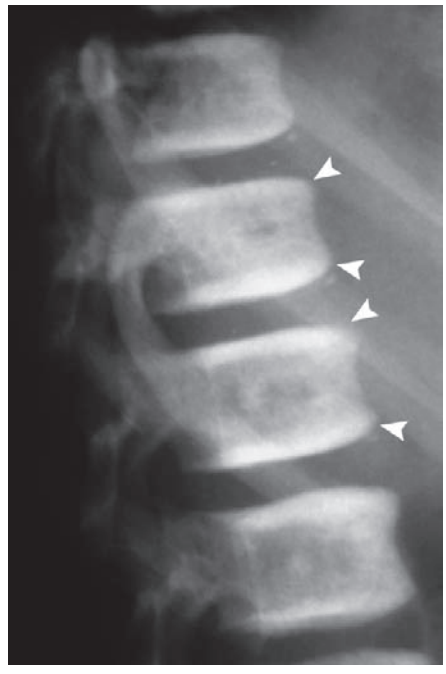

Fig. 5.10.4. Plain skeletal radiograph of the vertebral column shows sclerotic end plate vertebrae known as the "rugger-jersey spine" (*arrowheads*)

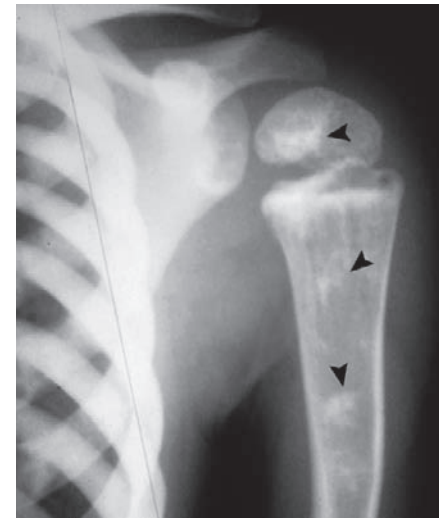

Fig. 5.10.5. Plain shoulder radiograph of a patient with autosomal dominant osteopetrosis shows multiple bony sclerotic lesions affecting the epiphysis and the metaphysis (*arrowheads*). This signs is known as "bone in bone appearance"

- **Autosomal Dominant Osteopetrosis**

Signs on Plain Skeletal Radiographs

In this form, there is a "bone in bone" appearance seen as small bony islands and sclerosis within the trabecular bone (Fig. 5.10.5).

Serum calcium and phosphate levels are normal, while the serum alkaline phosphatase level is typically elevated due to the high rate of new bone formation.

The most distinctive features of dysosteosclerosis differentiating it from osteopetrosis are flattening of the vertebrae and sclerosis of the base of the skull.

Dysosteosclerosis

Dysosteosclerosis is a rare disease characterized by dysplasia and excessive sclerosis of the base of the skull, often causing narrowing of the optic canals leading to blindness. There is sclerosis all over the body in a similar fashion to osteopetrosis.

Signs on Plain Skeletal Radiographs

- Sclerotic flat vertebra (diagnostic and characteristic).
- Erlenmeyer flask deformity of femoral metaphysis with dense sclerotic transverse bands.
- Dense sclerosis of the base of the skull (Fig. 5.10.6).

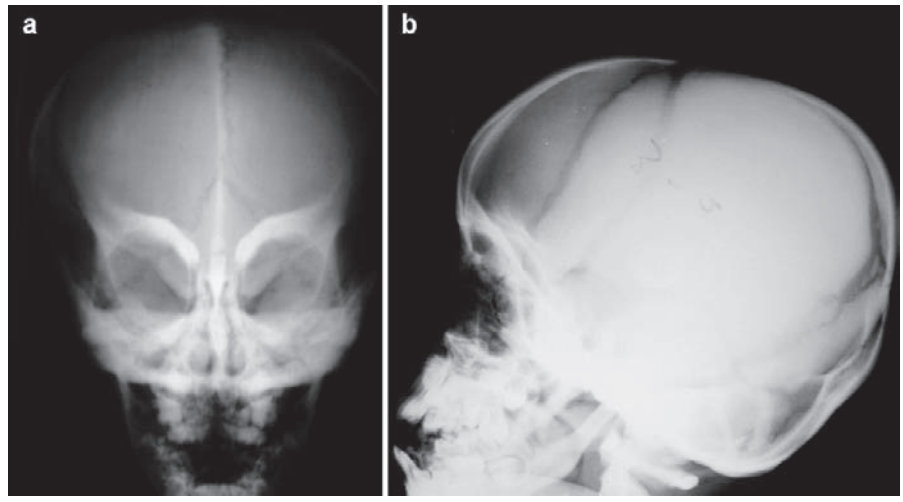

Fig. 5.10.6. Plain skull radiographs of two patients. One patient is affected by osteopetrosis **a**, while the other patient is affected by dysosteosclerosis **b**. Note the degree of skull sclerosis in dysosteosclerosis compared with a patient with autosomal dominant osteopetrosis

For Further Reading

1. Huston CS et al. Dysosteosclerosis. Am J Roentgenol 1978; 130:988–991.
2. Lund-Sorensen N et al. Autosomal dominant osteopetrosis: report of a Norwegian family with radiographic or anamnesic findings differing from the generally accepted classification. Skeletal Radiol 1997;26:173–176.

5.11

Mucopolysaccharidosis

Mucopolysaccharidosis is a group of metabolic disorders characterized by accumulation of mucopolysaccharides within body organs due to a genetic defect in the enzymes responsible for degrading mucopolysaccharides (defect in glycosaminoglycans metabolism).

There are ten known diseases; each is caused by a specific lysosomal enzyme deficiency normally involved in the degradation of mucopolysaccharides.

The diagnosis can be made by measuring the amount of mucopolysaccharides in the urine.

The most common diseases are the first four types: (all are autosomal recessive except Hunter disease, which is X-linked recessive).

- **Type I** is called Hurler disease (gargoylism).
- **Type II** is called Hurler-Hunter diseases.
- **Type III** is called Sanfilippo syndrome.
- **Type IV** is called Morquio syndrome.

Hurler disease is associated with cystic changes within the brain. These cysts are made up of dilated perineural spaces (Virchow-Robin spaces) filled with mucopolysaccharide gargoyle cells. The patients present with dwarfism, gargoyle-like face (Fig. 5.11.1), mental retardation, and spinal cord compression

Fig. 5.11.1. Illustration showing the typical facial features of a patient with gargoylism (Hurler syndrome)

Signs on Skeletal Radiographs

- A small hook seen at the anterior–inferior margin of the vertebra is a pathognomonic finding in mucopolysaccharidosis patients (Fig. 5.11.2). It is seen in Hurler and Hunter diseases.
- A small hook at the anterior margin of the vertebra is seen in Morquio and Sanfilippo syndromes, differentiating them from the first two types (Fig. 5.11.3).
- Thickened skull with frontal bossing and J-shaped sella (Fig. 5.11.4).
- Canoe paddle ribs: the ribs are narrowed at their vertebral articulation and widened anteriorly. They are commonly seen in Hurler disease (Fig. 5.11.5).
- Metacarpal bullet appearance: thickening of the metacarpal bones with tapering of the proximal ends. They are seen in all four types (Fig. 5.11.6).

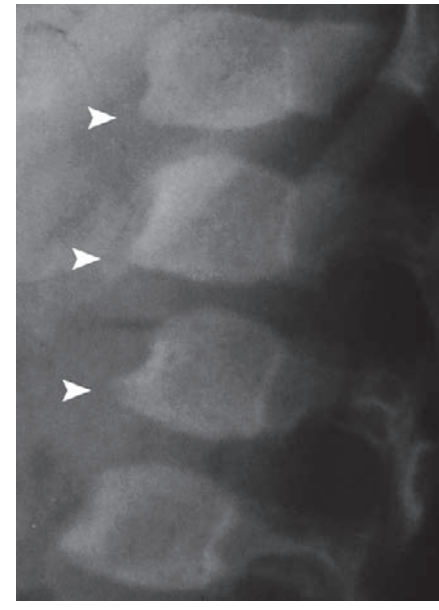

Fig. 5.11.2. Lateral plain radiograph of the spine in a patient with Hurler disease shows the typical vertebral hook at the anterior–inferior margin of the vertebral bodies (*arrowheads*)

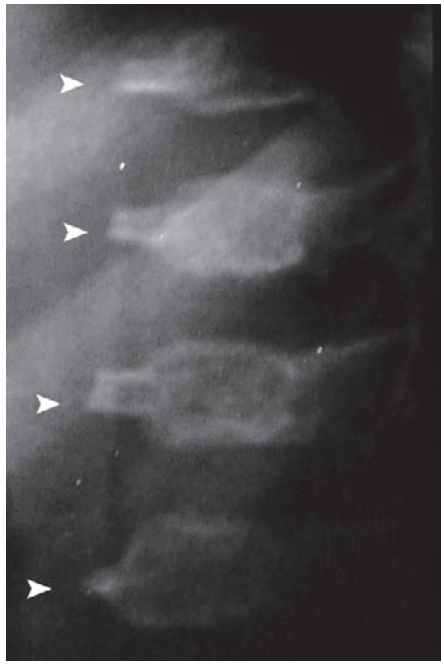

Fig. 5.11.3. Lateral plain radiograph of the spine in a patient with Morquio syndrome shows the typical vertebral hook at the anterior margin of the vertebral bodies (*arrowheads*)

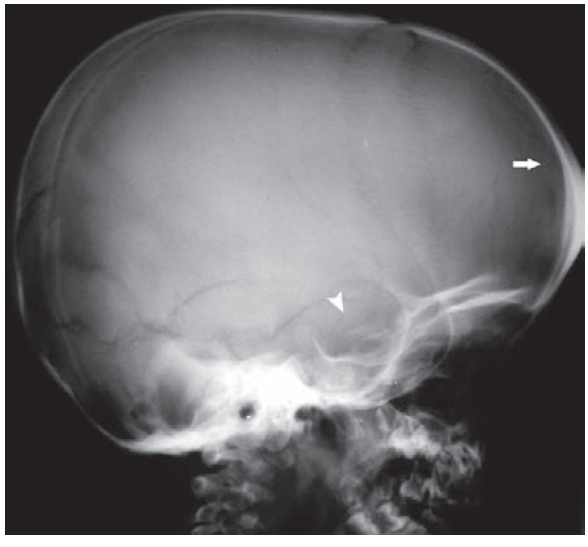

Fig. 5.11.4. Lateral plain radiograph of the skull in a patient with Sanfilippo syndrome shows typical frontal bossing (*arrow*) and J-shaped sella (*arrowhead*)

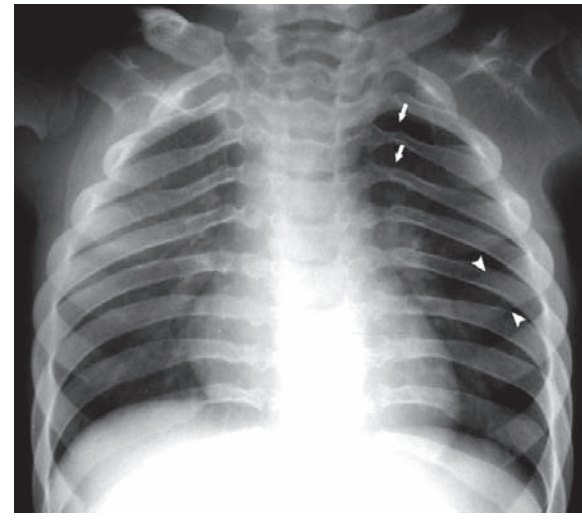

Fig. 5.11.5. Plain chest radiograph of a patient with Sanfilippo syndrome shows typical "canoe paddle ribs." Note the narrowed portion of the ribs at their vertebral articulation (*arrows*), with widening of their cartilaginous–sternal articulation (*arrowheads*)

Fig. 5.11.6. Plain hand radiograph of a patient with Sanfilippo syndrome shows metacarpal bullet appearance

Signs on Brain MRI

- Brain atrophy with hydrocephalus.
- Finding Virchow-Robin spaces within the corpus callosum is a pathognomonic feature in mucopolysaccharidosis (Figs. 5.11.7 and 5.11.8).
- Demyelinating periventricular white matter disease seen as high T2 signal intensity on T2-weighted images.

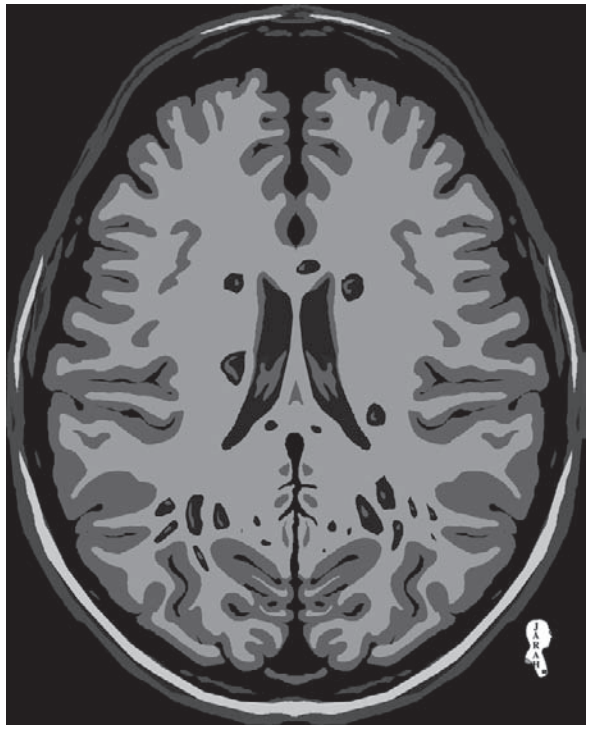

Fig. 5.11.7. Axial T1-weighted MR illustration shows multiple cystic lesions scattered within the brain and characteristically found in the genu and the splenium of the corpus callosum. These findings are typical in patients with mucopolysaccharidosis

Signs on Cardiac MRI

Metabolic storage diseases like mucopolysaccharidosis are characterized by left ventricular wall thickening (Fig. 5.11.9) and left ventricular diastolic dysfunction, usually with normal systolic function.

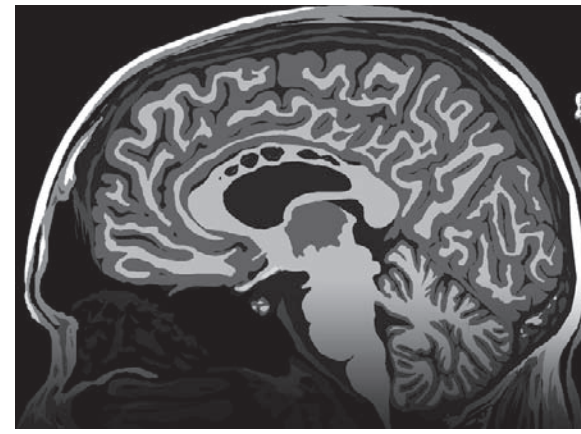

Fig. 5.11.8. Sagittal T1-weighted MR illustration shows the cystic lesions within the body of the corpus callosum

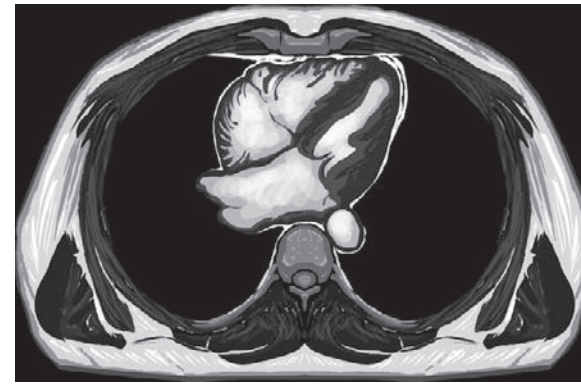

Fig. 5.11.9. Axial T1-weighted MR illustration shows hypertrophy of the left ventricle as it appears in patients with metabolic storage diseases like mucopolysaccharidosis

For Further Reading

1. Yamada Y et al. Mucopolysaccharidosis type I (Hunter disease): 13 gene mutation in 52 Japanese patients and carrier detection in four families. Hum Genet 1993;92:110–114
2. Guven G et al. Mucopolysaccharidosis type I (Hurler syndrome): Oral and radiographic findings and ultrastructural/chemical features of enamel and dentin. Oral Surg Oral Med Oral Pathol Oral Radiol Endod 2008;105:72–78
3. Tuschl K et al. Mucopolysaccharidosis type II in females: Case report and review of literature. Pediatr Neurol 2005; 32: 270–272
4. Neely J et al. Cerebral infarction in Hunter syndrome. J Clin Neurosci 2006;13:1054–1057
5. Laradi S et al. Mucopolysaccharidosis type IV: N-Acetylgalactosamine-6-sulfatase mutation in Tunisian patients. Mol Genet Metab 2006;87:213–218

5.12

Ollier Disease and Maffucci Syndrome

Enchondroma is a cartilaginous benign tumor that results from failure of the normal endochondral ossification, causing part of the cartilaginous physis to be embedded within the metaphyseal bone (cartilage within bone).

Ollier Disease (Multiple Enchondromatosis)

Ollier disease is characterized by noninheritable multiple enchondroma formation within the body, with a high risk of malignant transformation into chondrosarcoma.

The disease can lead to leg length discrepancy, angular deformity, and shortening due to defects in the growth plate (Fig. 5.12.1).

Fig. 5.12.1. Illustration showing an Ollier disease patient with a short leg

Signs on Plain Skeletal Radiographs

- Multiple enchondromas are seen in the body as radiolucent metaphyseal expanding lesions, with punctuated choroid matrix calcification described as "smoke-ring pattern" (Fig. 5.12.2). The calcified matrix is a characteristic feature of enchondromas, and it is seen in enchondromas all over the body except in the hands. Enchondromas in the hands usually do not calcify (Fig. 5.12.3).
- Enchondromas are sharply demarcated, while chondrosarcomas usually have lobulated and ill-defined margins. It is sometimes difficult to differentiate enchondroma from low-grade chondrosarcoma even by pathological examination.

Fig. 5.12.2. Plain radiograph of the left knee in a patient with Ollier disease shows metaphyseal, radiolucent, expanding lesions affecting the distal femoral metaphysis, the proximal tibial metaphysis, and the proximal fibular metaphysis (*arrowheads*). Note the pattern of the matrix calcification of the expanding radiolucent lesions

Fig. 5.12.3. Plain hand radiograph of the same patient shows multiple expanding, radiolucent lesions affecting the proximal metaphysis of the metacarpal bones (*arrowheads*). The lesions have sharp margins, with absent calcifications

Maffucci Syndrome

Maffucci syndrome is a rare, sporadic, genetic disease characterized by the presence of enchondroma plus vascular anomalies of the nearby soft tissue (hemangioma, venous malformation, or hemangioendothelioma).

The affected person appears normal at birth, and the lesions start to appear in early childhood as multiple, superficial, asymmetric, red-to-purple tender skin nodules (Fig. 5.12.4).

Maffucci syndrome involves all metaphyses of the short and long bones. It commonly affects the hands, and when it affects an extremity, it can cause hypertrophy and overgrowth of this extremity. The disease has a high risk for malignant transformation. Radiotherapy can be used to relieve the pain and the symptoms.

Signs on Plain Skeletal Radiographs

Multiple phleboliths can be seen due to calcifications within the abnormal hemangiomas in a limb near an enchondroma (pathognomonic).

Fig. 5.12.4. Illustration showing a hand with a severe form of Maffucci syndrome. Note the multiple red-to-purple skin nodules over the fingers and the hypothenar muscles, the whitish areas of the skin representing areas of ischemia and lines of demarcations, enlargement, and hypertrophy of the thumb, and the black skin over the thumb and over the thenar muscles representing gangrenous skin transformation due to ischemia from the hemangiomas

For Further Reading

1. Faik A et al. Maffucci's syndrome: A case report. Clin Rheumatol 2005;25:88–91
2. Oestreich AE et al. Both Trevor and Ollier disease limited to one upper limb. Skeletal Radiol 2002;31:230–234
3. Asirvatham R et al. Ollier's disease with secondary chondrosarcoma associated with ovarian tumor. Int Orthop (SICOT) 1991;15:393–395
4. Kosaki N et al. Bilateral multiple malignant transformation of Ollier's disease. Skeletal Radiol 2005;43:477–484
5. Mellon CD et al. Ollier's disease and Maffucci's syndrome: distinct entities or a continuum. Case report: Enchondromatosis complicated by an intracranial glioma. J Neurol 1988;235:376–378

5.13

Osteogenesis Imperfecta

Osteogenesis imperfecta (OI) is a group of diseases caused by genetic mutations in collagen type I formation. OI subtypes are characterized by increased bone fragility. The skeleton is osteoporotic and has thin cortices with reduced trabeculae. The bones contain varying amounts of woven bones that persist into adulthood. Woven bone is an immature bone with its fibers not arranged in any direction (nonlamellar).

There are three types of OI:

Osteogenesis Imperfecta Type I (Tarda/Lobstein Syndrome)

OI type I is characterized by generalized osteopenia, bone fragility, and blue sclera. It has an autosomal dominant mode of inheritance.

Signs on Plain Skeletal Radiographs

- General osteopenia with multiple healed fractures of the long bones (Fig. 5.13.1).
- Occipitalization of the atlas and biconcave (fish) vertebrae.

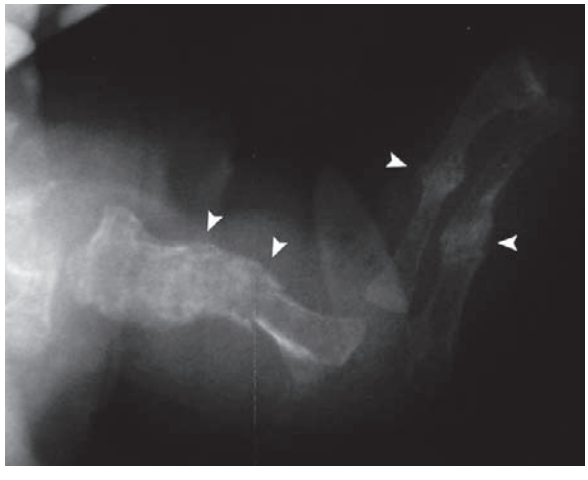

Fig. 5.13.1. Plain radiograph of the forearm in OI patient shows multiple healed fractures with callus formation (*arrowheads*)

Osteogenesis Imperfecta Type IIA

OI type IIA is a lethal form of OI, and is characterized by thick short bones, short extremities, and membranous caput. It has an autosomal dominant mode of inheritance.

Signs on Plain Skeletal Radiographs

- Osteopenia and multiple fractures at birth.
- Severe retarded mineralization of the calvarium (Fig. 5.13.2).
- Rectangular femurs with broad and short limb bones.
- Angulated tibia and fibula (Fig. 5.13.3).
- Beaded ribs.
- Flattened and deformed vertebra.

Fig. 5.13.2. Plain skull radiograph shows severe retarded mineralization of the calvarium in a patient with type IIA OI (membranous caput)

Fig. 5.13.3. Plain babygram shows angulated femurs, left tibia, and the right fibula (*arrowheads*)

Fig. 5.13.4. Plain radiograph of the right lower limb in a patient with type III OI shows severe deformity of both tibia and fibula, with signs of old, multiple fractures and callus formation (*arrowheads*)

Osteogenesis Imperfecta Type IIB/III

OI type IIB/III has the same features as OI type I, but with normal sclera and severely deformed limbs.

Signs on Plain Skeletal Radiographs

- Severe osteoporosis.
- Severe limb deformities, with multiple fractures and callus formation (Fig. 5.13.4).

For Further Reading

1. Herman TE et al. Inherited diseases of bone density in children. Radiol Clin N Am 1991;29(1):749–772
2. Castriota-Scanderbeg A et al. Abnormal skeletal phenotypes: From simple signs to complex diagnoses, 1st edn. Springer, Berlin, 2005

5.14

Caudal Regression Syndrome and Sirenomelia (Mermaid Syndrome)

Caudal regression syndrome (CRS) is a rare disease characterized by complete or incomplete absence of the sacrum. Sirenomelia is a severe form of CRS characterized by fusion of both lower limbs into one limb making the infant look like a mermaid.

The anomaly is sporadic, and can be associated with diabetic mothers and maternal folic acid deficiency.

CRS is associated with lack of growth of the lower extremities with disruption of the distal spinal cord.

The patient presents with neurological deficits in the lower limbs and loss of bladder and bowel control.

CRS can be associated with Klippel-Feil syndrome and VATER association.

Other anomalies associated with CRS include renal agenesis, hydrocephalus, myelomeningocele, Pierre-Robin sequence (micrognathia, glossoptosis, and U-shaped cleft palate), and anorectal anomalies.

Signs on Plain Radiographs

Complete or partial agenesis of the sacrum is a pathognomonic sign (Fig. 5.14.1).

Fig. 5.14.1. Plain pelvic radiograph shows complete agenesis of the sacrum in CRS, plus dislocated left hip joint (*arrowhead*)

Signs on Spinal MRI

CRS spinal cord anomalies are categorized according to the location and the shape of the conus medullaris. Type 1 CRS is characterized by sudden blunting of the cord (Fig. 5.14.2). Type 2 CRS is characterized by tethered cord (Fig. 5.14.3).

Fig. 5.14.2. Sagittal T1-weighted MR illustration of the spinal cord shows type 1 CRS spinal cord anomaly with sudden blunting of the spinal cord (*arrowhead*)

Fig. 5.14.3. Sagittal T1-weighted MR illustration of the spinal cord shows type 2 CRS spinal cord anomaly with tethering of the cord (*arrowhead*)

For Further Reading

1. Towfighi J et al. Spinal cord abnormalities in caudal regression syndrome. Acta Neuropathol 1991;81(4):458–466
2. Kozlowski K et al. Caudal regression syndrome and spondyloepiphyseal dysplasia in a 6-year-old child. A new syndrome? Pediatr Radiol 1990;21:75–77
3. Singh SK et al. Caudal regression syndrome – Case report and review of literature. Pediatr Radiol Int 2005;21:578–581
4. Meisheri IV et al. Sirenomelia: the mermaid syndrome. Pediatr Surg Int 1996;11:580–581
5. Rossi A et al. Imaging in spine and spinal cord malformation. Eur J Radiol 2004;50:177–200

5.15

Ellis-van Creveld Syndrome (Chondroectodermal Dysplasia)

Ellis-van Creveld (EvC) syndrome is a rare genetic disorder characterized by dwarfism, bilateral postaxial polydactyly in the hands or feet (Fig. 5.15.1), narrow chest, and distal limb shortening (acromelia). The disease arises due to abnormal formation of organs developing from the ectoderm such as cartilage, bones, nails, teeth, and sweat glands. Renal anomalies such as agenesis, mega-ureter, and nephrocalcinosis may be seen in patients with EvC syndrome.

The disease has an autosomal recessive mode of inheritance. Up to 50–60% of patients have congenital heart defects (most often atrial septal defect). Patients present with hypoplastic nails, bilateral postaxial polydactyly, dwarfism, and small teeth. Alopecia might be present.

Death in EvC syndrome patients usually results from respiratory insufficiency due to a narrow thorax. However, death due to cardiac failure from the congenital heart diseases also occurs.

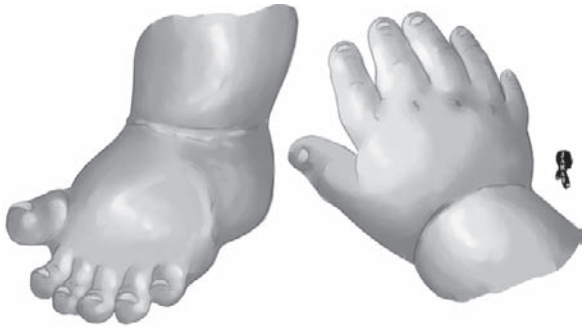

Fig. 5.15.1. Illustration shows postaxial polydactyly of the hand and foot in EvC syndrome

Signs on Skeletal Radiographs

- Bilateral postaxial (ulnar side) polydactyly (Fig. 5.15.2).
- Progressive limb shortening (short radius, ulna, metacarpals, and metatarsals).
- Short ribs with narrow thorax.
- Valgus deformity of the knee.

For Further Reading

1. Castriota-Scanderbeg A et al. Abnormal skeletal phenotypes: From simple signs to complex diagnoses, 1st edn. Springer, Berlin, 2005
2. Ghosh S et al. Report of a new syndrome: Focus on differential diagnosis and review of Ellis-van Creveld, Curry-Hall, acrofacial dysostosis, and orofacial digital syndromes. Oral Surg Oral Med Oral Pathol Oral Radiol Endod 2007;103: 670–676
3. Moudgil A et al. Nephronopthisis associated with Ellis-van Creveld syndrome. Pediatr Nephrol 1998;12:20–22
4. Sergi C et al. Ellis-van Creveld syndrome: A generalized dysplasia of enchondral ossification. Pediatr Radiol 2001; 31:289–293

Fig. 5.15.2. Plain radiograph shows bilateral postaxial polydactyly in a child with EvC syndrome (*arrowheads*)

5.16

SAPHO Syndrome (Anterior Chest Wall Syndrome)

SAPHO syndrome is a rare disease of unknown origin affecting the bones and the joints with skin manifestations. SAPHO is an acronym of the typical disease manifestations:

- Synovitis.
- Acne.
- Pustulosis of the palmar and plantar skin surface, usually psoriatic palmoplantar pustulosis or psoriasis vulgaris (Figs. 5.16.1 and 5.16.2).
- Hyperostosis of the bones due to inflammation and ossification of the bone and its ligaments.
- Ostitis.

Fig. 5.16.1. Illustration shows psoriasis vulgaris lesions on the palm of a SAPHO syndrome patient

Fig. 5.16.2. Illustration showing psoriasis vulgaris lesions on a plantar surface

Absence of skin lesions do not exclude SAPHO syndrome because the interval between skin manifestations and bone lesions seen on radiographs can take from 2 to 20 years.

The disease affects children and young adults. In adults, it presents with classic sternoclavicular joint hyperostosis and ostitis, while in children it presents with chronic recurrent multifocal osteomyelitis (CRMO) usually affecting the metaphyses of the long bones.

Fever and blood test results showing signs of inflammatory reaction, such as high C-reactive proteins and elevated erythrocyte sedimentation rate (ESR), are common features.

SAPHO syndrome should be suspected in a patient having rheumatic bone pain and skin manifestations with sterile inflammation of bones and joints (negative synovial fluid culture). The disease features are sometimes indistinguishable from features of chronic osteomyelitis. Absence of abscesses and bony sequestra, along with a history of psoriasis vulgaris or palmoplantar pustulosis, is a good clue for the diagnosis.

Tietze syndrome: is a rare syndrome of unknown origin characterized by nonsuppurative inflammation of the costosternal and sternoclavicular joints. Patients often present with painful tender swelling of the anterior chest wall with acute, sudden pain radiating to the arms and shoulders. The disease lacks the skin manifestations of SAPHO syndrome.

Signs on Skeletal Radiographs, Bone Scan, and CT in Adults

- Anterior chest wall lesions in the form of sternoclavicular, sternomandibular, and costochondral joint ostitis and hyperostosis are seen in 65–90% cases (Fig. 5.16.3).
- The thoracic spine is affected in up to 30% of cases in the form of end plate sclerosis and hyperostosis with multiple erosions (nonspecific spondylodiscitis).
- Paravertebral ossifications with ankylosis occur in advanced stages mimicking ankylosis spondylitis.
- Unilateral sacroiliitis with mandibular joint osteosclerosis can be seen in up to 10% of cases.
- On bone scan, high ^{99m}Tc uptake in the manubrium and both sternoclavicular joints gives a "bull's head" sign.

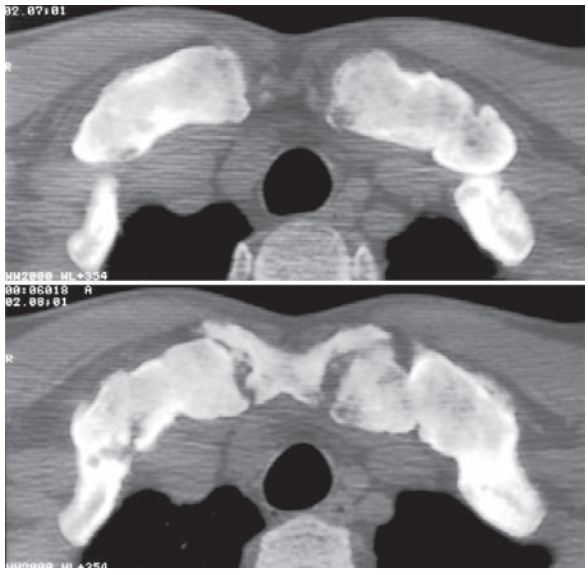

Fig. 5.16.3. Axial thoracic CT shows typical bilateral hyperostosis of the sternoclavicular joints in a patient with SAPHO syndrome

Signs on Skeletal Radiographs and CT in Children

- The lesions are commonly seen in the metaphyses of long bones, usually in the lower extremities in the form of CRMO.
- Minimal periosteal reaction with predominant osteolytic lesions is seen. The periosteal reaction can be extensive with onion-skin type mimicking malignancy (e. g., Ewing sarcoma).
- Osteolytic lesions in the medial end of the clavicles instead of hyperostotic lesions as in the adult form.
- In the spine, lesions are predominantly osteolytic affecting the end plates.

Q: What is the difference between ankylosing spondylitis and SAPHO syndrome regarding vertebral column manifestations?

Ankylosing spondylitis is characterized by syndesmophytosis, while syndesmophytosis is not a feature of SAPHO syndrome. Sacroiliitis in SAPHO syndrome is usually unilateral, while sacroiliitis in ankylosing spondylitis is typically bilateral.

For Further Reading

1. A. M. Davies et al. SAPHO syndrome: 20-year follow-up. Skeletal Radiol (1999) 28:159–162
2. H. Sugimoto et al. The SAPHO syndrome: defining the radiologic spectrum of disease comprising the syndrome. Eur Radiol. 8, 800–806 (1998)
3. A. Nachtigal et al. Vertebral involvement in SAPHO syndrome: MRI findings. Skeletal Radiol (1999) 28:163–168
4. J. W. S. Earwaker et al. SAPHO: syndrome or concept? Imaging findings. Skeletal Radiol (2003) 32:311–327
5. Massimo De Filippo et al. MRI findings of Tietze's syndrome mimicking mediastinal malignancy on MDCT. European Journal of Radiology Extra 65 (2008) 33–35

5.17

Fong Disease and Nail-Patella Syndrome

Nail-patella syndrome is a rare genetic disease characterized by dystrophic nail changes, patella hypoplasia or aplasia, iliac horns, and nephropathy with proteinuria.

The disease has an autosomal dominant mode of inheritance, with an incidence approaching 1 in 50,000 live births.

Iliac horns are seen in up to 70% of cases, and they are a specific sign of the disease. Horns are triangular bony processes that arise from a bony surface. The iliac horns afford a point of origin for the gluteus medius muscle.

The disease causes dystrophy of the nails in 95.1% of cases, and sometimes there is complete absence of the nails. Nail changes commonly affect the thumb and the index finger (Fig. 5.17.1). Recurrent subluxation or dislocation of the patella can be seen, but without gait abnormalities.

Elbow dysplasia, such as hypoplasia of the radial head, can be found in up to 92.5% of cases.

Renal problems present in the form of chronic glomerulonephritis that might rarely progress into renal failure and uremia.

When only iliac horns are present without other abnormalities, the name "Fong disease" is applied to the condition rather than nail-patella syndrome.

Signs on Plain Radiographs

- Bilateral iliac horns located at the site of attachment of the gluteus medius muscles (Fig. 5.17.2).
- Hypoplasia or absent patella.
- Hypoplasia of the capitellum or radial head.
- A conical spine projecting from the lateral and middle thirds of the clavicle might be seen occasionally, and is called "clavicular horn."

Fig. 5.17.1. Illustration showing typical nail dystrophic change affecting the index finger in nail-patella syndrome

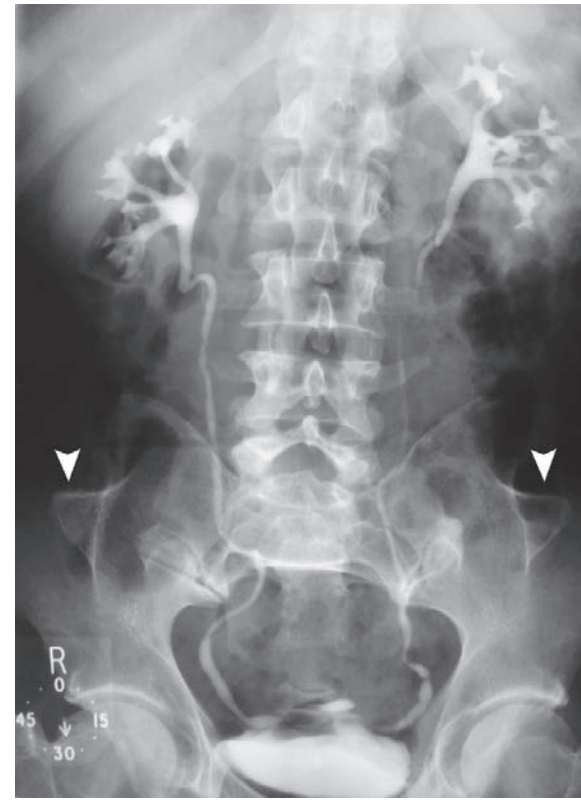

Fig. 5.17.2. Intravenous urography radiograph investigating renal function shows bilateral iliac horns (*arrowheads*). Iliac horns are characteristic findings in nail-patella syndrome and Fong disease

For Further Reading

1. Yarali HN et al. Clavicular horn: Another bony projection in nail-patella syndrome. Pediatr Radiol 1995;25:549–550
2. Castriota-Scanderbeg A et al. Abnormal skeletal phenotypes: From simple signs to complex diagnoses, 1st edn. Springer, Berlin, 2005
3. Reed D et al. Computed tomography of "iliac horns" in hereditary osteo-onychodysplasia (nail-patella syndrome). Pediatr Radiol 1987;17:168–169
4. Lazzeri S et al. Hereditary osteo-onychodysplasia or nail-patella syndrome: Description of one case and literature review. J Orthopaed Traumatol 2005;6:105–109
5. Bongers EM et al. Nail-patella syndrome. Overview on clinical and molecular findings. Pediatr Nephrol 2002;17:703–712

5.18

Progeria (Hutchinson-Gilford Syndrome)

Progeria is a very rare genetic pediatric disease characterized by an abnormal rapid premature-aging process, scleroderma-like skin changes, and progressive loss of the subcutaneous fat in a child. It is a very rare disease that is seen almost exclusively in Caucasians (1 in each 8 million live birth).

Patients usually present after the first year of life with profound failure to thrive, alopecia, prominent scalp veins, large head and small face, beaked nose, protruded ears, short stature, "horse rider's stance," and delayed dentition (Fig. 5.18.1).

Death in progeria occurs due to extensive atherosclerosis that leads to ischemic heart disease within the first three decades of life.

Pangeria: is an autosomal recessive premature-aging syndrome that manifests itself in the second to third decade of life (like progeria but occurs in adulthood).

Fig. 5.18.1. Illustration showing the facial features of progeria

Signs on Plain Skeletal Radiographs

- Large cranium with frontal bossing, open fontanelles and wormian bones (Fig. 5.18.2).
- Small face compared to the head (Fig. 5.18.2).
- Very short clavicle with resorption of distal ends (Fig. 5.18.3).
- Loss of terminal tufts of digits (acro-osteolysis) (Fig. 5.18.4).
- Coxa valga with acetabular degeneration (Fig. 5.18.5).
- Generalized osteoporosis.

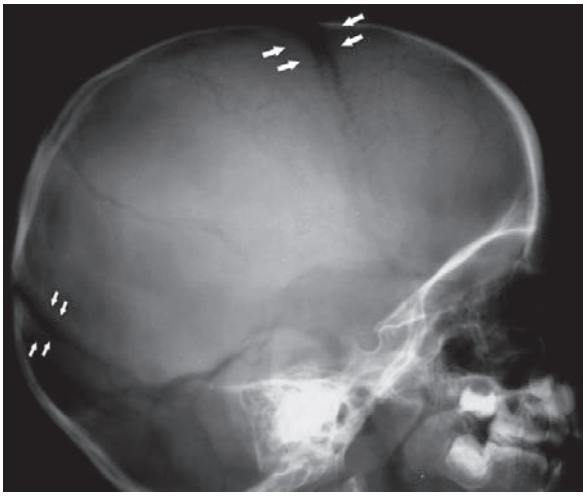

Fig. 5.18.2. Lateral plain radiograph of the skull shows open anterior and posterior fontanelles (*arrows*). Note the size of the face compared to the size of the skull

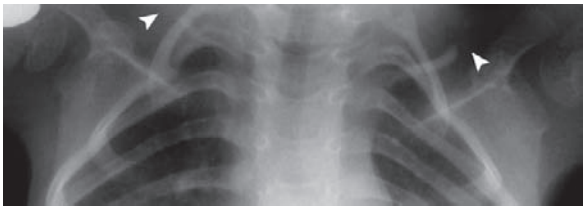

Fig. 5.18.3. Plain radiograph of the clavicles; note the small size of the clavicles with absence of the distal ends (*arrowheads*)

Fig. 5.18.4. Plain radiograph of the left hand shows acro-osteolysis of the thumb and the index finger (*arrowheads*)

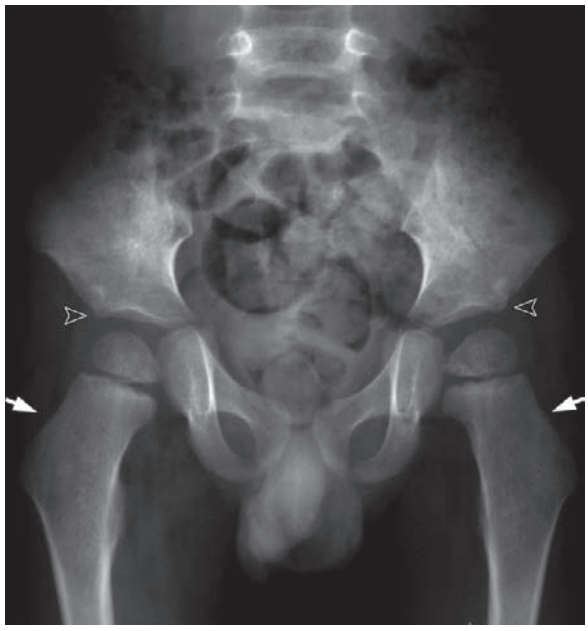

Fig. 5.18.5. Plain pelvic radiograph shows bilateral coxa valga (*white arrows*) with horizontal acetabulum (*open arrowheads*)

For Further Reading

1. Monu JUV et al. Hutchinson-Gilford progeria syndrome in siblings. Skeletal Radiol 1990;19:585–590
2. Harjacek M et al. Immunological aspects of progeria (Hutchinson-Gilford syndrome) in a 15-month-old child. Eur J Pediatr 1990;150:40–42
3. Wagle WA et al. Cerebral infarction in progeria. Pediatr Neurol 1992;8:476–477

5.19

Tarlov Cyst

Tarlov cyst is an out-pouching of the posterior sacral spinal nerve's perineural space at the junction of the root ganglion (Fig. 5.19.1). The cyst is filled with cerebrospinal fluid (CSF).

Tarlov cyst may have a valve, allowing the CSF to enter but not leave the cystic pouch. With time, an increase in the hydrostatic pressure of the CSF inside the cyst presses the spinal nerves against the cyst wall, creating neurological symptoms in rare situations.

Tarlov cyst can be asymptomatic, but when the sacral nerves are impinged, neurological symptoms start to develop, and the condition is called "*Tarlov disease*." The patient presents with low back pain, neurogenic claudication, and sensory and motor disturbance. Postural movements like bending, standing, and walking are typically painful; urinary dysfunction may occur. The pain from Tarlov cyst is similar to the pain from herniated discs and gynecological diseases.

Signs on MRI

Tarlov cyst is seen as a lesion located at the nerve roots with a typical fluid cyst signal of low T1 and high T2 signal intensities; there is no contrast enhancement after gadolinium injection (Figs. 5.19.2 and 5.19.3).

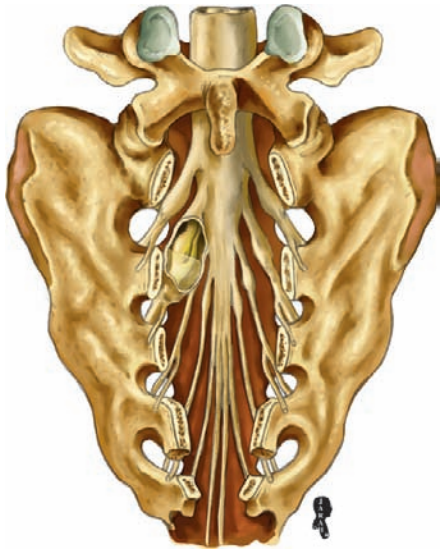

Fig. 5.19.1. Illustration of the gross pathological morphology and location of Tarlov cyst

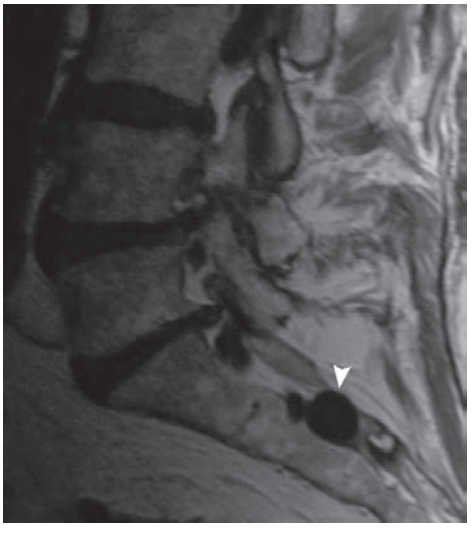

Fig. 5.19.2. Sagittal T1-weighted MR image shows low-intensity round cyst located at the sacral nerve roots, representing Tarlov cyst (*arrowhead*)

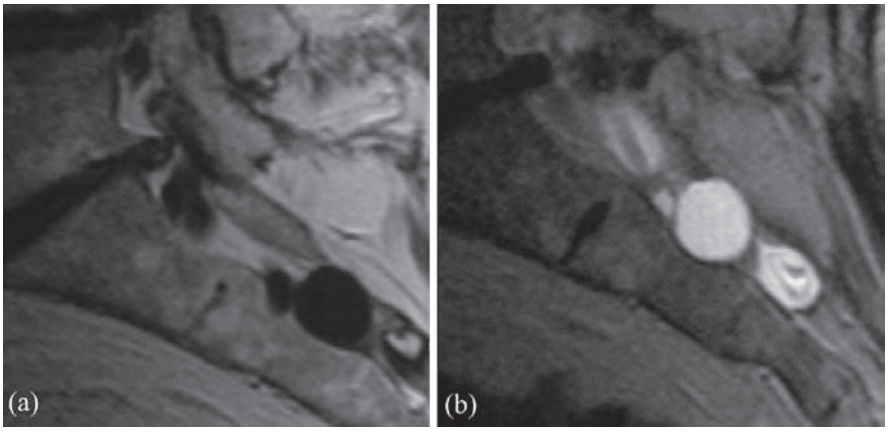

Fig. 5.19.3. Sagittal T1- and T2-weighted MR images show the low signal intensity of the cyst on the T1-weighted sequence **a**, and the high signal intensity of the cyst on the T2-weighted sequence **b**

For Further Reading

1. Nadler SF et al. Tarlov cyst as a rare cause of S1 radiculopathy: A case report. Arch Phys Med Rehabil 2001;82:689–690
2. Dehanie V et al. Coccygodynies révélant des kystes de Tarlov. Rev Med Interne 1990;11:280–284

5.20

Madelung Deformity and Dyschondrosteosis (Léri-Weill Syndrome)

Madelung deformity is a congenital hand deformity characterized by anterior subluxation of the carpal bones in relation to the distal radioulnar joint.

Madelung deformity usually appears between 10 and 15 years of age, and it is often unilateral. Patients with Madelung deformity present with a prominent dorsal end of the distal radioulnar joint.

Dyschondrosteosis (Léri-Weill syndrome): is a rare congenital disease characterized by bilateral Madelung deformities (Fig. 5.20.1). The disease has an autosomal dominant mode of inheritance with a female predominance.

Fig. 5.20.1. Illustration showing bilateral Madelung deformities in both hands (dyschondrosteosis)

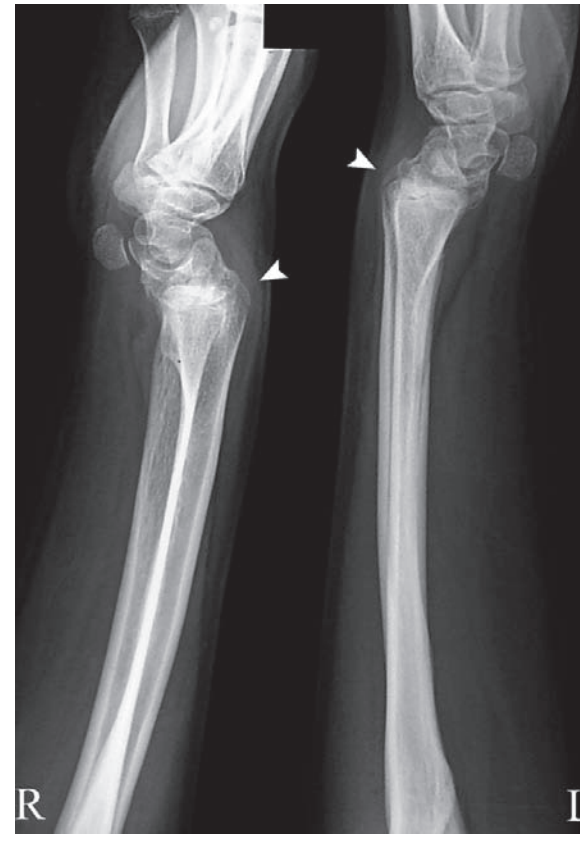

Fig. 5.20.2. Lateral plain radiograph of the wrists shows bilateral Madelung deformities in a patient with dyschondrosteosis. Note the anterior subluxation of the carpal bones with prominence of the posterior aspect of the distal radioulnar joints (*arrowheads*)

Signs on Skeletal Radiographs

- Madelung deformity is seen as an anterior projection of the carpal bone over the distal radioulnar joint (Fig. 5.20.2).
- Triangular shape of the distal radial epiphysis.

For Further Reading

1. Luchetti R et al. Carpal tunnel syndrome in Madelung's deformity. J Hand Surg 1988;13(1):19–22
2. Fagg PS. Wrist pain in the Madelung's deformity of dyschondrosteosis. J Hand Surg 1988l;13(1):11–15
3. Mohan V et al. Leri-Weill syndrome (dyschondrosteosis): A family study. J Hand Surg 1988;13(1):16–18

"*This page left intentionally blank.*"

Chapter 6

Phakomatoses (Neurocutaneous Syndromes)

Phakomatoses (neurocutaneous syndromes) are a group of chronic diseases characterized by neoplasms derived from the embryonic ectoderm (skin, central nervous system, peripheral nervous system, and eyes). They also affect structures derived from the mesoderm (blood vessels, bones, and cartilage) and the endoderm (epithelial lining of the gastrointestinal tract).

The phakomatoses concept was formulated early in the twentieth century by an ophthalmologist called van der Hoeve and initially described three disorders (neurofibromatosis, tuberous sclerosis, and von Hippel-Lindau syndrome) according to their ophthalmologic manifestations. Many of the phakomatoses have a genetic origin, although some are sporadic.

These syndromes result in the formation of angiomatous malformations, hamartomatoses, cystic lesions, and abnormalities in skin pigmentation. Phakomatoses also have high incidence of seizure disorders (75–90%).

For Further Reading

1. de Sousa C. The neurocutaneous syndromes. Curr Paediatr 1992; 2:86–89.
2. Korf BR. The phakomatoses. Clin Dermatol 2005;23:78–84.
3. Gardeur D et al. Cranial computed tomography in the phakomatoses. Neuroradiology 1983;25:293–304.

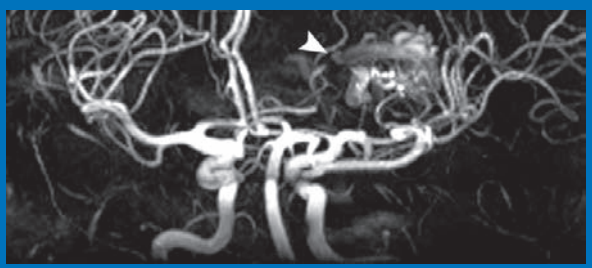

CONTENTS

6.1

Neurofibromatosis

Neurofibromatosis (NF) is a multisystemic, neurocutaneous (phakomatosis) disease characterized by the formation of multiple neurofibromas within the central or the peripheral nervous system. Neurofibromas are benign tumors composed of tortuous cord Schwann cells and neuronal axons.

NF is transmitted in an autosomal dominant fashion. There are two types of NF:

Peripheral Neurofibromatosis (Type 1/von Recklinghausen Syndrome)

Peripheral NF is more common than central NF, and it is characterized by numerous peripheral nerve sheath tumors (neurofibromas and schwannomas), skin manifestations (e.g., café-au-lait spots), ocular manifestations (e.g., Lisch nodules), and optic nerve or hypothalamic gliomas.

Diagnostic criteria of NF type 1

- Positive family history of NF.
- Dysplasia of the wings of the sphenoid bone.
- At least five café-au-lait spots larger than 5 mm.
- Two or more cutaneous neurofibromas or one plexiform neurofibroma.

Central Neurofibromatosis (Type 2)

Central NF is commonly associated with tumors of the brain, spinal cord, and meninges (spinal sheath schwannoma, glioma, and meningioma), and it is more fatal than peripheral NF.

Meningiomas of central NF occur early in life compared to the normal population (usually in the third decade of life rather than the fifth decade in normal subjects). Almost 25% of all childhood meningioma cases occur with NF type 2. Characteristically, meningiomas in NF type 2 are multiple (meningioma is usually a solitary lesion).

Bilateral schwannomas of the vestibulocochlear nerve (acoustic neuroma) is common and it is pathognomonic for NF type 2.

Diagnostic criteria of NF type 2:

- Positive family history of NF 2 with unilateral acoustic neuroma.
- Bilateral acoustic neuromas (Fig. 6.1.1).
- Multiple meningiomas (Fig. 6.1.2).

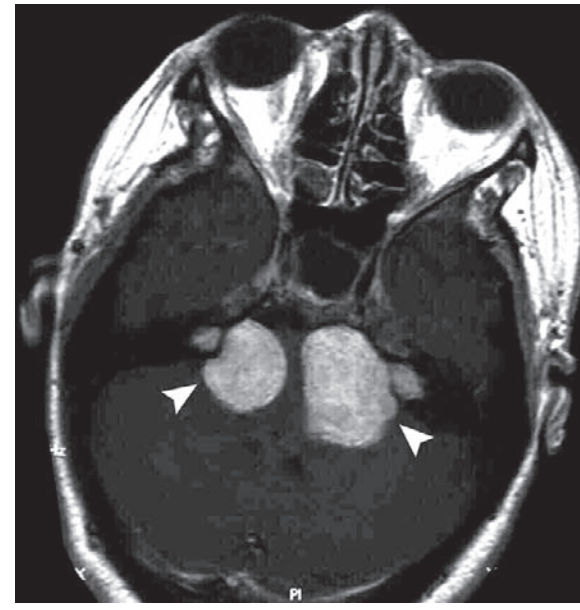

Fig. 6.1.1. Axial T1-weighted postcontrast MR image in a patient with a positive family history of NF type 2 showing bilateral acoustic schwannomas with homogeneous contrast enhancement (*arrowheads*)

Neurofibromatosis Abnormalities of the Orbit

NF abnormalities of the orbit can be classified into four categories:

- Plexiform NF.
- Orbital osseous dysplasia.
- Congenital glaucoma.
- Optic gliomas.

Plexiform Neurofibromatosis

Plexiform NF is a rare, congenital, diffuse, irregular tumor of the major nerve plexi, which has a cylindrical, fusiform, or globoid appearance (plexiform). The tumor

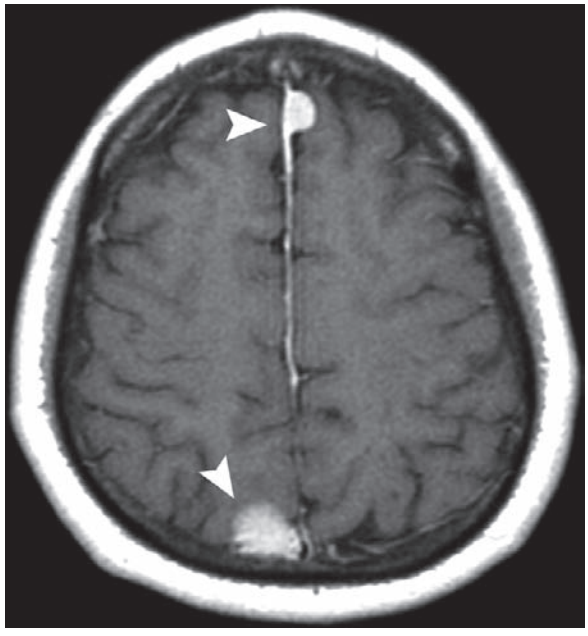

Fig. 6.1.2. Axial T1-weighted postcontrast MR image of the brain in another patient with NF type 2 showing two meningeal-based brain lesions with homogeneous enhancement characteristic of multiple meningiomas (*arrowheads*). The anterior meningioma has a dural tail connected to the falx cerebri

arises from any major nerve plexi (arms or legs), or rarely from peripheral nerves, such as nerves of the orbit. Microscopically, the tumor arises from the Schwann cells of the perineurial and endoneurial cells.

On clinical palpation, the tumor has the feeling of a bag of worms, and there will be overgrowth and thickening of the skin overlying it, termed "elephantiasis."

Signs on CT

The CT scan shows a very large, noncapsulated, poorly marginated, infiltrative mass that enhances moderately after contrast material administration (Fig. 6.1.3).

Orbital Osseous Dysplasia

The bony orbital dysplasia (malformation) in NF is a consequence of partial or complete absence of the greater wings of the sphenoid bone. The adjacent maxillary sinus and the ethmoid air cells might be hypoplastic, while the sella turcica might be dysplastic and abnormally formed.

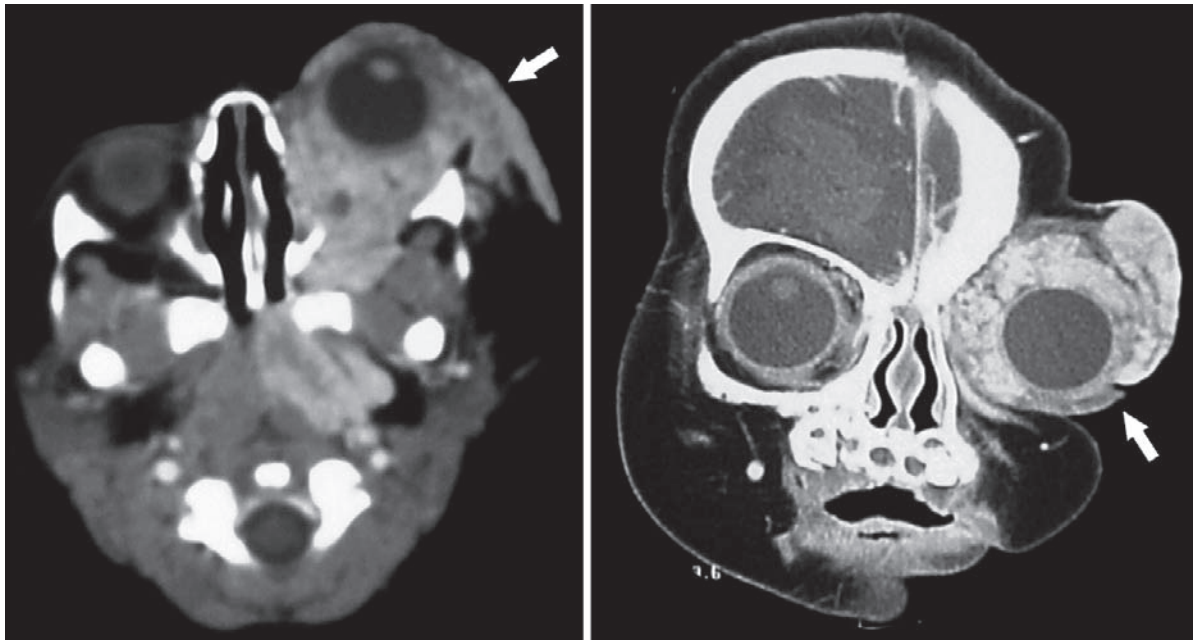

Fig. 6.1.3. Axial and coronal postcontrast CT images of the head in a patient with NF type 1 with plexiform neurofibromatosis (*arrows*). Note the shape of the tumor that is poorly marginated and extensive pushing the globe out of the orbital cavity

This bony defect will allow the adjacent temporal lobe of the brain to herniate anteriorly into the posterior aspect of the orbit causing exophthalmos, and when the cerebrospinal fluid pulsation is transmitted into the orbit, a pulsatile exophthalmos occurs.

Signs on Plain Radiographs

On plain frontal skull radiographs, there is absence of the oblique transverse orbital line, which is created when the X-rays passes over the greater wings of the sphenoid bone.

Signs on CT

- Hypoplasia of the greater wings of the sphenoid, with or without hypoplasia of the adjacent maxillary sinus and the ethmoid air cells (Fig. 6.1.4).
- The orbit might show enlargement deformity on coronal scans giving a radiographic "egg-shaped" appearance (Fig. 6.1.5).

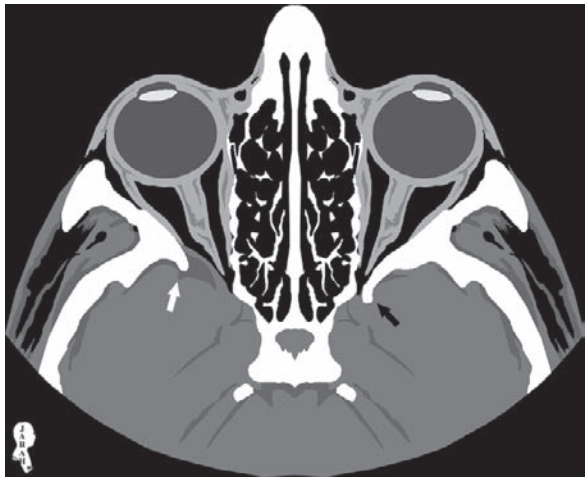

Fig. 6.1.4. Axial orbital CT illustration showing a classic defect in the greater wings of the sphenoid bone as seen in NF patients on CT examination (*white arrow*). Note the difference of the sphenoid bone shape compared to the other normal side (*black arrow*)

Fig. 6.1.5. Coronal orbital CT illustration showing widening deformity of the orbital cavity with radiographic "egg-shaped" appearance (*arrows*)

Congenital Glaucoma (Buphthalmos)

NF may increase intraocular pressure during the newborn period leading to stretching and enlargement of the cornea and breaks in the Descemet membrane. This causes eye bulging that is called buphthalmos or ox eye (Fig. 6.1.6).

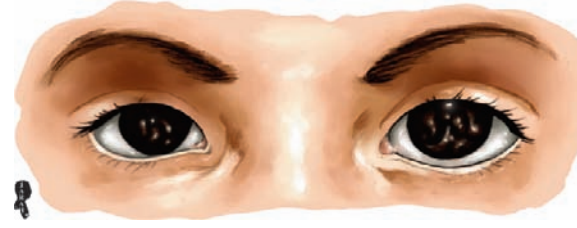

Fig. 6.1.6. Illustration showing congenital glaucoma of the left eye in a child. Note the difference in the size of the eye and the cornea compared with the normal right eye

Optic Glioma

Optic nerve glioma is a grade-I pilocytic astrocytoma. Up to 90% of cases occur before the age of 20 years. Bilateral optic nerve gliomas can be seen in NF type 1, and up to 40% of optic glioma cases have NF type 1 (Fig. 6.1.7). More than 50% of optic gliomas can extend to the optic chiasm and the hypothalamus. Patients usually present with painless exophthalmos and visual deterioration in late stages of the disease.

Signs on Plain Radiographs

The optic canal may show enlargement if extension to the canal occurs.

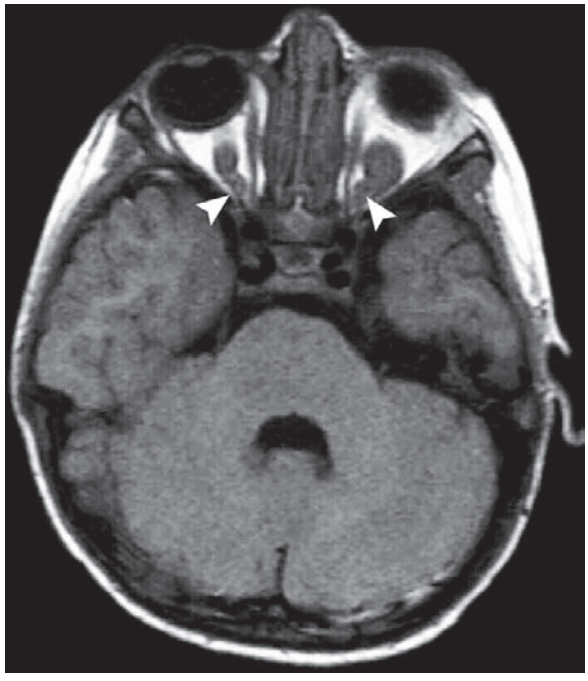

Fig. 6.1.7. Axial T1-weighted precontrast MR image in a patient with NF type 1 shows bilateral enlargement and tortuous thickening of the optic nerves, as a classic case of bilateral optic nerve gliomas (*arrowheads*)

Fig. 6.1.8. Lateral plain radiograph of the tibia and the knee joint in a patient with NF type 1 showing the classic appearance of tibial pseudoarthrosis. Note how the proximal end of the tibia is fractured and bowed posteriorly compared to the distal end (*arrow*). Also, note thickening and posterior bowing of the fibula

Signs on CT

- The optic nerve becomes thick, kinked, and tortuous (characteristic).
- Homogeneous enhancement of the nerve postcontrast.
- Widening of the optic canal might be seen if extension into the optic canal occurs.

Signs on MRI

- Isointense signal on T1-weighted images, with hyperintense signal intensity on T2-weighted images.
- Homogeneous contrast enhancement.

Pseudoarthrosis of Neurofibromatosis

Pseudoarthrosis is a bone deformity seen in only 10% of patients with NF. Pseudoarthrosis means a false joint. It is a clinical situation in which the bone is broken and the two broken ends do not join together, but make a false union instead which impedes movement. The most common bony pseudoarthrosis in NF is tibial pseudoarthrosis (Fig. 6.1.8).

NF causes gradual anterior bowing of the tibia until it fractures later in life. The two ends will not join together, making a pseudoarthrosis. Other bones can be involved such as the fibula, the radius, and the ulna.

For Further Reading

1. Linder B et al. CT and MRI of orbital abnormalities in neurofibromatosis and selected craniofacial anomalies. Radiol Clin North Am 1987;25(4):787–802
2. Tada M et al. Massive plexiform neurofibromatosis in the orbit in a child with von Recklinghausen's disease. Child's Nerv Syst 1998;14:210–212
3. Jacquemin C et al. Orbit deformities in craniofacial neurofibromatosis type 1. Am J Neuroradiol 2003;24:1678–1682.
4. Gardeur D et al. Cranial computed tomography in the phakomatoses. Neuroradiology 1983;25:293–304

6.2

Sturge-Weber Syndrome (Encephalotrigeminal Angiomatosis)

Sturge-Weber syndrome (SWS) is a rare, neurocutaneous (phakomatosis) disease characterized by the formation of multiple vascular malformations (angiomatoses) within the body. The incidence of this disease is 1 per 50,000 live births.

Two essential pathologic features must be found to diagnose SWS

- Cutaneous vascular lesion follows the course of the first branch of the trigeminal nerve known as "nevus flammeus" or "port-wine stain" in up to 85% of cases (Fig. 6.2.1). The lesion darkens with age and may develop nodular elevations.
- Leptomeningeal angiomatosis (vascular malformations) over the parieto-occipital lobe ipsilateral to the cutaneous vascular lesion. It is seen in all cases.

Fig. 6.2.1. Illustration of a young girl with a port-wine stain (nevus flammeus). The stain is typically seen on the forehead as a reddish–pinkish stain over the course of the ophthalmic division of the trigeminal nerve

Other features include angiomas in the gastrointestinal tract, glaucoma (30%), headache (30%), and stroke-like episodes with hemiparesis and mental retardation (50%).

Partial seizures occur in 75–90% of patients by the age of 3 years.

Signs on CT

- Atrophy of the affected side with gyral calcifications that can be seen on plain CT or radiography within the first 2 years of life. The gyral calcifications occur due to anoxia from blood stasis in the overlying angiomatous leptomeningeal vessels (Fig. 6.2.2). On plain radiographs, the gyral calcifications are described as "railroad track calcifications."
- Ipsilateral enlargement of the paranasal sinus and the skull (mainly frontal sinus).
- Ipsilateral choroid plexus hypertrophy seen within the ventricles.

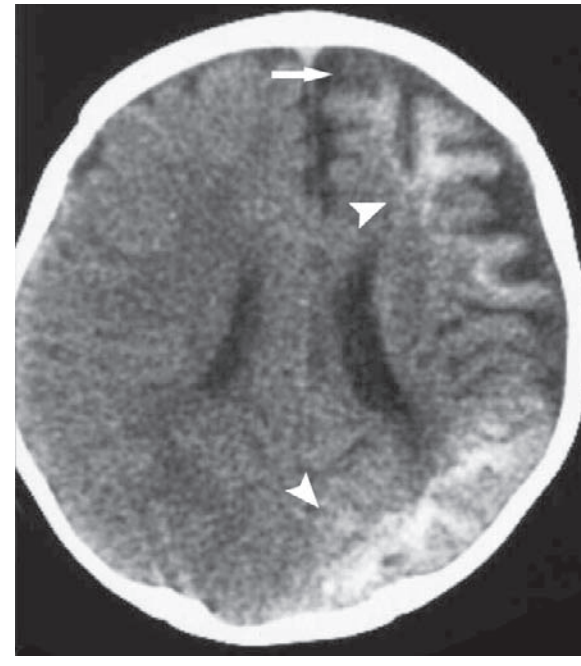

Fig. 6.2.2. Axial noncontrast-enhanced CT of the brain shows extensive gyral calcifications on the left side affecting the occipital, parietal, and the frontal lobe in a patient with SWS (*arrowheads*). Note the atrophy of the left side in comparison to the right one (*arrow*)

Signs on MRI

- Ipsilateral pia mater thickening with enhancement after contrast on T1-weighted images representing leptomeningeal angiomas (Fig. 6.2.3).
- Volume loss of the affected hemisphere (atrophy) with calvarial thickening of the affected side.

Fig. 6.2.3. Axial postcontrast T1-weighted MR illustration of the brain shows occipital leptomeningeal enhancement typically seen in patients with SWS

For Further Reading

1. Gardeur D et al. Cranial computed tomography in the phakomatoses. Neuroradiology 1983;25:293–304
2. Garzon MC et al. Vascular malformations. Part II: Associated syndromes. J Am Acad Dermatol 2007;56:541–64
3. Adamsbaum C et al. Accelerated myelination in early Sturge-Weber syndrome: MRI-SPECT correlation. Pediatr Radiol 1996;26:759–762
4. Kilickesmey O et al. Coexistence of pleomorphic xanthoastrocytoma with Sturge-Weber syndrome: MRI features. Pediatr Radiol 2005;35:910–913
5. Barath B et al. Cerebral venous drainage via the ophthalmic veins in the Sturge-Weber syndrome. Neuroradiology 1994; 36:318–320
6. Thomas-Sohl KA et al. Sturge-Weber syndrome: A review. Pediatr Neurol 2004;30:303–310

6.3

Tuberous Sclerosis (Bourneville-Pringle Disease)

Tuberous sclerosis (TS) is a neurocutaneous disease (phakomatosis) characterized by the formation of multiple hamartomas in the body. A hamartoma is composed of normal tissue in an abnormal configuration.

The disease has an autosomal dominant mode of inheritance, and an incidence of 1 in 15,000 live births.

TS forms hamartomas in different locations in the body, for example:

- **Retinal hamartomas:** found in 53% of patients with TS, which may calcify.
- **Adenoma sebaceum (facial angiofibroma):** consists of brownish–red papules found on the nasolabial folds, the temporal region, and the forehead (Fig. 6.3.1). They are found in 80% of patients with TS. Depigmentation of hair or eyebrows (poliosis) may occur as an early manifestation.
- **Shagreen patches:** are cutaneous lesions of variable sizes with leathery connective tissue proliferation seen at the lumbosacral region.
- **Renal angiomyolipomas:** are benign renal masses composed of three tissues (fat, blood vessels, and smooth muscles). They occur in 40–100% of patients with TS (Fig. 6.3.2).
- **Cardiac rhabdomyoma:** is a benign myocardial hamartoma that is found in children and neonates.
- **Pulmonary lymphangiomyomatosis:** is a rare obstructive airway disease occurring due to proliferation of the smooth muscles of the lymphatic vessels, bronchial walls, and alveolar walls. It is classically seen only in women with TS (Fig. 6.3.3).
- **Intracranial lesions:** a triad seen in 80% of TS patients consisting of seizures, mental retardation, and one of four lesions (cortical tuber, periventricular calcifications, subependymal nodules, and subependymal giant cell astrocytoma).

Diagnostic criteria of TS

- **Major (only one required for diagnosis):** facial angiofibroma, retinal hamartoma, subependymal nodules, renal angiomyolipoma, or cortical tuber.
- **Minor (two required for diagnosis):** infantile spasm, cardiac rhabdomyosarcoma, subependymal giant cell astrocytoma, shagreen patches, and first-degree relative with TS.

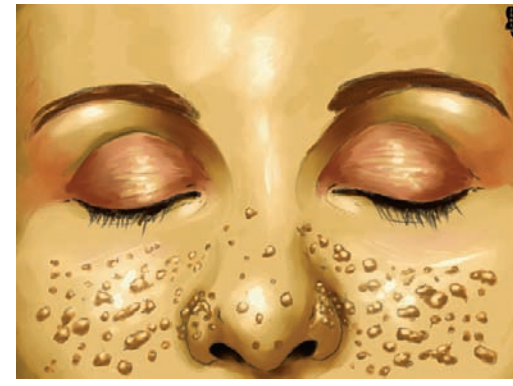

Fig. 6.3.1. Illustration showing multiple brownish papules scattered in a butterfly pattern along both nasolabial folds (facial angiofibroma)

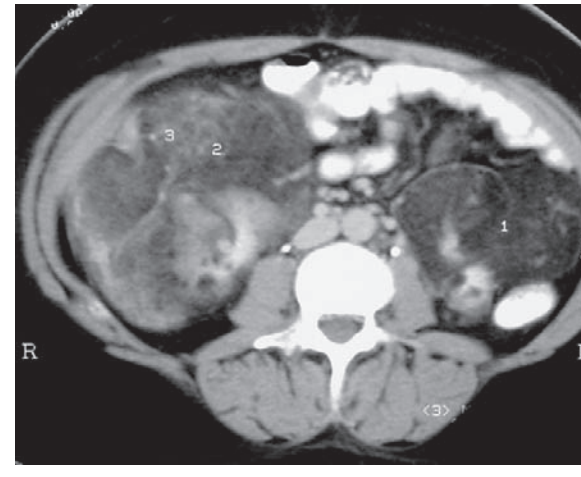

Fig. 6.3.2. Axial abdominal CT image with contrast shows bilateral renal masses with heterogeneous densities (numbers). Note the mixed densities of the bilateral masses, with the fat density component seen more profoundly in the left kidney, typical of angiomyolipoma

Fig. 6.3.3. Axial chest lung-window CT image shows bilateral, diffuse, cystic interstitial lung pattern in a patient with obstructive airway disease and TS. Diagnosis is "lymphangiomyomatosis"

Signs on CT and MRI

- **Cortical tuber:** is a hypodense/hypointense lesion, with gross appearance of gyral broadening (like pachygyria) of one side of the cerebral hemispheres. It affects the frontal lobe more than the occipital lobe, and on MRI the lesion exhibits low T1 and high T2 signal intensities (Fig. 6.3.4).
- **Periventricular calcifications:** they are seen in the periventricular area, and especially around the foramen of Monro (Figs. 6.3.5 and 6.3.6).
- **Subependymal nodules (hamartomas):** they occur on the surface of the caudate nucleus and most often on the sulcus of the thalamostriatus just posterior to the foramen of Monro. They are seen in up to 98% of patients with TS, and commonly calcify causing periventricular and subependymal calcifications. The uncalcified nodules enhance after contrast material injection. The differential diagnosis includes metastasis and gray matter heterotopia (Figs. 6.3.7 and 6.3.4).
- **Subependymal giant cell astrocytoma:** is a tumor that tends to occur near the foramen of Monro causing obstructive hydrocephalus. Calcification within the tumor is common. The tumor is highly enhanced after contrast material injection, and it is seen in up to 10% of cases of TS (Fig. 6.3.8).

Fig. 6.3.5. An axial brain CT image shows bilateral subependymal calcifications, typical of TS. These calcifications represent calcified subependymal nodules

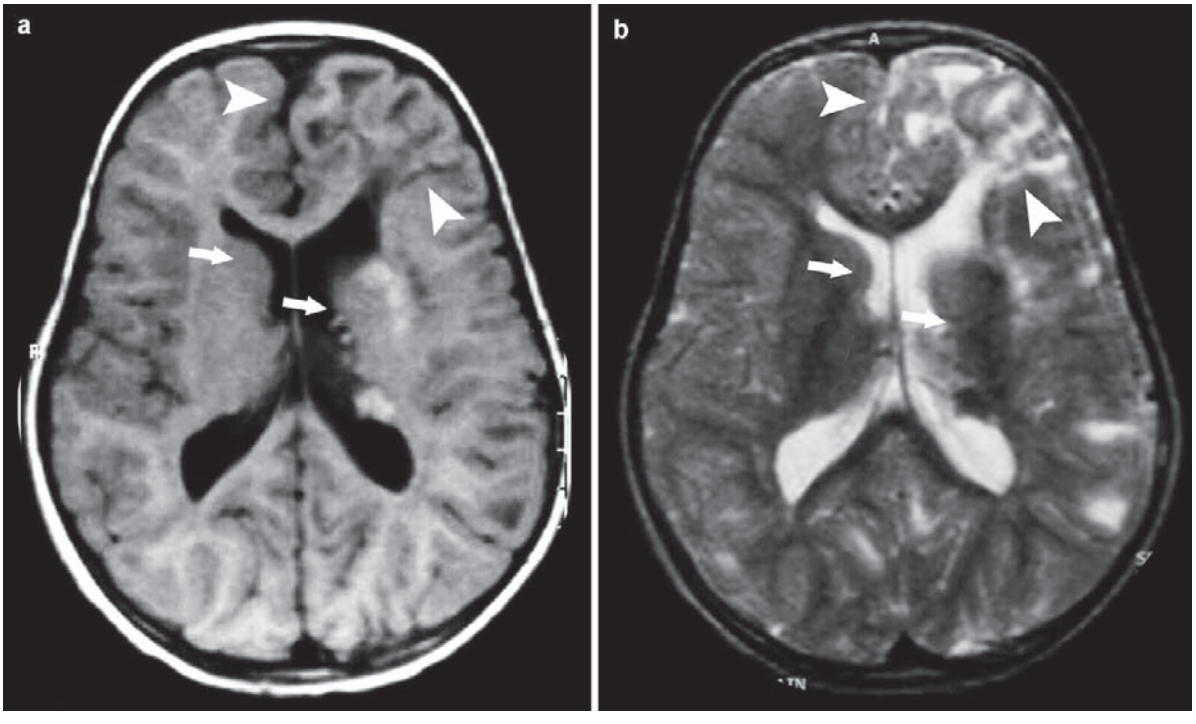

Fig. 6.3.4. Axial T1- and T2-weighted MR images show cortical tuber on the left frontal lobe (*arrowheads*). Note the gyral broadening mimicking pachygyria, with the low intensity on the T1-weighted image **a** and high signal intensity on the T2-weighted image **b**. Also, note the subependymal nodules (*arrows*)

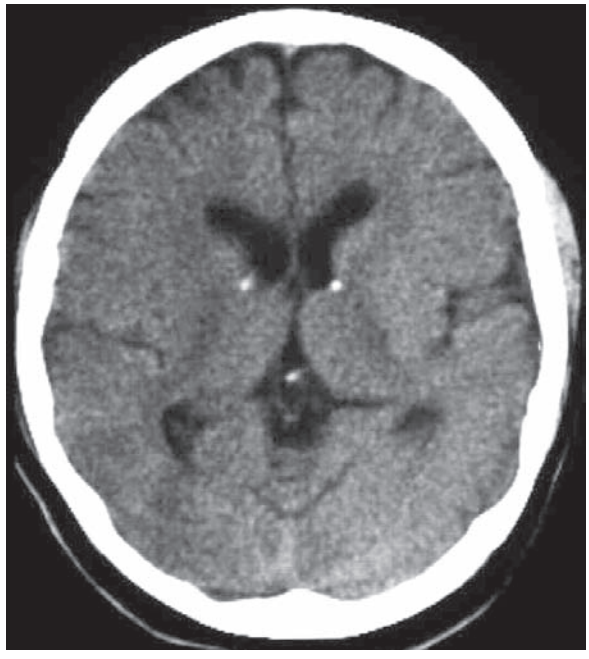

Fig. 6.3.6. An axial brain CT image shows bilateral symmetrical calcifications near the foramen of Monro, a classic finding in TS

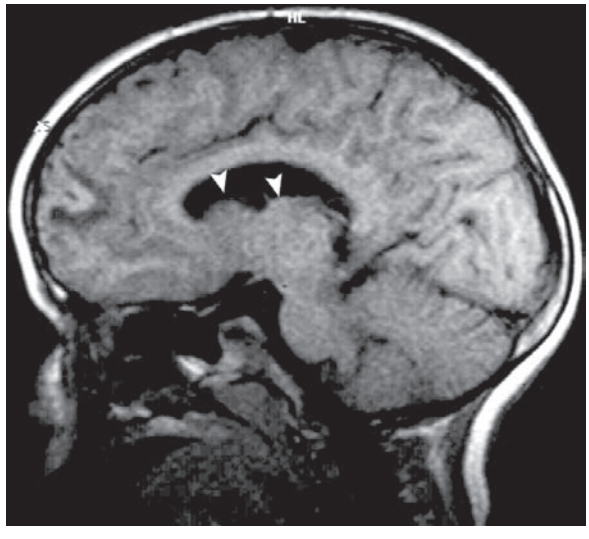

Fig. 6.3.7. Sagittal T1-weighted MR image shows subependymal nodules (*arrowheads*)

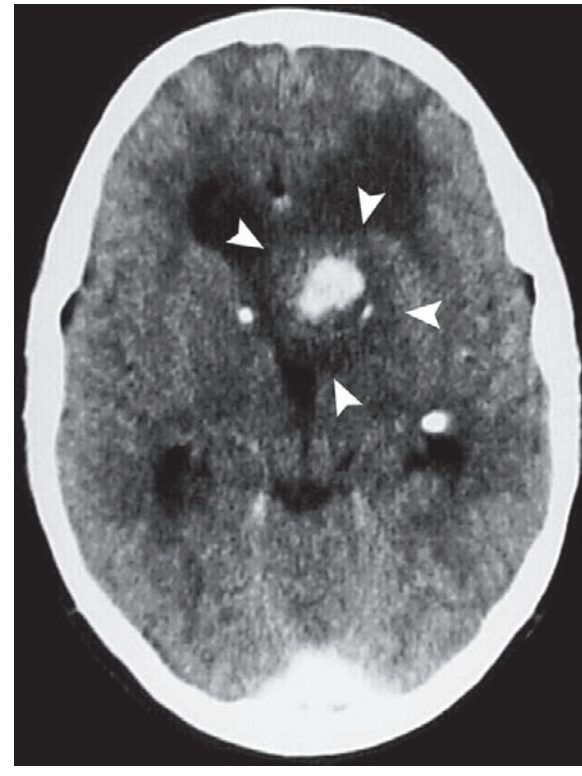

Fig. 6.3.8. An axial brain CT image shows subependymal giant cell astrocytoma. Note the location of the tumor in the subependymal region (*arrowheads*), and the calcification within the tumor. Also, note the calcification seen on the right side near the foramen of Monro

For Further Reading

1. Gardeur D et al. Cranial computed tomography in the phakomatoses. Neuroradiology 1983;25:293–304
2. Martin N et al. MRI evaluation of tuberous sclerosis. Neuroradiology 1987;29:437–443
3. de Sousa C. The neurocutaneous syndromes. Curr Paediatr 1992;2:86–89
4. Korf BR. The phakomatoses. Clin Dermatol 2005;23:78–84

6.4

Neurocutaneous Melanosis

Neurocutaneous melanosis (NCM) is a neurocutaneous disease (phakomatosis) characterized by an increased number of melanocytes in the leptomeninges (leptomeningeal melanosis) and by multiple giant hairy cutaneous nevi.

Patients characteristically present with "large" congenital cutaneous nevi, i.e., larger than 20 cm in diameter (66%). The giant nevi are usually located in a lumbosacral distribution (Fig. 6.4.1). Up to 50% of patients develop meningeal melanomas later in life.

Leptomeningeal melanosis can be a primary disease on its own, and can also be due to leptomeningeal metastasis from melanoma. Spinal involvement occurs in up to 20% of cases. A definitive diagnosis usually requires meningeal biopsy.

NCM can exist with other neurocutaneous syndromes like neurofibromatosis and Sturge-Weber syndrome. In up to 10% of cases, NCM can be associated with Dandy-Walker anomaly.

Primary leptomeningeal melanosis diagnostic criteria:

- High-density cerebrospinal fluid in the subarachnoid space on noncontrast-enhanced CT images due to proliferation of the melanocytes in the meninges.
- Absence of cutaneous, meningeal, or ocular melanomas to exclude melanotic metastasis.
- Extensive body search that reveals no metastasis, including bone scan and CT examination of the abdomen and lungs.
- Large or multiple congenital nevi.

Signs on MRI

- High signal intensity of the meninges on T1-weighted images and low signal on T2-weighted images due to the paramagnetic effect of melanin pigment. After gadolinium injection, the leptomeninges enhance markedly (Fig. 6.4.2).
- Hydrocephalus might be present due to disturbance of the cerebrospinal fluid ventricles by the meningeal melanosis proliferation (obstructive, noncommunicating hydrocephalus).

Fig. 6.4.1. Illustration of a baby with giant congenital nevus in the lumbosacral region, with numerous satellite nevi on the trunk, upper limb, and face. The lumbosacral distribution of the nevi is usually referred to as "bathing-trunk" distribution.

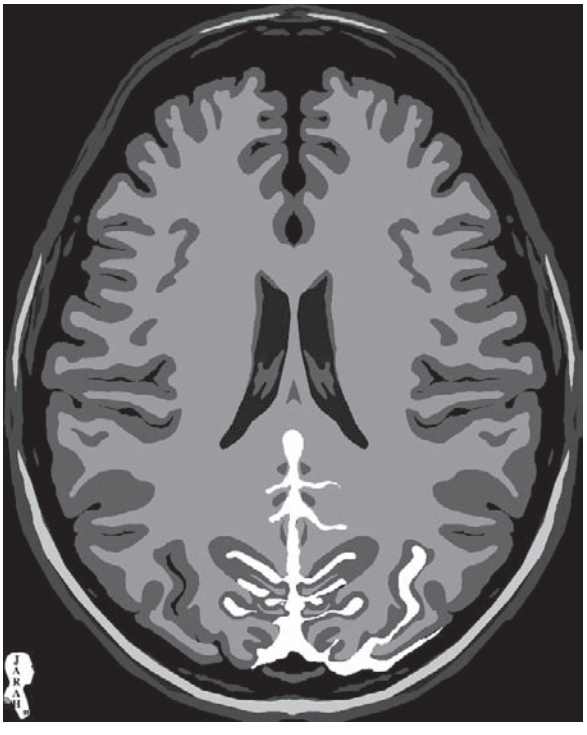

Fig. 6.4.2. Axial T1-weighted postcontrast MR illustration shows leptomeningeal thickening and enhancement in the occipital area due to infiltration by melanocytes in NCM

For Further Reading

1. Makkar HS et al. Neurocutaneous melanosis. Semin Cutan Med Surg 2004;23(2):138–144
2. Chaloupka JC et al. Neurocutaneous melanosis with Dandy-Walker malformation: A possible rare pathoetiologic association. Neuroradiology 1996;38:486–489
3. Di Rocco F et al. Neurocutaneous melanosis. Childs Nerv Syst 2004;20:23–28
4. Byrd SE et al. MR imaging of symptomatic neurocutaneous melanosis in children. Pediatr Radiol 1997;27:39–44

6.5

PHACE Syndrome

PHACE syndrome is a neurocutaneous (phakomatosis) disease characterized by posterior cranial fossa anomalies, hemangiomas, arterial anomalies, cardiac anomalies, and eye anomalies. Sternal clefting may occur in some cases, causing the syndrome to be termed "*PHACES syndrome*" according to some authors. More than 90% of patients are females (strong female predominance). The disease has a spectrum of lesions comprising:

- Posterior cranial fossa anomalies: the most common feature is Dandy-Walker anomaly.
- Hemangioma: is usually large and occurs in the cervicofacial region with a plaque-like appearance, which is a characteristic feature of this syndrome (Fig. 6.5.1). The facial hemangioma exists soon after birth with orbital involvement of the eyelids or the choroids.
- Arterial anomalies: include internal carotid artery aplasia or hypoplasia with arterial collateral formation in the brain resembling moyamoya disease but in an infant (Fig. 6.5.2).
- Cardiac anomalies: include coarctation of the aorta, atresia of the aortic arch, cor triatriatum, and patent ductus arteriosus (Fig. 6.5.3).
- Eye anomalies: include colobomas, choroidal hemangiomas, and optic nerve hypoplasia.

Fig. 6.5.1. Illustration showing a classic giant facial hemangioma in a child with PHACE syndrome

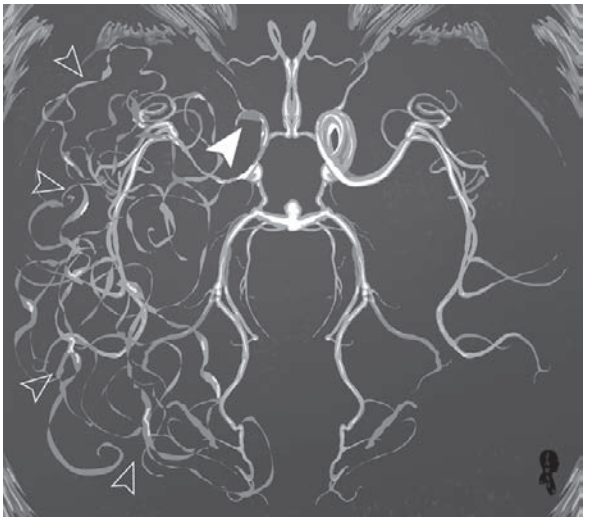

Fig. 6.5.2. Axial MR angiography illustration shows the circle of Willis with large network of collaterals in the territory of the right middle cerebral artery, giving the appearance of a "puff of smoke," which is a pathognomonic feature of moyamoya disease (*open arrowheads*). Hypoplasia of the right internal carotid artery can be seen (*white arrowhead*). Moyamoya disease is a progressive occlusion of the arteries of the circle of Willis due to intimal thickening of the distal internal carotid artery walls. The disease forms abnormal collateral networks that develop adjacent to the stenotic vessel

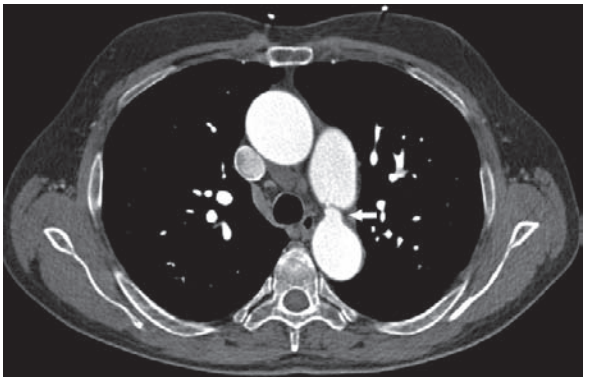

Fig. 6.5.3. Axial postcontrast CT image of the chest shows patent ductus arteriosus between the pulmonary artery and the descending aorta in a 9-year-old patient (*arrow*). The ductus arteriosus is a duct that connects the left proximal pulmonary artery to the descendant aorta just distal to the subclavian artery in the embryo. After birth, the high oxygen concentration in the blood from normal breathing causes constriction of the duct until it closes functionally within 24 h of birth. Anatomical closure occurs in 90% of cases within the first 2 months of life, and in 99% at 1 year of age

Key diagnosis

Presence of both Dandy-Walker anomaly and cervicofacial hemangioma in an infant.

For Further Reading

1. Bhattacharya JJ et al. PHACES syndrome: A review of eight previously unreported cases with late arterial occlusion. Neuroradiology 2004;46:227–233
2. Drosou A et al. Infantile midline facial hemangioma with agenesis of the corpus callosum and sinus pericranii: Another face of the PHACE syndrome. J Am Acad Dermatol 2006;54:348–352
3. Heyer GL et al. The neurologic aspects of PHACE: Case report and review of the literature. Pediatr Neurol 2006;35: 419–424

6.6

Von Hippel-Lindau Syndrome

Von Hippel-Lindau syndrome (VHL) is a multisystemic, neurocutaneous (phakomatosis), cancerous syndrome characterized by the formation of multiple central nervous system hemangioblastomas and cystic lesions in the viscera. Hemangioblastoma is a benign (grade I), mostly cerebellar, tumor that arises from abnormal blood vessel proliferation.

VHL syndrome has an autosomal dominant inheritance pattern, and it is linked to mutations in chromosome 3. The disease has an incidence of 1 in 36,000 live births.

Diagnostic criteria for VHL syndrome:

- A patient with a positive family history of VHL syndrome, central nervous system hemangioblastoma (including retinal hemangioblastoma), pheochromocytoma, or clear cell renal carcinomas.
- A patient with a family history must have more than one hemangioblastoma, or one hemangioblastoma and visceral tumors.

VHL syndrome other manifestations include:

- Cerebellar, spinal, or retinal hemangioblastomas (35–60%) (Fig. 6.6.1).
- Renal cell carcinoma (35%).
- Pheochromocytoma (10%).
- Visceral cysts (Fig. 6.6.2).
- Syringomyelia (80%).
- Endolymphatic sac tumor (Fig. 6.6.3).
- Pancreatic cystadenoma or cystadenocarcinoma (17%).

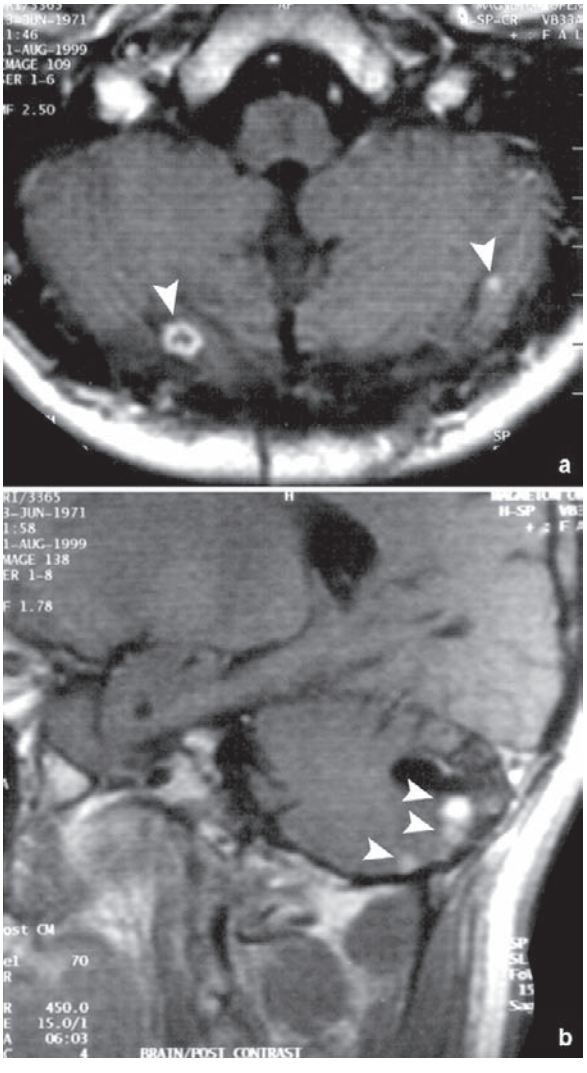

Fig. 6.6.1. Axial (**a**) and sagittal (**b**) T1-weighted postcontrast MR images of the cerebellum show multiple small enhancing lesions (*white arrowheads*). One of the lesions shows rim enhancement with mural nodule compatible with hemangioblastoma in a patient with a positive family history of VHL syndrome

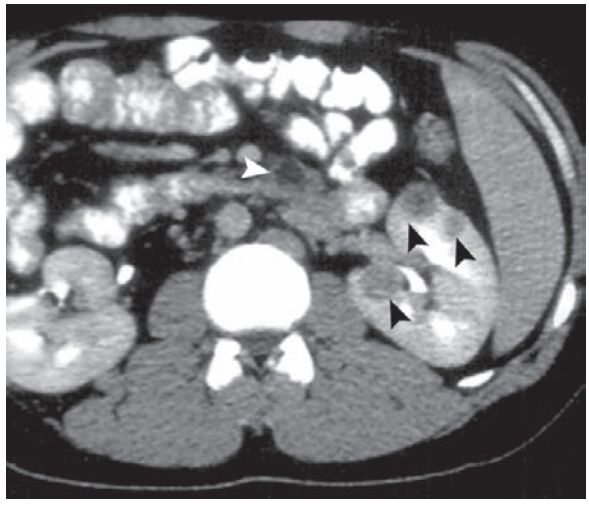

Fig. 6.6.2. Axial contrast-enhanced abdominal CT of the same patient reveals multiple renal cysts in the kidney (*black arrowheads*), with a pancreatic cyst (*white arrowhead*). Multiple cystic visceral lesions plus cerebellar hemangioblastomas are essential features of VHL syndrome

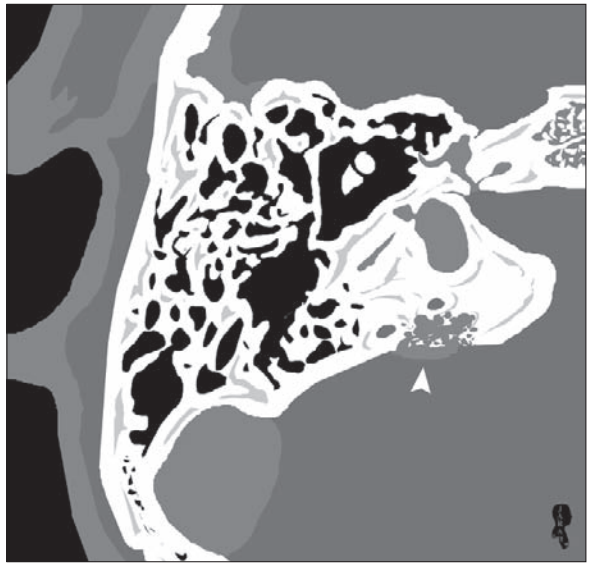

Fig. 6.6.3. Axial temporal bone CT illustration shows soft-tissue density lesion with bone destruction located at the region of the vestibular aqueduct (*white arrow*); the diagnosis is endolymphatic sac tumor

For Further Reading

1. McEvoy AW et al. Haemangioblastoma of a cervical sensory nerve root in Von Hippel-Lindau syndrome. Eur Spine J 2000;9:434–436
2. Gardeur D et al. Cranial computed tomography in the phakomatoses. Neuroradiology 1983;25:293–304

6.7

Cowden Syndrome (Multiple Hamartoma-Neoplasia Syndrome)

Cowden syndrome is a rare, multisystemic, autosomal dominant, neurocutaneous (phakomatosis) disease characterized by whitish skin nodules (trichilemmoma), gingival whitish papillomas, and formation of various types of papillomas from the mouth to the anus.

Trichilemmomas are whitish, benign skin papules derived from the outer root sheath of a hair follicle. The whitish stain is due to glycogen deposition within the lesion, and it is a pathognomonic feature of Cowden disease (Fig. 6.7.1).

The disease is characterized by the formation of multiple, sessile polyps in the esophagus, stomach, and colon. In upper gastrointestinal endoscopy, the esophageal polyps are diffuse giving a nodular appearance to the esophagus, known as "glycogenic acanthosis." The name "glycogenic" reflects the glycogen content of the polyps.

The disease manifests itself at 30 years of age, and affects mainly women and Caucasians for unknown reasons.

The disease forms multiple hamartomas with risk of malignancy in other areas of the body such as:

- **Breasts:** breast fibroadenomas occur in up to 70% of patients with Cowden disease, and appear at a younger age compared with the normal population (Fig. 6.7.2).
- **Thyroid gland:** thyroid adenomas and multinodular goiter can be seen in 40–60% of cases.
- **Cerebellar gangliocytomatosis (Lhermitte-Duclos disease):** is characterized by dysplastic enlargement of the cerebellar cortex (Fig. 6.7.3).

Screening for breast cancer monthly by self-examination and annually by mammography is advised for patients with Cowden syndrome after 25 years of age. Also, annual screening with ultrasound for thyroid nodules is advised for patients after 20 years of age.

Fig. 6.7.1. Illustration of a finger with whitish lesion in a patient with Cowden syndrome (trichilemmoma)

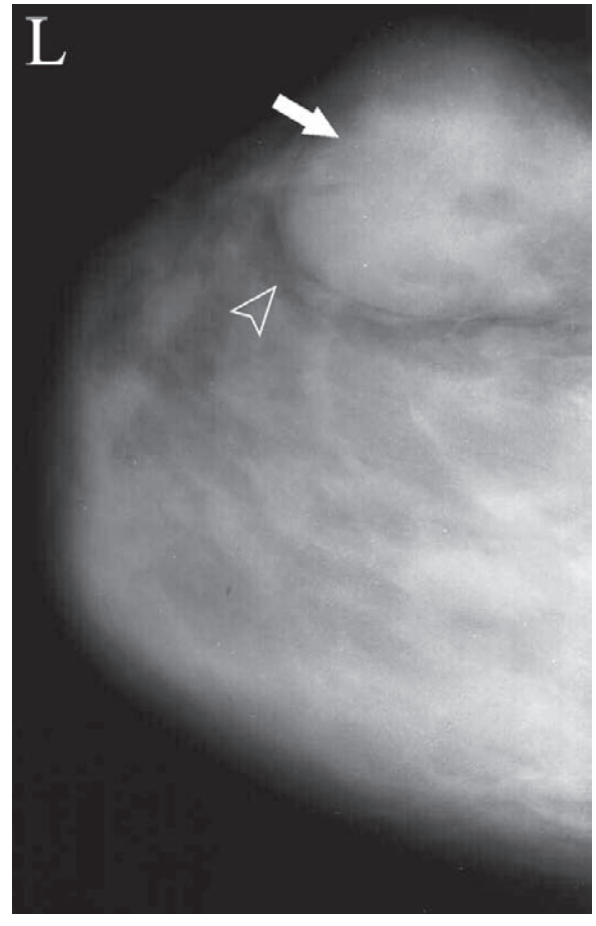

Fig. 6.7.2. Conventional mammogram shows large fibroadenoma (*arrow*). Fibroadenoma is a benign breast lesion arising from the connective tissue around the acini. It normally affects young women between 20 and 30 years of age. The lesion is seen as a round or oval well-defined mass with popcorn or dystrophic calcification. It is sometimes surrounded by a lucent halo seen as an optical illusion (*open arrowhead*)

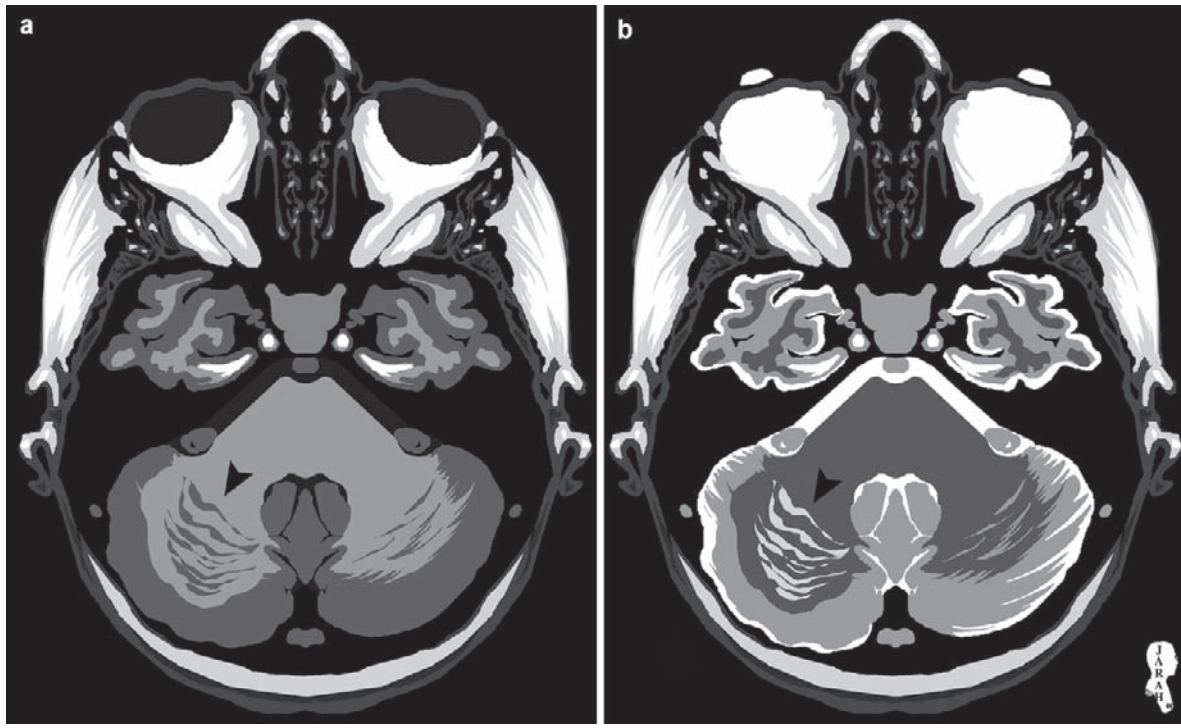

Fig. 6.7.3. Axial T1- and T2-weighted MR illustrations show Lhermitte-Duclos disease. The disease consists of a hamartoma that arises due to hypermyelination of the axons in the cerebellum. On MRI, it is seen as a focal or diffuse mass in the cerebellum with striation and thickening of the cerebellar folia (*arrowheads*). The lesion shows no contrast enhancement, and gives low T1 signal, with high-signal-intensity striations on T2 causing a "tiger-striped" appearance

For Further Reading

1. Kee Myung L et al. Cowden disease. Gastrointest Endosc 2006;63:151. doi10.1016/j.gie.2005.06.004
2. Campos FG et al. Cowden syndrome: Reports of tow cases and review of clinical presentation and management of a rare colorectal polyposis. Curr Surg 2006;63:15–19. doi 10.1016/j.cursur.2005.04.015
3. Vantomme N et al. Lehrmitte-Duclos disease is a clinical manifestation of Cowden's syndrome. Surg Neurol 2001; 56:201–205

6.8

Gorlin Syndrome (Basal Nevus Cell Carcinoma Syndrome)

Gorlin syndrome is an autosomal dominant neurocutaneous (phakomatosis) disease characterized by a triad of multiple basal cell nevi, jaw odontogenic keratocysts, and skeletal anomalies.

An odontogenic (primordial) keratocyst is a cyst that arises from a tooth before its calcification. It is most commonly located posterior to the premolar region of the mandible or maxilla. In the mandible, it mostly affects the third molar tooth. In men, the disease causes hypogonadism, while in women it causes calcified ovarian fibroids.

To diagnose Gorlin syndrome, two major or one major and two minor diagnostic criteria are needed:
Major diagnostic criteria:

- A patient under 20 years of age with basal cell carcinoma or more than two basal cell carcinomas in older age.
- Histologically proven odontogenic keratocysts of the jaw.
- More than three palmar pits (Fig. 6.8.1).
- Bifid or fused ribs (Fig. 6.8.2).
- First-degree relative with basal nevus cell carcinoma.

Fig. 6.8.1. Illustration showing multiple small skin pits on the palm. This sign is one of the characteristic and major diagnostic criteria of Gorlin syndrome

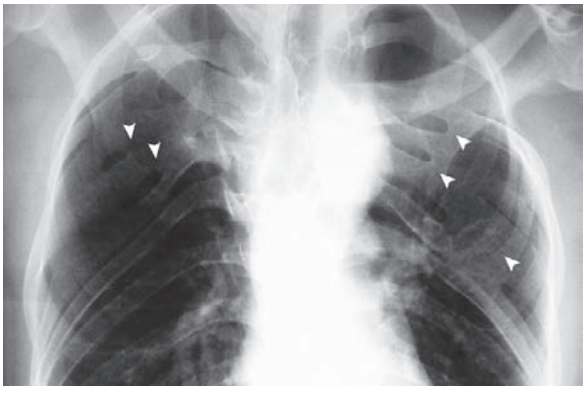

Fig. 6.8.2. Plain chest radiograph shows multiple congenital fused, bifid, and abnormally branched ribs (*arrowheads*). This is another major diagnostic sign of Gorlin syndrome when it is associated with multiple mandibular keratocysts or palmar pits

Minor diagnostic criteria:

- Macrocephaly.
- Medulloblastoma.
- Calcified ovarian fibroids.
- Sprengel deformity or syndactyly.
- Vertebral anomalies or bridging of the sella turcica.
- Hypertelorism, cleft-lip, or frontal bossing.
- Cardiac fibromas.

For Further Reading

1. Shand JM et al. Cysts of the jaws and advances in the diagnosis and management of nevoid basal cell carcinoma syndrome. Oral Maxillofacial Surg Clin N Am 2005;17: 403–414
2. Gardeur D et al. Cranial computed tomography in the phakomatoses. Neuroradiology 1983;25:293–304
3. Nassab R et al. Infected palmar pits: A rare presentation of Gorlin's syndrome. J Hand Surg (Br Eur Vol) 2005;30(5): 459–460
4. Rayner CRW et al. What is Gorlin syndrome? The diagnosis and management of the basal cell naevus syndrome, based on a study of thirty-seven patients. Br J of Plast Surg 1976; 30:62–67

6.9

Wyburn-Mason Syndrome

Wyburn-Mason syndrome (WMS) is a rare, congenital, nonhereditary, neurocutaneous disorder (phakomatosis) characterized by unilateral vascular abnormalities (arteriovenous malformations) affecting the brain, eye, and face.

The ocular manifestations are seen in the form of retinal arteriovenous malformation (AVM), optic atrophy, enlargement of the optic foramen, and pulsatile exophthalmus occasionally. The key for the diagnosis of WMS is to identify retinal AVM (Fig. 6.9.1).

The facial cutaneous manifestations vary from faint skin discoloration to extensive nevus distributed along the course of the trigeminal nerve ipsilateral to the cerebral and ocular lesions (Fig. 6.9.2).

A child or a young patient with facial skin discoloration and brain AVM should be referred to an ophthalmologist to check for retinal AVMs.

Signs on CT and MRI

Both scans show intraparenchymal AVM (Fig. 6.9.3) ipsilateral to the retinal AVM and the skin nevus, with or without intracerebral hemorrhage.

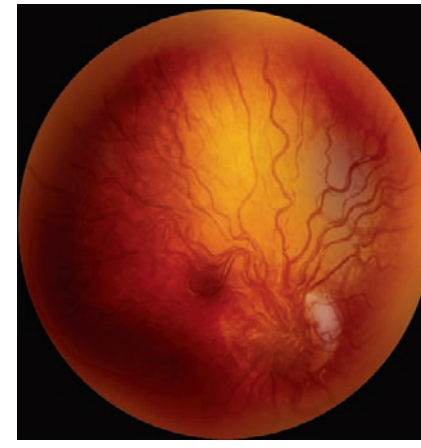

Fig. 6.9.1. A fundoscopic illustration showing a retinal arteriovenous malformation, a characteristic feature of WMS

Fig. 6.9.2. An illustration of a child with facial nevus distributed along the course of the trigeminal nerve

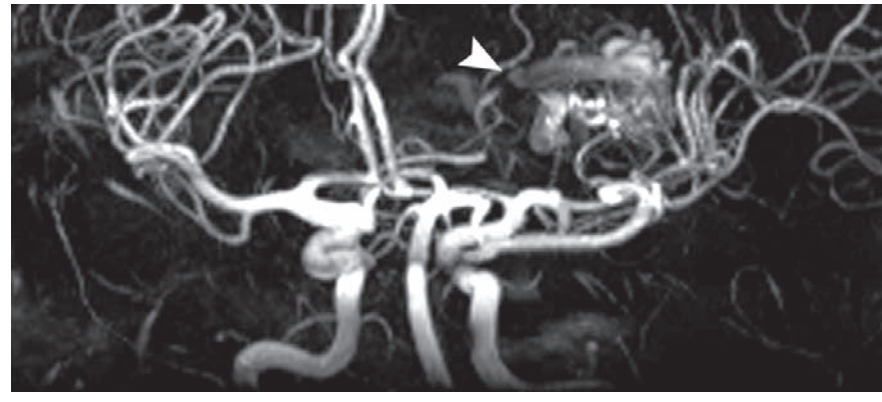

Fig. 6.9.3. 3D reconstructed MR angiography image showing arteriovenous malformation (*arrowhead*). Arteriovenous malformation is a congenital malformation in which large anastomoses exist between arteries and veins in a circumscribed area.

For Further Reading

1. Patel U et al. Wyburn-Mason syndrome. A case report and review of the literature. Neuroradiology 1990;31:544–546
2. Keswani T et al. Wyburn-Mason syndrome: A case report. Int Opthalmol 2008;28:437–438. doi 10.1007/s10792-007-9155-5
3. Jain IS, Sharma SK, Dhir SP, Kaul RL. Wyburn-Mason syndrome. Indian J Opthalmol 1980;28:161–163

"*This page left intentionally blank.*"

Index